Numerical simulations of surface winds and precipitation in Iceland

– Die zweite Aufgabe der theoretischen Meteorologie

Ólafur Rögnvaldsson

Dissertation for the degree of philosophiae doctor (PhD)

University of Bergen, Norway

2013

UNIVERSITY OF BERGEN

Numerical simulations of surface winds and precipitation in Iceland

– Die zweite Aufgabe der theoretischen Meteorologie

Ólafur Rögnvaldsson

Submitted in partial fulfillment
of the Philosophiæ Doctor degree
in meteorology at the
University of Bergen,
Geophysical Institute,
Allégaten 70, 5007 Bergen

November 2012

Contents

List of Figures

List of Tables

Acknowledgements

As this work started in 2002 I must acknowledge the trust and patience I have been shown by the University of Bergen, and in particular Prof. Sigbjørn Grønås. I hope this thesis is a proof that I was worth this trust.

Over the years the projects that make up the bulk of the work presented in this thesis have received financial support from numerous sources. These are:

- RANNÍS (e. the Icelandic Science Fund).
- Tækniþróunarsjóður (e. the Icelandic Innovation Fund).
- Orkusjóður (e. the Icelandic Energy Fund).
- Orkustofnun (e. the National Energy Authority).
- Landsvirkjun.
- Landsnet.
- Orkuveita Reykjavíkur (e. Reykjavík Energy).
- NORA, via the project "Vejrtjeneste for søberedskab", grant number 550-025.
- The Nordic Climate and Energy (CE), Climate, Water and Energy (CWE), and Climate and Energy Systems (CES) research projects and the corresponding Icelandic projects Veður og orka (VO), and Lofthjúpsbreytingar og áhrif þeirra á OrkuKerfi og Samgöngur (LOKS, see http://en.vedur.is/ces).

Working facilities have been provided by the Icelandic Meteorological Office (thanks to Magnús Jónsson), the Hydrological Service of the National Energy Authority (thanks to Árni Snorrason), and in recent years by Iceland GeoSurvey (thanks to Ólafur G. Flóvenz).

The work presented in the first paper was initiated by Tómas Jóhannesson, consequently his responsibility for what has happened since is considerable.

This thesis would not have been accomplished without the tremendous help I have received from my supervisor, Haraldur Ólafsson, especially during the final stage. I'm further indebted to all my co-authors over the years, whom without the papers would obviously never have been written. Many of the figures in chapter 5 were made by my colleague and friend Hálfdán Ágústsson, of which I'm immensely grateful.

I have had the pleasure of meeting and working with many wonderful and talented people during my frequent visits to NOAA/ESRL in Boulder, Colorado. Evelyn, Georg, John, and Sarah, just to name a few (and hopefully not pissing all the others off).

I'm deeply grateful for the time Carlo Casty spent in the shade in June 2011 reading the manuscript and giving me valuable comments and encouragement. Viva my friend.

Thanks to my friend Jian–Wen Bao for re-kindling my passion for science and for all the meaningful (as well as the less meaningful) discussions about life, the universe, and everything over the years. May you enjoy life to the fullest.

Last, but not the least, I'm grateful to my wife María for having walked down the aisle, in spite of my lack of higher education, and for having said yes. The kids are OK too.

This work is dedicated to the loving memory of my father, who taught me to think, and my brother Sigurður, who taught me to think again.

Fyrir mömmu.

Chapter 1

Introduction

1.1 Genesis

In the beginning there was a word, and the word was “application”. The reviewers saw that the word was good and so it was accepted. And because of the acceptance of the word, a small company with a big name (Institute for Meteorological Research – IMR) was founded. So begins the tale of many wonders, and even more pages, that eventually will culminate in perhaps the biggest wonder of them all: Yours truly getting a PhD degree in meteorology from the University of Bergen.

Our story begins in 2001 when a project called “Áhrif loftslagsbreytinga á úrkomu og veðurfar á Íslandi” (e. Impacts of climate changes on precipitation and weather in Iceland) was funded by the Icelandic Research Fund (RANNÍS) and was later to form the backbone of this PhD project, which started formally in February 2002, at the University of Bergen. The main purpose of this modest project was to map precipitation in Iceland in the current climate. A secondary goal was to describe possible changes in the precipitation pattern under different climatic conditions. Over the years there have been many side projects and spin-offs from the original project but, most importantly, there has always been a continuity in this work. There have further been many changes in the meteorological research environment in Iceland. Available computational power has increased by orders of magnitude and numerical models have become more advanced. As a consequence the number of end-users for meteorological products and know-how has increased, ranging from local fishermen to to the energy sector through the combination of weather- and runoff models. New development, which is of great importance, happened in early 2012 when IMR launched an on-demand weather forecasting system called SARWeather (Rögnvaldsson, 2011). One of the novelties of SARWEather (short for Search And Rescue Weather) is that it is run on the Amazon EC2 computing cloud. Hence, the need for powerful, and expensive, in-house computing facility is reduced.

On 30 March 2004, IMR started running numerical weather forecasts twice daily for Iceland and its surrounding waters. The model resolution was 9 km with a smaller 3 km resoulution domain covering SW-Iceland. The forecast range was 72 and 24 hours, respectively. Currently, IMR runs model simulations eight times a day for Iceland and various sub-domains in the North-Atlantic. The forecasts range from a day up to a week and the grid resolution is between 1 and 27 km. In addition IMR provides on-demand forecasting service to Iceland Search And Rescue association (ICE-SAR) and the Department of Civil Protection of the Icelandic Police as well as to GDACS – The Global Disaster Alerts and Coordination System. GDACS is a cooperation framework between the United Nations, the European Commission and disaster managers worldwide to improve alerts, information exchange and coordination in the first phase after major sudden-onset disasters.

1.2 Research questions

The subject of this research has mainly been twofold. Firstly, can one use a regional model to dynamically scale down a coarse resolution global atmospheric analysis to gain better understanding of temporal and spatial distribution of winds and precipitation in Iceland? Secondly, and closely related to the first one, what, if anything, is gained by increasing the horizontal resolution of the regional model?

The answer to the first question is of direct economical importance as the geographical distribution of precipitation and winds in Iceland is poorly known but very important for hydrological and wind energy applications, both in general and particularly in the context of climate change. It is also of importance regarding mapping potential wind energy in Iceland, a subject that is gaining increased interest from the local power sector. The answer to the second question relates directly to our ability to forecast winds and precipitation in as much detail as possible, and in so doing helping to save lives and property.

In this thesis new ways to validate numerical simulations of precipitation are presented and tested. Firstly, comparing simulated precipitation to observations of accumulated snow over large ice caps and glaciers. And secondly, using results from numerical model to force a hydrological runoff model. The resulting discharge is then compared to observed discharge from a large number of individual watersheds.

We will also explore the sensitivity of the numerical simulations to a number of parameters, including the growth of hydrometeors, mixing in the atmospheric boundary layer and of the numerical configurations of the models themselves.

1.3 The structure of this work

This thesis is structured as follows: In the next chapter we describe the weather and climate of Iceland in brief. Chapter three deals with the scientific challenges for studies of surface winds and precipitation in Iceland. In this chapter we focus on the availability and quality of observational data. We give a theoretical background to the meteorological processes related to surface winds and precipitation and how these processes are modeled by state of the art atmospheric models. Chapter four contains a short abstract from each of the seven peer reviewed papers presented in this thesis, followed by general discussions in chapter five. Chapter six gives general conclusions followed by discussions of future work in chapter seven. Thereafter, each of the seven research papers is presented in a chronological order.

Chapter 2

Surface winds and precipitation in Iceland

The objectives of this work is to improve our understanding of how the orography of Iceland modifies the impinging atmospheric flow. Especially, how the orography shapes the wind- and precipitation fields. The primary tools chosen for this work have been the MM5 atmospheric model (Grell et al., 1995), and from 2007, the WRF model (Skamarock et al., 2008). Through the study of available observational data and model results a comprehensive and detailed picture of both spatial and temporal distribution of these important variables has emerged.

2.1 Climate and weather in Iceland

Iceland is a mountainous island and is located in the N-Atlantic storm track. Due to this the climate of Iceland is largely governed by the effects orography has on the flow of extra-tropical cyclones. The weather and climate of most parts in Iceland is characterized by strong winds, frequent precipitation, mild winters and relatively cool summers. Mean temperatures are typically close to 0°C in the winter and 10°C in the summer. Annual precipitation varies considerably. In the lowlands in the southern part of Iceland, where orographic effects are not dominating, the mean annual precipitation is about one thousand millimeters but in general less in the north. Although the amplitute of the seasonal cycle is moderate, there can be large fluctuations in the weather on a daily basis. These fluctuations are reflected by the observed weather extremes shown in table 2.1.

The mountains of Iceland contribute to an enhancement of the fluctuations in the weather. The mountains also cause a large spatial variability of both the weather and the climate and they lead to local amplification of weather extremes. The extreme temperatures, precipitation and winds shown in table 2.1 are all enhanced

Table 2.1: *Observed weather extremes from the beginning of instrumental records. Data from Veðurstofa Íslands (e. The Icelandic Meteorological Office).*

Parameter	**Value**	**Location**	**Date**
Min temperature	-38 °C	Möðrudalur & Grímsstaðir, NE-Iceland	22 January 1918
Max temperature	30.5 °C	Teigarhorn, SE-Iceland	22 June 1939
Max 24 hour precipitation	293.3 mm	Kvísker, SE-Iceland	9–10 January 2002
Max one month precipitation	971.5 mm	Kollaleira, E-Iceland	November 2002
Max one year precipitation	4630.4 mm	Kvísker, SE-Iceland	2002
Max ten minute wind speed	62.5 ms^{-1}	Mt. Skálafell, SW-Iceland	20 January 1998
Max wind gust	74.2 ms^{-1}	Mt. Gagnheiði, E-Iceland	16 January 1995
Min sea level pressure	919.7 hPa	Vestmannaeyjar islands, S-Iceland	2 December 1929
Max sea level pressure	1058.5 hPa	Reykjavík, SW-Iceland	3 January 1841

by mountains, either through damming of cold air, warm downslope descent, local acceleration of the airflow or by forced ascending motion as in the Kvísker case of extreme precipitation at the foothills of Mt. Öræfajökull. The fact that the weather in Iceland is to a large extent dominated by synoptic scale weather systems together with the impact of the terrain offers many scientific challenges. As these systems, and their interaction with terrain, can be described quite accurately by present day atmospheric models, this meteorological framework provides conditions where increased spatial resolution in numerical weather prediction models is likely to produce substantial improvements in the quality of local weather forecasts. Furthermore, downscaling of the climate, using limited area models, can give valuable information about spatial and temporal distribution of temperature, precipitation and winds, especially in the data-sparse highlands. The impact of orography on precipitation in the mountains has an economic aspect, since hydraulic power is generated only by water that has fallen as precipitation in the mountains, and not in the lowland. However, most precipitation observations, including long time series, are from the lowland. Hence, data coverage is poor in the interior and in other high altitude regions.

Chapter 3

Scientifical challenges for studies of surface winds and precipitation in Iceland

3.1 Availability and quality of observational data

Figure 3.1 shows the observational network of weather stations in Iceland. The network consists of stations from Veðurstofa Íslands (e. The Icelandic Meteorological

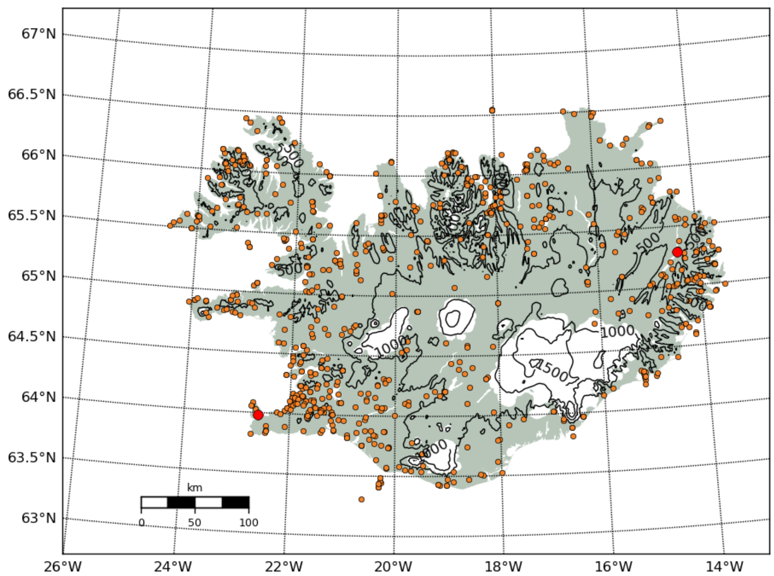

Figure 3.1: *Location of observational stations in Iceland. Rawinsonde stations at Keflavík (SW-Iceland) and Egilstaðir (E-Iceland) airports are marked in red. Contour lines (black) of the terrain are plotted every 500 meters.*

Office), Vegagerðin (e. The Icelandic Road Administration), Landsvirkjun (e. The Icelandic Power Company) and Siglingastofnun (e. The Icelandic Maritime Institute). The observational instruments are fairly homogeneous, except that anenometer height at the Vegagerð stations is around 6 meters and not 10 meters. From the figure it is clear that the bulk of the stations are located in coastal and lowland areas. Upper air observations are only done at two stations, Keflavík airport in SW-Iceland and Egilstaðir airport in E-Iceland, where rawinsondes are released twice a day.

Figure 3.2 shows the location of the operational GPS (e. Global Position System) network run by Háskóli Íslands (e. The University of Iceland), Veðurstofa Íslands, and Landmælingar Íslands (e. The National Land Survey). Only few of these stations provide real-time data and could therefore be used to extract information regarding the vertical profile of water vapor content. As of September 2010, two stations are part of the International GNSS Service network, in Reykjavík and Höfn í Hornafirði. Although observational data from satellites and automatic weather sta-

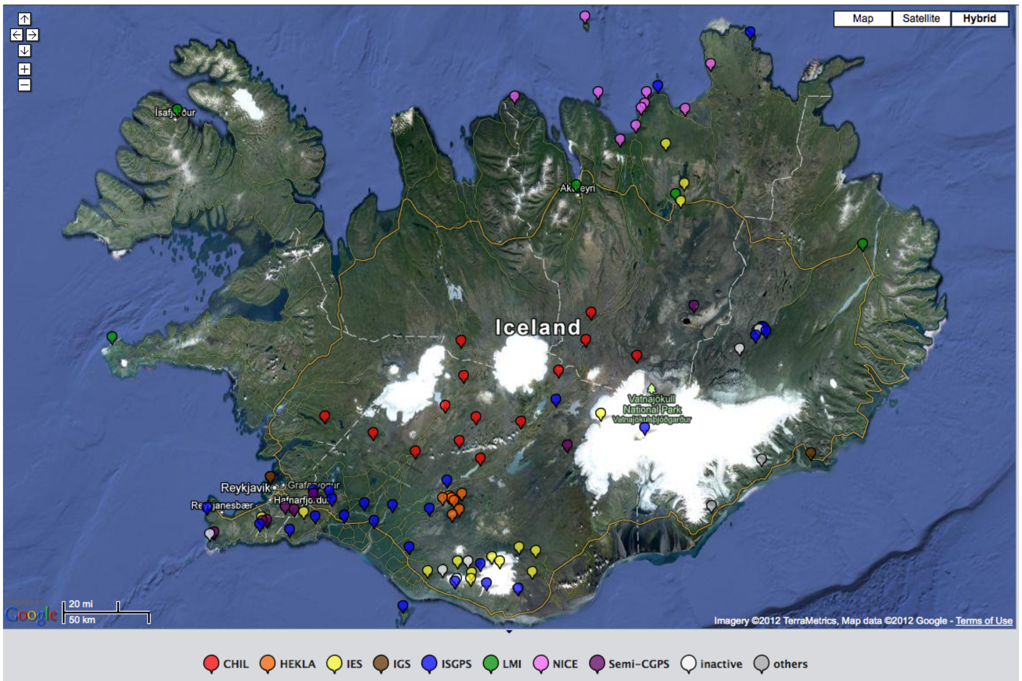

Figure 3.2: *Location of GPS stations in Iceland in November 2012. Figure courtesy of the University of Iceland* [1].

tions is ever increasing there is still a lack of observations throughout the boundary layer and in the interior of Iceland. Without these types of data, it is unclear how

[1] https://notendur.hi.is/runa/cgps.html. Retrieved on 2012-11-08.

much useful information, if any, data assimilation of available surface observations can add to atmospheric analysis from global models like the ECMWF[2] and GFS[3].

3.2 Meteorological processes – Theoretical background

In the late 1940s Charney and Eliassen (1949) showed that topographic Rossby waves, on the horizontal scale of order 10^4 km, seemed to explain the existence of the major 500 hPa trough in the lee of the Himalayas and the Rocky Mountains. This theory is however not applicable to airflow over Iceland, due to its smaller horizontal scale. The reason is that stationary waves only occur when $U = \beta/k^2$. Here U is the wind speed, β is the change in the Coriolis parameter with latitude and k is the zonal wave number. This implies a wavelength given by $L = 2\pi\sqrt{U/\beta}$. With the low β-parameter of Iceland and a typically observed wind speed of 10 m/s this would result in a wavelength of the order 6800 km, which is totally unrealistic for such a narrow "mountain" as Iceland (e.g. Kristjánsson and McInnes (1999)). A more useful approach to understand airflow over and around Iceland would be to use Smith's regime diagram (Smith, 1989).

3.2.1 Smith's theorem

Smith (1989) showed that in order to describe a steady Boussinesq, hydrostatic, non-rotating flow on a free-slip surface, unbounded above for a given mountain shape, one only needs two non-dimensional control parameters. The former is the dimensionless mountain height (also known as the inverse Froude number), $\hat{h} = Nh/U$, where N is the Brunt-Väisälä frequency, h is the mountain height and U is the upstream, horizontal wind. The latter parameter r is the horizontal aspect ratio[4], which must be taken into account to describe the dimensions of the mountain.

3.2.1.1 Flow regimes

There are two phenomena that can alter the kinematic or geometric nature of the flow field. The former is when the flow goes around the mountain instead of over (i.e. flow splitting) and the latter is when wave breaking occurs above the mountain. Each of these begins with the formation of a stagnation point (i.e. a point where

[2]http://www.ecmwf.int

[3]http://www.noaa.gov

[4]$r = a_y/a_x$ where a_x is the cross-mountain width and a_y the along-mountain width. The cross-mountain width is parallel to the upstream wind direction but the along-mountain width is perpendicular to it.

the horizontal wind speed becomes close to zero). For small $\hat{h}$, as is usually the case for small isolated hills, airflow tends to diverge around the hill, but the center streamline (for a hill with left-right symmetry, but some other streamline if the hill shape is complex) is still able to climb over the hill top. For larger hills, a stagnation point can develop on the windward slope. There the center streamline splits and passes around the hill on both sides.

A stagnation point can also form aloft. At such a point $u \ll U$, where U is the main upstream flow speed, the streamline becomes steeply sloping and overturning may follow (Smith, 1989).

3.2.1.2 Regime diagrams

Figure 3.3 summarizes the onset of stagnation as a function of the horizontal aspect ratio r of the mountain and the dimensionless mountain height $\hat{h}$. Note that there are no vertical variations in the upstream values of U and N. The diagram should be used by fixing a value of r and increasing $\hat{h}$ from a small value to a larger one until one of the critical curves is met. If curve A is met first, stagnation begins aloft. If curve B is met first, stagnation begins on the windward slope.

It can be seen that stagnation begins aloft (curve A) for mountain ridges with a large aspect ratio, $r > 1$. Curve B (small dotted line) above curve A should not be taken too seriously since the influence of wave breaking is not taken into consideration in linear theory (Smith, 1989). For a small aspect ratio, $r < 1$, stagnation begins on the windward side of the mountain (curve B). We can now construct three regimes for hydrostatic flow:

1. Below the critical curves, gravity waves propagate vertically and there is neither any flow blocking nor wave breaking.

2. Above curve A (large r), wave breaking occurs.

3. Above curve B (large $\hat{h}$ and small r), stagnation at the surface leads to flow splitting.

A weakness in Smith's theory is that it is both inviscid and irrotational,[5] and unlike in nature, the vertical profiles of wind and stability are uniform. According to Ólafsson and Bougeault (1997) the combined effect of rotation and friction will actually lead to an extension of linear theory resulting in that the qualitative results of Smith's theory should still apply for flow with rotation and friction. Ólafsson (2000) extended Smith's regime diagram by taking into account the effects of rotation and surface friction. His results are depicted in figure 3.4. It is interesting to note that the flow is considerably simpler now. Stagnation aloft does not occur and the flow

[5]It is irrotational in the sense that the Coriolis "force" is absent.

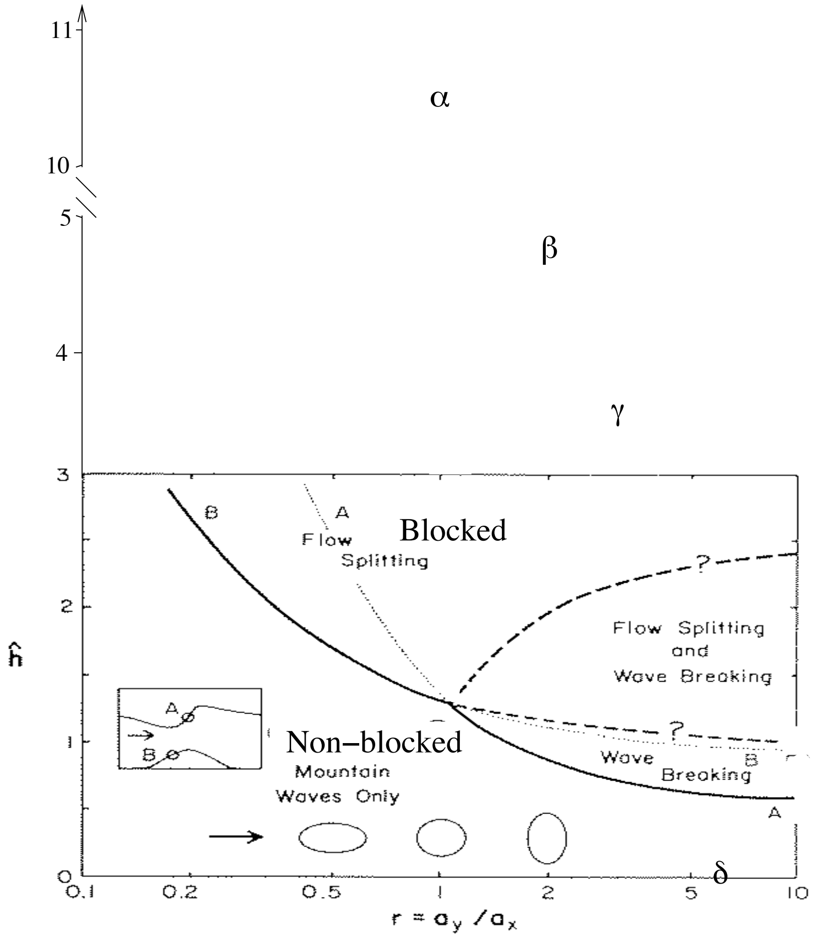

Figure 3.3: *Regime diagram for hydrostatic flow over a mountain. The diagram axes describe the horizontal aspect ratio, r, and the non-dimensional mountain height, $\hat{h}$. Solid curves A and B are linear theory estimates of flow stagnation, suggesting where wave breaking aloft (curve A) and flow splitting (curve B) will begin as $\hat{h}$ increases. Other regime boundaries above the A and B curves (dashed lines) are not yet known. Adapted and redrawn from Smith (1989).*

is simply either blocked or not blocked. It should be emphasized that this is only valid for an atmosphere where both U and N are constant with height. The effects of rotation on the flow are typically described by the non-dimensional Rossby number, *Ro*, defined as U/fL, were U is the mean windspeed, f is the Coriolis parameter and L is the mountain length scale. The Rossby number is a measure of the relative importance of the Coriolis term in the momentum equations. For Iceland it is in order to assume $L = 300\text{km}$, $U = 10\text{ms}^{-1}$ and $f = 10^{-4}\text{s}^{-1}$ resulting in a Rossby

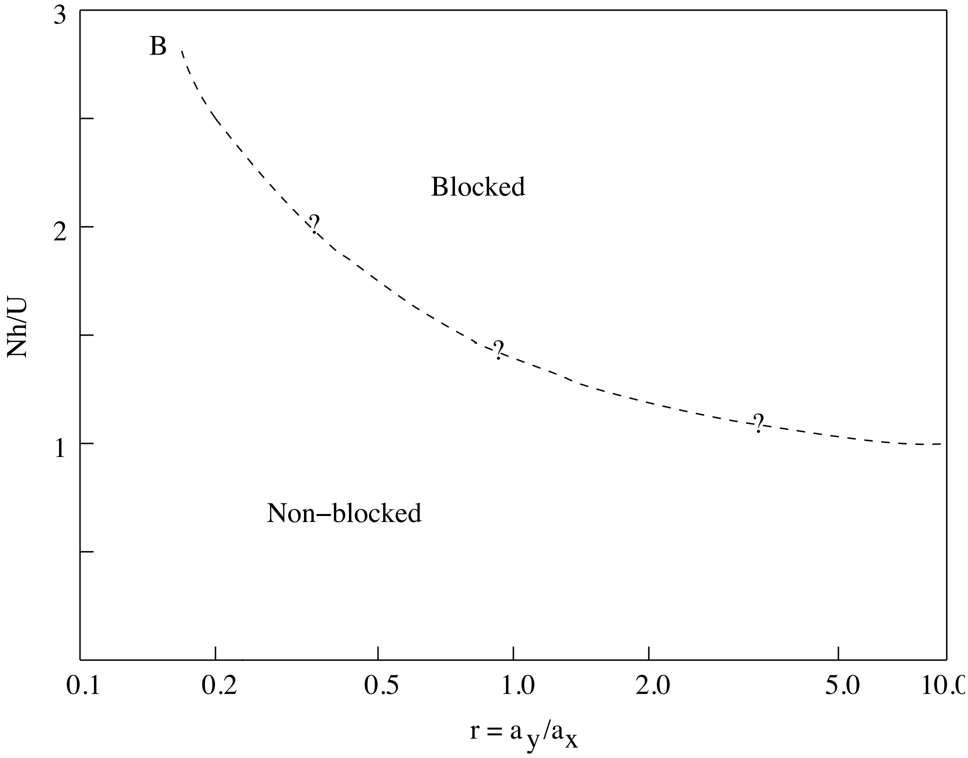

Figure 3.4: *Extension of Smith's regime diagram, where the effects of rotation and surface friction are taken into account. Note that stagnation aloft (curve A in figure 3.3) does not occur anymore. Question marks indicate that the exact position of the line is not known. Adapted and redrawn from Ólafsson (2000).*

number close to 1/3. At that value, the Coriolis force is important, but the flow is not geostrophic. As the length scale is reduced as to represent individual mountain ranges and mountains, the Rossby number increases and the flow becomes less and less affected by the rotation.

The combined effects of the Rossby number (*Ro*) and the inverse Froude number (Nh/U) on the atmospheric flow is shown in Fig. 3.5. The diagramme shows schematically the patterns of speed-up and slow-down of flow in the vicinity of mountains as a function of the governing non-dimensional numbers, Nh/U and *Ro*. The upper part of the diagramme represents flow at high Rossby numbers (*Ro*), where the Coriolis force plays a minor role. At low values of Nh/U, the flow is able to overcome the potential barrier of the mountain. The maximum wind speed is at the top of the mountain (hill), but there is relatively little horizontal variability in the wind speed. At high values of Nh/U, the flow is blocked on the upstream side and it is deflected on each side of it. In this type of flow, the flow speed is significantly reduced both inside a so-called upstream blocking as well as in a wake, downstream

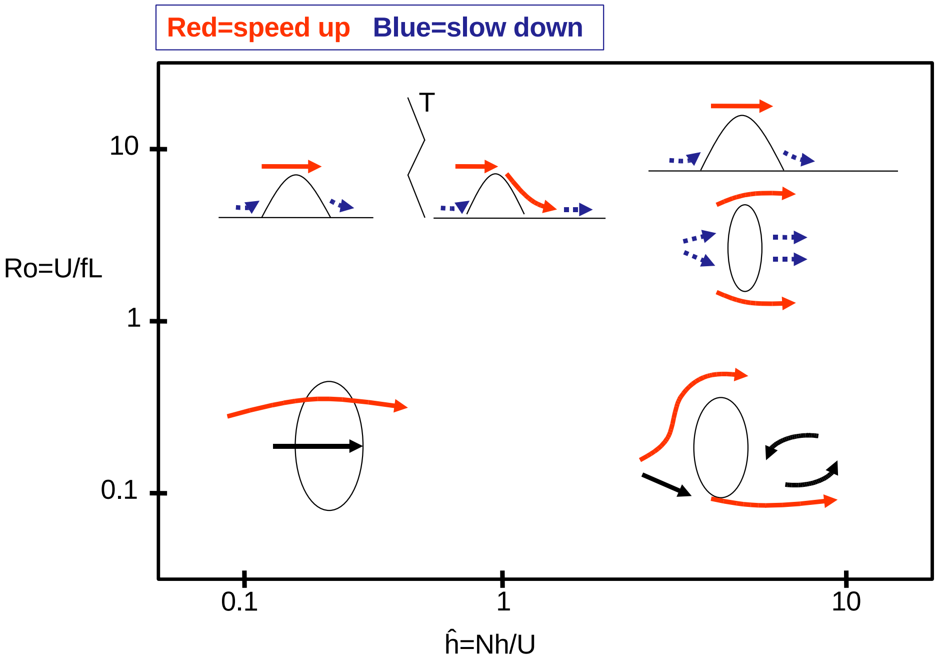

Figure 3.5: *Schematic diagram showing the combined effects of Rossby number (vertical axis) and the inverse Froude number (horizontal axis). Adapted and redrawn from Ólafsson (2003).*

of the mountain. There is, on the other hand, speed-up at the edges of the mountain. These speed-ups are sometimes referred to as corner winds or tip jets. Such a wind inbetween two mountains is called a gap wind. At high Nh/U, there may be substantial areas with hardly any wind inside the blocking and the wake, while the edges of the mountain may experience more than twofold the upstream flow speed. An intermediate flow pattern exists at values of the Nh/U close to unity (typically $0.5 < Nh/U < 3$). Here, vertically propagating gravity waves dominate the flow field. Aloft, the flow oscillates and on its way down, the flow accelerates, giving maximum surface wind speed above the slope, at the downstream foothills of the mountain. Particular structures of the flow, such as inversions or vertical variability of wind speed may enhance the wave activity, giving extreme surface winds at the bottom of the wave, downstream of the mountain.

3.2.2 Cloud microphysics

Improving quantitative precipitation forecasting (QPF) over complex topography has long been a target of research campaigns organized in the numerical weather prediction (NWP) community. Recent examples of such campaigns are the Mesoscale

Alpine Program – MAP (Bougeault et al., 2001) and the Improvement of Microphysical Parameterization through Observational Verification Experiment – IMPROVE (Stoelinga et al., 2003). Although forecasting skills of NWP models have improved considerably for many variables (e.g. geopotential height and temperature) over the past years and decades, precipitation has remained somewhat elusive (Bosart, 2003). One reason for this is that the physics governing the formation of precipitation are highly complicated, rendering parameterization difficult. Another reason is that the distribution of precipitation (particularly solid precipitation) over complex topography as simulated by NWP models is very sensitive to the dynamic and thermal characteristics of impinging wind (e.g. Chiao et al. (2004)).

According to Stensrud (2007) the reason microphycs parameterization is so challenging is twofold. Firstly, the phase changes of water that can occur in the atmosphere are numerous:

- Vapor to liquid (condensation).
- Liquid to vapor (evaporation).
- Liquid to solid (freezing).
- Solid to liquid (melting).
- Vapor to solid (deposition).
- Solid to vapor (sublimation).

As these phase changes do not occur at ideal thermodynamic equilibrium, one has both to take into account the surface tension of water drops and the surface free energy for solid particles (Stensrud, 2007). Secondly, the type of precipitation (liquid vs. solid) is strongly dependent on temperature, and as such, altitude. If the temperature is below 0°C precipitation is in general solid (exception is supercooled water). Solid precipitation can take many forms, ice crystals, snow flakes, hail, graupel, all of which vary in shape and size (different shapes and sizes are called “habits”). Furthermore, the growth of ice crystal habits is both dependent on temperature and the excess vapor density over ice. Even liquid raindrops are not homogeneous in size of shape, drops tend to grow as they fall through the atmosphere and collide with other drops that are in the way. There is however a limit to how big individual raindrops can get, and large drops have the tendency to split up when they collide with other drops.

But how does precipitation begin, how does a liquid droplet[6] form in terms of thermodynamical principles? To answer this we need to look at a modified version

[6]The distinction between a droplet and drop is usually such that the droplet is assumed to have sufficiently small terminal fall velocity that it is advected with the ambient flow. Raindrop, on the other hand, has a significant fall speed $v(R)$, where R is the radius of the drop (Cotton et al., 2011).

of the Clausius-Clapeyron equation, describing the equilibrium state for a system of water vapor over curved surface, such as a rain droplet (Stensrud, 2007) [eq. 7.1]:

$$e_s(r) = e_s(\infty)e^{2\sigma/rR_v\rho_w T} \tag{3.1}$$

Here, e_s is the equilibrium vapor pressure, σ is the surface tension, r is the radius of the droplet, R_v is the gas constant for water vapor, ρ_w is the density of water and T is temperature. Finally, $e_s(\infty)$ is the saturation vapor pressure over flat liquid surface given by the unmodified Clausius-Clapeyron equation. Equation 3.1 is often rearranged to give the saturation ratio S:

$$S = \frac{e_s(r)}{e_s(\infty)} = e^{2\sigma/rR_v\rho_w T} \tag{3.2}$$

Note that the value of S increases as r (the radius of the droplet) is reduced. A saturation ratio of 1 indicates a 100% relative humidity and that the atmosphere is just saturated. Observed ratios are typically less than 1.01, i.e. less than 1% supersaturation (Stensrud, 2007). Observations show that the first droplets to form are small ones and that the observed size of r for these droplets result in a saturation value around, or over 2, indicating a 100% supersaturation. As said before, supersaturation in the nature seldom exceeds 1%, so it is clear that droplet formation from clear water is rear.

Aerosols are microscopic particles that are present in the atmosphere. When mixed with water vapor they act to reduce the evaporation pressure and as such speed up the formation of droplets. The aerosols act as centers for condensation and are therefor called “cloud condensation nuclei” (or CCN). The size and volume of CCN’s varies greatly in the atmosphere, both as a function of height, temperature and underlying surface. CCN’s in a maritime air mass are bigger than CCN’s in a continental air mass. This size difference leads to continental air masses having more numerous, and smaller, droplets than maritime air. Thus, in general, the collision and coalescence process is inhibited in nuclei-rich continental air. The fundamental assumption of many microphysics schemes is that the cloud droplet concentration, or activated CCN concentration, at cloud base, determine whether or not a cloud will precipitate (Cotton et al., 2011).

The presence of CCN’s lead to further refinement of the saturation ratio equation for a diluted solution (Stensrud, 2007) [eq. 7.3]:

$$S = \frac{e_s(r)}{e_s(\infty)} = \left(1 - \frac{b}{r^3}\right) e^{2\sigma/rR_v\rho_w T} \tag{3.3}$$

Here, the parameter b is a function of the solute mass and density, the molecular weight of the solute and water as well as the degree of ionic dissociation[7] of the

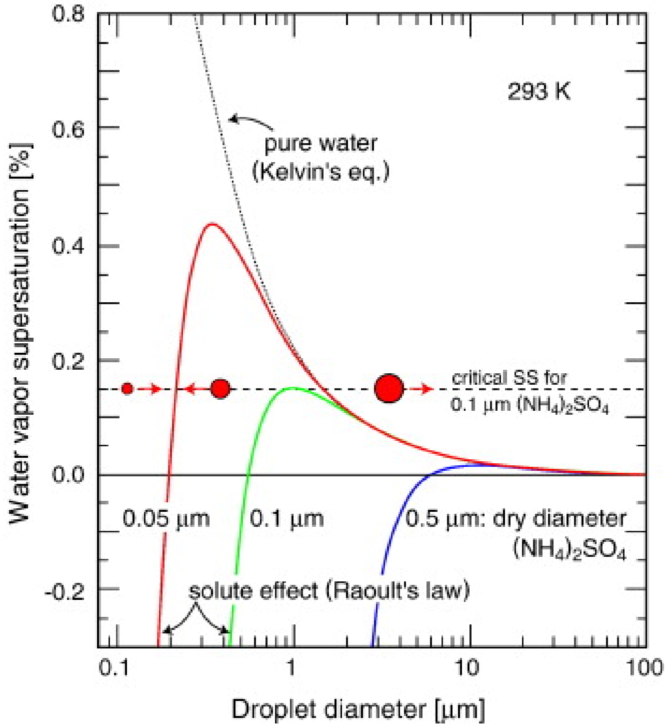

Figure 3.6: *Köhler curves showing the equilibrium water vapor supersaturation at 293 K for droplets of pure water (dotted curve) and for droplets containing various masses of dissolved* $(NH_4)_2SO_4$ *(solid curves) vs. diameter of the droplet. The water vapor supersaturation,* $S(\%) = \left(\frac{e_s}{e_s(\infty)} - 1\right) 100$, *where* e_s *is the partial pressure of the water vapor and* $e_s(\infty)$ *is the saturated vapor pressure over a plane surface of water at this temperature. In the indicated example, an ambient water vapor S of 0.15% (dashed line) exceeds the critical value for all ammonium sulfate aerosols with dry diameter* $\geq 0.1\mu m$. *These aerosols will therefore activate and grow into cloud droplets, whereas smaller aerosols remain as unactivated haze particles. Droplets below their corresponding equilibrium curve will shrink by evaporation whereas those above will grow by condensation (the indicated droplets correspond, for example, to a dry diameter of 0.05 µm). From Andreae and Rosenfeld (2008), reprinted with permission from Elsevier.*

solute. Figure 3.6 shows the radius r as a function of the saturation ration S at a fixed temperature, solute type and mass. The shape of r is called a Köhler-curve, it shows

[7] Dissociation is a general process in which ionic compounds (complexes, or salts) separate or split into smaller particles, ions, or radicals, usually in a reversible manner. The dissociation degree is the fraction of original solute molecules that have dissociated. From Wikipedia: http://en.wikipedia.org/wiki/Dissociation_(chemistry), retrieved on 2012-06-15.

that for a small radii the solution effect dominate and for large radii the surface tension effect dominates. Initially, the growth of the droplet is due to condensation and is proportional to $(S-1)/r$ (Stensrud, 2007). Consequently, as the droplet increases in size, its growth becomes slower and droplet growth from collisions and coalescence becomes the driving factor in transforming a droplet to a raindrop.

Freezing of cloud droplets does not necessarily happen immediately as the temperature drops below 0°C. This is because water droplets are able to maintain supersaturation relative to ice (remain as liquid water droplets and not freeze) because of the high surface tension of each micro droplet, which prevents them from expanding to form larger ice crystals (Rogers and Yau, 1989). Without ice nuclei supercooled liquid water droplets can exist down to about -40°C. If the ambient temperature is higher than -40°C, the formation of ice requires ice nuclei (IN), just as the formation of liquid droplets requires the presence of CCN.

According to Stensrud (2007) there are four processes that are believed to lead to ice nucleation. These are vapor-deposition, condensation-freezing, immersion-freezing, and contact-freezing nucleation. Contact-freezing happens when a supercooled droplet comes to a contact with an ice nucleus and freezes. Immersion-freezing is the freezing of a supercooled droplet that has an ice nuclei immersed within itself. Condensation-freezing is the condensation of water onto an ice nuclei to form a embryonic drop, followed by freezing of the embryonic drop. Once ice crystals have formed they can grow by vapor-deposition, as long as the environment is supersaturated with respect to ice. Saturation pressure with respect to water is higher than with respect to ice, this means that a cloud that is saturated with respect to water, is supersaturated with respect to ice. As ice crystals grow by vapor-deposition, the cloud can become sub saturated with respect to water but still be supersaturated with respect to ice. When this happens, water droplet start to evaporate, hence enhancing ice crystal growth. This process is called Bergeron-Findeisen mechanism of ice crystal growth (Stensrud, 2007).

As with liquid drops, collisions and coalescence can also lead to ice crystal growth. This process is called aggregation and is more complicated than for liquid phase. This is because ice crystals can come in many different forms, or habits, which affects how they interlock after collision. For liquid drops, the coalescence efficiency is near unity, but this is not the case for ice crystals. Snowflakes are formed via this process.

The process when ice crystals collide with droplet of supercooled cloud water is called riming. As the initial ice crystal collects more and more supercooled water it is gradually transformed into a particle called graupel. Although graupel density varies across a large range it is considerably greater than that of ice crystals and snowflakes. Graupel particles have typical fall speeds of 1-3 ms^{-1}, they also serve as embryos for hailstones, which have much greater fall speeds (10-50 ms^{-1}). Initiation of riming can take a long time as the original particles have very small fall speeds as they are light and often flat in shape. But once the particles begin to fall, riming can be very effective in growing the ice crystals into graupel particles, assuming there is sufficient supercooled cloud water.

3.3 Modeling of surface winds and precipitation

Atmospheric models are systems of differential equations derived from the basic laws of physics, fluid motion, and chemistry. These are the momentum equations that represent Newtons second law of motion[8], and the thermodynamic equation that accounts for both diabatic and adiabatic changes in temperature. In addition there are the continuity equations for total mass and water vapor and the gas law, that relates temperature, pressure and density. These equations were first described in Bjerknes's 1904 paper *Das Problem der Wettervorhersage, betrachtet vom Standpunkte der Mechanik und der Physik*. The details of the equations where set out by Lewis Fry Richardson and published in his book *Weather prediction by numerical process* in 1922. Following Warner (2011) we now write these equations in their primitive form for a spherical earth:

$$
\begin{aligned}
\frac{\partial U}{\partial t} &= -U\frac{\partial U}{\partial x} - V\frac{\partial U}{\partial y} - W\frac{\partial U}{\partial z} + \frac{UV\tan\phi}{a} - \frac{UW}{a} - \frac{1}{\rho}\frac{\partial p}{\partial x} \\
&\quad - 2\Omega(W\cos\phi - v\sin\phi) + \mathbf{Fr_x} && (3.4) \\
\frac{\partial V}{\partial t} &= -U\frac{\partial V}{\partial x} - V\frac{\partial V}{\partial y} - W\frac{\partial V}{\partial z} + \frac{U^2\tan\phi}{a} - \frac{UW}{a} - \frac{1}{\rho}\frac{\partial p}{\partial y} \\
&\quad - 2\Omega U\sin\phi + \mathbf{Fr_y} && (3.5) \\
\frac{\partial W}{\partial t} &= -U\frac{\partial W}{\partial x} - V\frac{\partial W}{\partial y} - W\frac{\partial W}{\partial z} - \frac{U^2+V^2}{a} - \frac{1}{\rho}\frac{\partial p}{\partial z} \\
&\quad + 2\Omega U\cos\phi - g + \mathbf{Fr_z} && (3.6) \\
\frac{\partial T}{\partial t} &= -U\frac{\partial T}{\partial x} - V\frac{\partial T}{\partial y} + (\lambda - \lambda_d)W + \frac{1}{c_p}\frac{\mathbf{dH}}{\mathbf{dt}} && (3.7) \\
\frac{\partial \rho}{\partial t} &= -U\frac{\partial \rho}{\partial x} - V\frac{\partial \rho}{\partial y} - W\frac{\partial \rho}{\partial z} - \rho\left(\frac{\partial U}{\partial x} + \frac{\partial V}{\partial y} + \frac{\partial W}{\partial z}\right) && (3.8) \\
\frac{\partial q_v}{\partial t} &= -U\frac{\partial q_v}{\partial x} - V\frac{\partial q_v}{\partial y} - W\frac{\partial q_v}{\partial z} + \mathbf{Q_v} && (3.9) \\
p &= \rho RT && (3.10)
\end{aligned}
$$

[8]Newton's second law of motion states that the net force on a particle is equal to the time rate of change of its linear momentum **p** in an inertial reference frame: $F = \frac{d\mathbf{p}}{dt} = m\frac{d\mathbf{v}}{dt}$, where m is mass, and **v** is speed (Feynman et al., 1963)

where U, V, and W represent the three dimensional winds, ρ is the density of air, p is pressure, T is temperature. Ω is the rotational frequency of earth, ϕ is latitude, λ is the lapse rate and λ_d is the dry adiabatic lapse rate, c_p is the specific heat at constant pressure, g is gravitational acceleration, and R is the gas constant for ideal gas. Here, Fr represents frictional terms, and H and Q_v represent sources and/or sinks of heat and humidity, respectively. These terms, which are written in bold, need to be parameterized within the model.

These equations cannot be solved analytically but have to be converted to a form that can be solved by numerical methods on fast computers. Traditionally this is done by a method called Reynolds averaging, where a variable is split into a *mean* (defined as a mean value over a grid cell) and *turbulent* part. The time development of the mean part of a variable can be directly resolved by the model (often referred to as the *dynamical core* of the model) but the turbulent part represents unresolved effects. These effects need to be described, or parameterized, in terms of resolved parts of the equations. Methods to do so will be described in section 3.3.1.

In addition to Reynolds averaging, the equations need to be formulated on a grid of some sort. There are a number of methods to do so, but the two most common are the method of finite differences (also known as the grid-point method) and the spectral method. The spectral method dominates global modeling as it levitates singularities at the poles that early global models, using finites differences, were riddled with. This is done be replacing the finite expansions of the variables with Fourier series, or Fourie-Legendre functions, to represent the horizontal spatial variation. In the finite difference method a procedure is defined for organizing grid points in a systematic way over the area of interest, the grid needs not even be regular (Warner, 2011).

In order to solve the equations the whole planet, or a sub-region of interest, is covered by a 3-dimensional grid to which the basic equations are applied and evaluated. At each grid point the motion of the air (winds), heat transfer (thermodynamics), radiation (solar and terrestrial), moisture content (relative humidity) and surface hydrology (precipitation, evaporation, snow melt and runoff) are calculated as well as the interactions of these processes among neighboring points (cf. Fig. 3.7). The computations are stepped forward in time from days to seasons, or even to centuries depending on the study. State-of-the-art coupled ocean-atmosphere models now include interactive representations of the ocean, the atmosphere, the land, hydrologic and cryospheric processes, terrestrial and oceanic carbon cycles, and atmospheric chemistry. The accuracy of these models is limited by lack of observations, grid resolution and our ability to describe the complicated atmospheric, oceanic, and chemical processes mathematically. Despite some imperfections, models simulate remarkably well current climate and its variability (IPCC, 2007). More capable supercomputers enable significant model improvements by allowing for more accurate representation of currently unresolved physics.

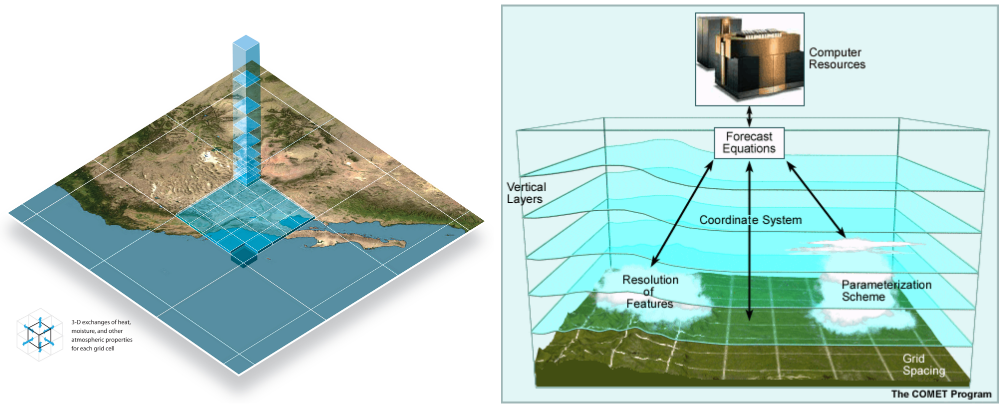

Figure 3.7: *Atmospheric models are systems of differential equations based on the basic laws of physics. The models calculate winds, heat transfer, radiation, relative humidity, and surface hydrology within each grid box and evaluate interactions with neighboring points. Figure courtesy of UCAR*[9].

As of autumn 2012, the horizontal grid resolution of the two most widely used global atmospheric forecast models is about 14 and 28 km (0.125°and 0.25°). These models are the European Centre for Medium range Weather Forecasts – ECMWF model, and the Global Forecast System – GFS model, respectively. Both modeling system simulate weather forecasts four times a day for the whole globe that span over two weeks.

Even at such high horizontal resolution, many important flow features are left unresolved. To tackle this shortcoming of the global models, one can use regional, or local area, weather models. These models only cover a fraction of the globe (hence the name regional, or local area) and are typically forced by initial and boundary data from a global model. Consequently they can be run at a higher horizontal resolution for the fraction of the computation power that would otherwise have been needed to run the global models at the same resolution. As the true orography is better resolved, so to the interaction between the surface and the atmospheric flow can be better resolved. These improvements in the simulated flow can be expected to be especially evident in mountainous regions like Iceland.

But how are winds and precipitation simulated within an atmospheric model, global or regional? An important feature of any numerical atmospheric model are the parameterization schemes. It is within these schemes, and through their interaction, that the various processes within the atmosphere are simulated. We will now look in more detail on two types of parameterization schemes that are of great importance when simulating surface winds and precipitation. These are the planetary

[9] http://www2.ucar.edu/news/understanding-climate-change-multimedia-gallery, left figure, and http://www.meted.ucar.edu/mesoprim/models/print.htm, right figure. Retrieved on 2012-06-23.

boundary layer schemes and the microphysics schemes.

3.3.1 Planetary boundary layer schemes

The lowest part of the atmosphere is generally called the atmospheric boundary layer, the planetary boundary layer, or simply the boundary layer. The depth, or thickness, of the boundary layer is typically defined as the distance through which energy fluxes from the earth's surface (e.g. temperature change or a forced ascend due to an obstacle) can reach within one hour. Stull (1988) [p. 2] defines the boundary layer as "the part of the troposphere that is directly influenced by the presence of the earth's surface, and responds to surface forcings with a timescale of an hour or less[10]". It is within this part of the atmosphere that we humans spend the bulk of our live.

The depth of the boundary layer typically varies between 1 and 2 km, but can range from tens of meters to 4 km or more (Stull, 2006) [p. 375]. In atmospheric modeling the generation of these surface energy fluxes are parameterized using different models from the PBL models. These Land Surface Models (LSM) handle the interaction between the earths surface (both land and water) and the atmosphere as well as modeling the interaction between soil and vegetation and the atmosphere. It is through the LSM's that the surface energy fluxes are described and in turn form a lower boundary condition for the PBL models. How these energy fluxes influence the lower atmosphere depends on the PBL scheme.

The transport of energy up through, and within, the boundary layer is turbulent in nature. The source of turbulence can both be sensible heat flux from the ground (warm air being more buoyant than cold) and wind shear. The relevant importance of these two main sources of turbulence varies both temporarily (e.g. more heat flux during the daytime than at night) and spatially.

The equations of motion could in theory be applied directly to turbulent flow. This would however require very small grid spacing in order for the model to correctly simulate the flow behavior. Even with a grid spacing of 50 meters, there would still be sub-grid eddies whose influence on the flow would need to be accounted for. A common method to describe the effects of sub-grid eddies in contributing to the overall mixing in the boundary layer is called Reynolds averaging. Reynolds averaging gives a statistical approach to the eddy effects. The idea behind the technique is to separate a variable into a time averaged part and a perturbing part.

$$U = \bar{u} + u^{'} \tag{3.11}$$

[10] It should be noted that this only applies to fluxes of moisture, heat and momentum. Perturbations due to surface-generated gravity waves are obviously outside the framework of this definition, as such waves may travel fast through the entire troposphere and further upwards

The $\bar{u}$ can also be regarded as the part of U that can be resolved on the grid of the numerical model in question. Consequently, the perturbation part, the $\overline{u'}$, is the sub-grid fluctuation around the grid-resolved value. The perturbations are defined such that their time average equals zero (i.e. $\overline{u'} = 0$). Also, the product of two variables, U, and V, give:

$$UV = \overline{uv} + \overline{u'v'} \tag{3.12}$$

When using this technique on the momentum equations, the perturbations are assumed to represent the effects of turbulence. For a detailed description of how this is done, we refer to Stull (1988) and Stensrud (2007). Following Stensrud (2007) we define the following:

- x_j as a generic distance, with $x_1 = x, x_2 = y, x_3 = z$
- u_j as a vector, with $u_1 = u, u_2 = v, u_3 = w$
- δ_j as a unit vector, with $\delta_1 = i, \delta_2 = j, \delta_3 = k$

and δ_{mn} as the Kronecker delta which equals 1 when $m = n$ but is zero otherwise. Finally, we define the unit tensor ε_{ijk} as:

$$\varepsilon_{ijk} = \begin{cases} +1, & \text{if } i,j,k \text{ are in ascending order} \\ -1, & \text{if } i,j,k \text{ are in descending order} \\ 0, & \text{otherwise} \end{cases}$$

using this, the equations of motions, assuming the Boussinesq assumption and after Reynolds averaging, can be written like this (eq. 5.12 in Stensrud (2007)):

$$\frac{\partial \bar{u}_i}{\partial t} + \bar{u}_j \frac{\partial \bar{u}_j}{\partial x_j} = -\delta_{i3} g + f \varepsilon_{ij3} \bar{u}_j - \frac{1}{\bar{\rho}} \frac{\partial \bar{p}}{\partial x_i} + \nu \frac{\partial^2 \bar{u}_i}{\partial x_j^2} - \frac{\partial \overline{(u_i' u_j')}}{\partial x_j} \tag{3.13}$$

The second term on the right hand side represents the Coriolis effect and the fourth term represents molecular viscosity, and is generally ignored in praxis. The last term on the right hand side is the covariance, or Reynolds stress, term. As this term is not predicted explicitly it can either be parameterized, or additional equations can be derived to predict it. Doing the latter will however result in yet more terms that are not explicitly predicted (namely $\partial \overline{u_i' u_j' u_k'} / \partial x_j$). The unknown is now a triple correlation term. If one would derive equations to solve for these, one would in turn create a quadruple term, and so on, and so on. This cascade of creation of unknown terms is referred to as the *turbulence closure* problem.

As there will always be more unknowns than there will be equations one needs, at some point, to parameterize the solution for the unknown terms by relating them in some way to known variables. It is these unknown terms that contain the unresolved sub-grid motion. It is through the closure formulation (or parameterization) that the mixing from the sub-grid is introduced into the equations for large scale motions (the resolved part of the motion) within the PBL scheme. It is important to note that this sub-grid mixing, as handled by PBL schemes, is one-dimensional. That is, mixing in the horizontal is assumed to be an order, or orders, of magnitude less than in the vertical. Hence, its effects are dismissed when the equations of motion are derived for the various PBL schemes. This assumption breaks down when the horizontal scale of the model becomes of the same order of magnitude as the length scale of the energy- and flux-containing turbulence. This numerical region is termed "Terra Incognita" by Wyngaard (2004).

The "order" (also called "level") of a PBL scheme refers to where in this cascade of terms one decides to parameterize the correlation terms. First order schemes only include equations for the state variables (u, v, w, T, q), i.e. winds, temperature and humidity (also known as first moments). The covariance terms, like $\overline{u'v'}$, are parameterized. Second order schemes in turn include explicit description of both the first moments and the covariance terms, but parameterize the triple correlations terms. There are also PBL schemes were not all of the covariance terms are explicitly described, such schemes are referred to as 1.5-order schemes. The main reason for using higher order is the assumption that crude description of the third moments (i.e. parameterization of the triple correlation terms) will give a better forecast of the second moments.

Another deciding factor for a PBL scheme is how the equations are integrated vertically. If only neighboring points are used, the scheme is referred to as being "local" (or "local closure" scheme). On the other hand, if information from the whole vertical column is used, the scheme is called "non-local" (also known as "non-local closure" schemes). Local and non-local PBL schemes both have their pros and cons. In general, non-local scheme are better equipped to describe dry convective boundary layers that typically evolve over warm areas such as summertime Arizona. Under such conditions the day-time boundary layer can become very deep. Bright and Mullen (2002) report of 2 km deep boundary layer, and even exceeding 3 km depth. In this study, Bright and Mullen (2002) also showed that local PBL schemes consistently under predicted the depth of the day-time Arizona boundary layer, often by a factor of two. The local schemes also over predicted the convective available potential energy (CAPE) by a factor of two, whilst non-local schemes performed well under these conditions. The reason local closure scheme have difficulties under these conditions is that the vertical mixing is to a large extent governed by very large eddies. Hence, relative difference in the vertical transport between few model levels is negligible. In short, the local models don't see the "big picture". A clear benefit local closure models of order 1.5, or higher, do have over non-local ones is the ability to predict the intensity of turbulent kinetic energy

(TKE). Information about TKE is important for air quality studies and dispersion studies in general, e.g. to model the distribution of volcanic ash in the atmosphere.

The dominant mechanism for boundary layer development is turbulence. During daytime production of turbulence is in general dominated by buoyancy gradients produced by surface forcing. Wind shear is usually the dominant factor in turbulence production at night. As horizontal resolution is increased horizontal gradients of wind shear may contribute to the production of turbulence. At present, only vertical movement is taken into consideration, the PBL schemes are one dimensional. Direct influences of clouds on the development of the boundary layer are not included either.

Closure constants for PBL schemes are in general estimated from observed data. This data in turn stems from relatively few observations periods and/or locations. Generally, the data is collected in areas where the terrain is flat and the land use characteristics is homogeneous. This is done in order to observe the boundary layer development under pristine conditions. This may however result in the development of BL schemes that have considerable problems simulating the development of arctic boundary layer or the boundary layer in complex terrain.

3.3.2 Microphysics schemes

Warner (2011) lists up a number of microphysical processes that need to be parameterized in a numerical model:

- Condensation – Liquid droplets form when water saturation is exceeded at temperature from -40°C to above freezing. The condensation takes place on CCN particles.

- Accretion – In the warm-cloud process, i.e. within clouds that the ice phase does not play a significant role, droplets with different masses have different fall velocities, and the resulting collisions between droplets can result in coalescence and droplet growth. As a droplet grows, so does its vertical velocity relative to smaller droplets, thus increasing the rate of collisions.

- Accretion by frozen particles – Snow, graupel, or hail collect other solid or liquid particles as they fall.

- Evaporation – Cloud droplets and raindrops can evaporate.

- Ice and snow aggregation – Aggregation is the process when ice crystals and snow flakes collide and coalesce.

- Vapor deposition – Ice crystal growth via the Bergeron-Findeisen mechanism.

- Melting – As snow flakes fall into the lower troposphere, below the freezing level, they may melt and form raindrops. Similarly, hail and graupel begin to melt as they fall below freezing level.
- Freezing – Water droplets freeze in the presence of IN, riming involves the freezing of water droplets that collide with ice crystals, and raindrops can freeze to form graupel.

Microphysical schemes are typically grouped into "bulk" and "bin" models. Bulk models use a distribution function (e.g. that of Marshall and Palmer (1948)) to describe the distribution of hydrometeors in the atmosphere. These models predict the particle mixing ratio (total mass per unit volume of air), and sometimes the total particle concentration as well. The former are named single-moment schemes, and the latter double moment schemes. The benefit of using double-moment compared to single-moment methods is that they predict both number concentration and mixing ratio and are therefore able to derive the broad features of the drop size distribution. In doing so, the double-moment scheme improves the representation of growth processes and precipitation formation (Cotton et al., 2011) and as such can be used over a wider range of environments. Triple-moment scheme also exist, but only if the distribution is described using a Gamma[11] function. In that case, the third moment describes the shape parameter k (Warner, 2011). In contrast, bin models do not use distribution functions but instead divide the particle distribution into a finite number of categories (or "bins"). The particle distribution into bins requires considerable more computing power than the bulk approach and a poor knowledge on ice phase physics results in potentially inaccurate representation of the evolution of ice particle concentrations (Stensrud, 2007). Due to this, bin models are currently not part of any operational models, unlike bulk schemes, and are used only in a few research models.

3.3.2.1 Bin parameterizations

The approach to model microphysics processes in clouds by explicitly resolving the evolution of hydrometeor size spectra is referred to as the bin-resolving technique. The temporal evolution of the spectral density $f(m)$ of cloud droplets of mass m to $m \pm \delta m/2$ can be written as (Cotton et al., 2011):

$$\begin{aligned}\frac{\partial f(m)}{\partial t} =& N(m) - \frac{\partial[\dot{m} f(m)]}{\partial m} + G(m)|_{\text{gain}} + G(m)|_{\text{loss}} \\ &+ B(m)|_{\text{gain}} + B(m)|_{\text{loss}} + \tau(m)\end{aligned} \tag{3.14}$$

[11] In probability theory and statistics, the gamma distribution is a two-parameter family of continuous probability distributions. It is common to parameterize it with a shape parameter k and a scale parameter θ. From Wikipedia: http://en.wikipedia.org/wiki/Gamma_distribution, retrieved on 2012-06-18.

where $\dot{m}$ is the total derivative of the mass, $\dot{m} = \frac{Dm}{Dt} = \frac{\partial m}{\partial t} + u\frac{\partial m}{\partial x} + v\frac{\partial m}{\partial y} + w\frac{\partial m}{\partial z}$.

In (3.14) N represents nucleation, G represents collection, B represents breakup, and τ represents the sum of both mean and turbulent transport processes. N is the production of droplets of mass m by the nucleation of such droplets on activated CCN. This term is kept in (3.14) only if the droplet spectrum $f(m)$ is truncated at some small droplet mass. The second term on the right hand side is the divergence of $f(x)$ due to continuous vapor mass deposition on droplets growing at a rate of $\dot{m}$, where $\dot{m}$ is a function of the droplet mass, its solubility in water, and the local cloud supersaturation. The third and fourth terms represent, respectively, the gain and loss due to the collision and coalescence of cloud droplets. The fifth and sixth terms represent, respectively, the gain and loss of the spectral density $f(m)$ due to breakup of droplets.

A common approach to solve (3.14) is to discretize $f(m)$ into 40 to 70 elements and then integrate the equations by finite element approach (Cotton et al., 2011).

3.3.2.2 Bulk parameterizations

The distribution of ice and liquid particles in the atmosphere can, to a certain extent, be described by an inverse exponential function, first suggested by Marshall and Palmer (1948):

$$n(D) = n_0 e^{-\lambda D} \tag{3.15}$$

where D is the particle diameter (m), n is the number of particles per unit volume (m^{-4}), λ is the slope parameter that defines the fall off of particles as the diameter increases (m^{-1}), and n_0 is the intercept parameter that defines the maximum number of particles per unit volume at $D = 0$ size (Stensrud, 2007). The gamma distribution has also been used to describe particle distribution, it differs from that of Marshall and Palmer mainly for very small droplets.

An important assumption that is generally made within bulk models is that non-precipitating hydrometeors have zero fall speed, i.e. they simply move with the ambient flow. It is not until the droplet (liquid or solid) has reached a certain size that it can be regarded as a precipitating particle (raindrop, snowflake, hail, or graupel particle). Berry and Reinhardt (1974) demonstrated that a natural break between cloud and raindrops occurs at a radius of 50 μm.

The bulk microphysics schemes differ greatly in complexity, both with regard to how many types of interactions between particles are assumed (phase and habit changes) and also how the interactions between different particles are described. The equations that describe the evolution of the microphysical variables do however all follow a similar structure:

$$\frac{\partial q_x}{\partial t} = -ADV(q_x) + TURB(q_x) + (P_1 + P_2 + P_3 + P_4 + P_5 + \cdots) \tag{3.16}$$

where q_x is any microphysical variable (e.g. mixing ratios of water vapor, cloud water, rainwater, ice, snow, and graupel), ADV represents the advective processes, $TURB$ the turbulent processes and P_i represents the various tendencies from the microphysics parameterization (Stensrud, 2007).

Parameterization of warm rain condensation The approach to create condensed particles in microphysical parameterization schemes differs somewhat from what happens in nature and was described in section 3.2.2. Rather than predicting the aerosol composition itself (like size, shape and chemical properties), and from it predict the droplets formation and growth the scheme rather try to forecast the droplet formation based on other known model parameters, in particular the mixing ratios. To predict aerosol development and resulting droplet formation would be a fiendishly complex task.

Following Stensrud (2007) we now describe how the increase in cloud water, due to condensation, over a single integration time step is approximated. The methodology follows that of Asai (1965) and is used in most bulk microphysics schemes.

When water vapor condenses and cloud droplets are formed the following supersaturation conditions is assumed to hold:

$$q_v - q_{vs} = \delta M > 0 \tag{3.17}$$

where q_v is the water vapor mixing ratio, q_{vs} is the saturation vapor mixing ratio, and δM represents the total possible condensed water. Note that δM is the sum of two variables; δM_1 is condensed water and δM_2 is the increase in the water vapor mixing ratio stored in the air. The latter variable is due to latent heat release from condensation that increase the air temperature and consequently the saturation mixing ratio. The equation for latent heat

$$\theta = T \left(\frac{p_0}{p}\right)^{R/c_p} \tag{3.18}$$

can be used to express the warming due to condensation

$$\delta\theta = \frac{L_v}{c_p} \left(\frac{p_0}{p}\right)^{R/c_p} \delta M_1 \tag{3.19}$$

where L_v is the latent heat of vaporization that is needed to be given to a unit mass of material to convert it from liquid to vapor without changing the temperature. The specific heat at constant pressure is denoted by c_p, p_0 is the surface pressure, and p is the pressure. The Clausius-Clapeyron equation for the variation of the equilibrium vapor pressure e_s with temperature T can be written as (Wallace and Hobbs, 2006):

$$\frac{de_s}{dT} = \frac{L_v}{T(\alpha_v + \alpha_l)} \tag{3.20}$$

where α_v is the unit mass of vapor and α_l is the unit mass of liquid. As $\alpha_v \gg \alpha_l$, equation (3.20) can be approximated as:

$$\frac{de_s}{dT} \simeq \frac{L_v}{T\alpha_v} \tag{3.21}$$

Because α_v is the specific volume of water vapor that is in equilibrium with liquid water at temperature T, the pressure it exerts at T is e_s. Therefore, from the ideal gas equation for water vapor, $e_s\alpha_v = RT$, we can rewrite equation (3.21) as:

$$\frac{de_s}{dT} = \frac{L_v e_s}{R_v T^2} \tag{3.22}$$

The partial pressure exerted by any constituent in a mixture of gases is proportional to the number of moles of the constituent in the mixture. Therefore, the pressure e due to water vapor in air is given by (Wallace and Hobbs, 2006):

$$e = \frac{n_v}{n_v + n_d} p = \frac{\frac{m_v}{M_w}}{\frac{m_d}{M_d} + \frac{m_v}{M_w}} p \tag{3.23}$$

Here, n_v and n_d are the number of moles of water vapor and dry air in the mixture, respectively, M_w is the molecular weight of water, M_d is the apparent molecular weight of dry air, and p is the total pressure of the moist air. As the mixing ratio q_v is defined as m_v/m_d (i.e. the ratio between the mass of water vapor to that of the mass of dry air) one can re-write equation (3.23) as:

$$e = \frac{q_v}{q_v + \varepsilon} p \tag{3.24}$$

where

$$\varepsilon = \frac{R_d}{R_v} = \frac{M_w}{M_d} = 0.622$$

where R_d and R_v are the individual gas constants for dry air and water vapor, respectively. As $\varepsilon \gg q_v$ equation (3.24) can be simplified to:

$$e \simeq \frac{q_v p}{\varepsilon} \tag{3.25}$$

We can now use equation (3.25) to rewrite equation (3.22) as:

$$d\left(\frac{q_{vs}p}{\varepsilon}\right) = \frac{L_v(q_{vs}p/\varepsilon)}{R_vT^2}dT$$

which, at a constant pressure, simplifies to

$$dq_{vs} = \frac{L_vq_{vs}}{R_vT^2}dT \tag{3.26}$$

We now use the equation for potential temperature (3.18) to replace dT for $d\theta$ in equation (3.26), such that

$$dq_{vs} = \frac{L_vq_{vs}}{R_v\theta^2}\left(\frac{p_0}{p}\right)^{\kappa} d\theta \tag{3.27}$$

where $\kappa = R/c_p$. Finally, replace $d\theta$ with $\delta\theta_1$ to represent the warming effect of condensation and dq_{vs} with δM_2 to represent the increased saturation mixing ratio due to warming. This leads to (Stensrud, 2007)

$$\delta M_2 = \frac{L_v^2}{c_pR_v}\left(\frac{p_0}{p}\right)^{2\kappa}\frac{q_{vs}}{\theta^2}\delta M_1 \tag{3.28}$$

and so the ratio of $\delta M_1/\delta M$ is

$$\frac{\delta M_1}{\delta M} = r_1 = \frac{1}{[1+(L_v^2/c_pR_v)(p_0/p)^{2\kappa}(q_{vs}/\theta^2)]} \tag{3.29}$$

The increase in cloud water over a single model time step Δt due to condensation, P_{COND}, is

$$P_{COND} = (r_1\delta M)/\Delta t \tag{3.30}$$

The value of P_{COND} is the number of droplets created by condensation over the integration time step Δt. In some microphysics schemes, the value of the adjustment factor r_1 is held constant, but in general it varies between values of 0.25 to 0.9 for a lapse rate of 6.5°C/km^{-1} (Asai, 1965). If the supersaturation of the environment is less than a chosen critical value, evaporation occurs using the same parameterization. In theory this value should be 1, i.e. 100% Relative Humidity, but in reality it often needs to be less in order for the scheme to be able to start producing droplets via condensation. The reason is that it may be very difficult for a scheme to make a whole grid box supersaturated, especially if the model resolution is relatively coarse. Currently, for the GFS global model (which has a horizontal resolution of 0.25° $\simeq$ 28km) this critical value is set to 0.85, i.e. at 85% Relative Humidity, the scheme starts producing droplets via warm rain condensation.

Parameterization of ice initiation The representation of ice-phase microphysical processes in a cloud model is greatly complicated by the variety of forms of the ice phase, as well as by the numerous physical processes that determine the crystal forms. Moreover, in contrast to the physics of warm rain formation, the physics of ice-phase is less understood. The result is that in many cases the formulation of parameterization schemes for ice-physics, based on detailed theoretical models and/or observations, cannot be done (Cotton et al., 2011).

Stensrud (2007) states that observed concentrations of ice nuclei appears to be sufficient to explain ice crystal concentration in some atmospheric clouds. Knowing the ice nuclei concentrations makes it possible to calculate the concentration of vapor-activated ice crystals. Given the ice crystal concentration, knowledge of the mass of a typical ice crystal is sufficient to calculate the value for the cloud ice mixing ratio. Consequently, most parameterization schemes assume that cloud ice forms when in the presence of ice nuclei when the air is supersaturated with respect to ice and the air temperature is below freezing. This assumption allows observations of ice nuclei to be used as the basis for these schemes.

Fletcher (1965) derived an empirical formulation relating the formation of ice nuclei with temperature:

$$N_{IN} = A\exp(\beta T_s) \tag{3.31}$$

where N is the number concentration of active ice nuclei per liter of air, T_s is the number of supercooling (the temperature in °C), β varies from about 0.3 to 0.8 and A is about 10^{-5} liter^{-1} (Cotton et al., 2011). The initiation rate of cloud ice is then described as (Stensrud, 2007):

$$P_{ICE} = \left(\frac{m_i n_c}{\rho} - q_i\right)\frac{1}{\Delta t} \tag{3.32}$$

where q_i is the cloud ice mixing ratio, m_i is the mass of a typical ice particle and Δt is the integration time step of the model. A different relationship between ice particle number concentration and temperature is proposed in Meyers et al. (1992):

$$n_c = 1000\exp\left[-0.639 + 12.96\left(\frac{q_v}{q_{vsi}} - 1\right)\right] \tag{3.33}$$

where q_{vsi} is the saturation water vapor mixing ratio over ice. Dudhia (1989) uses the Fletcher parameterization for ice initiation but Reisner et al. (1998) indicate that the Fletcher scheme overestimates ice nucleation at very low temperatures. Consequently, the value of T is not allowed to go below a certain threshold value ($T = 246$K) in the Reisner scheme. Equation (3.33) is used in the scheme of Schultz (1995), but is not allowed if ice is already present. This is done because ice nucleation is a much slower process than deposition growth of ice crystals (Stensrud, 2007).

The simple Dudhia (1989) scheme regards solid hydrometeors either as snow or ice if the temperature is less than 273 K, with these hydrometeors turning into rain and cloud water, respectively, if the temperature rises. The interactions between the hydrometeor types are also relatively simple; ice can turn into snow and water vapor, water vapor can turn into ice or snow, but snow can only turn into vapor. If the temperature is above the freezing level of water than vapor can only turn into cloud water, cloud water can turn into vapor or rain, and rain can only turn into vapor (cf. Fig. 3.8). Other schemes can be considerably more complicated, allowing for

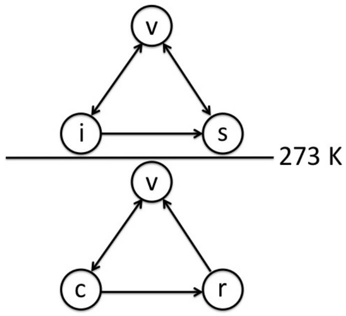

Figure 3.8: *Illustration of the michrophysical processes available in Dudhia (1989) microphysics scheme. Adapted from Stensrud (2007).*

the existence of all hydrometeors at the same time and various interactions between said hydrometeors.

As most microphysics schemes assume that non precipitating hydrometeors are advected with the ambient flow it is clear that the description of the boundary layer can greatly affect the precipitation field. It should however be noted that the description of the microphysical processes do also affect the boundary layer behavior. This can be explained by a simple thought experiment. Envision a parcel of moist air being advected towards a mountain. As the parcel approaches the obstacle it is forced to ascend and is no longer in equilibrium with its environment. Through adiabatic processes there will be a change (either positive of negative) of heat due to forced phase change of the parcel. This heat change in turn can affect the static stability of the layer, and if this layer is near the mountain height, upstream of the mountain, this can enhance, or diminish, the likelihood of a down-slope wind-storm. The importance of this mechanism was demonstrated in Rögnvaldsson et al. (2011).

3.4 Dynamical downscaling

Dynamical downscaling is a method for obtaining high resolution climate, or climate change, information from relatively coarse resolution global climate models (GCMs). Typically, GCMs have a resolution of 100-200 km by 100-200 km. Figure 3.9 shows how the resolution of global models, used for the IPCC evaluation reports, has increased over the years. Many impact-models require information at

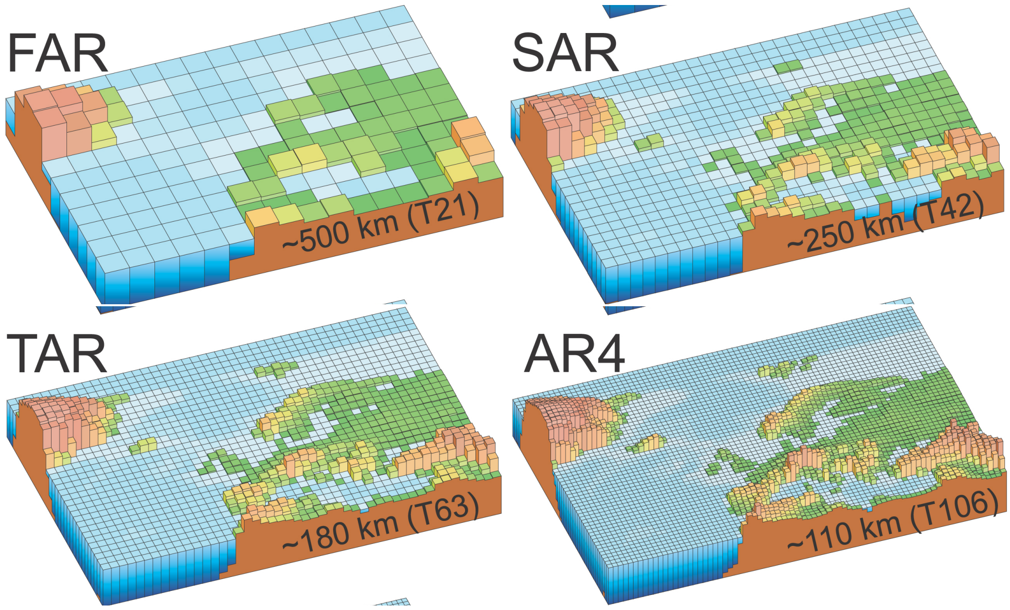

Figure 3.9: *The horizontal grid resolution of the global models used for the IPCC climate evaluation reports has steadily increased. Figure courtesy of IPCC, http://www.icpp.ch.*

scales of 10 km or less, so some method is needed to estimate the smaller-scale information.

The idea behind dynamical downscaling is relatively simple. Take output from a coarse resolution model, e.g. a Global Circulation Model (GCM), and use it to force a Limited Area Model (LAM) at a higher horizontal and vertical resolution. As resolution is increased, processes governed by the interaction of the large scale flow and topography become better resolved by the models. One drawback of this approach, which is not present in global climate models, is that the simulations are dependent on the lateral boundary conditions. These can constrain the model dynamics and hence affect the results (e.g. Warner et al. (1997)). To minimize the constraining effects of the boundary conditions, Qian et al. (2003) suggested consecutive short term integration, overlapping in time as to minimize the effects of spin-up, instead of a single long term integration. Other investigators (e.g. Giorgi and Mearns (1999)) opt for longer integration times, emphasizing the importance of the model to be free to develop its own internal circulations.

It should be pointed out that state of the art LAM, such as the WRF model, have the possibility of “nesting”, i.e. one can create a relatively coarse outer domain and “nest” smaller domains, at a higher horizontal resolution, within this “mother of all domains” (MOAD). This approach can than be used to minimize the negative effects of coarse resolution boundary effects, granted that the MOAD is sufficiently large to allow the LAM to create its own atmospheric flow.

Chapter 4

Overview of peer reviewed articles

4.1 Paper I: Mapping of precipitation in Iceland using numerical simulations and statistical modeling

Precipitation in Iceland during a period of 10 years is simulated with the PSU/NCAR MM5 model. The results are compared with precipitation estimated by a statistical model based on observations and a number of topographic and geographic predictors. The simulated precipitation pattern agrees with the statistical model in areas where data is available and gives a credible precipitation pattern in data-sparse mountainous regions. The simulation is however in general overestimating the precipitation, but the magnitude and the seasonal and geographical distribution of the overestimation indicate that it is to some extent associated with observation errors that are due to wind-loss of solid precipitation. There are also uncertainties associated with the representativeness of the observations as well as with the reference model itself.

4.2 Paper II: Numerical simulations of precipitation in the complex terrain of Iceland – Comparison with glaciological and hydrological data

Atmospheric flow over Iceland has been simulated for the period September 1987 through June 2003, using the PSU/NCAR MM5 mesoscale model driven by initial and boundary data from the European Centre for Medium-range Weather Forecasts (ECMWF). The simulated precipitation is compared with two types of indirect precipitation observations. Firstly, snow accumulation on two large ice caps in SE-

Iceland and on two large glaciers in central Iceland. Secondly, model output is used as input to theWaSiM-ETH hydrological model to calculate and compare the runoff with observed runoff from six watersheds in Iceland for the water years 1987–2002. Model precipitation compares favourably with both types of validation data. The seasonal and inter-annual variability of precipitation is investigated at low as well as high altitudes. The simulations reveal a negative trend in the winter precipitation in W-Iceland, but a positive trend in the ratio of lowland precipitation to mountain precipitation in E-Iceland. There is in general a substantial inter-annual variability in the ratio of lowland precipitation to precipitation in the mountains, especially in E-Iceland, emphasizing the limitation of precipitation observations in the lowlands as a proxy for precipitation in the mountains. In order to assess the impact of orography on the precipitation climate of Iceland, precipitation is simulated with flat Iceland and compared to a simulation with true orography. It is found that the mountains contribute to a total increase of precipitation in Iceland of the order of 40%.

4.3 Paper III: Sensitivity simulations of orographic precipitation with MM5 and comparison with observations in Iceland during the Reykjanes EXperiment

This paper presents a study of the sensitivity of numerically simulated precipitation across a mesoscale mountain range to horizontal resolution, cloud condensation nuclei (CCN) spectrum, initiation of cloud ice, numerical treatment of horizontal diffusion and initial and boundary conditions. The fifth generation Penn State/National Center for Atmospheric Research (PSU/NCAR) Mesoscale Model (MM5) is used in the study, in which the model is run at 8, 4 and 2 km horizontal resolutions and with a number of microphysical and numerical configurations. The model simulated precipitation is compared to the observed precipitation over the Reykjanes mountain ridge during the Reykjanes Experiment in Southwest Iceland in the autumn of 2002. Improvements in representation in topography at increasing horizontal resolutions yield large improvements in the accuracy of the simulated precipitation. At 8 km horizontal resolution the simulated maximum precipitation is too low, but the simulated precipitation upstream of the mountains is too high. The absolute values and the pattern of the precipitation field improve stepwise when going from horizontal resolutions of 8 km to 2 km, with the main contribution being when going from 8 km to 4 km. Calculations of diffusion and ice initiation do not seem to have a large impact on the simulated precipitation, which is on the other hand quite sensitive to the CCN spectrum. The simulations underestimate the precipitation over the downstream slopes of the mountain ridge by factors of 2–3. There are indications that this underestimation may be associated with a systematic overestimation of downslope winds, and possibly descending motion, by the model.

4.4 Paper IV: Extracting statistical parameters of extreme precipitation from a NWP model

Precipitation simulations on an 8 km grid using the PSU/NCAR Mesoscale Model MM5 are used to estimate the M5 and C_i statistical parameters in order to support the M5 map used for flood estimates by Icelandic engineers. It is known a priori that especially wind anomalies occur on a considerably smaller scale than 8 km. The simulation period used is 1962–2005 and 73 meteorological stations have records long enough in this period to provide a validation data set. Of these only one station is in the central highlands, so the highland values of the existing M5 map are estimates. A comparison between the simulated values and values based on station observations set shows an M5 average difference (observed-simulated) of -5 mm/24 h with a standard deviation of 17 mm, 3 outliers excluded. This is within expected limits, computational and observational errors considered. A suggested correction procedure brings these values down to 4 mm and 11 mm, respectively.

4.5 Paper V: Validation of Numerical Simulations of Precipitation in Complex Terrain at high Temporal Resolution

Atmospheric flow over Iceland has been simulated for the period January 1961 to July 2006, using the mesoscale MM5 model driven by initial and boundary data from the ECMWF. A systematic comparison of results to observed precipitation has been carried out. Undercatchment of solid precipitation is dealt with by looking only at days when precipitation is presumably liquid or by considering the occurrence and non-occurrence of precipitation. Away from non-resolved orography, the long term means (months, years) of observed and simulated precipitation are often in reasonable agreement. This is partly due to a compensation of the errors on a shorter timescale (days). The probability of false alarms (the model predicts precipitation, but none is observed) is highest in N Iceland, particularly during winter. The probability of missing precipitation events (precipitation observed but none is predicted by the model) is highest in the summer and on the lee side of Iceland in southerly flows.

4.6 Paper VI: Dynamical Downscaling of Precipitation in Iceland 1961–2006

Atmospheric flow over Iceland has been simulated for the period January 1961 to July 2006, using the mesoscale MM5 model driven by initial and boundary data from the European Centre for Medium Range Weather Forecasts (ECMWF). Firstly, the simulated precipitation is compared to estimates derived from mass balance measurements on the Icelandic ice caps. It is found that the simulated precipitation compares favourably with the observed winter balance, in particular for Hofsjökull, where corrections to take liquid precipitation and/or winter ablation into account have been made, and for the outlet glaciers Dyngjujökull and Brúarjökull. Secondly, the model output is used as input to the WaSiM hydrological model to calculate and compare the runoff with observed runoff from six watersheds in Iceland. It is found that model results compare favourably with observations. Overall, the MM5 V3–7 is somewhat better than the MM5 V3–5. The V3–7 is drier than V3–5 on upstream slopes.

4.7 Paper VII: Downslope windstorm in Iceland – WRF/MM5 model comparison

A severe windstorm downstream of Mt. Öræfajökull in Southeast Iceland is simulated on a grid of 1 km horizontal resolution by using the PSU/NCAR MM5 model and the Advanced Research WRF model. Both models are run with a new, two equation planetary boundary layer (PBL) scheme as well as the ETA/MYJ PBL schemes. The storm is also simulated using six different micro-physics schemes in combination with the MYJ PBL scheme in WRF, as well as one "dry" run. Output from a 3 km MM5 domain simulation is used to initialise and drive both the 1 km MM5 and WRF simulations. Both models capture gravity-wave breaking over Mt. Öræfajökull, while the vertical structure of the lee wave differs between the two models and the PBL schemes. The WRF simulated downslope winds, using both the MYJ and 2EQ PBL schemes, are in good agreement with the strength of the observed downslope windstorm. The MM5 simulated surface winds, with the new two equation model, are in better agreement to observations than when using the ETA scheme. Micro-physics processes are shown to play an important role in the formation of downslope windstorms and a correctly simulated moisture distribution is decisive for a successful windstorm prediction. Of the micro-physics schemes tested, only the Thompson scheme captures the downslope windstorm.

Chapter 5

General discussions

5.1 Discussions on peer reviewed papers

In the first paper *Mapping of Precipitation in Iceland using Numerical Simulations and Statistical Modeling* (Rögnvaldsson et al., 2004) we presented our initial findings on the matter. The ten year simulations, run at 8 km horizontal resolution, were compared to the results of a statistical model based on observations, as well as observations for the same period. The initial results where promising as the atmospheric model did capture the observed precipitation pattern, as interpreted by the statistical model, in areas where there was good geographical coverage of rain gauges. The simulations also revealed plausible precipitation pattern in the data sparse high-lands, e.g. more precipitation in the mountains and a rain shadow in sheltered areas north of Vatnajökull ice cap (cf. Fig. 5.1 Compared to observations the model did overestimate precipitation in certain regions and more so during colder months. This lead us to speculate that part of the discrepancy was due to wind-loss of solid precipitation in the observations. It was also not clear for how large an area some of the observational sites, where precipitation was measured, were representative.

In light of these observational issues, in our next paper *Numerical Simulations of Precipitation in the complex Terrain of Iceland – Comparison with Glaciological and Hydrological Data* (Rögnvaldsson et al., 2007b), we compared simulated precipitation to accumulated winter precipitation on four ice caps and to simulated river-runoff. To be precise, the simulated precipitation, and other meteorological variables, were used as input to the WaSiM-ETH hydrological runoff model. The runoff, as simulated by the WaSiM-ETC model, was then compared to observed runoff from six watersheds. The simulation period was longer than for the first experiment (Rögnvaldsson et al., 2004), fifteen years instead of ten, but the simulation domain was kept unchanged. This extended simulation period allowed more focus to be put on investigating temporal trends in precipitation. The seasonal and inter-

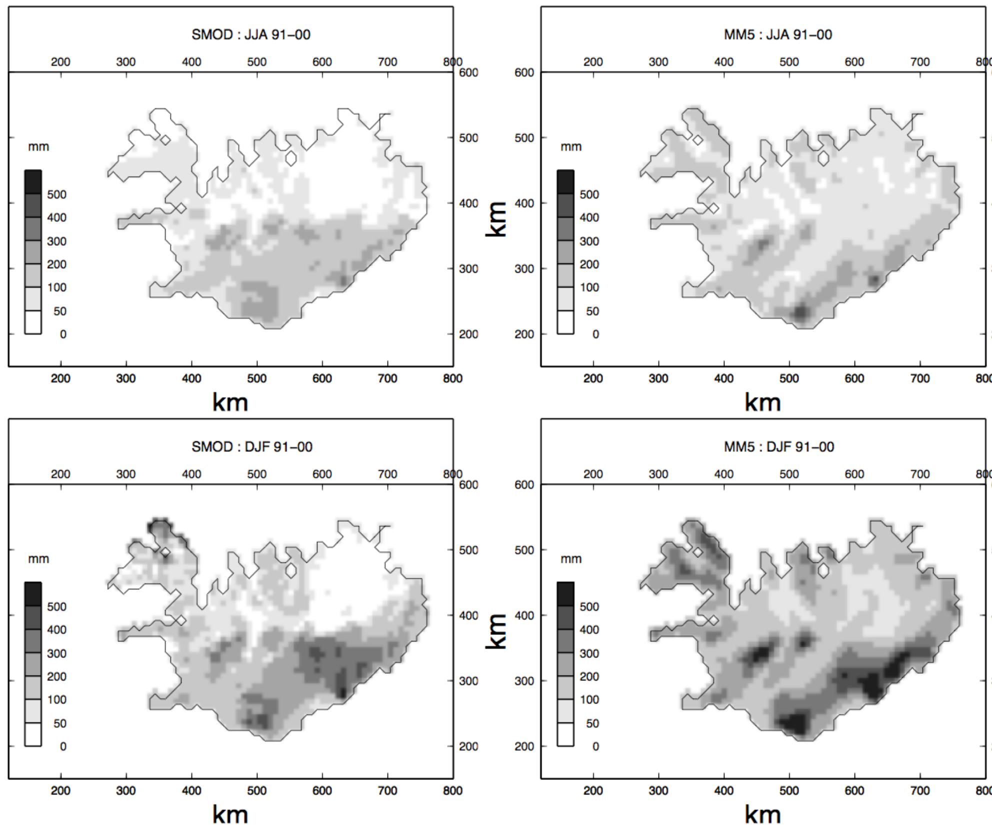

Figure 5.1: *Season average monthly precipitation for June, July, and August (JJA) 1991–2000 [mm] (top) and December, January, and February (DJF, bottom). Reference precipitation as simulated by the statistical model is shown on left panels and precipitation simulated by MM5 on the right panels. Same as Fig. 5 in Rögnvaldsson et al. (2004).*

annual variability of precipitation is investigated at low as well as high altitudes. The simulated precipitation (cf. Fig. 5.2) was found to be in good agreement with the two independent data sets used for comparison and generally within observational errors. In areas where there is substantial subgrid orography, changes in the horizontal resolution will inevitably lead to locally different simulated precipitation. Such a difference may, however, not give a proportionally large signal in tests of the kind that are presented in this paper. This is because the glacier observations are not in the vicinity of substantial subgrid variability in orography, and because the runoff calculations are all based on averaging over a large area. At 8 km horizontal resolution, the finer details of the orography are to some extent lost. This is especially true for geographical features where the ratio between mountain width and height is small, such as narrow ridges or stand-alone mountains. The Rögnvaldsson et al.

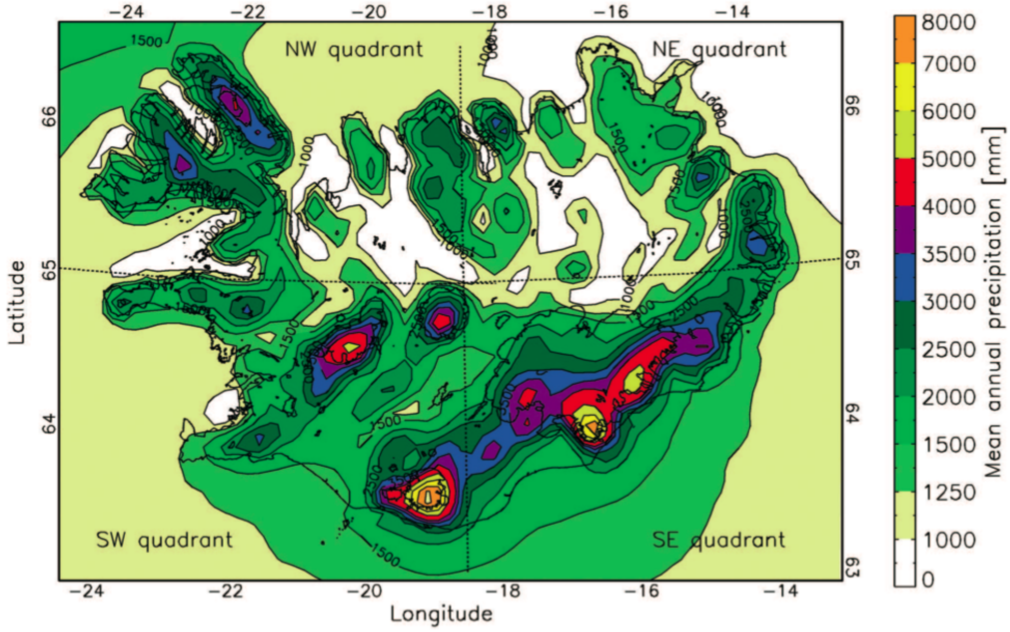

Figure 5.2: *Mean annual precipitation from March 1988 through February 2003 as simulated by the MM5 model. Dashed lines show the definition of NW, NE, SE and SW quadrants. Same as Fig. 7 in Rögnvaldsson et al. (2007b).*

(2007b) paper did therefore not address the question how increased model resolution would modify the precipitation pattern. However, in order to assess the impact of orography on the precipitation climate of Iceland, precipitation was simulated with flat Iceland and compared to a simulation with true orography for a one year period (cf. Fig. 5.3).

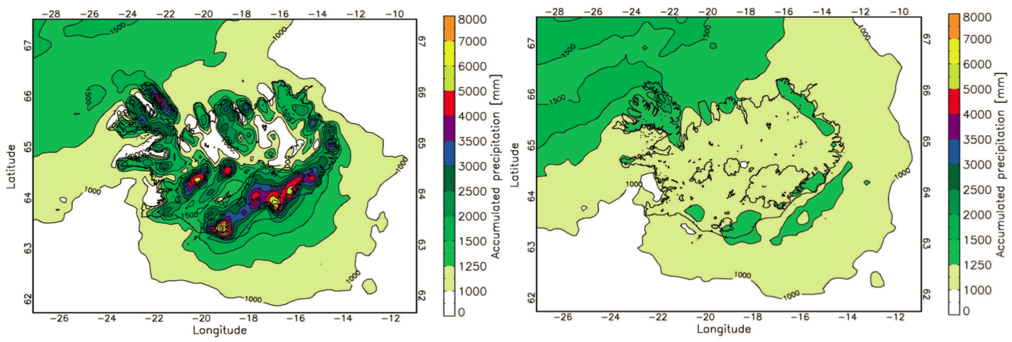

Figure 5.3: *Simulated precipitation [mm] for 2001–02 (September through August) with unmodified terrain (left) and with the orography reduced to one meter (right). Same as Fig. 11 in Rögnvaldsson et al. (2007b).*

In the third paper, *Sensitivity Simulations of Orographic Precipitation with MM5 and comparison with Observations in Iceland during the Reykjanes EXperiment* (Rögnvaldsson et al., 2007a), we did investigate the sensitivity of simulated precipitation to model resolution. Figure 5.4 shows the location of observational stations during the REX intensive observation periods (IOP's) as well as simulated precipitation at 4 km model resolution during IOP5. In addition a number of sensitivity

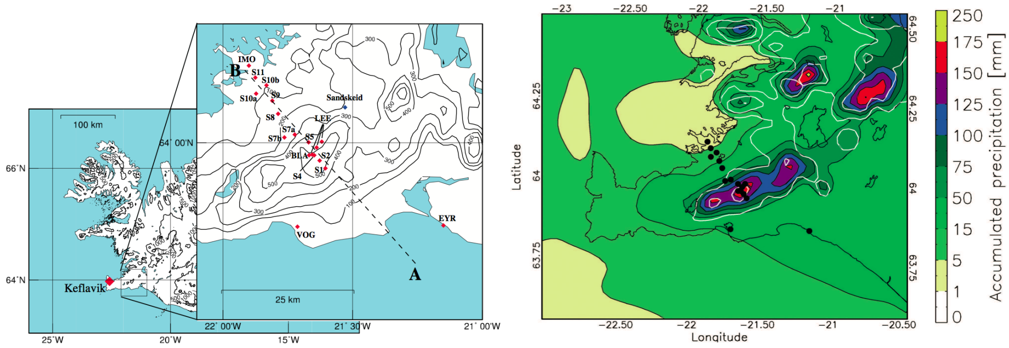

Figure 5.4: *Overview of station location during REX (left). Stations EYR (Eyrarbakki), VOG (Vogsósar), BLA (Bláfjöll), IMO (Icelandic Meteorological Office, WMO 4030) and Keflavík (WMO 4018) are part of the operational network in Iceland. Other stations, S1, S2, S4, S5, LEE (taken as mean of three stations), S7a, S7b, S8, S9, S10a, S10b and S11 were installed specifically for the Reykjanes EXperiment. Station Sandskeið is shown in blue. Topography is shown with height intervals of 100 meters. On the right, terrain and accumulated precipitation during IOP5 is shown, as simulated in the REX2_CNP30 run (cf. Table 1 in Rögnvaldsson et al. (2007a)). Contour lines (white) of the terrain are plotted every 250 meters. Location of observation sites are shown by black dots. Same as Figs. 2 (left panel) and 3 (right panel) in Rögnvaldsson et al. (2007a).*

tests where done in order to see how changes to the microphysical parameterizations would affect the simulated precipitation. The simulation results revealed most sensitivity to the CCN spectra (cf. Fig. 5.5), which in turn was tuned by modifying the droplet concentration, i.e. the minimum number of droplets per unit volume needed before warm rain condensation can be initiated. By modifying the microphysics scheme towards a more maritime climate, i.e. less droplet concentration per unit volume (equivalent to assuming larger droplets), resulted in simulated precipitation that was closer to observed values. The simulation showed limited sensitivity to changes made to how cloud ice was initiated and how horizontal diffusion was calculated. This indicates that the precipitation process, as modeled by the microphysics scheme, was to a large extent warm rain. Increasing model resolution did reveal large sensitivity, both for upslope precipitation (reduced when model reso-

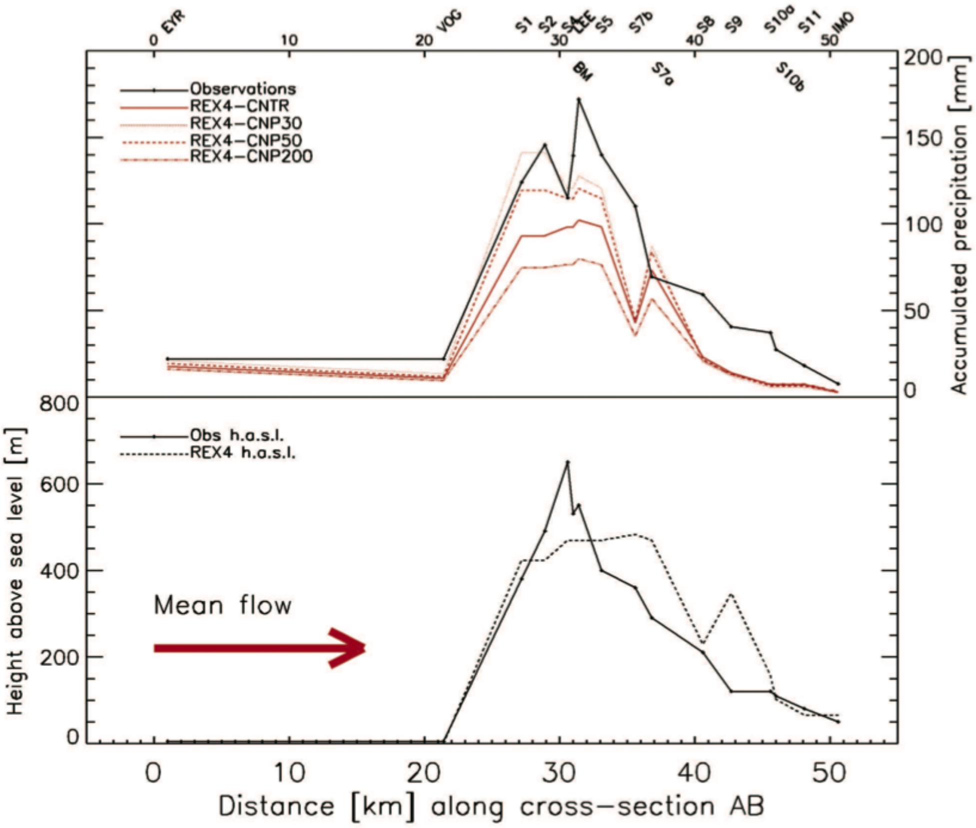

Figure 5.5: *Sensitivity to different values of CNP at 4 km horizontal resolution, CNP = 100 (CNTR, solid line), CNP = 30 (dotted line), CNP = 50 (dashed line) and CNP = 200 (dot-dashed line). Bottom panel shows the model and actual orography along cross section AB in Fig. 5.4. Same as Fig. 6 in Rögnvaldsson et al. (2007a).*

lution was increased) and precipitation at mountain crest (increased when model resolution was increased). All simulations did however underestimate precipitation downstream of the mountain. This behavior indicates that the model did indeed not capture the true quantity of solid hydrometeors, i.e. it underestimated the amount of ice being initiation and/or the amount of ice and snow being formed via various processes, such as aggregation. The reason is that solid hydrometeors (e.g. snowflakes) have much lower fall velocities than liquid drops. These hydrometeors can therefore be advected by the flow, in this case over the mountain ridge. Another possible reason for the lee-side dryness is too much downdraft, leading to an overestimation of evaporation. Comparison with observations did indeed reveal overestimation of surface winds on the lee-side of the mountain ridge. The results from this study indicate that the precipitation mapped at 8 km resolution as in

Bromwich et al. (2005) and Rögnvaldsson et al. (2004, 2007b) gives too small maxima over the mountain crest and far too little precipitation directly downstream of the crest. This can have considerable economical implications, as the spatial distribution of precipitation plays a key part in planning and use of water resources.

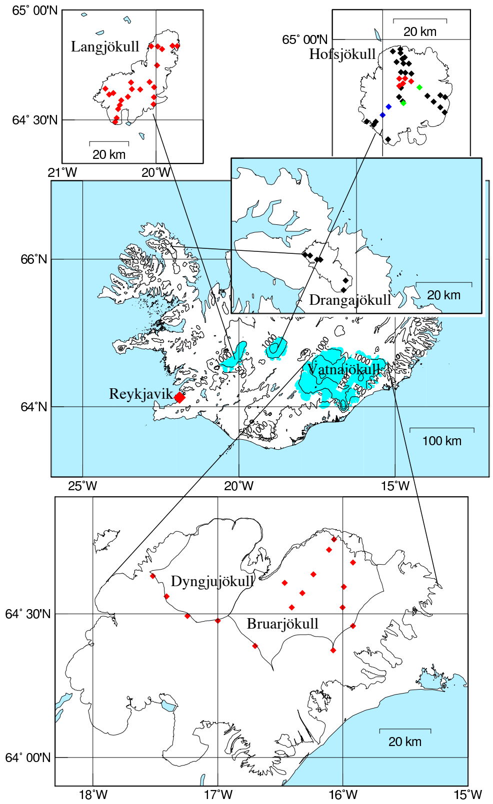

Figure 5.6: *Overview of the six ice caps and glaciers used for validation purposes, where dots indicate a typical location of an observation site. Red dots on Hofsjökull glacier are along profiles HN (N part), blue dots along profile HSV (SW part) and green dots along profile HSA (SE part). Observations at locations shown in black at Hofsjökull have not been used in this study. Drangajökull is split up in two regions, NW and SE parts (cf. Table 2 in Rögnvaldsson et al. (2010)). See Figure 1 in Rögnvaldsson et al. (2007b) for comparison. Same as Fig. 2 in Rögnvaldsson et al. (2010).*

In the sixth paper, *Dynamical Downscaling of Precipitation in Iceland 1961–2006* (Rögnvaldsson et al., 2010), we extended the study presented in Rögnvaldsson et al. (2007b). The simulation period was considerably longer than in the earlier investigation, or 45 years. This gave us the opportunity to extend the simulated runoff series and compare to earlier observations, more glaciological data was also available (cf. Fig. 5.6). In this study a newer version of the MM5 atmospheric model was used (version 3.7 vs. version 3.5 in earlier studies). The simulated precipitation was again compared to non-conventional observations of precipitation, i.e. snow accumulation and runoff. As before, the simulated precipitation did compare favorably with observations. There where noticeable differences from the earlier simulation for the overlapping 15 year period 1987–2003 (cf. Fig. 5.7). Most notably the newer version of MM5 simulated less precipitation on the upstream slopes of mountains that are well represented at the model horizontal resolution. This is believed to be caused by changes made in the microphysics scheme used (the Reisner2 scheme, (Reisner et al., 1998)). Notably, version 3.5 of MM5, used in Rögnvaldsson et al. (2007b)

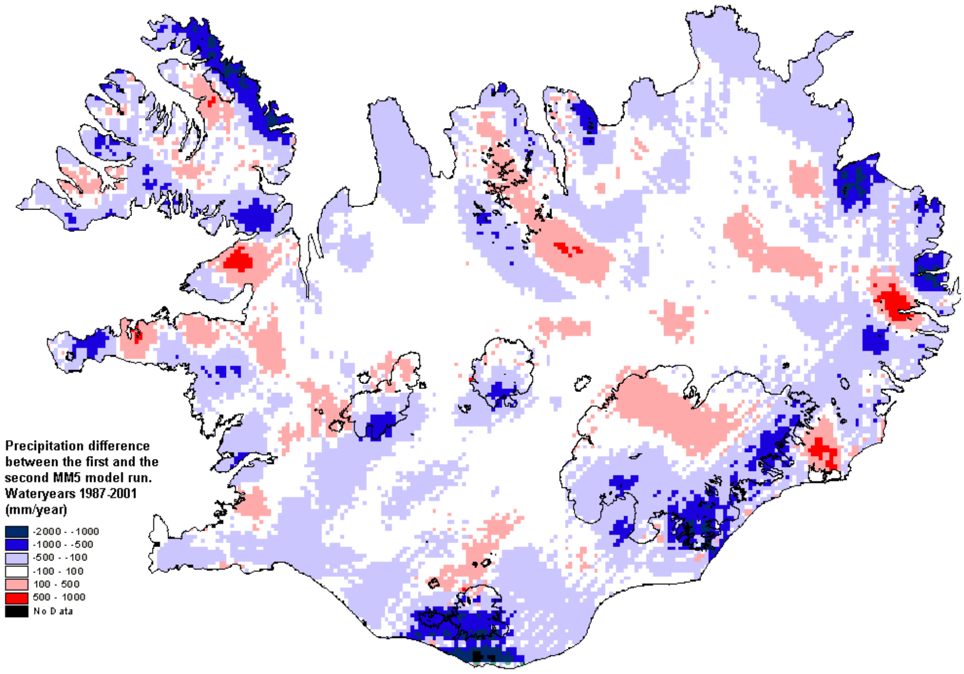

Figure 5.7: *Difference (MM5 V3.7 minus MM5 V3.5) in simulated mean annual precipitation for the water years 1987–2002. Same as Fig. 8 in Rögnvaldsson et al. (2007b).*

used the Kessler autoconversion[1] scheme. As of version 3.6 of MM5, this scheme was swapped with that of Berry and Reinhardt as implemented by Walko et al. (1995). The Kessler scheme has been known to produce too much precipitation upstream of mountains. The glaciological and runoff data only provides validation on a much longer timescale than conventional rain-gauge data, and the daily error in the precipitation downscaling remains unclear. However, the comparison with the observational data shows that the climatological values of the simulated precipitation are of good quality.

The temporal and spatial accuracy of precipitation simulated in Rögnvaldsson et al. (2010) was investigated for the period 1987–2003 in the fifth paper *Validation of Numerical Simulations of Precipitation in Complex Terrain at high Temporal Resolution*, (Arason et al., 2010). The main findings where that away from non-resolved orography, long term (months, years) sums of simulated precipitation are quite correct in the south but too high in the north. This was partly due to compensating errors on a smaller timescale (days). Figure 5.8 shows the relative

[1] Autoconversion is the process where cloud droplets collide and coalesce with each other and eventually form raindrops.

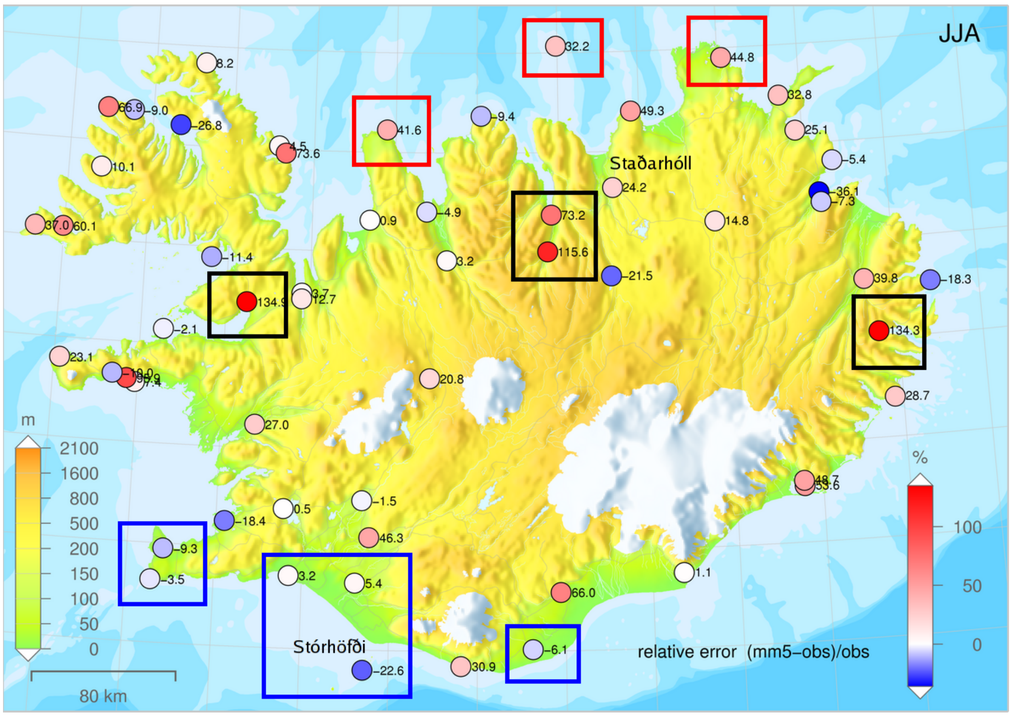

Figure 5.8: *A topographic map of Iceland showing relative difference between simulated and observed accumulated precipitation, (mm5-obs)/obs, in June, July and August (JJA). Each colored circle corresponds to a synoptic weather station. Station names are included at the stations referred to in the Arason et al. (2010) paper. The color of the circle denotes the relative error in the simulations (colorbar to the right). The blue boxes enclose a few stations on flat land in S Iceland where the observations and simulations are in reasonable agreement. The red boxes draw attention to stations in N Iceland where the model overestimates precipitation, despite these stations being on flat land. Stations that have huge overestimation, which is almost certainly due to non-resolved orography, are enclosed in black boxes. Same as Fig. 1 in Arason et al. (2010).*

difference between simulated and observed accumulated precipitation during the summer months June, July, and August for the period 1987–2003. The probability of false alarms (the model predicts precipitation, but none is observed) is highest in N Iceland, particularly during winter. The probability of missing precipitation events is highest in the summer and on the lee side of Iceland in southerly flows. Precipitation is underestimated in southeasterly flows at the SW coast of Iceland and is overestimated at the N coast of Iceland. This cannot only be explained by non-resolved orography.

In spite of the shortcomings of the downscaled precipitation demonstrated in

Arason et al. (2010), it is still possible to gain valuable statistical information from the data set. The fourth paper, *Extracting statistical parameters of extreme precipitation from a NWP model*, (Elíasson et al., 2009), demonstrates just that. In this paper the authors use the simulated precipitation from Rögnvaldsson et al. (2010) to estimate the M5 and C_i statistical parameters in order to support the M5 map used for flood estimates in Iceland.

In the seventh paper, *Downslope Windstorm in Iceland – WRF/MM5 Model Comparison*, (Rögnvaldsson et al., 2011), we take a closer look at a severe windstorm in SE Iceland. In this study we compared the MM5 and WRF models. Both models are run with a new, two equation planetary boundary layer (PBL) scheme as well as the ETA/MYJ PBL schemes. The storm was also simulated using six different micro-physics schemes in combination with the MYJ PBL scheme in WRF. The new two equation PBL scheme, when implemented within the MM5 model, did capture the downslope windstorm better than the ETA scheme. There was however less difference seen between the two WRF simulations, i.e. the one using the MYJ scheme and the two equation scheme. The sensitivity tests using different microphysics scheme revealed that thermodynamical processes can play a very important role in the formation of downslope windstorms. Forced ascend, or descend, can cause changes in phases of hydrometeors and hence modifications in the temperature field via release (or uptake) of heat due to the phase changes. This change in temperature can in turn modify the stability of the impinging flow, and as explained by e.g. Durran (1990), upslope stability at mountain height can be a crucial factor in the formation of a downslope windstorm.

5.2 Climatology of winds

A preliminary study on surface winds from a fifteen year period (1987–2002) of simulated MM5 data was done by Rögnvaldsson and Ólafsson (2005a). In this study observations from thirteen stations where compared to simulated winds (cf. Fig.5.9). The stations were both near the coast and at higher altitudes. Two points show the greatest discrepancies, stations Stórhöfði and Reykjavík. The anemometer at Stórhöfði is on a 120 meter high cliff whilst the corresponding grid cell in MM5 is at sea level. This discrepancy between the topography in the model and reality explains the large difference between the measured (10.4 m/s) and simulated (7.6 m/s) wind speed. The Reykjavík weather station is at 50 meter altitude but the nearest model grid cell is at 150 meter altitude. There is further a strong coastal gradient in the wind field, the next inland grid cell having considerably less wind speed (5.7 m/s).

In this study the authors conclude that the simulated wind speeds agreed fairly well with observations and that the observed discrepancies could to a large extent

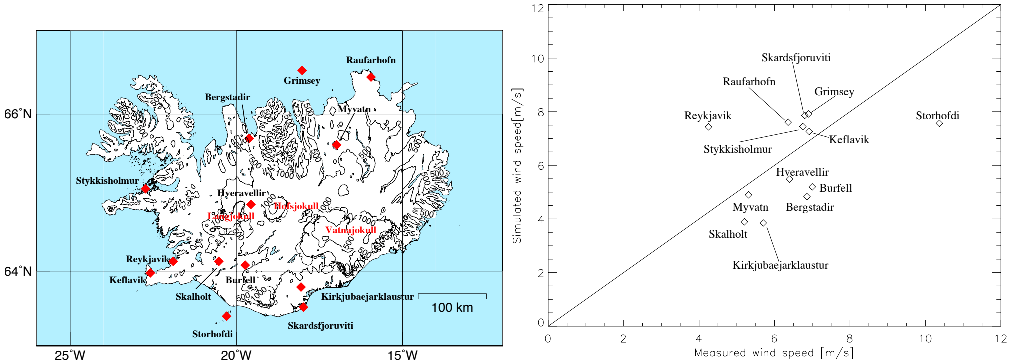

Figure 5.9: *Observation stations (red diamonds) used for comparison with the MM5 simulations (left panel) and comparison between measured (x-axis) and simulated (y-axis) annual mean wind speed at the thirteen observation sites (right panel). Same as Figs. 1 (left) and 4 (right) in Rögnvaldsson and Ólafsson (2005a).*

be explained by the model coarse resolution and corresponding errors in land use parameters and orography. Another source of discrepancies was the inherited uncertainty of anemometers. The authors further speculated that too little mixing near the surface in the PBL scheme used could have contributed to too low simulated wind speeds in the interior of Iceland.

Long term downscaling experiments have also been done using the WRF atmospheric model, both version 2.2 and 3.0.1. These simulations range from fall 1957 to spring 2011 and 2012, respectively. Data from the older version of WRF, which was run at a 9 km horizontal resolution, have been used to calibrate a runoff model developed by the Vatnaskil Engineering company[2]. This runoff model is now being driven in operational mode with data from an ensemble forecasting system operated by IMR. The resulting runoff data are in turn used for day-to-day decision making at Landsvirkjun, Iceland's largest electrical power producer. The series created with version 3.0.1 of WRF was run at a 27 km resolution for the period September 1957 to September 2009. The model was also run at a 9 km resolution for the whole 1957–2012 period, and at a 3 km resolution for the period 1994–2012, using one-way nesting in on-line mode. A further 1 km domain was run for part of S Iceland for the seven year period September 2002 to September 2009. The various model domains are shown in Fig. 5.10. The model was run with the two equation PBL scheme discussed earlier and described in detail in Bao et al. (2008). Table 5.1 shows the various parameterization schemes used for the two downscaling experiments. Comparisons of the heights of various pressure levels, wind speed and direction, and temperature with upper air observations at Keflavík airport show that the large scale flow is well captured by the simulations (cf. Fig. 5.11).

[2]http://www.vatnaskil.is

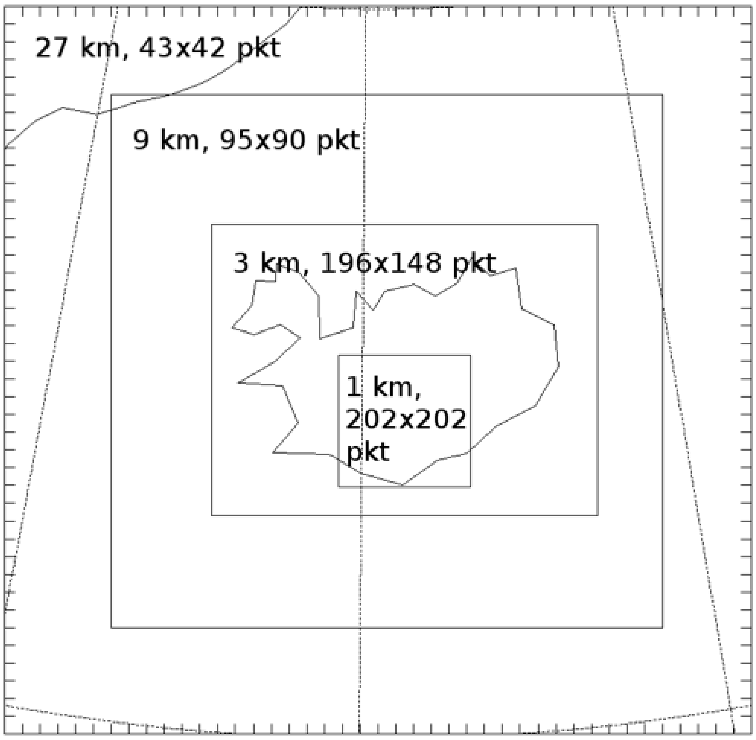

Figure 5.10: *WRF domain configurations for the various downscaling experiments of ERA-40 and ECMWF re-analysis data. The 9 and 3 km domains are the same for both version 2.2 and 3.0.1 simulations but the 27 and 1 km domains were only used with version 3.0.1.*

Table 5.1: *Various parameterization schemes used for dynamical downscaling experiments using two different versions of the WRF model.*

Parameterization scheme	**Version 2.2**	**Version 3.0.1**
Microphysics	Thompson graupel	Thompson graupel
Cumulus	Kain-Fritsch	Betts-Miller-Janjic
Planetray boundary layer	Mellor-Yamada-Janjic	Two equation
LW radiation	RRTM	RRTM
SW radiation	Dudhia	Dudhia
Surface physics	NOAH LSM	NOAH LSM
Surface layer physics	Monin-Obukhov	Monin-Obukhov

Comparison of surface observations of wind direction, wind speed and temperature

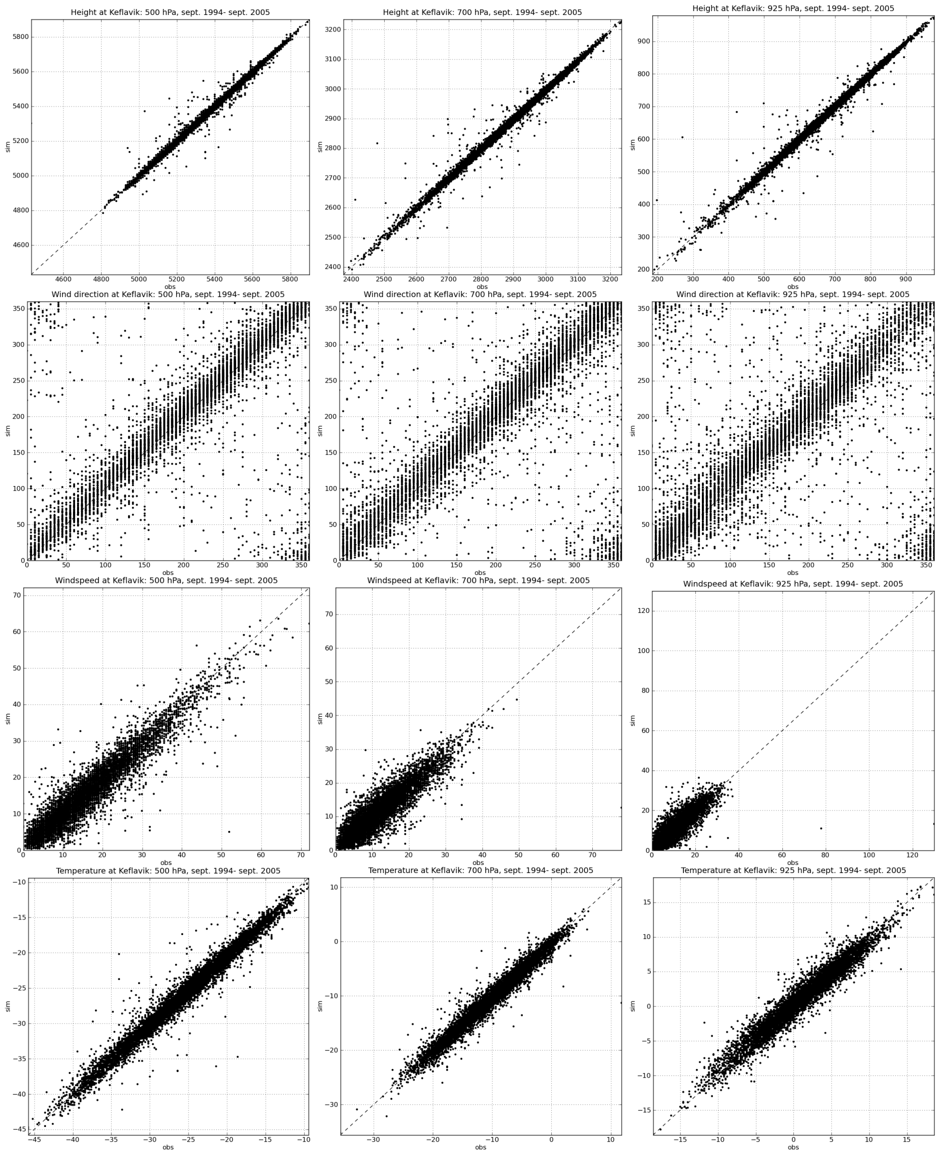

Figure 5.11: *Comparison of observed 500, 700, and 925 hPa heights (top) [m], wind direction (second from top) [°], wind speed (second from bottom) [m/s] and temperature (bottom) [°C] at 500 (left), 700 (middle) and 925 hPa (right). Horizontal axis shows observations and vertical axis simulated results at 3 km resolution. The comparison period is from September 1994 until September 2005 (both months included).*

with simulations are also favorable (cf. Fig. 5.12).

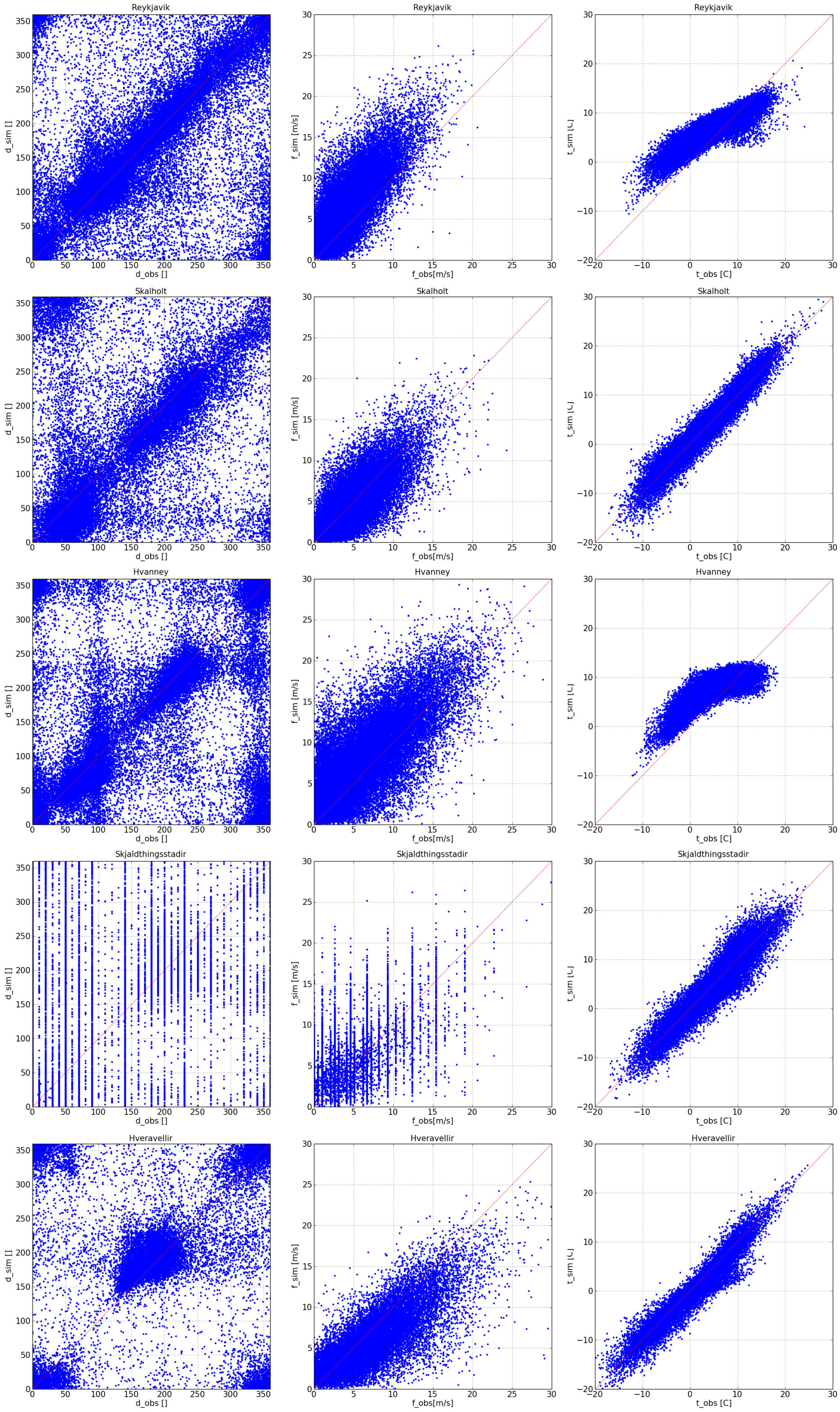

Figure 5.12: *Comparison of observed ten meter wind direction (left) [°] and wind speed (middle) [m/s], and two meter temperature (right) [°C] at Reykjavík (top), Skálholt (second from top), Hvanney (middle), Skjaldþingsstaðir (second from bottom), and Hveravellir (bottom). Horizontal axis shows observations and vertical axis simulated results at 3 km resolution. The comparison period is from September 1994 until September 2005 (both months included).*

Observed errors at various stations can, to some extent, be explained by:

- Sub-grid orography.
- Proximity to water bodies.
- Inaccurate landuse characteristics, e.g. incorrect surface roughness.

The 10 meter mean winds are shown for different classes of sub-periods in Figures 5.13 to 5.15. The patterns revealed in these figures correspond to features

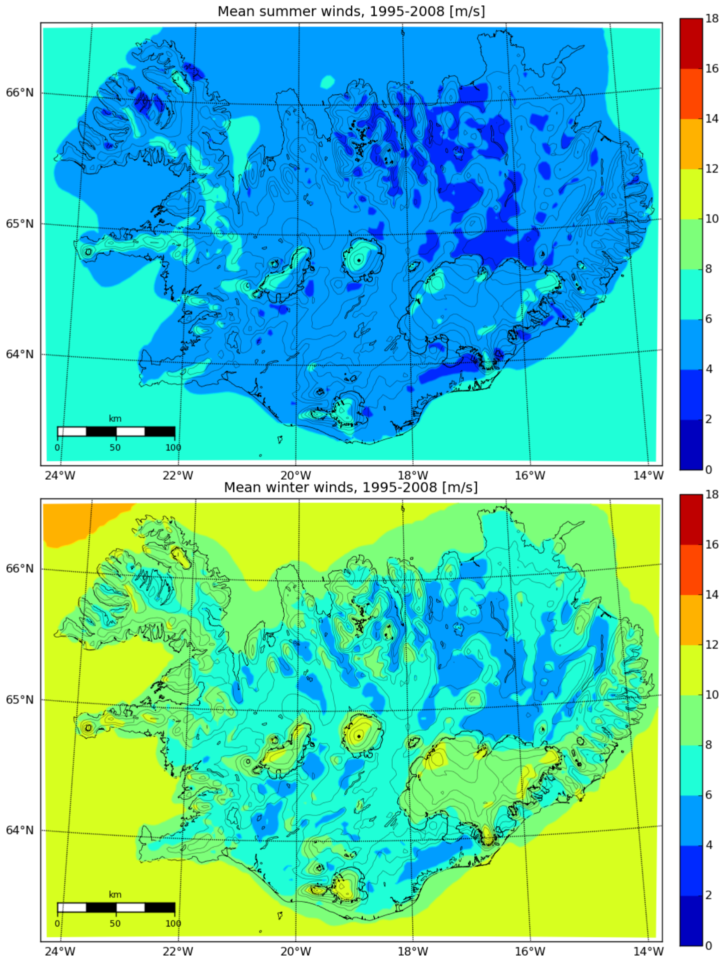

Figure 5.13: *Simulated mean summer (June, July, and August) ten meter windspeed (top) and winter (December, January, and February) windspeed (bottom) [m/s] for the period 1995–2008 (both years included).*

produced in flows at high Rossby numbers and values of Nh/U close to unity or above (upper central and upper right parts of the mountain wind diagramme in Fig. 3.5). In this parameter space, strong winds can be expected where the flow

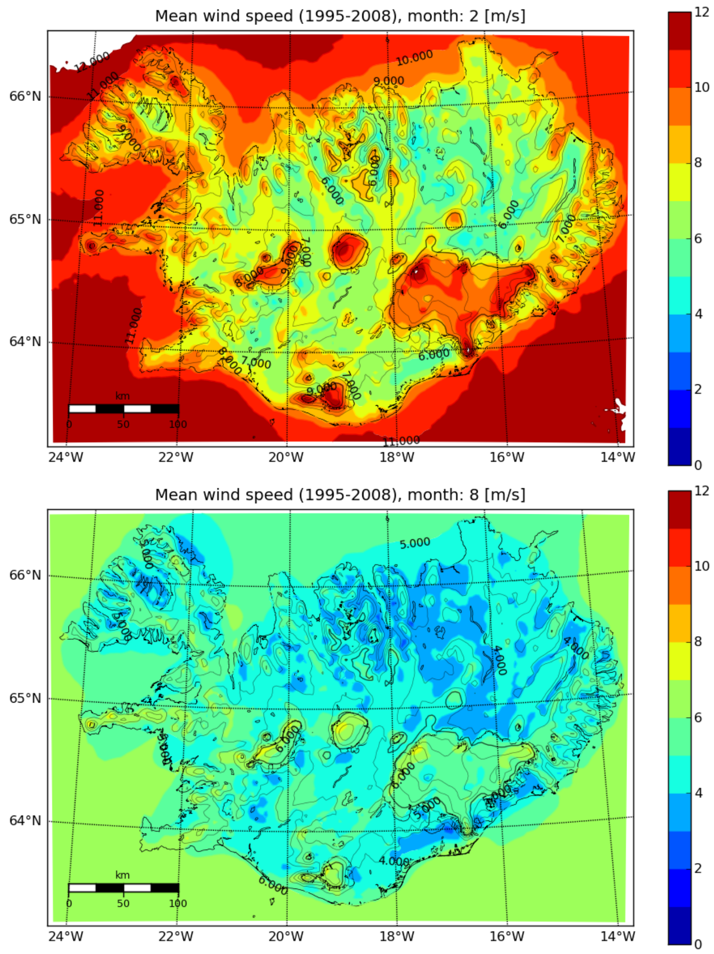

Figure 5.14: *Simulated mean monthly ten meter windspeed [m/s] for February (top) and August (bottom) for the period 1995–2008 (both years included).*

escapes past mountain ranges (corner winds) and above the downsream slopes of mountains. Weak winds are immediately upstream (blockings) and downstream (wakes) of mountains. At the scale of Iceland as a whole, the Coriolis force has an significant impact on the flow pattern. Here, we move downwards in the right part of the diagramme in Fig. 3.5 to intermediate or low Rossby numbers. In this parameter space, there is speed-up on the left side of the mountains. This speed-up may explain that the mean winds are stronger along the south coast than along the north coast of Iceland. Winds from the SE, E and NE are much more frequent than winds from the westerly directions. The easterlies accelerate at the south coast, while the infrequent westerlies accelerate at the north coast. Figure 5.15 illustrates this effect nicely with a speed-up at the SW-coast in flow from the SE. In the mean

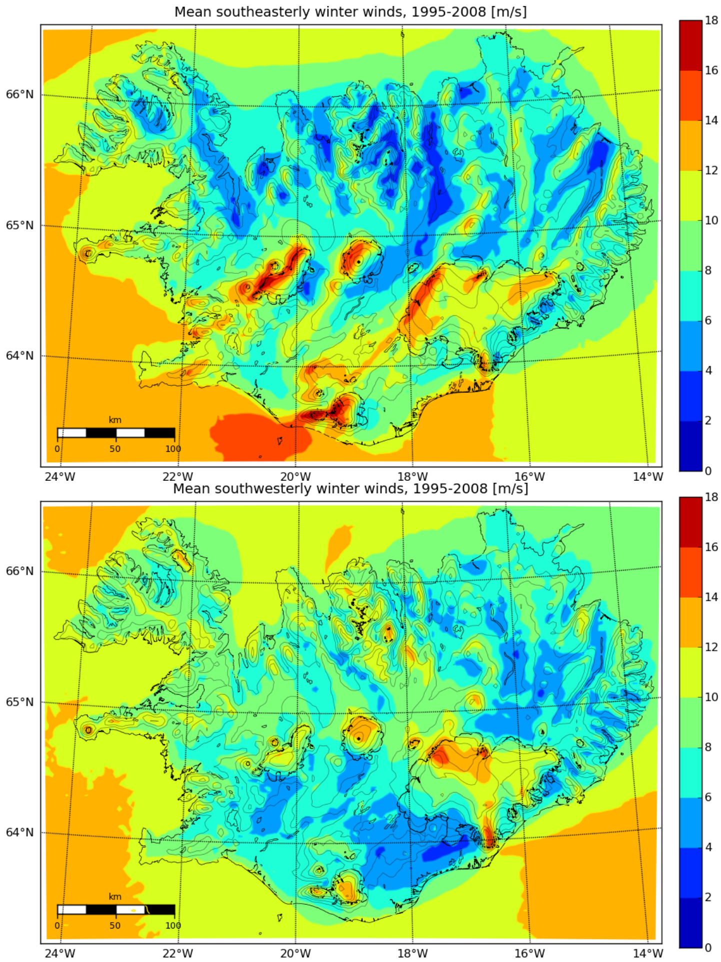

Figure 5.15: *Simulated mean ten meter windspeed [m/s] for southeasterly (top) and southwesterly (bottom) winds for the winter (January, February and March) months for the period 1995–2008 (both years included).*

flow, areas of strong winds in the mountains are not above the mountain tops, but in the western slopes. This suggests strong persistency of gravity waves in easterly winds. This pattern becomes particularly clear in winds from individual directions as in Fig. 5.15.

In the winter, the difference between mean wind speed in the lowlands and over the ocean is much greater than in the summer. This difference reflects the high static stability of the winter boundarylayer over cold land surface, compared to low static stability over the relatively warm ocean. In the summer, the situation is opposite; the ocean surface is often colder than the overlying airmass, while the daytime surface over land is in general warmer than the airmass, leading to lower static stability over land than over the ocean. Low static stability leads to much vertical miximg of momentum and consequently, the mean summer winds are only a little weaker over land than over the sea, while in the winter the mean winds at sea are much greater than inland.

Comparing flow from SE and flow from SW (cf. Fig. 5.15), the SE-flow features much stronger gravity-wave signal and weaker mean winds in N-Iceland (wake). Both these features may be attributed to higher static stability (and Nh/U) in winds from the SE than in winds from the SW. The flow from SE is often associated with advection of warm air ahead of an extratropical cyclone, while the flow from the SW is often associated with outbreak of a cold airmass over relatively warm ocean.

5.3 Dynamical downscaling of future climate

Rögnvaldsson and Ólafsson (2005b) investigated two simulations of future climate, focusing on Iceland and surrounding waters. The simulations were done with the numerical model HIRHAM (a version of the NWP model HIRLAM) at a horizontal resolution of 0.5° and with boundary conditions from global simulations by the Hadley centre, based on scenarii A2 and B2. The study indicated that precipitation in a future climate might increase substantially in NE-Iceland during mid-winter and mid-summer and in S-Iceland in the autumn. The simulated precipiation increase in mid-winter and autumn was found to be much greater in the mountain slopes than at the coast, indicating that a future climate might have a new and different precipitation change with height.

As part of the Nordic CES (Climate and Energy Systems) and Icelandic LOKS (LOfthjúpsbreytingar og áhrif þeirra á orkuKerfi og Samgöngur) projects (Thorsteinsson and Björnsson, 2012) we have used the WRF model to dynamically scale down simulations of both control period and future climate. In order to assess the impact of horizontal resolution on the simulated climate, the atmosphere has been simulated for selected areas at different resolutions (cf. Fig. 5.16). The forcing data are from the Bjerknes climate model, run at the Bjerknes Centre for Climate Research[3] (BCCR) in Bergen, Norway. Two periods were chosen, a control period 1961–1990 and a future period 2020–2050.

The modeling approach used in this experiment is that of Giorgi and Mearns (1999), i.e. we opt for a very large MOAD and long simulation times (one year).

[3]http://www.bjerknes.uib.no/

The atmosphere model used by BCCR is the Arpege model (Déqué et al., 1994), run

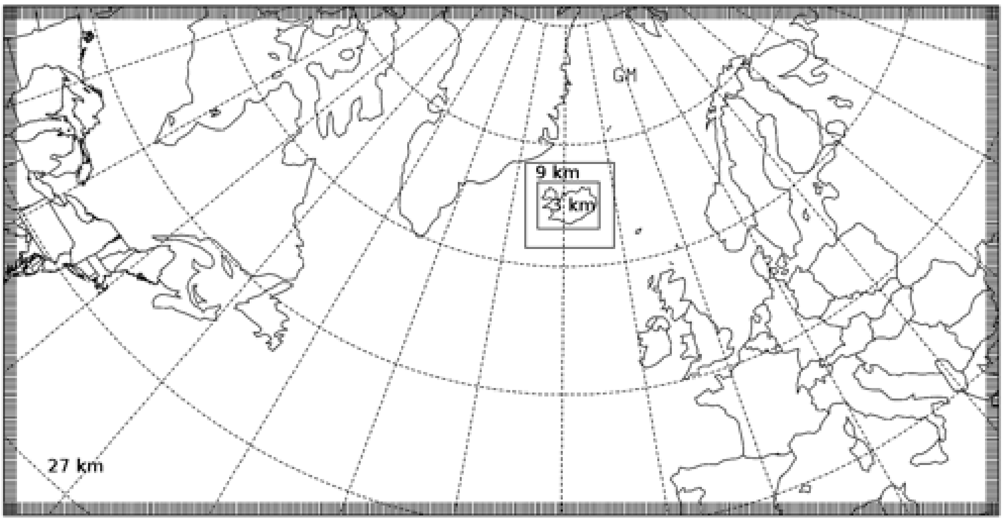

Figure 5.16: *WRF domain configurations for the Arpege control and future climate downscaling experiments. The outermost 27 km MOAD is 400×200 points, the 9 and 3 km domains covering Iceland are 94×91 and 196×148 points, respectively.*

on a T159c3 irregular grid. The scenario chosen was the SRES A1B (Nakićenović et al., 2000).

Prior to being pre-processed be the WRF model the Arpege data were regridded to a regular 1.125°× 1.125° grid. The reason for this relatively coarse resolution was to prevent the creation of spurious high frequency noise by the regridding process in areas far from the high resolution part of the original Arpege simulation.

5.3.1 Results

The model resolution has a big impact on the simulated precipitation (cf. Fig. 5.17).

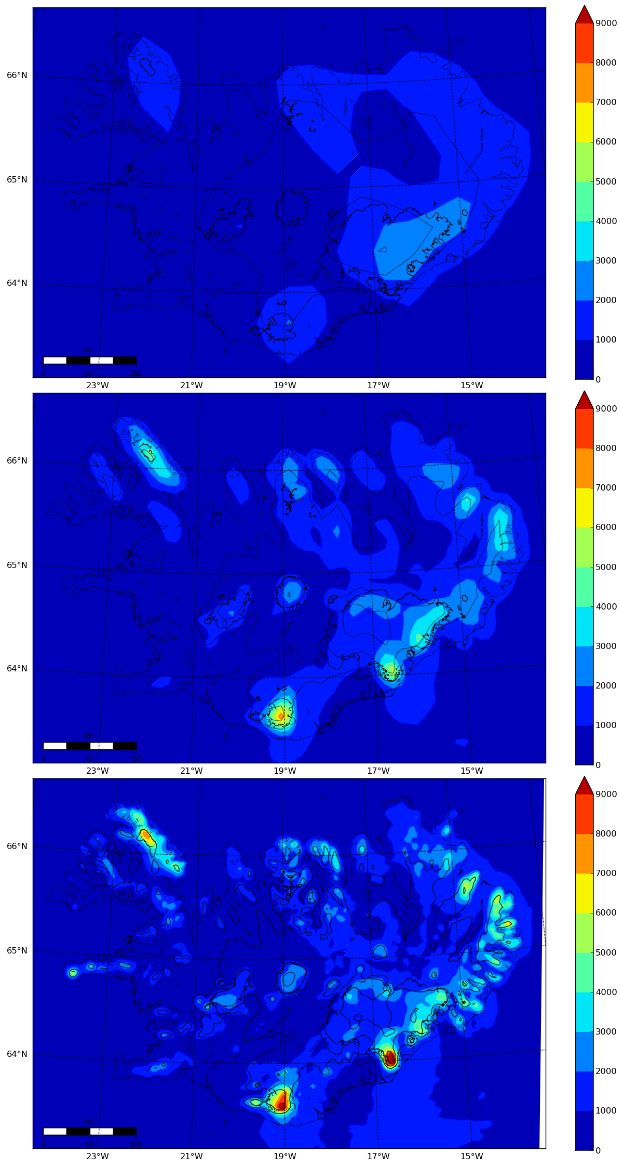

Figure 5.17: *The simulated annual precipitation [mm] for the period 2020 to 2021 increases as the horizontal resolution goes from 27 (top), to 9 (middle) and 3 km (bottom).*

As the model resolution is increased the terrain is better represented and the maximum precipitation values increases. The precipitation pattern also becomes more realistic and detailed, with high values in mountainous regions and over the large ice caps in S-, SE-, and Central Iceland. Comparison of simulated precipitation from this particular future climate scenario with the control period reveals both spatial and temporal changes. There is less annual precipitation in W-, SW-, and E-Iceland but more in SE- and Central Iceland (cf. Fig. 5.18). This pattern is even more pronounced for large events (not shown).

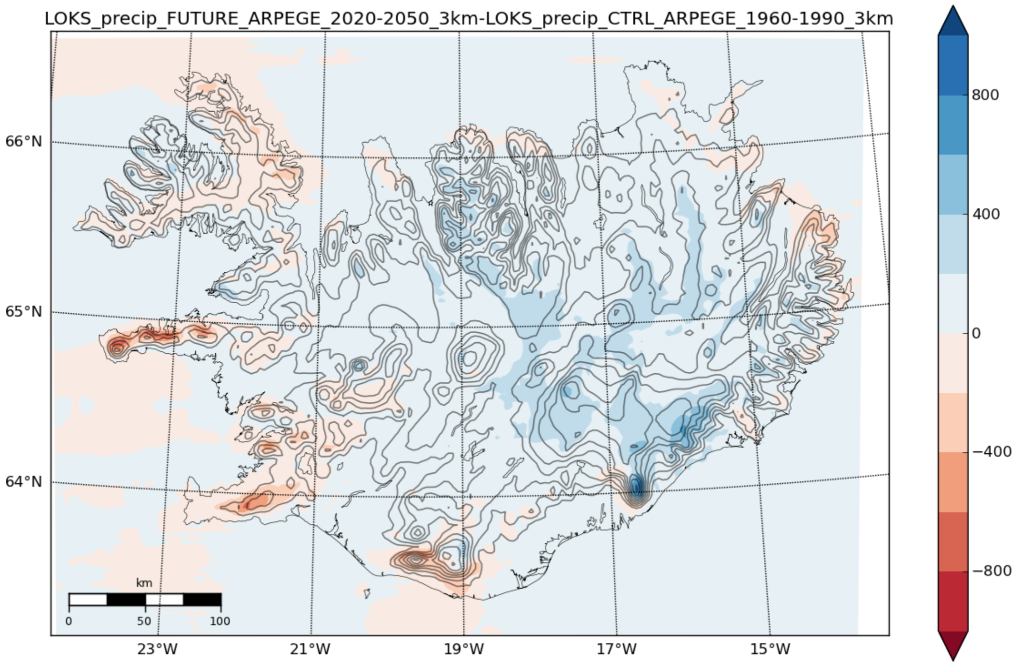

Figure 5.18: *Difference in simulated mean annual precipitation for the period 2020–2050 and 1960–1990 (future minus control).*

There are also signs of seasonal changes in the precipitation pattern, in particular for heavy precipitation events. Figure 5.19 shows a histogram of daily precipitation, separeted into different bins. There is little change in light precipitation events, but as daily precipitation increases there is a clear shift from winter and spring to summer and fall.

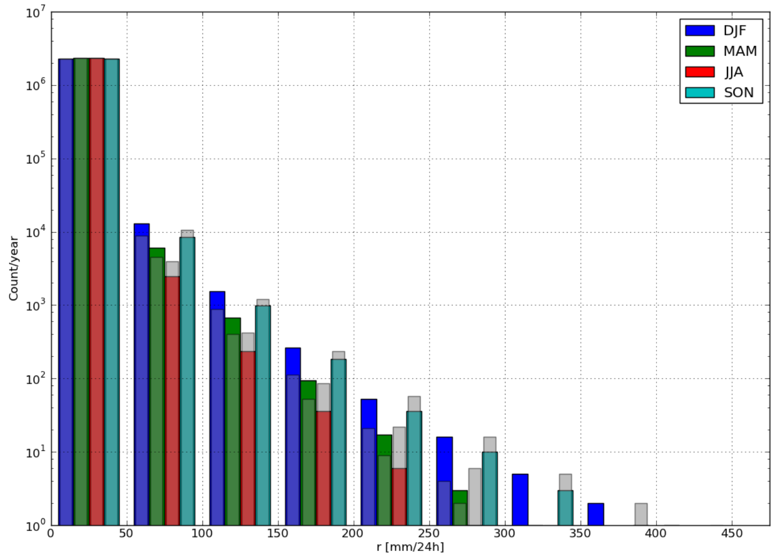

Figure 5.19: *Difference in simulated precipitation for the period 2020–2050 and 1960–1990 for different daily amounts, simulated at 3 km resolution. Vertical axis shows the number of grid cells within each precipitation amount bin shown on the horizontal axis. The control period is shown with coloured bars (different color for each three month period) and the future period is shown with shaded, slightly narrower bars.*

This trend can also be seen at 9km resolution, cf. Fig. 5.20. These seasonal vari-

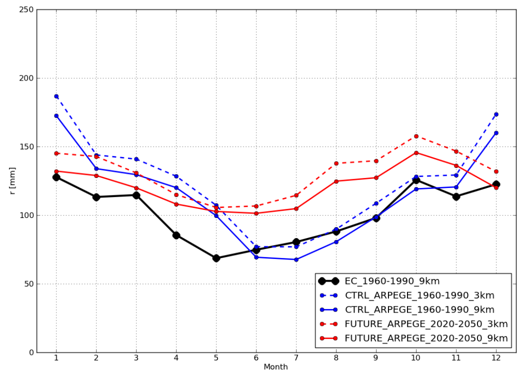

Figure 5.20: *Annual cycles of monthly mean precipitation for the control (red) and future (blue) periods at 9 (solid lines) and 3 (dashed lines) km resolution. The black line shows the same, but for the downscaled ERA40 data set at a 9 km resolution.*

ations in precipitation are not seen when looking at the 15-member multi-model ensemble mean changes from the CES (Thorsteinsson and Björnsson, 2012) project (cf. Fig.5.21). These result indicate an increase in precipitation in future climate,

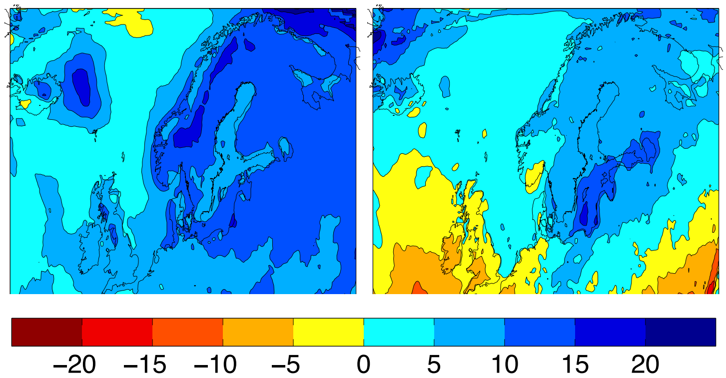

Figure 5.21: *Change in precipitation (%) in DJF (left panel) and JJA (right panel) comparing 2021–2050 with 1961–1990 (future minus control) for the 15-member multi-model ensemble mean from the CES project. Adapted from Fig. 3.1 in Thorsteinsson and Björnsson (2012).*

regardless of season. However, when one looks at results from individual scenario simulations the picture is quite different. Figure 5.22 shows relative changes in

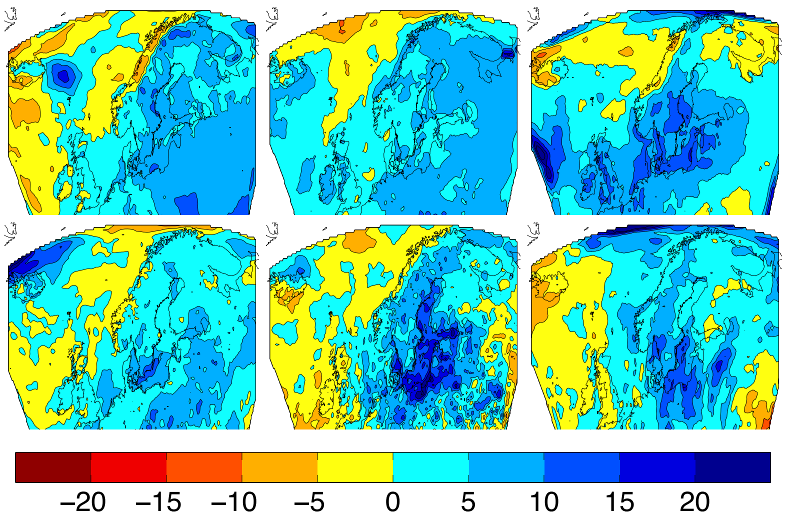

Figure 5.22: *Change in precipitation (%) in DJF (top panel) and JJA (bottom panel) comparing 2021–2050 with 1961–1990 (future minus control) for the DMI-HIRHAM-ECHAM5 (left), Met.No-HIRHAM-HadCM3Q0 (middle), and SMHI-RCA3-BCM simulations from the CES project. Same as Fig. 3.3 in Thorsteinsson and Björnsson (2012).*

precipitation for the three so-called recommended CES scenarios (cf. Table 3.1 in Thorsteinsson and Björnsson (2012)). These three reference simulations show considerable variability, both seasonal and spatial, with no clear consencus.

Similar seasonal variations, albeit for wind, have been reported for Ireland in Nolan et al. (2012). In this paper the authors use the COSMO-CLM model to scale down future climate scenarios (i.e. A1B and B1) from the ECHAM5. From a tvelwe member ensamble the authors conclude that the simulations show a marked increase in the amplitude of the annual cycle in wind strength with 9–13% more energy available during winter and 5–8% less during summer.

Chapter 6

General conclusions

Let us now restate our original research questions:

- Can one use a regional model to dynamically scale down a coarse resolution global atmospheric analysis to gain better understanding of temporal and spatial distribution of winds and precipitation in Iceland?
- What, if anything, is gained by increasing the horizontal resolution of the regional model?

As we have shown, than the answer to the first question is a definite "yes". The climate of Iceland is to a large extent governed by synoptic scale flow that impinges the topography. Both the flow and the topographical influence are relatively predictable. Therefore, this downscaling approach may work better for Iceland and surrounding waters, than for places with less predictable weather.

As for the second question, much additional information can be gained on both temporal and spatial variability of winds and precipitation by increasing the model resolution. The validity of model results is however strongly dependent on the quality of the initial atmospheric analysis and the ability of the model to correctly resolve the relevant physical processes, as well as parameterize the relevant sub-grid processes.

There are also limits to at which horizontal resolution current atmospheric models can operate. We will address these, and other eminent problems that emerge as one increases horizontal model resolution below 1 km, in the final chapter of this thesis.

Our main findings can be summarized as follows:

- Improvements in representation of topography in the numerical system lead to large and clear improvements in the accuracy of the simulated precipitation. This is both important for short range weather forecasts as well as for dynamical downscaling of past, present, and model scenarios of future climate.

- High resolution simulations are a useful and valuable tool to describe the temporal and spatial pattern of precipitation in the complex terrain of Iceland. A new methodology has been successfully applied:

  Validation of simulated annual precipitation with independent hydrological data from many watersheds.

  Validation of simulated winter precipitation by comparison with comparison of observed accumulated snow on a number of large ice caps.

- On a timescale of a day, or less, there are still substantial errors in simulated precipitation. Results on larger timescales (30 days and beyond) are better, but this is due to compensating errors on shorter timescales.

- The MM5 numerical simulations underestimate systematically precipitation immediately downstream of narrow (10 km) mountain ridges, independent of model resolution (8, 4, or 2 km). This underlines the need for high resolution observations of the atmospheric flow in the vicinity of the mountain ridge, as well as of the microphysical parameters.

- In spite of errros on short time scales, the numerical output is of great value for statistical analysis of various meteorological parameters.

- High resolution numerical simulations produce realistic orographic wind patterns. However, an in-depth investigation of a downslope windstorm reveals substansial sensitivity of the simulated surface winds to microphysical processes upstream of the mountain, through their influences on static stability.

- A new two-equation planetary boundary layer scheme, with a prognostic mixing length, captures well the magnitude of an extreme downslope windstorm.

Chapter 7

Onwards – yet more questions

The subtitle of this thesis, *Die zweite Aufgabe der theoretischen Meteorologie*, is taken from the 1904 *Das Problem der Wettervorhersage, betrachtet vom Standpunkte der Mechanik und der Physik* paper of Vilhelm Bjerknes. The work described in this thesis has to a large extent focused on atmospheric physics, how it is represented in atmospheric models, and consequently how these models can be used to gain a better understanding of the nature. An undertaking Bjerknes described as the second task of theoretical meteorology. Second indicates a *first*, and indeed Bjerknes describes the *erste Aufgabe* as well as the second one.

7.1 First task of theoretical meteorology

Numerical weather predictions are generated by integrating systems of differential equations forward in time. The equations are derived from the basic laws of physics and fluid motion. The initial state of this global modeling system is derived by merging observations from satellites, radio-sondes, and other sources, with the latest forecasting cycle. These measurements are taken all over the world, and over a certain period, usually the last six hours prior to the initiation time. This data assimilation methodology ensures that the initial state of the atmosphere, as simulated by the modeling system, is in close agreement with available observations, as well as being a solution to the system of differential equations.

The importance of data assimilation, albeit not called by that name at the time, was already realized by Vilhelm Bjerknes in early 1900s. In his 1904 paper Bjerknes expressed his vision and program for weather forecasting (Grønås, 2005). In this paper he states that “Based on the observations made, the first task of theoretical meteorology will then be to derive the clearest possible picture of the physical and dynamical state of the atmosphere at the time of the observations. This picture must be in a form that is appropriate to serve as a starting point for a weather prediction according to rational dynamical-physical methods[1]". Bjerknes realized that this task was not possible at the time, essential data was missing from over the oceans and upper-air observations were lacking as well.

7.1.1 Data assimilation

As stated by A. J. Simmons in his Vilhelm Bjerknes medal lecture at the EGU conference in Vienna in 2012: "The key to addressing Bjerknes's first task has been the development of data assimilation. Data assimilation provides a sequence of analyses of atmospheric and related oceanic and land-surface conditions. It uses information from the latest observations to adjust a background model forecast initiated from the preceding analysis in the sequence. The model carries information from earlier observations forward in time, and information is spread in space and from one variable to another by the model forecast and through the background-error structures used in the adjustment process. The set of observations may comprise many different types of measurement, each with its own accuracy and spatial distribution." Essentially, the core of any data assimilation system is to balance the observational and forecast uncertainty (cf. Fig. 7.1).

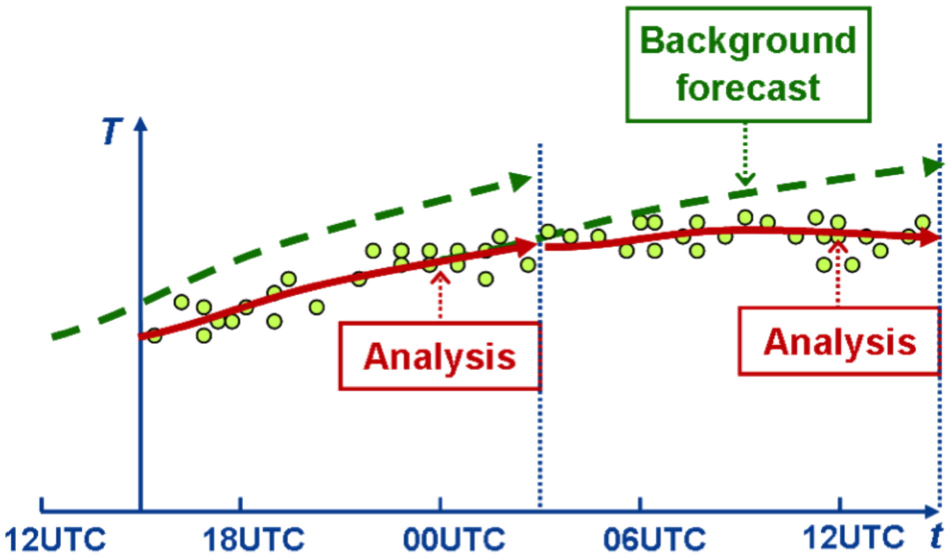

Figure 7.1: *To produce an estimate of the atmospheric state, data assimilation blends information from observations, short background forecast, estimates of observational and background errors, and dynamical relationships built into the representation of background errors. From Simmons (2012).*

[1]From the english translation of the Bjerknes 1904 paper, Bjerknes (2009).

Edward Lorenz argues in his 1982 paper that the Root Mean Square (RMS) difference curve (cf. Fig. 7.2) is the limit of the forecast improvement that is possible without reducing the day-1 forecast error, assuming that the model has realistic intrinsic error-growth characteristics. As can clearly be seen in Fig. 7.2 about half of

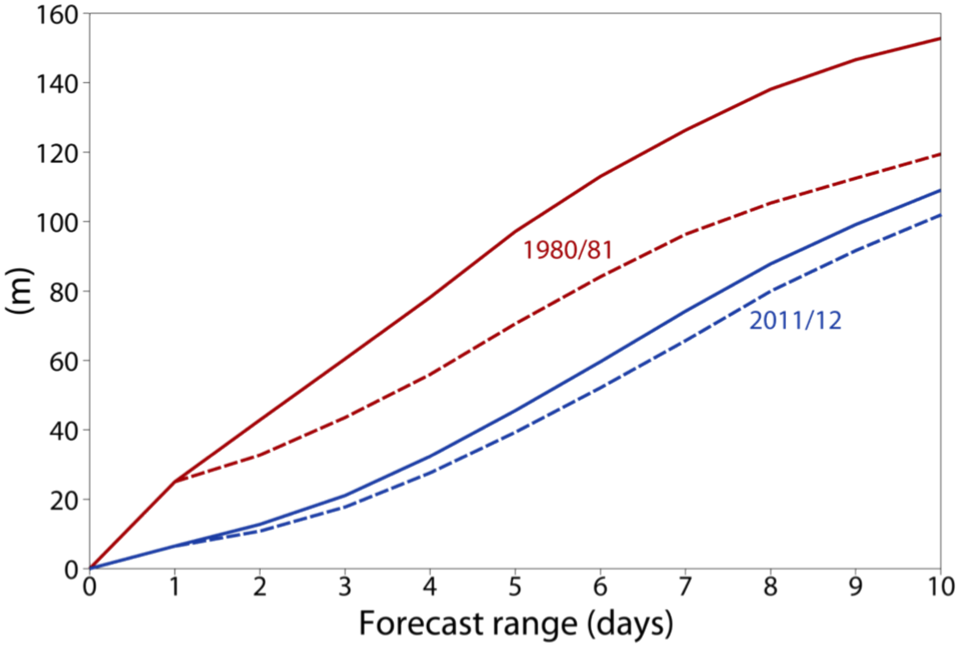

Figure 7.2: *Root Mean Square (RMS) error of the forecast (solid line) and RMS difference between successive daily forecasts (dashed lines) for the 500 hPa height for the period December to February in the extratropical northern hemisphere. Red lines are for 1980/81 and blue curves for 2010/11. From Simmons (2012).*

the ECMWF forecast improvements from 1980/81 to 2010/11 stems from improving the knowledge of the initial state of the atmosphere.

7.1.2 Potential of regional data assimilation

In recent years considerable advances have been made in data assimilation for regional models. Ready to use assimilation systems are now available for the WRF modeling system (e.g. DART[2], GSI[3] and WRFDA[4]), offering 3D-VAR, 4D-VAR, FDDA and EnKF methods. One can now also assimilate radiances data from satellites and/or ground based radars, although care must be taken when choosing which

[2]http://www.image.ucar.edu/DAReS/DART
[3]http://www.dtcenter.org/com-GSI/users
[4]http://www.mmm.ucar.edu/wrf/users/wrfda

channels should be used. One should also keep in mind that the quality of certain satellite data can be reduced if there is cloud cover. Global Positioning System (GPS) Radio Occultation (RO) data can provide high-resolution vertical profiles of refractivity, independent of cloud cover, and hence high-resolution profiles of temperature and humidity. Assimilation of this type of data has been shown to improve the operational forecasts of the Central Weather Bureau of Taiwan (Hong and Fong, 2012). In light of this, it would be a very interesting research task to investigate the potential of using data from the extensive GPS network in Iceland (cf. Fig. 3.2) to improve the atmospheric analysis, and consequently provide a better weather forecast.

7.2 Second task of theoretical meteorology

In the 1904 paper Bjerknes also describes the second task of theoretical meteorology as "...the second and most challenging task of theoretical meteorology will be to construct the pictures of the future states of the atmosphere from the picture of the current state of the atmosphere as a starting point, either according to the method outlined here, or according to a method of a similar kind[5]". The details of the second task were outlined in Lewis Fry Richardson's book *Weather prediction by numerical process* in 1922. The first numerical forecast, using an electronic computer, was then done by Charney, Fjörtoft and von Neumann in 1950 (Charney et al., 1950) The computer in question was named ENIAC and was the first general purpose computer ever built, a historical overview of this accomplishment can be found in Platzman (1979).

The methods used to tackle this task have continuously been improved upon to this day.

7.2.1 Terra Incognita

There are limitations that current one-dimensional planetary boundary layer (PBL) schemes face as the horizontal model resolution (Δ) approaches the scale, l, of the flux- and turbulent containing eddies. Current PBL schemes were simply not designed to be used when Δ and l are of the same order. This numerical region is termed "Terra Incognita" by Wyngaard (2004), and it is this region we now fast approach as the need for even higher horizontal resolution and more detailed model results is emerging.

The limits of running the WRF model below 1 km resolution was demonstrated in a recent study by Elíasson et al. (2011). In this study a comparison was made between measured and simulated in-cloud ice loading in E-Iceland. The simulated ice

[5]From the english translation of the Bjerknes 1904 paper, Bjerknes (2009)

loading was based on numerical data from the WRF model, describing the state of the atmosphere at high spatial and temporal resolution, ranging from 9 to 0.33 km. It is found that the model performance increases as the resolution is increased, especially when going from 3 km to 1 km, but only moderately when going from 1 km to 0.33 km.

A promising substitute to conventional PBL schemes is the 3D-TKE method, but flux issues need to be addressed and fixed (Rögnvaldsson et al., 2011) before this scheme can be used for real case applications.

7.2.1.1 Use of additional observations

The Elíasson et al. (2011) case study further shows that the results from the atmospheric model improve considerably when, in addition to the atmospheric analysis, the model is forced through nearby surface based observations of weather. This is especially important when the temperature is close to or just below 0°C as a small error in simulated temperature will strongly influence whether icing is taking place or not. Care must be taken when nudging the WRF model using only surface observations as the data may not be representative for the lowest part of the boundary layer in the case of low-level inversion.

As was pointed out in Jonassen et al. (2012), a clear advantage of using data from Unmanned Aerial Systems (UAS) rather than from automatic weather stations (AWS) is that it provides observations not only from near the surface, but also from an atmospheric column further aloft. Thereby, one can avoid several issues connected to e.g. the assimilation of only surface temperature observations, which are known to be especially problematic, e.g. Reen and Stauffer (2010).

Lack of observational turbulence data has also often been stated as a hindrance to improving PBL schemes (e.g. Lorsolo et al. (2010) and references therein). In this paper Lorsolo et al. describe a new method to assess the distribution of the turbulent energy in a hurricane using airborne Doppler measurements. The authors point out that when combined with surface wind and thermodynamic information, an accurate assessment of the TKE in the PBL could be used to estimate other important parameters, such as eddy diffusivity and dissipation, necessary to evaluate model parameterization schemes.

The kind of observations described in Lorsolo et al. require quite expensive observational platforms and can only be carried out by large governmental agencies such as NOAA. Another, and a much cheaper, approach was introduced by Reuder and Jonassen (2012). Here, the unmanned aerial system SUMO (Reuder et al., 2009), equipped with a miniaturized 5-hole probe, was used to observe the 3D turbulence field within a wind farm in Denmark. Granted, one cannot expect the SUMO, weighing less than one kilogram, to operate within a tropical cyclone. This platform has however proved quite useful in a number of field experiments in

Iceland, Norway, and Spitsbergen (e.g. Reuder et al. (2012); Jonassen et al. (2012)).

We must keep in mind that fluxes of momentum and heat are necessary lower boundary conditions for any PBL scheme. Hence, even if we have a "perfect" PBL scheme that could handle equally well sub filter-scale turbulences at a 10 km grid as on a 10 m grid, we would still be riddled with errors in the model results if the lower boundaries are not of equal quality. Hence, the quality of the land surface model is becoming ever greater as well as the accuracy of the underlying landuse characteristic and topography data. The quality and availability of the latter, i.e. the altitude data, has greatly improved with the emerging of the ASTER[6] (and most recently the ASTER2) data sets that has a 25 meter resolution and spans the globe from 85°south to 85°north.

Observations of hydrometeors are necessary to determine why the model does not capture lee side precipitation (i.e. the REX cases). Two theories were proposed in Rögnvaldsson et al. (2007a), but neither one can be verified or refuted without additional observations. This is needed in order to be able to see what parts of the model need to be improved upon. Recent research (Nicoll and Harrison, 2012) indicate that it may be possible to observe these cloud properties using relatively cheap and lightweight sensors, either via radio-sondes or deployed on UAS's. If proven useful, this kind of observations could become an option compared to expensive remote sensing measurements that can also be used for model evaluation and data assimilation. Han et al. (2012) use observations from a space-borne radiometer and a ground-based precipitation profiling radar to study the impact different cloud microphysics schemes in the WRF model have on the simulated microwave brightness temperature, radar reflectivity, and Doppler velocity, during a winter storm in California. Four microphysics schemes were tested, each having unique assumptions of particles size distributions, number concentrations, shapes, and hydrometeor fall speeds. These information are implemented into a satellite simulator and customized calculations for the radar are performed to ensure consistent representation of precipitation properties between the microphysics schemes and the radiative transfer models. This methodology of integrating an atmospheric model with a forward radiative transfer model has recently been used to evaluate model simulations and to improve model microphysics schemes (e.g. Matsui et al. (2009); Han et al. (2010); Li et al. (2010); Shi et al. (2010)). It is also one of the key components in algorithm development to retrieve or assimilate remote sensing data (Han et al., 2012).

[6]http://asterweb.jpl.nasa.gov/gdem.asp

7.3 Modeling of volcanic ash dispersion

Contrary to the data assimilation methodology used for global (and in some cases regional) weather forecasting, predictions of ash cloud dispersion make very limited use of observations far from the source of the eruption. The dispersion forecast starts at the source, e.g. an eruption column in Iceland, and the material is then transported along the wind track. Under normal weather conditions the atmospheric flow reaches Europe in a few days. During this time a variety of unknown natural processes affect the exact constituent and distribution of the ash cloud. Without the support of in-situ measurements, not only at the source (i.e. the erupting volcano), but also along the dispersion track, the simulated volcanic ash concentration will inevitably be too high as a consequence of the "safety first rule". This prediction technique needs to be improved by reducing the error that is generated during the propagation calculations.

The most important parameters used as input to the dispersion model, be it an Eulerian or Lagrangian one, are:

1. The scale of the eruption, including the erupted mass of ash.
2. The initial altitudes of the ash particles.
3. Eruption rate.
4. Grain size spectrum of the ash particles.

It should be stressed that in-situ and/or remote sensing observations at, or near, the source can improve the distribution forecast close to the erupting volcano (i.e. parameters 1 to 4 above). However, it is very difficult, if not impossible, to observe these parameters with adequate accuracy at the source, or even just to get the order of magnitude correct.

On the other hand, it is possible (up to a certain altitude) to observe parameters 2 and 4 (ash cloud height and grain size spectrum) downwind of the eruption using known and relatively simple techniques (Weber et al., 2012). When the eruption has been ongoing for some hours, and the ash cloud has been distributed some distance, these are the most important parameters to measure. The reason for this is twofold:

1. These parameters are advected with the atmospheric flow and are ultimately the parameters that affect air traffic safety.
2. Using observations, these parameters can be assimilated with the volcanic ash dispersion simulation, improving the ash distribution forecast.

As the eruption prolongs, and the volcanic ash is distributed over greater and greater distances it becomes necessary to observe parameters 2 and 4 over as much part of the affected area as possible.

A research project has been proposed to develop a new method, based on Kalman filtering, to assimilate measurements of volcanic ash density into a Eulerian dispersion model such as the Volcanic-WRF (Stuefer et al., 2012)[7]. The observations are to be collected in-situ from an airborne platform in the near-field of the crater (up to 200-300 km from the source). The objective is to generate more accurate forecasts than are available today where Lagrangian dispersion models are used to propagate the variables of the ash dispersion process for days without making corrections to the state variables, or model parameters, based on airborne measurements. The scientific value of this research project lies in the capability to predict and detect at any point in time with a high degree of accuracy the geographical boundaries where the concentration of volcanic ash exceeds the level that can be safely navigated by modern jet transport aircraft. For this purpose it is imperative that the measurements will be used in an optimal manner in order to correct the forecast variables and the model parameters where appropriate. Research done in other environmental areas, in particular in the Netherlands, has proven the value of applying certain types of Kalman filters for this purpose (Segers, 2002; Heemink and Segers, 2002). Hence this general approach is being proposed for the new research project focused on volcanic ash. The financial stakes are enormous as the disruption of air transport operations in Iceland has been very costly to the airlines and the tourism industry. It is also clear that this subject is of great interest to other European states that have experienced major disruptions of air transport due to volcanic ash emanating from volcanic eruptions in Iceland.

It should also be kept in mind that there is an actual possibility that, during an eruption, all international airports in Iceland may be closed, due to inaccurate ash distribution forecasts. The consequences of such airport, and airspace, closures could indeed proof dire.

[7] This version of WRF has been used to simulate the ash dispersion from the Mt. Eyjafjallajökull eruption in 2010 (Webley et al., 2012)

Bibliography

Andreae, M. O. and Rosenfeld, D., 2008. Aerosol cloud precipitation interactions. Part 1. The nature and sources of cloud-active aerosols. *Earth Science Reviews*, **89**: 13–41.

Arason, T., Rögnvaldsson, Ó. and Ólafsson, H., 2010. Validation of Numerical Simulations of Precipitation in Complex Terrain at high Temporal Resolution. *Hydrol. Res.*, **41**(3–4): 164–170.

Asai, T., 1965. A Numerical Study of the Air-Mass Transformation over the Japan Sea in Winter. *J. Meter. Soc. Japa.*, **43**: 1–15.

Bao, J. W., Michelson, S. A., Kantha, L. H. and Brown, J. W., 2008. Implementation of a Two–Equation Vertical Turbulent Mixing Scheme in a Mesoscale Atmospheric Model. NOAA Technical Memorandum OAR PSD–311. National Oceanic and Atmospheric Administration, Boulder, CO, 33 pp.

Berry, E. X. and Reinhardt, R. L., 1974. An Analysis of Cloud Drop growth by Collection: Part I. Double Distribution. *J. Atmos. Sci.*, **31**: 1814–1824.

Bjerknes, V., 1904. Das problem der wettervorhersage, betrachtet vom standpunkte der mechanik und der physik. *Meteorolog. Z.*, **21**: 1–7.

Bjerknes, V., 2009. The problem of weather prediction, considered from the viewpoints of mechanics and physics. *Meteorolog. Z.*, **18**(6): 663–667. Translated and edited by Volken E. and S. Bronnimann.

Bosart, L. F., 2003. Whither the Weather Analysis and Forecasting Process? *Weather and Forecasting*, **18**: 520–529.

Bougeault, P., Binder, P., Buzzi, A., Dirks, R., Houze, R., Kuettner, J., Smith, R., Steinacker, R. and Volkert, H., 2001. The map special observing period. *Bull. Amer. Meteor. Soc.*, **82**(3): 433–462.

Bright, D. R. and Mullen, S. L., 2002. The Sensitivity of the Numerical Simulation of the Southwest Monsoon Boundary Layer to the choice of PBL Turbulence Parameterization in MM5. *Wea. Forecasting*, **17**: 99–114.

Bromwich, D. H., Bai, L. and Bjarnason, G. G., 2005. High-resolution regional climate simulations over iceland using polar mm5. *Mon. Weather Rev.*, **133**(12): 3527–3547.

Charney, J. G. and Eliassen, A., 1949. A Numerical Method for predicting the Perturbations of the middle Latitude Westerlies. *Tellus*, **1**: 38–54.

Charney, J. G., Fjörtfoft, R. and Von Neumann, J., 1950. Numerical integration of the barotropic vorticity equation. *Tellus*, **2**(4): 237–254.

Chiao, S., Lin, Y.-L. and Kaplan, M. L., 2004. Numerical Study of the Orographic Forcing of Heavy Precipitation during MAP IOP-2B. *Mon. Weather Rev.*, **132**: 2184–2203.

Cotton, W. R., Bryan, G. and van den Heever, S. C., 2011. Chapter 4 - the parameterization or modeling of microphysical processes in clouds. G. B. William Cotton and S. van den Heever, editors, *Storm and Cloud Dynamics The Dynamics of Clouds and Precipitating Mesoscale Systems*, volume **99** of *International Geophysics*, pp. 87–142. Academic Press.

Déqué, M., Dreveton, C., Braun, A. and Cariolle, D., 1994. The ARPEGE/IFS atmosphere model: a contribution to the French community climate modelling. *C*limate Dynamics, **10**: 249–266.

Dudhia, J., 1989. Numerical study of convection observed during the winter monsoon experiment using a mesoscale two–dimensional model. *J. Atmos. Sci.*, **46**: 3077–3107.

Durran, D. R., 1990. Mountain Waves and Downslope Winds. W. Blumen, editor, *Atmospheric Processes Over Complex Terrain*, pp. 59–81. American Meteorological Society, Boston.

Elíasson, J., Rögnvaldsson, Ó. and Jónsson, T., 2009. Extracting Statistical Parameters of extreme Precipitation from a NWP Model. *Hydrol. Earth Syst. Sci.*, **13**: 2233–2240.

Elíasson, Á. J., Thorsteins, E., Ágústsson, H. and Rögnvaldsson, Ó., 2011. Comparison between simulations and measurements of in-cloud icing in test spans. *14th IWAIS (International Workshop on Atmospheric Icing of Structures) conference*. Chongqing, China. Extended abstract, 8 pages. Available on-line: http://www.wire1002.ch/fileadmin/user_upload/Major_events/WS_Nice_2011/-Spec._posters/ES1002_extended_abstract_Agustsson_ICING.pdf.

Feynman, R. P., Leighton, R. B. and L., S. M., 1963. The Feynman Lectures on Physics. Addison-Wesley Pub. Co.

Fletcher, N. H., 1965. The Physics of Rain Clouds. Cambridge University Press, Cambridge, first edition.

Giorgi, F. and Mearns, L. O., 1999. Introduction to special section: Regional climate modeling revisited. *J. Geophys. Res.*, **104**(D6): 6335–6352.

Grell, G. A., Dudhia, J. and Stauffer, D. R., 1995. A Description of the Fifth–Generation Penn State/NCAR Mesoscale Model (MM5). NCAR/TN–398+STR. National Center for Atmospheric Research, Boulder, CO, 107 pp.

Grønås, S., 2005. Vilhelm bjerknes vision for scientific weather prediction. *The Nordic Seas: an integrated perspective. Geophysical Monograph Series*, pp. 357–366. Am. Geophys. Union. 158.

Han, M., Braun, S. A., Matsui, T. and Williams, C. R., 2012. Evaluation of cloud microphysics schemes in simulations of a winter storm using radar and radiometer measurements. To appear in *J. Geophys. Res., Atmosphere*.

Han, M., Braun, S. A., Olson, W. S., Persson, P. O. G. and Bao, J.-W., 2010. Application of TRMM PR and TMI Measurements to Assess Cloud Microphysical Schemes in the MM5 for a Winter Storm. *J. Appl. Meteor. Climatol.*, **49**(6): 1129–1148.

Heemink, A. W. and Segers, A. J., 2002. Modeling and prediction of environmental data in space and time using kalman filtering. *Stochastic Environmental Research and Risk Assessment (SERRA)*, **16**(3): 225–240.

Hong, J.-S. and Fong, C.-T., 2012. Highlights of the Operational WRF-Based Numerical Prediction System at Central Weather Bureau of Taiwan. *13th Annual WRF Users' Workshop*. Boulder, Colorado. Available on-line: http://www.mmm.ucar.edu/wrf/users/workshops/WS2012/ppts/2.4.pdf.

IPCC, 2007. Stationary and quasi-stationary eddies in the extratropical troposphere: theory. Solomon, S., D. Qin, M. Manning, Z. Chen, M. Marquis, K.B. Averyt, M. Tignor and H.L. Miller, editor, *Contribution of Working Group I to the Fourth Assessment Report of the Intergovernmental Panel on Climate Change*. Cambridge University Press, Cambridge, United Kingdom and New York, USA.

Jonassen, M. O., Ólafsson, H., Ágústsson, H., Rögnvaldsson, Ó. and Reuder, J., 2012. Improving high resolution numerical weather simulations by assimilating data from an unmanned aerial system. *Mon. Weather Rev.*, **140**(11): 3734–3756. Available on-line: http://journals.ametsoc.org/doi/abs/10.1175/MWR-D-11-00344.1journalCode=mwre.

Kristjánsson, J. E. and McInnes, H., 1999. The impact of Greenland on cyclone evolution. *Q. J. R. Meteorol. Soc.*, **125**: 2819–2834.

Li, X., Tao, W.-K., Matsui, T., Liu, C. and Masunaga, H., 2010. Improving a spectral bin microphysical scheme using trmm satellite observations. *Q. J. R. Meteorol. Soc.*, **136**(647): 382–399.

Lorenz, E. N., 1982. Atmospheric predictability experiments with a large numerical model. *Tellus*, **34**(6): 505–513.

Lorsolo, S., Zhang, J. A., Marks, F. and Gamache, J., 2010. Estimation and mapping of hurricane turbulent energy using airborne doppler measurements. *Mon. Weather Rev.*, **138**(9): 3656–3670.

Marshall, J. S. and Palmer, W. M., 1948. The Distribution of Raindrops with Size. *J. Atmos. Sci.*, **5**: 165–166.

Matsui, T., Zeng, X., Tao, W.-K., Masunaga, H., Olson, W. S. and Lang, S., 2009. Evaluation of long-term cloud-resolving model simulations using satellite radiance observations and multifrequency satellite simulators. *J. Atmos. Oceanic Technol.*, **26**: 1261–1274.

Meyers, M. P., DeMott, P. J. and Cotton, W. R., 1992. New Primar Ice-Nucleation Parameterization in an Explicit Cloud Model. *J. Appl. Meteor.*, **31**: 708–721.

Nakićenović, N., Alcamo, J., Davis, G., de Vries, B., Fenhann, J., Gaffin, S., Gregory, K., Grübler, A., Jung, T. Y., Kram, T., Lebre La Rovere, E., Michaelis, L., Mori, S., Morita, T., Pepper, W., Pitcher, H., Price, L., Riahi, K., Roehrl, A., Rogner, H. H., Sankovski, A., Schlesinger, M., Shukla, P., Smith, S., Swart, R., van Rooijen, S., Victor, N. and Dadi, Z., 2000. IPCC Special Report on Emissions Scenarios (SRES). Cambridge University Press, UK.

Nicoll, K. and Harrison, R. G., 2012. Cloud detection using disposable airborne sensors. *Geophysical Research Abstracts*, volume **14**. Vienna, Austria. Available on-line: http://meetingorganizer.copernicus.org/EGU2012/EGU2012-8218.pdf.

Nolan, P., Lynch, P. and Sweeney, C., 2012. Simulating the future wind energy resource of Ireland using the COSMO-CLM model. *Wind Energy*. Available on-line: http://dx.doi.org/10.1002/we.1554.

Ólafsson, H., 2000. Comment les Montagnes Ralentissent-Elles le Vent? *La Mètèorologie*, **8**(31): 19–24.

Ólafsson, H., 2003. Forecasting winds in the vicinity of mountains. Tech.rep., The Eumetcal Library. Available on the web: http://www.eumetcal.org/intralibrary/open_virtual_file_path/i204n4542t/forecasting_winds_in_the_vicinity_of_mountains.ppt.

Ólafsson, H. and Bougeault, P., 1997. The effect of rotation and surface friction on orographic drag. *J. Atmos. Sci.*, **54**: 193–210.

Platzman, G. W., 1979. The ENIAC Computations of 1950-Gateway to Numerical Weather Prediction. *Bull. Amer. Meteor. Soc.*, **60**: 302–312.

Qian, J.-H., Seth, A. and Zebiak, S., 2003. Reinitialized versus continuous simulations for regional climate downscaling. *Mon. Weather Rev.*, **131**(11): 2857–2874.

Reen, B. and Stauffer, D., 2010. Data assimilation strategies in the planetary boundary layer. *Boundary-Layer Meteorology*, pp. 1–33–33.

Reisner, J., Rasmussen, R. M. and Bruintjes, R. T., 1998. Explicit forecastin of supercooled liquid water in winter storms using the MM5 mesoscale model. *Q. J. R. Meteorol. Soc.*, **124B**: 1071–1107.

Reuder, J., Ablinger, M., Ágústsson, H., Brisset, P., Brynjólfsson, S., Garhammer, M., Jóhannesson, T., Jonassen, M., Kühnel, R., Lämmlein, S., Lange, T., Lindenberg, C., Malardel, S., Mayer, S., Müller, M., Ólafsson, H., Rögnvaldsson, Ó., Schäper, W., Spengler, T., Zängl, G. and Egger, J., 2012. Flohof 2007: an overview of the mesoscale meteorological field campaign at hofsjökull, central iceland. *Meteorol. Atmos. Phys.*, **116**: 1–13.

Reuder, J., Brisset, P., Jonassen, M., Müller, M. and Mayer, S., 2009. The small unmanned meteorological observer sumo: A new tool for atmospheric boundary layer research. *Meteorolog. Z.*, **18**(2): 141–147.

Reuder, J. and Jonassen, M. O., 2012. Turbulence measurements in a wind park with the Micro-UAS SUMO. *Geophysical Research Abstracts*, volume **14**. Vienna, Austria. Available on-line: http://meetingorganizer.copernicus.org/EGU2012/EGU2012-3471.pdf and http://presentations.copernicus.org/EGU2012-3471_presentation.pdf.

Richardson, L., 1922. Weather prediction by numerical process. University Press.

Rogers, R. and Yau, M., 1989. A short course in cloud physics. International series in natural philosophy. Pergamon Press.

Rögnvaldsson, Ó., 2011. Search and Rescue Software, Weather Prediction System assists Humanitarian Aid. *Meteorological Technology International*, pp. 76–78.

Rögnvaldsson, Ó., Bao, J.-W., Ágústsson, H. and Ólafsson, H., 2011. Downslope Windstorm in Iceland - WRF/MM5 Model Comparison. *Atmospheric Chemistry and Physics*, **11**: 103–120.

Rögnvaldsson, Ó., Bao, J.-W. and Ólafsson, H., 2007a. Sensitivity Simulations of Orographic Precipitation with MM5 and Comparison with Observations in Iceland during the Reykjanes EXperiment. *Meteorolog. Z.*, **16**(1): 86–98.

Rögnvaldsson, Ó., Crochet, P., and Ólafsson, H., 2004. Mapping of Precipitation in Iceland using Numerical Simulations and Statistical Modeling. *Meteorolog. Z.*, **13**(3): 209–219.

Rögnvaldsson, Ó., Jónsdóttir, J. F., and Ólafsson, H., 2007b. Numerical Simulations of Precipitation in the Complex Terrain of Iceland – Comparison with Glaciological and Hydrological Data. *Meteorolog. Z.*, **16**(1): 71–85.

Rögnvaldsson, Ó., Jónsdóttir, J. F., and Ólafsson, H., 2010. Dynamical Downscaling of Precipitation in Iceland 1961-2006. *Hydrol. Res.*, **41**(3–4): 153–163.

Rögnvaldsson, Ó. and Ólafsson, H., 2005a. Numerical simulations of the climatology of winds in the complex terrain of Iceland. Proc. Int. Conf. Alp. Meteorol. (ICAM), p. 4. Available on-line: http://www.map.meteoswiss.ch/map-doc/icam2005/pdf/poster-sesion-e/E39.pdf.

Rögnvaldsson, Ó. and Ólafsson, H., 2005b. The response of precipitation to orography in simulations of future climate. Proc. Int. Conf. Alp. Meteorol. (ICAM), p. 4. Available on-line: http://www.map.meteoswiss.ch/map-doc/icam2005/pdf/poster-sesion-d/D33.pdf.

Rögnvaldsson, Ó., Ágústsson, H. and Ólafsson, H., 2011. WRFLES – A system for high-resolution limited area numerical simulations. Tech.Rep. 1, Institute for Meteorological Research. Available on-line: ftp://betravedur.is/pub/wrf/icam2011/UniRes_WRFLES.pdf.

Schultz, P., 1995. An Explicit Cloud Physics Parameterization for Operational Numerical Weather Prediction. *Mon. Weather Rev.*, **123**: 3331–3343.

Segers, A., 2002. Data assimilation in atmospheric chemistry models using Kalman filtering. Ph.D. thesis. Available on-line: http://resolver.tudelft.nl/uuid:113b6229-c33a-4100-93be-22e1c8912672.

Shi, J. J., Tao, W.-K., Matsui, T., Hou, A., Lang, S., Peters-Lidard, C., Jackson, G., Cifelli, R., Rutledge, S. and Petersen, W., 2010. Microphysical Properties of the January 20-22 2007 Snow Events over Canada: Comparison with in-situ and Satellite Observations. *J. Appl. Meteor. Climatol.*, **49**: 2246–2266.

Simmons, A. J., 2012. Vilhelm Bjerknes's "First task of theoretical meteorology": Assimilation of observational data for atmospheric monitoring and forecasting. *Geophysical Research Abstracts*, volume **14**. Vienna, Austria. Available on-line: http://meetingorganizer.copernicus.org/EGU2012/EGU2012-14441.pdf and http://presentations.copernicus.org/EGU201214441_presentation.pdf.

Skamarock, W. C., Klemp, J. B., Dudhia, J., Gill, D. O., Barker, D. M., Duda, M. B., Huang, X.-Y., Wang, W. and Powers, J. G., 2008. A Description of the Advanced Research WRF Version 3. NCAR Technical Note, NCAR/TN–475+(STR). National Center for Atmospheric Research, Boulder, CO, 113 pp.

Smith, R. B., 1989. Hydrostatic Airflow over Mountains, volume 31 of *Advances in Geophysics*. Academic Press.

Stensrud, D. J., 2007. Parameterization Schemes. Cambridge University Press, Cambridge, first edition.

Stoelinga, M. T., Hobbs, P. V., Mass, C. F., Locatelli, J. D., Colle, B. A., Houze, Jr., R. A., Rangno, A. L., Bond, N. A., Smull, B. F., Rasmussen, R. M., Thompson, G. and Colman, B. R., 2003. Improvement of Microphysical Parameterization through Observational Verification Experiment. *Bull. Amer. Meteor. Soc.*, **84**: 1807–1826.

Stuefer, M., Freitas, S. R., Grell, G., Webley, P., Peckham, S. and McKeen, S. A., 2012. Inclusion of Ash and SO_2 emissions from volcanic eruptions in WRF-CHEM: development and some applications. *Geoscientific Model Development Discussions*, **5**(3): 2571–2597.

Stull, R. B., 1988. An Introduction to Boundary Layer Meteorology. Atmospheric Sciences Library. Kluwer Academic Publisher, London.

Stull, R. B., 2006. The Atmospheric Boundary Layer. J. M. Wallace and P. V. Hobbs, editors, *Atmospheric Science. An Introductory Survey*, volume 92 of *International Geophysics Series*, pp. 375–418. Elsevier, London.

Thorsteinsson, T. and Björnsson, H., editors, 2012. Climate Change and Energy Systems: Impacts, Risks and Adaptation in the Nordic and Baltic countries. Nordic Council of Ministers, Copenhagen.

Walko, R. L., Cotton, W. R., Meyers, M. P. and Harrington, J. Y., 1995. New RAMS cloud microphysics parameterization. Part I: The single–moment scheme. *Atmos. Res.*, **38**: 29–62.

Wallace, J. M. and Hobbs, P. V., 2006. Atmospheric Science: An Introductory Survey. Academic Press, New York.

Warner, T. T., 2011. Numerical Weather and Climate Prediction. Cambridge University Press, Cambridge, first edition.

Warner, T. T., Peterson, R. A. and Treadon, R. E., 1997. A Tutorial on Lateral Boundary Conditions as a Basic and Potentially Serious Limitation to Regional Numerical Weather Prediction. *Bull. Amer. Meteor. Soc.*, **78**: 2599–2617.

Weber, K., Eliasson, J., Vogel, A., Fischer, C., Pohl, T., van Haren, G., Meier, M., Grobéty, B. and Dahmann, D., 2012. Airborne in-situ investigations of the Eyjafjallajökull volcanic ash plume on Iceland and over north-western Germany with light aircrafts and optical particle counters. *Atmospheric Environment*, **48**: 9–21.

Webley, P. W., Steensen, T., Stuefer, M., Grell, G., Freitas, S. and Pavolonis, M., 2012. Analyzing the Eyjafjallajökull 2010 eruption using satellite remote sensing, lidar and WRF-Chem dispersion and tracking model. *J. Geophys. Res.*, **117**.

Wyngaard, J. C., 2004. Toward Numerical Modeling in the "Terra Incognita". *J. Atmos. Sci.*, **61**: 1816–1826.

Peer reviewed papers

Paper I: Mapping of Precipitation in Iceland using Numerical Simulations and Statistical Modeling

Meteorologische Zeitschrift, Vol. **13**, No. 3, 001-010 (June 2004)
© by Gebrüder Borntraeger 2004

Article

Mapping of precipitation in Iceland using numerical simulations and statistical modeling

ÓLAFUR RÖGNVALDSSON[23], PHILIPPE CROCHET[1] and HARALDUR ÓLAFSSON[124]

[1]Icelandic Meteorological Office, Reykjavík, Iceland
[2]Institute for Meteorological Research, Reykjavík, Iceland
[3]University of Bergen, Iceland
[4]University of Iceland, Reykjavík, Iceland

(Manuscript received August 8, 2003; in revised form January 8, 2004; accepted May 5, 2004)

Abstract

Precipitation in Iceland during a period of 10 years is simulated with the PSU/NCAR MM5 model. The results are compared with precipitation estimated by a statistical model based on observations and a number of topographic and geographic predictors. The simulated precipitation pattern agrees with the statistical model in areas where data is available and gives a credible precipitation pattern in data-sparse mountainous regions. The simulation is however in general overestimating the precipitation, but the magnitude and the seasonal and geographical distribution of the overestimation indicate that it is to some extent associated with observation errors that are due to wind-loss of solid precipitation. There are also uncertainties associated with the representativeness of the observations as well as with the reference model itself.

Zusammenfassung

Niederschlag in Island wurde mit dem PSU/NCAR MM5 Modell für eine 10-Jahresperiode simuliert. Die Modellresultate werden mit Niederschlagsschätzungen eines statistischen Modells verglichen, das auf Beobachtungen und auf einer Reihe von topographischen und geographischen Prediktoren basiert. Das simulierte Niederschlagsmuster stimmt für Gebiete, in denen Daten verfügbar sind, mit dem statistischen Modell überein und liefert in Gebirgsregionen mit schlechter Datenabdeckung glaubwürdige Niederschlagsmuster. Die Simulation ueberschätzt jedoch generell die Niederschlagsmengen. Dabei deuten die Amplitude und die saisonale und geographische Verteilung der Abweichung darauf hin, dass dies zu einem Teil mit Beobachtungsfehlern verknüpft ist, die durch windbedingte Verluste von festem Niederschlag entstehen. Zudem existieren Unsicherheiten in Zusammenhang mit der Repräsentativität der Beobachtungen, sowie des Referenzmodells selbst.

1 Introduction

The aim of this study is to verify the precipitation simulated by a limited area atmospheric model, the PSU/NCAR MM5 (WANG et al., 2001), in Iceland. One of the reasons for using a limited area model to simulate precipitation is to obtain a dataset of the current climate for comparison with down-scaling of future climate from coupled atmospheric and oceanic simulations by GCMs.

Attempts have been made to simulate precipitation in mountainous terrain. In the recent PRUDENCE project simulations with five numerical models were compared to an observation-based reference in the Alps. The models performed quite satisfactorily, but produced consistently too little precipitation (FREI et al., 2003).

Precipitation in Iceland is largely associated with extra-tropical synoptic systems. It often occurs during strong winds and can be greatly enhanced locally by the mountainous terrain (VRIES M. DE and ÓLAFSSON, 2003). Due to this and a coarse observation network, the direct use of an interpolation method for mapping precipitation is considered not to be sufficiently reliable. To map the reference precipitation and to minimize the uncertainties related to scale issues (see TUSTISON et al. (2001)), some further modeling is therefore needed.

In the past years, various studies have described the statistical links between precipitation and topographic parameters (see for instance BENICHOU and BRETON (1987); DALY et al. (1994); BASIST et al. (1994); WOTLING et al. (2000); KIEFFER et al. (2001) and DROGUE et al. (2002)) and the joint effect of topographic and atmospheric parameters (KYRIAKIDIS et al., 2001). In the present paper, a similar approach is considered to model and map the precipitation of reference (hereafter called REF) used to verify the MM5 simulations.

This paper is organized as follows: In the next section we will give a short introduction to the observational data, followed by a short description of the mod-

*Corresponding author: Haraldur Ólafsson, Bústaðavegur 9, IS-150 Reykjavík, Iceland, e-mail: haraldur@vedur.is

0941-2948/04/0013-0001 $ 3.15
DOI: 10.1127/0941-2948/2004/0013-0001
© Gebrüder Borntraeger, Berlin, Stuttgart 2004

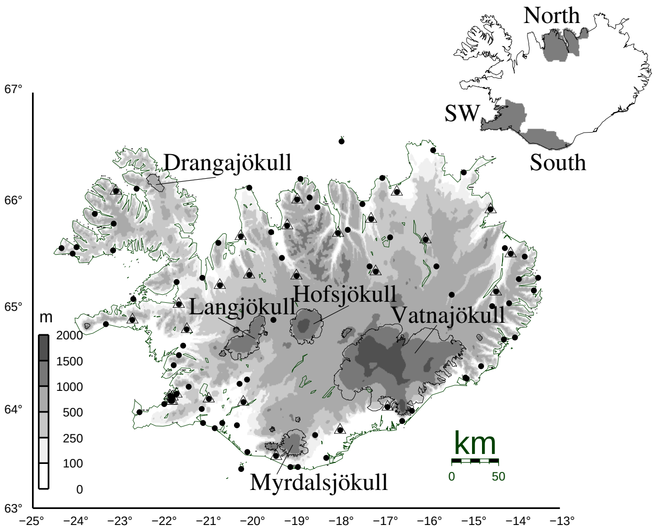

Figure 1: Map of Iceland showing regions North, South and SW (upper right corner) as well as position of rain gauges. Circles indicate the calibration network whilst triangles show the validation network. The largest glaciers are also shown.

Table 1: The geographic (top two) and topographic (bottom three) predictors used in SMOD.

	Geographic predictors:
1	D_{min} – minimum distance to the sea [km]
2	Y coordinates (lambert conformal) [km]
	Topographic predictors:
3	Smooth elevation [m]
4	Average slope steepness [%]
5	Average hillslope orientation, $-180° < \theta < 180°$ $0° < \theta < 180°$ clockwise from N to S $-180° < \theta < 0°$ clockwise from S to N

els. The results will be presented in section 4, followed by discussions and concluding remarks. A more detailed description of the mapping procedure is given in an appendix at the end of the paper.

2 Observational data

The observational precipitation data used in this study originates from 90 rain-gauges measuring daily precipitation (see Figure 1). The density of this network varies over Iceland. Most of the stations are located near the coast at elevations lower than 200 m, hence, data coverage is poor in the interior and in other high altitude regions. The measured precipitation may underestimate the true ground precipitation. The magnitude of the error depends on the wind-speed and the under-catch is more pronounced for solid (especially snow) than liquid precipitation (see review by HARALDSDÓTTIR et al. (2001), citing FØRLAND et al. (1996)).

In the present study, no correction was considered to account for the wind loss, or loss due to wetting or evaporation. This is mainly due to the fact that wind data is not available.

The season average monthly precipitation was derived over a ten year period from January 1991 to December 2000. The four seasons are defined as follows: March through May (MAM), June through August (JJA), September through November (SON) and finally December through February (DJF).

3 Model description

3.1 Statistical modeling

The statistical model (SMOD) used in this study makes use of five predictors. Two of them are related to the geographic position of the sites whilst the other three are related to the broad-scale topographic environment around the gauge sites (Table 1). The three topographic predictors were derived from a digital elevation model (DEM) of 1 km resolution (Figure 1), considering a 10 km averaging window. This choice was somehow arbitrary but in line with results suggested by other studies (see for instance DALY et al. (1994), and KYRIAKIDIS et al. (2001)). The slope steepness and orientation were defined with respect to a North (y) and East (x) plane. The statistical relationship between the season average monthly precipitation and the five predictors was evaluated individually for nine regions D and each season k by multivariate least-squares regression:

$$R(u,k) = a_{0,k,D} + \sum_{j=1}^{5} a_{j,k,D}\, p_{j,u} \quad (u \in D) \qquad (3.1)$$

Where $R(u,k)$ is the season average monthly precipitation at location u and season k. Further, $p_{j,u}$ is the j^{th} predictor at location u and $a_{j,k,D}$ is the j^{th} regression coefficient for season k and region D. The nine regions were defined by merging together different topographic domains in order to have enough observations to calibrate the statistical model. These topographic domains were delineated by applying the method of the watershed transform (see for instance ROERDINK and MEIJSTER (2001)) to the reverted DEM, (DREM). In the DREM, the reverted elevation of each grid point rh_u, is defined by subtracting the DEM elevation h_u from the maximum DEM elevation h_{max}:

$$rh_u = h_{max} - h_u \qquad (3.2)$$

In doing so, the valleys become peaks and the peaks valleys, and the delineated "watersheds" defined the different massifs. Figure 2 presents the different regions. Table 2 gives the number of gauges and the approximate size of each region, of which some overlap. Table 3 summarizes the results of the multiple linear regressions.

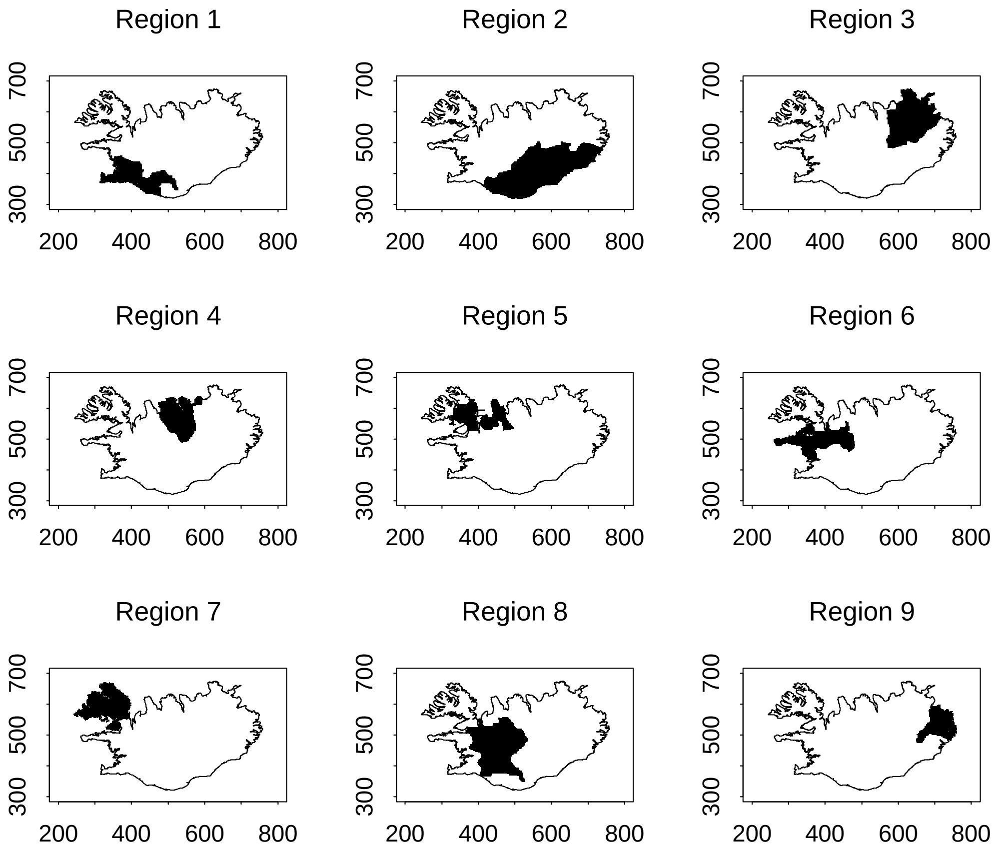

Figure 2: The nine different regions of SMOD (*D*). Scales are in km.

The predictors explain in average more than 80% of the variance of the season average monthly precipitation in Iceland for the considered period. The winter season (DJF) displays in average the poorest R-squared. This result suggests that the predictors are not as powerful to explain the complexity of the spatial variability of precipitation for this season with mixed precipitation phases and stronger wind regime as for the other seasons. Table 5, in the appendix, presents the regression equations. The poor network density makes the uncertainty of the regression coefficients relatively large. Nevertheless, it is worth noting that a positive relationship is observed between precipitation and elevation in most cases, with a more pronounced effect during SON and DJF than MAM and JJA. The exception is for region 3 at all seasons where higher precipitation amounts are observed by the coast than in the highlands, leading to a negative contribution of the elevation. The same negative contribution of elevation is observed during JJA for regions 7 and 9 where the network is mainly located in the bottom of steep narrow fjords or valleys. The relationship between precipitation and slope is negative in the north and northwest (regions 4, 5 and 7) at all seasons and positive elsewhere except in region 9 during DJF. This, together with the sign of the regression coefficient related to the orientation describe a precipitation enhancement and/or rain shadow effects along the hillslope according to its steepness and orientation. There is a negative relationship between precipitation and the latitude in the south and a positive relationship in the north. The contribution of the minimum distance to the sea is not clearly defined, but the tendency is a reduction of precipitation from the coast towards the inland, with some exceptions for regions where the available network is mainly coastal and where there is some correlation between elevation and distance to the sea.

A more comprehensive description of the precipitation mapping is given in the appendix.

Table 2: Region, number of gauges per region and the area of each region in km^2.

	MAM	*JJA*	*SON*	*DJF*
Region 1 (12276)	19	20	20	19
Region 2 (31060)	13	13	13	13
Region 3 (16628)	9	9	9	9
Region 4 (11208)	11	11	11	11
Region 5 (9528)	7	7	7	8
Region 6 (12492)	10	9	9	9
Region 7 (12816)	8	8	7	8
Region 8 (21272)	12	12	12	12
Region 9 (7636)	10	8	8	9

Table 3: Multiple R-squared and F ratio (in brackets).

	MAM	*JJA*	*SON*	*DJF*
Region 1	0.84 (13)	0.89 (22.5)	0.845 (15)	**0.7 (6)**
Region 2	0.65 (2.6)	0.75 (4.25)	0.61 (2.23)	**0.58 (1.9)**
Region 3	0.93 (8.2)	0.89 (5.2)	0.96 (13.4)	**0.87 (4.1)**
Region 4	0.76 (3.2)	**0.59 (1.5)**	0.73 (2.7)	0.72 (2.5)
Region 5	0.75 (0.6)	0.95 (3.7)	0.98 (9.8)	**0.55 (0.5)**
Region 6	0.92 (10.14)	**0.7 (1.4)**	0.9 (5.6)	0.89 (4.7)
Region 7	**0.83 (2)**	0.99 (59)	0.99 (818)	0.89 (3.4)
Region 8	0.89 (10.2)	**0.87 (8)**	0.88 (9.37)	0.9 (11.4)
Region 9	0.86 (5.1)	0.99 (74)	**0.83 (1.9)**	0.89 (5.2)
Mean R-squared	0.852	0.846	0.858	**0.777**

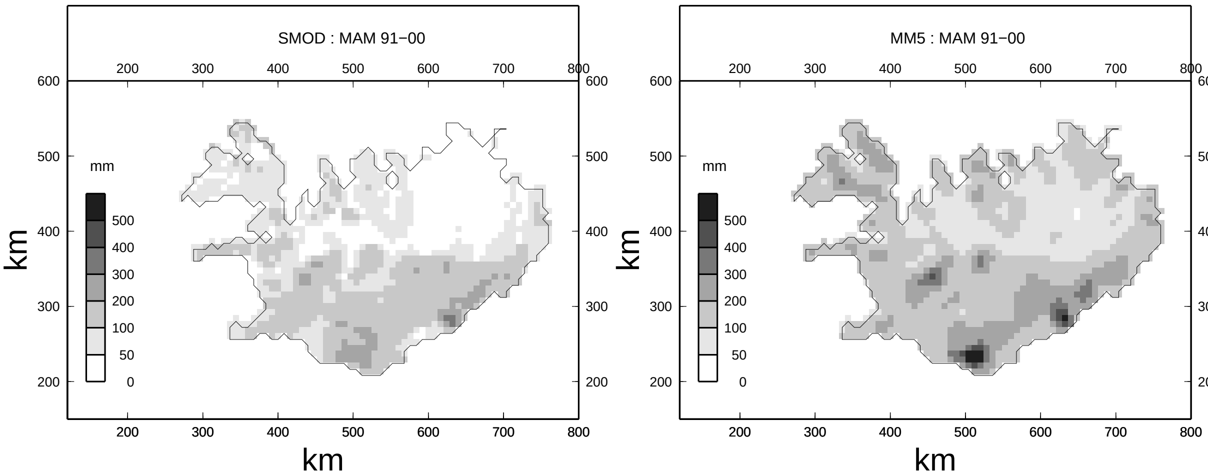

Figure 3: Season average monthly precipitation for MAM 1991–2000 [mm]. Reference precipitation is shown in (a) and simulated by MM5 in (b).

3.2 Numerical modeling

The PSU/NCAR MM5 model is a state of the art non-hydrostatic limited area model. It solves the pressure equations and the three dimensional momentum and thermo-dynamical equations that describe the atmosphere, using finite difference methods. The equations are integrated in time on an Arakawa-Lamb B grid using a second-order leapfrog scheme. Some terms, like the fast moving sound waves, are handled using a time-splitting scheme (DUDHIA, 1993). There is a terrain following vertical coordinate, σ, defined as:

$$\sigma = \frac{p_0 - p_t}{p_s - p_t}$$

Here p_0 is the reference pressure in a constant reference state, p_t is the constant pressure at the model top and p_s is the reference pressure at the surface.

3.2.1 Experimental setup

The domain used is 123 $\times$ 95 points, centered at 64° N and 19.5° W, with a horizontal grid spacing of 8 km. There are 23 vertical levels with the model top at 100 hPa.

In this study, the turbulent boundary layer is parameterized according to HONG and PAN (1996) and cloud physics and precipitation (microhpysics) processes according to GRELL et al. (1995) and REISNER et al. (1998), respectively. The version of the microphysical scheme used (Reisner2) includes cloud and rain water, as well as ice phase and super-cooled water. It further includes graupel and ice number concentration prediction equations. At the model top the radiation boundary condition formulated by KLEMP and DURRAN (1983) has been applied in order to minimize the reflection of vertically propagating gravity waves. Atmospheric long wave radiation is parameterized by the RRTM scheme, (MLAWER et al., 1997), and short wave radiation by DUDHIA (1993). For ground temperature we use the OSU/LSM scheme (CHEN and DUDHIA, 2001). The model, being run in a distributed memory mode, is forced by initial and boundary conditions from the European Centre for Medium range Weather Forecasts (ECMWF). The data used is from the ERA40 reanalysis project, having been interpolated from a horizontal grid of 1.25° to 0.5° prior to being applied to the MM5 modeling system.

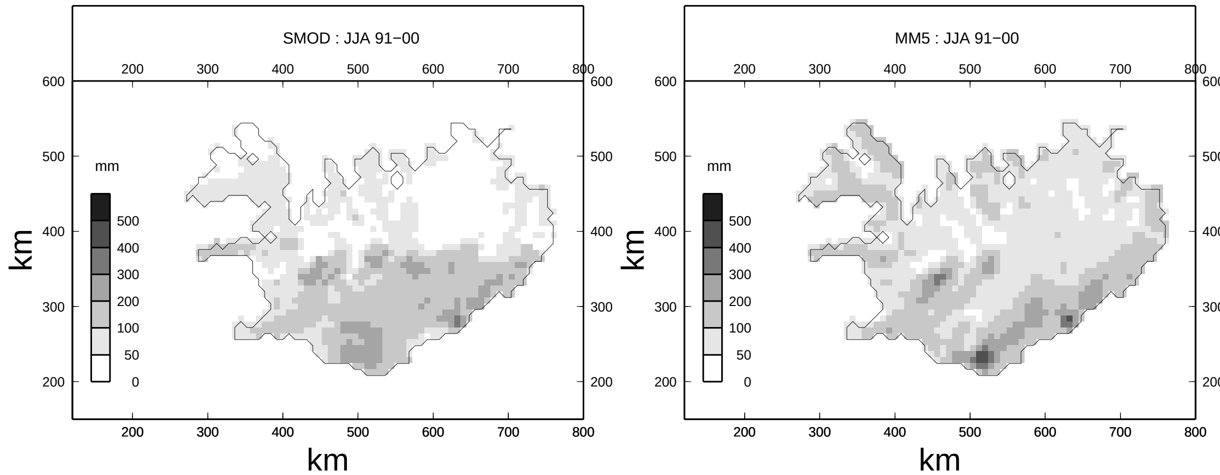

Figure 4: Season average monthly precipitation for JJA 1991-2000 [mm]. Reference precipitation is shown in (a) and simulated by MM5 in (b).

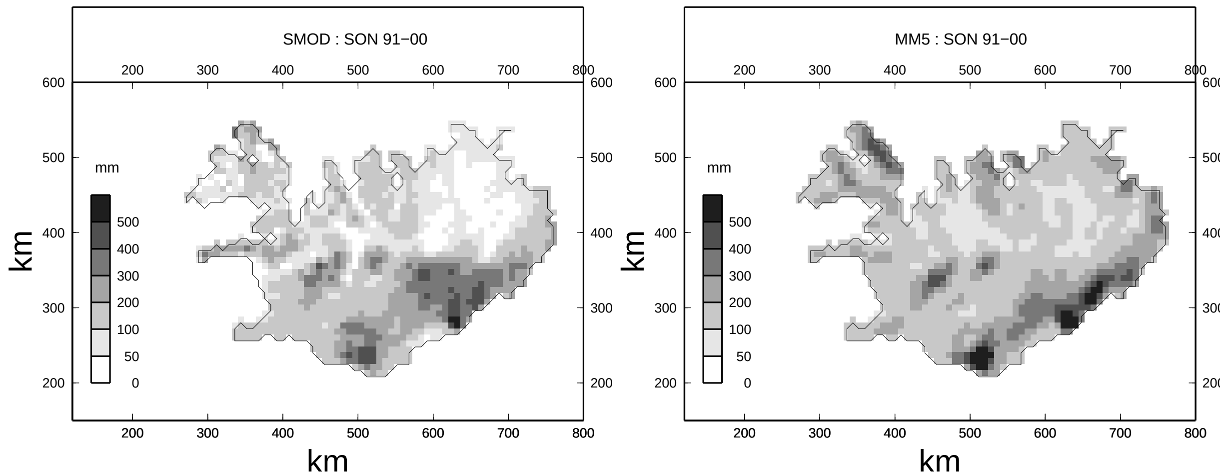

Figure 5: Season average monthly precipitation for SON 1991-2000 [mm]. Reference precipitation is shown in (a) and simulated by MM5 in (b).

4 Results

4.1 Qualitative comparison

The season average monthly precipitation for the period 1991 to 2000 is given in Figures 3 to 6. The overall pattern in the MM5 simulation is in a good agreement with REF, the greatest precipitation being along the south- and southeast-coast of Iceland. The precipitation gradient from southwest-Iceland to the northeast, towards Langjökull and Hofsjökull glaciers, is also present in both models. The precipitation gradients and the variability looks in general similar to REF, although being somewhat stronger in MM5. The most noticeable exceptions are in northwest-Iceland and at the northwest-part of Vatnajökull glacier. Estimation of precipitation in both these regions is uncertain, both due to lack of observations and the unrepresentative sampling of the topography of the regions by the observation network.

4.2 Quantitative validation

For quantitative validation of the numerical simulation, three regions have been defined. These regions are named North, South and SW and they are shown in the upper right corner of Figure 1. All these regions have a relatively dense observation network. In all regions, MM5 produces a precipitation pattern which agrees fairly well with the reference. Figure 7 shows the mean absolute relative error of precipitation simulated by MM5 compared to the reference precipitation. In the North the numerical simulation overestimates the observed precipitation from December to May by $110-130\%$, while the overestimation in summer and fall is around 80%. In the SW region the mean simulated precipitation is overestimated by about $20-50\%$ with the largest error being in the winter and spring. In the South the overestimation during summer and fall is about 30% and about 50% during spring and the winter months.

Figure 8 shows the precipitation as a function of altitude for all grid points in regions North and SW for both REF and MM5 during JJA. Figure 9 shows the same but for season DJF. It is clear that both the precipitation variability and the increase of precipitation with altitude (slope) is greater in MM5 than in REF in region North

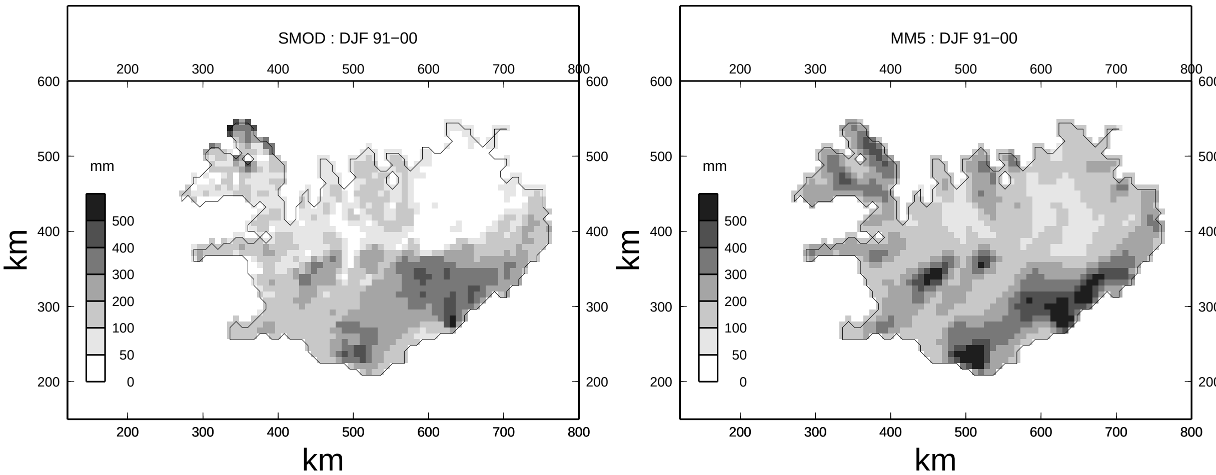

Figure 6: Season average monthly precipitation for DJF 1991-2000 [mm]. Reference precipitation is shown in (a) and simulated by MM5 in (b).

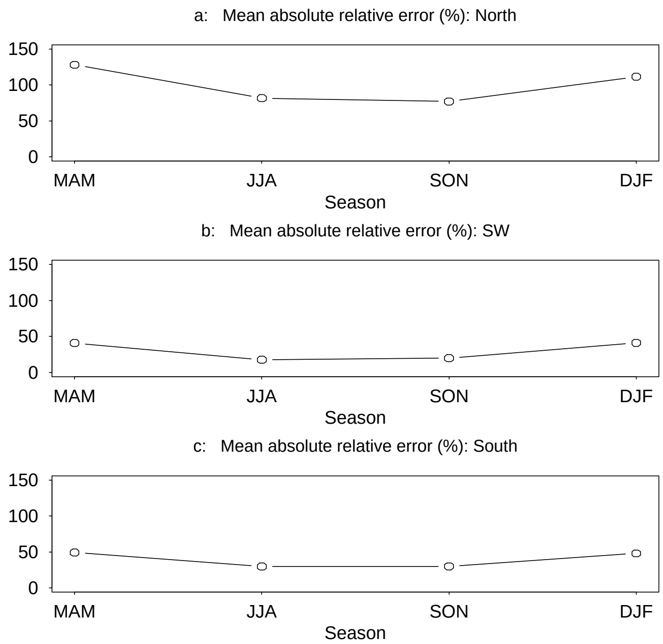

Figure 7: Mean absolute relative error [%], defined as $100 \cdot \frac{|MM5--REF|}{REF}$, of MM5 for regions (a) North, (b) SW and (c) South.

for both seasons. The slope is about four times that of REF in JJA and about double in DJF. It is also worth noting that the intercept, i.e. the precipitation at zero elevation, is higher in MM5 than REF, especially during the winter months. During these months the intercept in MM5 is about twice that of REF in region North. In JJA the intercept in MM5 is about 50% greater than in REF. In DJF the precipitation variability in regions SW and South (not shown) is similar to REF in MM5. The same holds true for JJA, but to a less extent. During the winter months the intercept is also slightly higher in MM5 and the slope being nearly twice the slope of REF. During JJA the intercept is nearly identical but the slope being again greater in MM5 than REF.

5 Discussion

The overestimation of precipitation in the MM5 simulations is greater in the north than it is in the south and southwest of Iceland. This is presumably due to both problems in the MM5 modeling system as well as greater uncertainties of the reference precipitation in the north. One source of uncertainty in the reference is the unrepresentativeness of the observation network. In fact, mapping of precipitation in complex terrain is highly depended upon the density of observations (e.g. FREI and SCHÄR (1998)). In Iceland, there is significant small scale variability in the orography and the observation sites are situated at low altitudes and close to the coast. This is particularly true for region North. The small scale variability in the orography introduces problems in the MM5 simulations as it is not resolved with the current resolution. Associated with this is that MM5 could be simulating to much precipitation at high altitudes, i.e. the precipitation gradient (slope) being to strong. The model could further be overestimating the background precipitation in the northern part of Iceland.

Another possible source of the discrepencies between REF and MM5 is that the reference is underestimating the true precipitation because of wind loss, wetting of the gauges and evaporation. This could explain to some extent the larger overestimation of MM5 during winter and spring than summer and fall. In strong winds conventional observations of solid precipitation underestimate grossly the true ground precipitation. Observation studies of solid precipitation (see review by HARALDSDÓTTIR et al. (2001)) suggest that at wind speeds greater than about 7 m/s, conventional precipitation gauges capture less than half of the true precipitation. Precipitation during winter and spring in region North (Figure 1) falls largely in the form of snow and often during strong winds. A large part of the overestimation of the simulated precipitation there may therefore

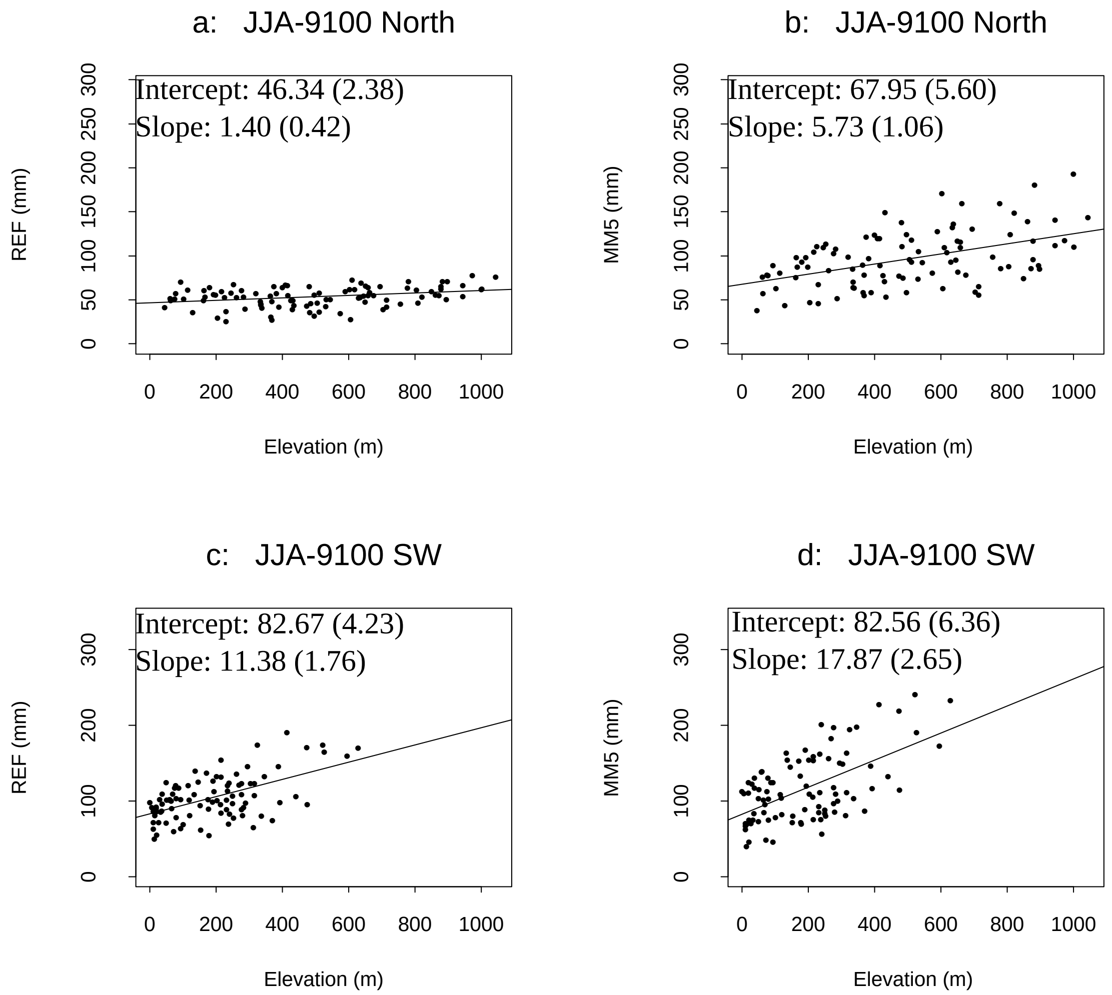

Figure 8: Season average precipitation as a function of elevation in JJA. (a) REF – region North, (b) MM5 – region North, (c) REF – region SW and (d) MM5 – region SW. Upper left corner of the figures shows the intercept [mm] and the slope [mm/100m].

be considered to be due to wind loss in the observations. If the precipitation is liquid, the wind loss is much less than if the precipitation is solid. This corresponds to the overestimation being less in the period June to November when most of the precipitation is liquid. In the summer and fall, there is still considerable overestimation of the precipitation in region North. The observed precipitation in the summer in the northern lowlands is typically only about 40 mm a month, but distributed over a relatively large number of days. In such weather, loss of observed precipitation due to wetting of the precipitation gauges and evaporation can also be expected to be of importance and observation errors therefore still account for some part of the difference between the two models.

In regions South and SW a much smaller part of the precipitation is solid, even during the winter. Accordingly, the simulation gives a much less overestimation than in the North. As in the North the greatest overestimation is in the winter and spring and loss of observed precipitation due to strong winds must still be regarded as an important source of error in the reference. The amount of precipitation in summer and fall is also considerably greater than in the North, and accordingly, loss due to wetting and evaporation is a smaller proportion of the total precipitation.

The results indicate that MM5 is overestimating the difference between upslope and downstream slopes as there is more precipitation variability for a given elevation than in REF. This may be related to the coarse resolution of the MM5 simulations.

Simulations that were made over a number of subperiods revealed little sensitivity of the MM5 simulations to both the land surface scheme and the domain size for the domain used in the current simulations and a 45% larger domain.

As previously stated, almost all precipitation observation sites in Iceland are located below 200 m.a.s.l. and REF must therefore be considered to be less reliable at high elevations than in the lowlands. The relatively high simulated values of precipitation in the mountains within the three regions may therefore be more realistic than a direct comparison with the current REF suggests.

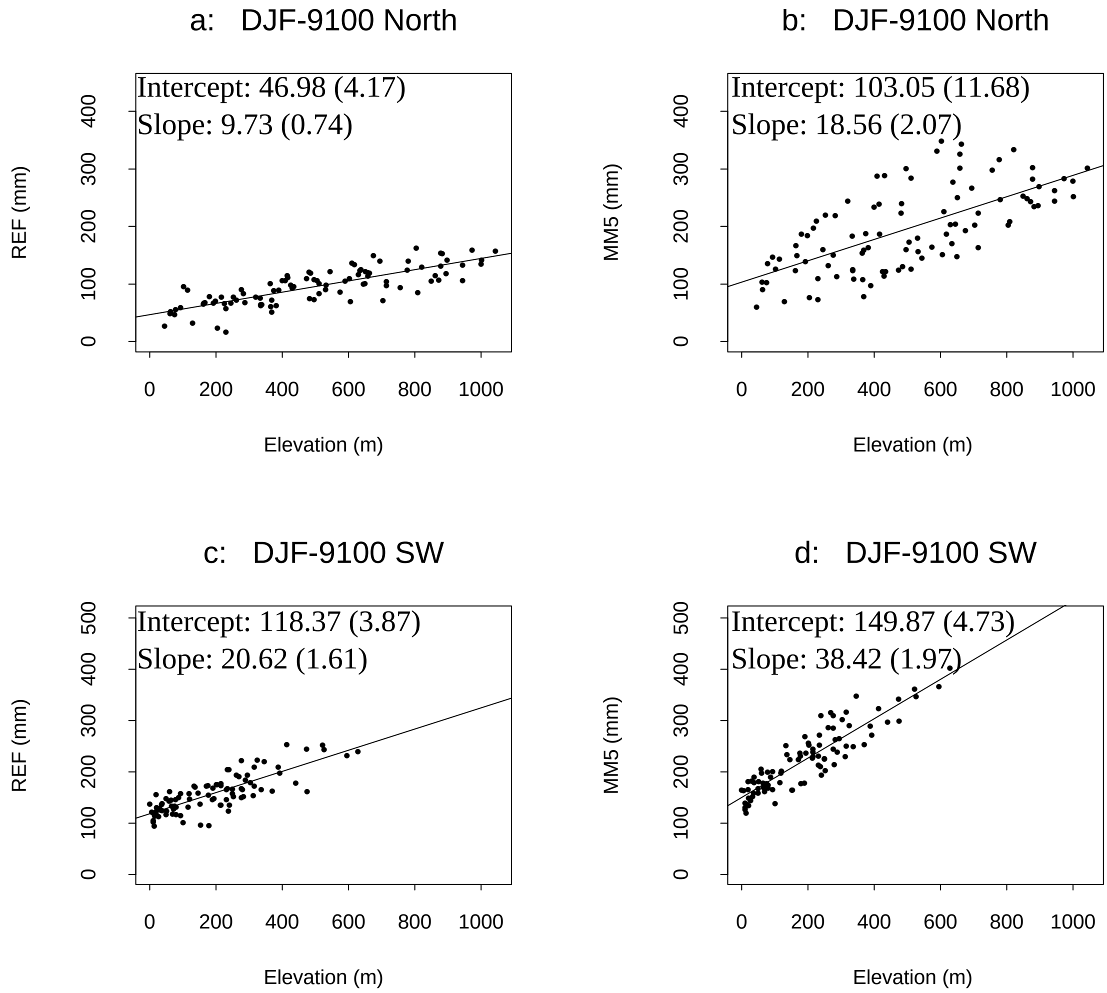

Figure 9: Season average precipitation as a function of elevation in DJF. (a) REF – region North, (b) MM5 – region North, (c) REF – region SW and (d) MM5 – region SW. Upper left corner of the figures shows the intercept [mm] and the slope [mm/100m].

Table 4: Cross validation – statistics of the estimation error for the 28 stations. Value found without using interpolation of residuals is shown in brackets.

	MAM	*JJA*	*SON*	*DJF*
MAE (%)	27.5 (27.7)	23.2 (23.9)	28.4 (28)	41.2 (40)
ME (mm)	3.38 (4.42)	2.5 (3.2)	7.7 (8.6)	4.6 (5.8)
STDEV (mm)	18.5 (18.8)	20.6 (20.6)	36.9 (36.4)	32.6 (32.1)

6 Concluding remarks

A general conclusion is that the simulated precipitation agrees quite well with observed precipitation when taking into account errors in observations and modelling errors in REF. Considering the uncertainty of the reference in relation to both the precipitation loss and the modeling errors (MAE being about 30%, see Table 4), the MM5 simulations seem to reproduce the precipitation quite well in regions South and SW, but to much precipitation is simulated in the steep terrain in region North. The only obvious systematic errors in the simulations are most likely related to the horizontal resolution. At higher resolution more precipitation can be expected to be simulated at mountain peaks and less downstream of mountain ranges. Large differences between the two models in the mountains in the north underline the need for observations at high altitudes, both for the validation of the numerical simulations as well as for the development of SMOD and the precipitation mapping of Iceland. Due to strong winds and higher proportion of snow, estimation of precipitation by observations of snow accumulation may be a more feasible option than conventional rain-gauge observations.

Acknowledgements

The authors wish thank Trausti JÓNSSON and Tómas JÓHANNESSON for discussions and for initiating the

Table 5: Regression coefficients for each season: (a) MAM, (b) JJA, (c) SON and (d) DJF. Standard error is shown in brackets.

MAM	*Intercept*	D_{min}	*Y*	*Elevation*	*Slope*	*Orientation*
Region 1	279 (77)	1.93 (0.64)	–0.55 (0.19)	0.024 (0.09)	7.21 (3.8)	–0.02 (0.08)
Region 2	413 (97)	0.52 (1.9)	–0.91 (0.28)	0.049 (0.36)	12.9 (12.2)	0.16 (0.13)
Region 3	–73 (87)	0.638 (0.62)	0.167 (0.13)	–0.09 (0.07)	5.36 (2.24)	0.09 (0.06)
Region 4	–196 (127)	–0.43 (0.71)	0.364 (0.2)	0.109 (0.06)	–0.69 (2.6)	–0.09 (0.09)
Region 5	149 (116)	0.24 (0.9)	–0.159 (0.2)	0.353 (0.32)	–14.8 (13)	–0.08 (0.16)
Region 6	177 (137)	–1.685 (1.6)	0.264 (0.26)	0.17 (0.21)	6.14 (3.9)	0.42 (0.14)
Region 7	–72 (325)	–25.3 (26)	0.49 (0.65)	0.218 (0.2)	–22.2 (12)	–0.20 (0.37)
Region 8	425 (54)	–0.39 (0.46)	–0.88 (0.14)	0.084 (0.06)	16.9 (5.8)	0.096 (0.08)
Region 9	33 (313)	–0.64 (1.24)	–0.003 (0.5)	0.01 (0.1)	4.83 (5.7)	0.36 (0.17)
JJA	*Intercept*	D_{min}	*Y*	*Elevation*	*Slope*	*Orientation*
Region 1	380 (74)	2.36 (0.6)	–0.83 (0.18)	0.015 (0.08)	7.6 (3.5)	–0.02 (0.08)
Region 2	404 (80)	1.37 (1.6)	–0.89 (0.23)	0.01 (0.29)	14.8 (10)	0.16 (0.11)
Region 3	110 (80)	–0.14 (0.57)	–0.98 (0.12)	–0.017 (0.06)	0.48 (2)	0.08 (0.56)
Region 4	–221 (135)	0.11 (0.77)	0.45 (0.21)	0.058 (0.07)	–2.28 (2.8)	–0.024 (0.1)
Region 5	78 (23)	0.2 (0.18)	–0.05 (0.04)	0.2 (0.06)	–8.4 (2.6)	–0,085 (0.03)
Region 6	68 (256)	–0.58 (3.13)	–0.065 (0.5)	0.05 (0.42)	7.6 (7.1)	0.18 (0.28)
Region 7	311 (57)	–1.13 (4.5)	–0.34 (0.11)	–0.05 (0.03)	–5.8 (2.25)	–0.003 (0.06)
Region 8	458 (64)	–0.64 (0.55)	–0.95 (0.16)	0.12 (0.08)	19 (6.9)	0.12 (0.1)
Region 9	–343 (50)	0.65 (0.29)	0.72 (0.08)	–0.14 (0.015)	6.9 (0.98)	0.34 (0.034)
SON	*Intercept*	D_{min}	*Y*	*Elevation*	*Slope*	*Orientation*
Region 1	441 (101)	2.18 (0.81)	–0.91 (0.25)	0.1 (0.1)	6.6 (4.8)	0.03 (0.11)
Region 2	465 (139)	–0.006 (2.7)	–0.97 (0.4)	0.19 (0.5)	15 (17)	0.24 (0.18)
Region 3	148 (128)	0.15 (0.9)	–0.13 (0.19)	–0.1 (0.1)	7.9 (3.3)	0.18 (0.09)
Region 4	–300 (251)	–1.4 (1.4)	0.62 (0.4)	0.21 (0.12)	–4.75 (5.2)	0.036 (0.18)
Region 5	88 (39)	0.08 (0.3)	–0.005 (0.06)	0.54 (0.1)	–23 (4.3)	–0.08 (0.05)
Region 6	–87 (230)	–5 (2.8)	0.26 (0.4)	0.6 (0.37)	5.2 (6.4)	0.7 (0.25)
Region 7	–695 (25)	–61 (1.5)	1.8 (0.05)	0.59 (0.01)	–50 (1.3)	–0.81 (0.02)
Region 8	603 (79)	–1.24 (0.7)	–1.26 (0.2)	0.2 (0.09)	24.9 (8.4)	0.16 (0.12)
Region 9	903 (1329)	–4.71 (6.2)	–1.36 (2.2)	–0.006 (0.25)	0.57 (19.8)	0.25 (0.579
DJF	*Intercept*	D_{min}	*Y*	*Elevation*	*Slope*	*Orientation*
Region 1	420 (140)	1.19 (1.16)	–0.8 (0.34)	0.16 (0.17)	5.4 (6.8)	0.08 (0.16)
Region 2	431 (127)	0.65 (2.5)	–0.86 (0.37)	0.17 (0.46)	12.5 (15.9)	0.17 (0.179)
Region 3	–48 (161)	0.53 (1.15)	0.14 (0.24)	–0.1 (0.13)	7.56 (4.1)	0.05 (0.11)
Region 4	–104 (237)	–1.46 (1.3)	0.22 (0.37)	0.19 (0.12)	–0.88 (4.9)	–0.13 (0.17)
Region 5	152 (174)	–1.01 (1.11)	–0.17 (0.29)	0.26 (0.34)	–6.9 (13.1)	0.0015 (0.2)
Region 6	346 (254)	–3.64 (3.1)	–0.54 (0.48)	0.4 (0.4)	0.65 (7)	0.65 (0.28)
Region 7	–1669 (553)	–92 (38)	3.9 (1.2)	1.04 (0.35)	–92 (31)	–1.28 (0.64)
Region 8	617 (74)	–1.11 (0.63)	–1.28 (0.19)	0.19 (0.09)	23.5 (7.9)	0.16 (0.11)
Region 9	953 (825)	–3.9 (2.6)	–1.5 (1.39)	0.21 (0.18)	–4.7 (13)	0.23 (0.31)

project. Comments from two anonymous reviewers further improved the article.

Appendix

Precipitation mapping

After the multiple linear regression equations are determined for each region D and each season k, the precipitation can be decomposed as the sum of two variables:

$$R(u,k) = SMOD(u,k) + e(u,k) \qquad (6.1)$$

where $SMOD(u,k)$ is the predicted precipitation from the statistical model and $e(u,k)$ is a random residual with zero mean and variance σ_e^2.

$$\begin{aligned} SMOD(u,k) &= SMOD(u,k,D) \\ &= a_{0,k,D} + \sum_{j=1}^{5} a_{j,k,D} p_{j,u} \quad (u \in D) \qquad (6.2) \end{aligned}$$

For the locations belonging to more than one region, the mean of the different predictions is taken:

$$SMOD(u,k) = E[SMOD(u,k,D)] \qquad (6.3)$$

The SMOD precipitation maps were produced for the following seasons: SON, DJF, MAM and JJA, by applying (6.2) and (6.3) to a regularly spaced grid of 2 km resolution. No spatial inconsistency was found in these maps after merging the different sectors together. Then, the residuals were interpolated using a spline function in tension (see SMITH and WESSEL (1990)) and added to the SMOD precipitation maps in order to produce to the final estimate, $\hat{R}(u,k)$:

$$\hat{R}(u,k) = SMOD(u,k) + \hat{e}(u,k) \qquad (6.4)$$

In order to assess the efficiency of the precipitation mapping, a cross-validation procedure was defined. A set of 28 validation stations located between 20m and 400m height were chosen (see Figure 1). One station was removed at the time, the statistical model re-calibrated each time and a new value estimated using (6.2), (6.3) and (6.4). Three statistical tests were then used to assess the mapping procedure.

The mean absolute error in %:

$$MAE\ [\%] = 100 \cdot E\left[\left|\frac{\hat{R}(u,k) - R(u,k)}{R(u,k)}\right|\right] \qquad (6.5)$$

The mean error:

$$ME = \left[\left(\hat{R}(u,k) - R(u,k)\right)\right] \qquad (6.6)$$

The standard deviation of the error:

$$STDEV = \sqrt{E\left[\left(\left(\hat{R}(u,k) - R(u,k)\right) - ME\right)^2\right]} \qquad (6.7)$$

The results (summarized in Table 4) show that according to MAE, the accuracy of the estimate is quite comparable for three seasons, and largest during DJF. These results are in agreement with the R-squared values of Table 3 and show the difficulty to model winter precipitation. The bias (ME) is always positive and largest during the wettest seasons (SON and DJF), and lowest for the driest seasons (MAM and JJA). The standard deviation of the error is also largest for the wettest seasons (SON and DJF) and lowest for the driest seasons (MAM and JJA).

Reference precipitation used to verify MM5

The horizontal resolution of MM5 is 8 km. A reference precipitation is defined for each MM5 grid point i and season k by taking the mean of all the point estimates (6.4) located within a 10 km circular window centered on that grid point:

$$REF(i,k) = E[\hat{R}(u,k)] \quad \| u - i \| \leq 5\text{km} \qquad (6.8)$$

Regression coefficients

Table 5 shows the regression coefficients for each season.

References

BASIST, A., G. D. BELL, V. MEENTEMEYER, 1994: Statistical Relationship between Topography and Precipitation Patterns. – J. Climate **7**(9), 1305–1315.

BENICHOU, P., O. L. BRETON, 1987: Prise en Compte de la Topographie pour la Cartographie des Champs Pluviométriques Statistiques. *La Météorologie* **7(19)**, 23–24.

CHEN, F., J. DUDHIA, 2001: Coupling an Advanced Land-Surface/Hydrology Model with the Penn State/NCAR MM5 Modeling System. Part I: Model Implimentation and Sensitivity. – Mon. Weather Rev. **129**, 569–585.

DALY, C., R. NELSON, D. PHILLIPS, 1994: A Statistical-Topographic Model for Mapping Climatological Precipitation over Mountainous Terrain. – J. Appl. Met. **33**, 140–158.

DROGUE, G., J. HUMBERT, J. DERAISME, N. MAHR, N. FRESLON, 2002: A Statistical-Topographic Model using an Omnidirectional Parametrization of the Relief for Mapping Orographical Rainfall. – Int. J. Climatol. **22**, 599–613.

DUDHIA, J., 1993: A Nonhydrostatic Version of the Penn State-NCAR Mesoscale Model: Validation Tests and Simulation of an Atlantic Cyclone and Cold Front. – Mon. Weather Rev. **121**, 1493–1513.

FREI, C., J. H. CHRISTIANSEN, M. DÉQUÉ, D. JACOB, R. JONES, P. L. VIDALE, 2003: Daily precipitation statistics in regional climate models: Evaluation and intercomparison for the European Alps. – J. Geophys. Res. **108(D3)**, ACL9–1–ACL9–19.

FREI, C., C. SCHÄR, 1998: A Precipitation Climatology of the Alps from High-Resolution Rain-Gauge Observations. – Int. J. Climatol. **18**, 873–900.

FØRLAND, E. P., P. ALLERUP, B. DAHLSTRÖM, E. ELOMA, T. JÓNSSON, H. MADSEN, J. PERÄLÄ, P. RISSANEN, H. VEDIN, F. VEJEN, 1996: Manual for operational correction of Nordic precipitation data. – Klima Report **24/96**, The Norwegian Meteorological Institute, Norway.

GRELL, G. A., J. DUDHIA, D. R. STAUFFER, 1995: A Description of the Fifth-Generation Penn State/NCAR Mesoscale Model (MM5). NCAR/TN-398+STR. National Center for Atmospheric Research, Boulder, CO, 107 pp.

HARALDSDÓTTIR, S. H., H. ÓLAFSSON, Y. DURAND, L. MÉRINDOL, G. GIRAUD, 2001: SAFRAN-Crocus snow simulations in an unstable and windy climate. – Annals of Glaciology **32**, 339–344.

HONG, S. Y., H. L. PAN, 1996: Nonlocal boundary layer vertical diffusion in a medium-range forecast model. – Mon. Weather Rev. **124**, 2322–2339.

KIEFFER, A., WEISSE, P. BOIS, 2001: Topographic Effects on Statistical Characteristics of Heavy Rainfall and Mapping in the French Alps. – J. Appl. Met. **40**, 720–740.

KLEMP, J. B., D. R. DURRAN, 1983: An Upper Boundary Condition permitting Internal Gravity Wave Radiation in Numerical Mesoscale Models. – Mon. Weather Rev. **111**, 430–444.

KYRIAKIDIS, P. C., K. JINWON, N. L. MILLER, 2001: Geostatistical Mapping of Precipitation from Gauge Data using Atmospheric and Terrain Characteristic. – J. Appl. Met. **40**, 1855–1877.

MLAWER, E. J., S. TAUBMAN, P. BROWN, M. IACONO, S. CLOUGH, 1997: Radiative Transfer for Inhomogenious Atmosphere: RRTM, a Validated Correlated-K Model for the Longwave. – J. Geophys. Res. **102 (D14)**, 16663–16682.

REISNER, J., R. J. RASSMUSSEN, R. T. BRUINTJES, 1998: Explicit forecasting of supercooled liquid water in winter storms using the MM5 mesoscale model. – Q. J. R. Meteor. Soc. **124B**, 1071–1107.

ROERDINK, J. B., A. MEIJSTER, 2001: The Watershed Transform: Definitions, Algorithms and Parallelization Strategies. – Fundamenta Informaticae **41**, 187–228.

SMITH, W. H. F., P. WESSEL, 1990: Gridding with continuous curvature splines in tension. – Geophysics **55**, 293 – 305.

TUSTISON, B., DANIEL HARRIS, EFI FOUFOULA GEORGIOU, 2001: Scale issues in verification of precipitation forecasts. – J. Geophys. Res. **106**(**D11**), 11,775–11,784.

VRIES M. DE, H. ÓLAFSSON, 2003: Precipitation across a mesoscale mountain ridge: The Reykjanes EXperiment (REX). In – International Conference on Alpine Meteorology and MAP-Meeting 2003, MeteoSwiss, No. 66, Brig, Switzerland, 113–116.

WANG, W., J. DUDHIA, D. GILL, Y. R. GUO, K. MANNING, J. CHISZAR, 2001: PSU/NCAR Mesoscale Modeling System Tutorial Class Notes and User Guide: MM5 Modeling System Version 3. www.mmm.ucar.edu/mm5/doc.html.

WOTLING, G., C. BOUVIER, J. DANLOUX, J. M. FRITSH, 2000: Regionalization of Extreme Precipitation Distribution using the Principal Components of the Topographical Environment. – J. Hydro. **233**, 86–101.

Paper II: Numerical Simulations of Precipitation in the complex Terrain of Iceland – Comparison with Glaciological and Hydrological Data

Meteorologische Zeitschrift, Vol. **16**, No. 1, 071-085 (February 2007)
© by Gebrüder Borntraeger 2007

Article

Numerical simulations of precipitation in the complex terrain of Iceland – Comparison with glaciological and hydrological data

Ólafur Rögnvaldsson*[1,2], Jóna Finndís Jónsdóttir[3,4] and Haraldur Ólafsson[1,5,6,7]

[1]Institute for Meteorological Research, Reykjavík, Iceland
[2]University of Bergen, Bergen, Norway
[3]Hydrological Service, National Energy Authority, Reykjavík, Iceland
[4]Dept. Water Resources Engineering, Lund University, Lund, Sweden
[5]University of Iceland, Reykjavík, Iceland.
[6]Icelandic Meteorological Office, Reykjavík, Iceland
[7]currently at Bergen School of Meteorology, Geophysical Institute, University of Bergen, Norway

(Manuscript received June 26, 2006; in revised form October 9, 2006; accepted October 27, 2006)

Abstract

Atmospheric flow over Iceland has been simulated for the period September 1987 through June 2003, using the PSU/NCAR MM5 mesoscale model driven by initial and boundary data from the European Centre for Medium-range Weather Forecasts (ECMWF). The simulated precipitation is compared with two types of indirect precipitation observations. Firstly, snow accumulation on two large ice caps in SE-Iceland and on two large glaciers in central Iceland. Secondly, model output is used as input to the WaSiM-ETH hydrological model to calculate and compare the runoff with observed runoff from six watersheds in Iceland for the water years 1987–2002. Model precipitation compares favourably with both types of validation data. The seasonal and inter-annual variability of precipitation is investigated at low as well as high altitudes. The simulations reveal a negative trend in the winter precipitation in W-Iceland, but a positive trend in the ratio of lowland precipitation to mountain precipitation in E-Iceland. There is in general a substantial inter-annual variability in the ratio of lowland precipitation to precipitation in the mountains, especially in E-Iceland, emphasizing the limitation of precipitation observations in the lowlands as a proxy for precipitation in the mountains. In order to assess the impact of orography on the precipitation climate of Iceland, precipitation is simulated with flat Iceland and compared to a simulation with true orography. It is found that the mountains contribute to a total increase of precipitation in Iceland of the order of 40 %.

Zusammenfassung

Die atmosphärische Strömung über Island wurde für den Zeitraum von September 1987 bis Ende Juni 2003 mit Hilfe des mesoscaligen PSU/NCAR MM5-Modells und unter Benutzung von Anfangs- und Randwerten aus dem European Centre for Medium-range Weather Forecasts (ECMWF) simuliert. Der simulierte Niederschlag wird mit zwei Arten indirekter Niederschlagsbeobachtungen verglichen. Zum einen mit der Schneeansammlung auf je zwei großen Gletschern in SO-Island und in Zentralisland. Zum anderen werden die Modellergebnisse des MM5 als Ausgangsdaten für das hydrologische Modell WaSiM-ETH verwendet, um die anfallende Wassermenge zu berechnen. Diese wird dann mit der angefallenen Wassermenge von sechs Einzugsgebieten in Island für die Wasserjahre 1987–2002 verglichen. Der im Modell ermittelte Niederschlag ist mit beiden Arten der Vergleichsdaten im Einklang. Die jahreszeitliche und interannuelle Variabilität von Niederschlag wird für niedere und hohe Höhenlagen untersucht. Die Simulationen zeigen einen negativen Trend im Winterniederschlag in Westisland, jedoch einen positiven Trend im Verhältnis von Flachlandniederschlag zu Bergniederschlag in Ostisland. Es gibt im allgemeinen eine grundlegende interannuelle Variabilität im Verhältnis von Flachlandniederschlag zu Niederschlag in den Bergen, besonders in Ostisland, was die eingeschränkte Übertragbarkeit von Niederschlagsbeobachtungen in den Niederungen auf den Niederschlag in den Bergen hervorhebt. Um die Auswirkungen der Orographie auf das Niederschlagsklima von Island zu beurteilen, wird der Niederschlag für das flache Island simuliert und mit einer Simulation für die wahre Orographie verglichen. Es stellt sich hierbei heraus, dass die Berge um 40 % zu einer Gesamtzunahme des Niederschlags in Island beitragen.

*Corresponding author: Ólafur Rögnvaldsson, Institute for Meteorological Research, Orkugarður Grensásvegur 9, 108 Reykjavík, Iceland, e-mail: or@os.is

0941-2948/2007/0174 $ 6.75
DOI: 10.1127/0941-2948/2007/0174
© Gebrüder Borntraeger, Berlin, Stuttgart 2007

1 Introduction

The idea of using limited area models (LAMs) for regional climate simulations was introduced by DICKINSON et al. (1989) and refined by GIORGI (1990). One of the benefits of such an approach is that it is relatively inexpensive in terms of necessary computer resources used for simulations of the atmospheric flow at relatively high spatial and temporal resolutions. As resolution is increased, processes governed by the interaction of the large scale flow and topography become better resolved by the models. One drawback of this approach which is not present in global climate models is that the simulations are dependent on the lateral boundary conditions. These can constrain the model dynamics and hence affect the results (e.g. WARNER et al., 1997). To minimize the constraining effects of the boundary conditions, QIAN et al. (2003) suggested consecutive short term integration, overlapping in time as to minimize the effects of spin-up, instead of a single long term integration. Other investigators (e.g. GIORGI and MEARNS, 1999) opt for longer integration times, emphasizing the importance of the model to be free to develop its own internal circulations. LIANG et al. (2004) used this approach when simulating precipitation over the U.S. during 1982-2002 using the MM5-based regional climate model CMM5. Several case studies investigating orographic forcing of precipitation have been made in recent years. CHIAO et al. (2004) used the MM5 model at a 5 km horizontal resolution to simulate a heavy precipitation event during MAP IOP-2B. The precipitation was satisfactorily reproduced by the model although the total amount of precipitation was slightly higher than measured by rain-gauges. BUZZI et al. (1998) simulated a 1994 flooding event in northwestern Italy. The role of orography was found to be crucial in determining the precipitation distribution and amount. Orographic precipitation has also been investigated by use of linear theory models (e.g. BARSTAD and SMITH, 2005; SMITH et al., 2005). By using a relatively simple model they identified the cloud delay time (i.e. the rate of conversion of cloud water to hydro-meteors and the rate of evaporation) as a primary unknown parameter.

The climate of Iceland is largely governed by the interaction of orography and extra-tropical cyclones, both of which can be described quite accurately by present day atmospheric models. As a result, dynamical downscaling of the climate, using limited area models, gives valuable information about precipitation distribution, especially in the data-sparse highlands.

The impact of orography on precipitation and precipitation in the mountains have an economic aspect, since hydraulic power is generated only by water that has fallen as precipitation in the mountains, and not in the lowland. However, most precipitation observations, including long time series, are from the lowland.

RÖGNVALDSSON et al. (2004) simulated precipitation in Iceland over a 10-year period using the PSU/NCAR MM5 model (GRELL et al., 1994). Simulations were compared to conventional precipitation measurements (i.e. rain-gauge data) and to precipitation estimated by a statistical model based on observed rain-gauge data and a number of topographic and geographic predictors. It was found that the simulated precipitation was in general greater than observed precipitation. However, the magnitude and the seasonal and geographic distribution of the overestimation indicated that it was to some extent associated with observation errors due to wind loss of solid precipitation and with limitations in the representativeness of the observations as well. BROMWICH et al. (2005) simulated the same 10-year period (1991–2000) using the Polar MM5 model (BROMWICH et al., 2001; CASSANO et al., 2001) and with the same horizontal resolution as in RÖGNVALDSSON et al. (2004). They concluded that simulations of the time-averaged near-surface temperature, moisture, wind and precipitation were in relatively good agreement with observations. Trends in simulated precipitation were linked to changes in the NAO index for the region.

BENOIT et al. (2000) reported some of the advantages of using one-way coupling of atmospheric and hydrological models, calibrated with observed discharge data, for validation of precipitation calculated by the atmospheric models. They conclude that stream flow record gives a better estimate of the precipitation that has fallen over a region than point measurements, and even though there were uncertainties related to their hydrological model (WATFLOOD), it was sufficiently sensitive to help improve atmospheric models. HAY et al. (2002) used output from the RegCM2 model (GIORGI et al., 1996) as input to a distributed hydrological model for four basins in the USA. Their research indicated that precipitation averaged over a large area could have the daily variations necessary for basin scale modeling. Studies focussing on one-way coupling between atmospheric models and the WaSiM-ETH watershed model in alpine landscapes have earlier been reported by JASPER et al. (2002), JASPER and KAUFMANN (2003) and by KUNSTMANN and STADLER (2005). The WaSiM-ETH model has further been integrated with a glacier sub model (KLOK et al., 2001) to simulate the discharge of a heavily glaciated drainage basin. JASPER et al. (2002) compared WaSiM-ETH simulations that were driven by observed meteorological data, with simulations driven by data from high-resolution numerical weather prediction (NWP) models. JASPER and KAUFMANN (2003) compared results from WaSiM-ETH watershed models that were on one hand driven by meteorological observations and on the other hand driven by data from atmospheric models. They concluded that the hydrological model was sufficiently sensitive to provide substantial information for the validation of atmospheric models. KUNSTMANN and STADLER (2005) were able to reproduce observed stream flow reasonably well in an alpine and orographically complex basin in Germany by driving the WaSiM-ETH watershed model with MM5 output data.

In a recent study by JÓNSDÓTTIR and ÞÓRARINSSON (2004) the HBV watershed model (SÆLTHUN, 1996) was calibrated and driven both with observed and simulated data from the MM5 model. The main results were that the correlation between daily values of measured discharge and discharge calculated by the MM5 data was fairly good. The correlation was somewhat higher when data from nearby weather stations were used. Using the MM5 data, however, improved the water balance for each water year. TÓMASSON et al. (2005) simulated a short winter flood in the Þjórsá-Tungnaá river basin in S-Iceland, using precipitation as simulated by the MM5 model and the HEC-HMS (HYDROLOGICAL MODELING SYSTEM, 2000) runoff model. They concluded that the runoff model showed results that were in good agreement with observed discharge in the river basin. The MM5 model output has also been used as input to the University of Washington Distributed-Hydrology-Soil-Vegetation Model (DHSVM) to form an automated riverflow forecasting system (WESTRICK et al., 2002).

A atmospheric flow over Iceland has been simulated for the period September 1987 through June 2003 using version 3-5-3 of the MM5 model and initial and boundary data from the European Centre for Medium-range Weather Forecasts (ECMWF). The results are compared with two types of indirect precipitation observations. Firstly, snow accumulation on two large glaciers in SE-Iceland and on two large ice caps in central Iceland. Secondly, model output was used as input to the WaSiM-ETH hydrological model (JASPER et al., 2002; JASPER and KAUFMANN, 2003) to calculate the runoff from six Icelandic watersheds for the water years 1987–2001. The hydrological model is calibrated against measured discharge from six watersheds in different parts of Iceland where neither glaciers nor groundwater play an important role in the hydrological cycle. Hence, the hydrological model output gives a fully independent evaluation of the simulated precipitation in addition to the glaciological data.

The seasonal and inter-annual variability of precipitation is investigated at low as well as high altitudes. In order to assess the impact of orography on the precipitation climate of Iceland, precipitation is simulated with flat Iceland and compared to a simulation with true orography.

The remainder of this paper is organized as follows: In section 2 we discuss the hydrological and atmospheric model configurations. Section 3 gives a description of the validation data. Results are presented in section 4 and discussed in section 5 followed by summary and conclusions.

2 Model configurations

2.1 Atmospheric model

The PSU/NCAR MM5 model (GRELL et al., 1994) is a state of the art non-hydrostatic limited area model. It has been used to simulate the atmospheric flow over Iceland over a more than 15-year period from September 1987 through June 2003. The domain used is 123 x 95 points, centered at 64°N and 19.5°W, with a horizontal resolution of 8 km. There are 23 vertical levels with the model top at 100 hPa. A more detailed description of the model configuration can be found in RÖGNVALDSSON et al. (2004).

2.2 Modeling approach

The MM5 model was used with initial and lateral boundaries from the ERA40 re-analysis project as to 1999. After that date, operational analysis, from the ECMWF were used. The ERA40 data were interpolated from a horizontal grid of 1.125° to 0.5° prior to being applied to the MM5 modeling system. The modeling approach differs from that used by BROMWICH et al. (2005). Instead of applying many short term (i.e. of the order of days) simulations and frequently updating the initial conditions, the model was run over a period of approximately six months with only lateral boundary conditions updated every six hours. This was made possible by taking advantage of the OSU land surface model (CHEN and DUDHIA, 2001).

The period from September 2001 through August 2002 was further simulated with the orography of Iceland being reduced down to one meter.

2.3 Hydrological model

The WaSiM-ETH hydrological model is a fully distributed catchment model using physically based algorithms and parameters for the description of hydrological processes (JASPER et al., 2002; JASPER and KAUFMANN, 2003). The model offers various methods of calculating the different water balance elements depending on the availability of input data. The input data from the MM5 model used in the hydrological model were precipitation, temperature at 2 metres above ground and wind speed at 10 metres above ground. The Penman-Monteith estimate of actual evaporation requires definition of vegetation parameters that were not available, and also data on humidity and radiation that could not be used directly from the MM5 model. An attempt to use Penman-Monteith with the limited data available therefore proved unsuccessful. The Hamon approach (FEDERER and LASH, 1983) was therefore used to calculate evaporation. A temperature-wind index method

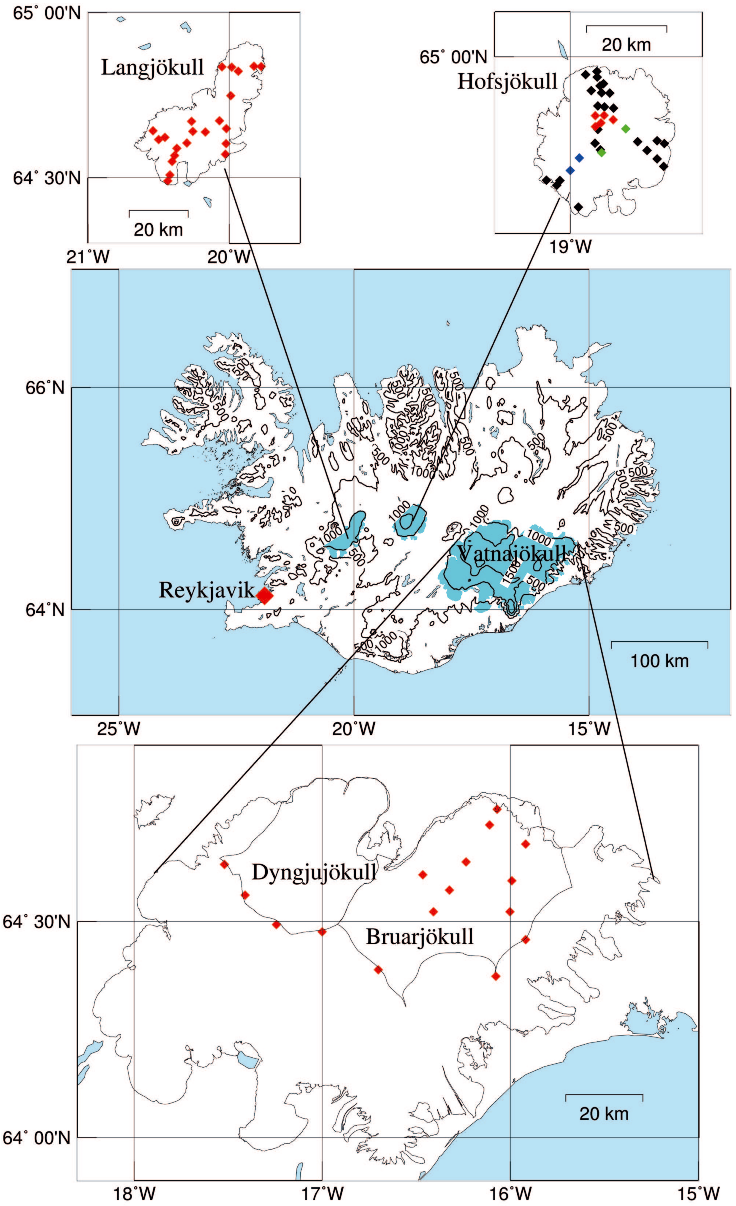

Figure 1: Overview of the four ice caps used for validation purposes, dots indicate typical location of observation sites. Red dots on Hofsjökull glacier are along profile HN (Npart), blue dots along profile HSV (SWpart) and green dots along profile HSA (SEpart), observations at locations shown in black have not been used in this study.

was used to account for higher melting when wind speed is high. The soil model used Richards equation (RICHARDS, 1931; PHILIP, 1969) for the unsaturated zone, but no groundwater model was applied.

In this study, ten parameters describing both the unsaturated zone and snow accumulation and melt were fitted to each watershed. For the unsaturated zone, the following six parameters were fitted: (1) storage coefficient of direct runoff, k_d, (2) storage coefficient of inter flow, k_i, (3) drainage density, d, (4) recession constant for base flow, k_b, and (5) saturated hydrological conductivities of the uppermost aquifer and (6) the fraction of surface runoff on snow melt. The four snow model parameters that were fitted were (7) temperature limit between rain and snow, $T_{R/S}$ (8) temperature at which snow melt starts, T_0, (9) degree-day factor without wind consideration, c_1, and (10) degree-day factor with wind consideration, c_2.

A one-way coupling between the MM5 and WaSiM-ETH model was applied by using the output from the MM5 model as input to the WaSiM-ETH model. The MM5 output was on an 8×8 km horizontal grid, while the grid of the watershed model was set to 1×1 km resolution to catch more of the characteristics of the landscape. Each grid point in the MM5 model was treated as a meteorological station, and the input to each grid

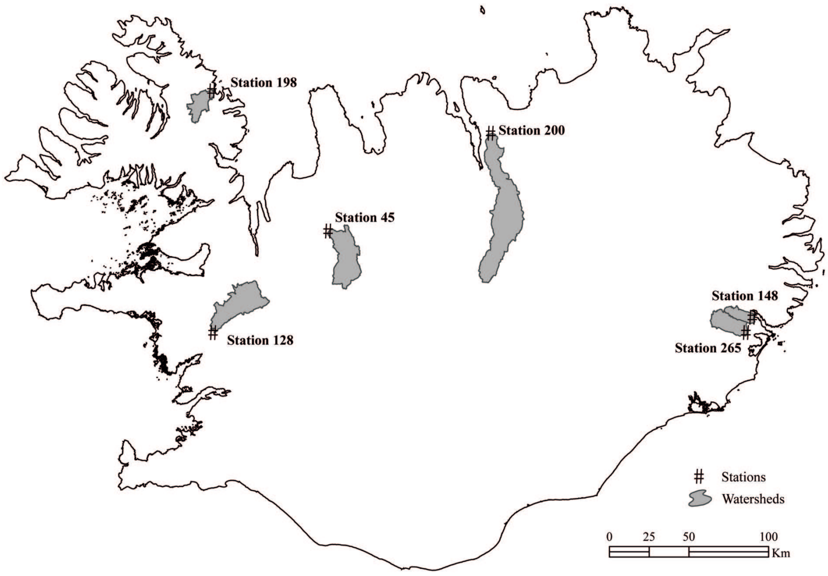

Figure 2: The location of the six watersheds and corresponding gauging stations used for validation of the MM5 precipitation data.

cell in WaSiM-ETH was evaluated by inverse distance weighting between the grid points of the MM5 model. The MM5 model output values are available for every six hours, while the watershed model was run at a daily time step because of the time resolution of observed data. The MM5 model output was therefore regridded to a daily time step, with precipitation from each of the four within-day time steps being accumulated, and with daily averages calculated for temperature and wind speed.

3 Validation data

3.1 Glaciological data

The spatial variability of the mass balance on large ice masses, such as Vatnajökull and Langjökull ice caps, can be mapped given data along several profiles extending over the elevation range of the ice caps. Since 1991 annual mass balance has been observed on parts of Vatnajökull ice cap in SE-Iceland (BJÖRNSSON et al., 1998) and from 1996 on Langjökull ice cap, central Iceland (BJÖRNSSON et al., 2002). Here, we only use measurements of accumulated wintertime snow, expressed in terms of liquid water equivalents. BJÖRNSSON et al. (1998) estimated the uncertainty of the areal integrals of the mass balance to be a minimum of 15 %. Due to surging of the Dyngjujökull glacier in 1998–2000 the uncertainty is considerably greater for this period and the foolowing winter (PÁLSSON et al., 2002a). The ice caps and typical locations of the mass balance stakes are depicted in Figure 1.

Precipitation on Hofsjökull ice cap has been observed at sites along profile HN (cf. Figure 1) since 1987 and along profiles HSV and HSA since 1988 (SIGURÐSSON et al., 2004). In our model configuration the maximum elevation of the Hofsjökull ice cap

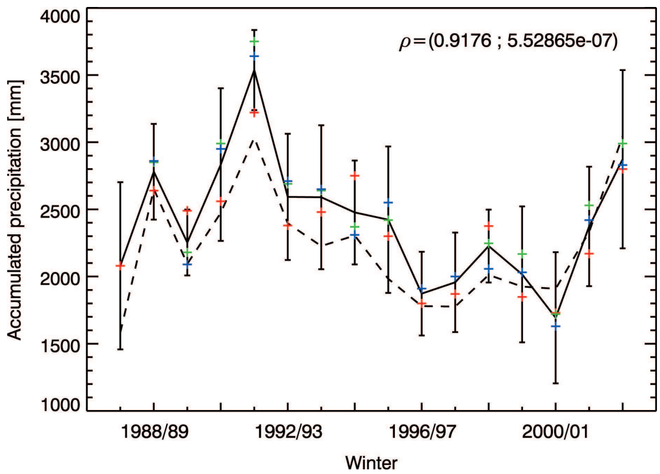

Figure 3: Estimated mean accumulated winter precipitation [mm] along profiles HN (N-part), HSA (SE-part) and HSV (SW-part) at altitudes between 1450 and 1650 metres (solid line, JÓHANNESSON et al., 2006). Dashed line represents simulated precipitation by MM5 from a single grid cell over Hofsjökull ice cap at altitude 1540 metres. Red, green and blue crosses represent mean values along profiles HN, HSA and HSV respectively on the altitude interval 1440–1680 metres (cf. Figure 1). Error bars indicate the standard deviation of the observations. Observed values from individual snow stakes are from SIGURÐSSON (1989, 1990, 1993), SIGURÐSSON and SIGURÐSSOn (1998) and Sigurðsson et al. (2004).

is approximately 1540 metres, i.e. more than 250 metres lower than in reality. Hence, we use area-integrated data from an elevation range of approximately 1450–1650 metres along the three profiles HN, HSV and HSA (JÓHANNESSON et al., 2006).

Table 1: Comparison of observed and calculated discharge at six discharge stations and Nash-Sutcliffe coefficients of model fit.

Station	$Q_{meas}[m^3/s]$	$Q_{calc}[m^3/s]$	Difference [%]	R2	R2log
198	26.8	25.4	-5.2	0.62	0.60
265	19.6	20.8	6.1	0.70	0.74
45	12.3	13.4	8.9	0.69	0.62
128	29.4	29.4	9.7	0.61	0.64
148	9.1	10.4	10.4	0.64	0.71
200	48.4	11.4	11.4	0.53	0.53

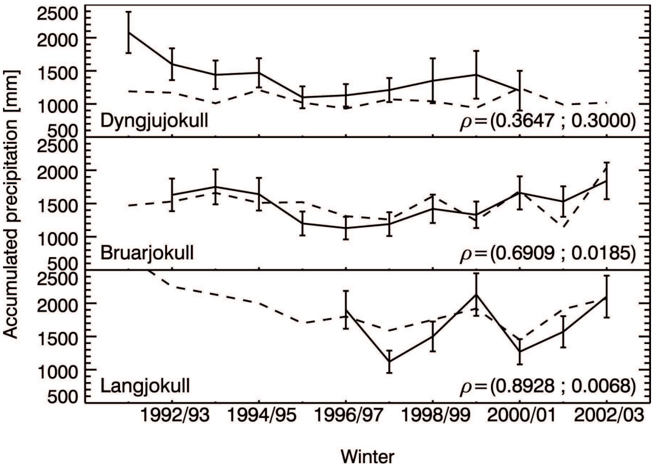

Figure 4: Estimated from observations (solid) and simulated by MM5 (dashed) accumulated winter precipitation for Dyngjujökull (top) and Brúarjökull (middle) glaciers and Langjökull (bottom) ice cap. Error bars indicate 15 % uncertainty of the observations, except for 1998–2001 at Dyngjujökull where it is 25 %. Glaciological data for Dyngjujökull and Brúarjökull are from BJÖRNSSON et al. (1998, 2002) and PÁLSSON et al. (2002a, 2002b, 2004b, 2004c). Data for Langjökull ice cap are from BJÖRNSSON et al. (2002) and PÁLSSON et al. (2004a).

3.2 Hydrological data

Large areas of Iceland are covered with post-glacial lava. In those areas, precipitation infiltrates through the porous surface, to the groundwater aquifers and in some cases through the groundwater aquifers to the ocean. Furthermore, the temperature at high altitudes in Iceland remains below zero for some months during the winter, so that some of the autumn and winter precipitation is stored until spring and glaciers may store precipitation from one season, year or decade to the next. The complexity of the hydrological cycle therefore varies from one area to the other. In this study, six watersheds were selected where the rivers are primarily direct-runoff rivers and are therefore relatively free from the complications of groundwater components and glacier mass balance changes. The locations of the six selected watersheds are shown in Figure 2. However all the watersheds have substantial snow cover during the winter, so that the models were run on the basis of a water year, i.e. from September 1, 1987 to August 31, 2002. Average daily discharges from the database of the Hydrological Service of the National Energy Authority were used to calibrate the model. A 500-m digital elevation model (ICELANDIC METEOROLOGICAL OFFICE et al., 2004), a soil map from the Agricultural University of Iceland and a digital vegetation map from the Icelandic Institute of Natural History were used in WaSiM-ETH to describe the watersheds. The geographical data were all regridded to a 1 x 1 km spatial resolution.

4 Results

4.1 Comparison with glaciological data

The simulated wintertime precipitation at Hofsjökull ice cap is in good agreement with observations (cf. Figure 3) over the northern part of Hofsjökull (HN, red dots, cf. Figure 1), the SE-part (HSA, green dots, cf. Figure 1) and the SW-part of the ice cap (HSV, blue dots, cf. Figure 1). The solid line in Figure 3 shows the estimated wintertime precipitation, taking into account ablation due to liquid precipitation and/or melting, at altitude between 1450 and 1650 metres at locations HN, HSA and HSV. The dashed line shows the wintertime precipitation simulated by MM5 at a single grid cell over Hofsjökull ice cap at altitude 1540 metres. The simulated precipitation is within one standard deviation of snow accumulation for the whole observation period (1987–2003), observed at snow stakes between 1440 and 1680 metres altitude. The Spearman's rank correlation[1] is 0.92 with a significance value of $5.5 \cdot 10^{-7}$.

When compared with estimated areal integrals of wintertime precipitation over the Dyngjujökull (1040 km^2) and Brúarjökull (1695 km^2) glaciers and the Langjökull ice cap (925 km^2), the rank correlation decreases somewhat (see Figure 4). The model shows the least skill on Dyngjujökull (ρ =0.365;0.300) and the greatest skill on Langjökull (ρ =0.893;0.007). The correlation for Brúarjökull is 0.691 with a significance

[1] We used the *r_correlate* function within the IDL® software package. The function computes the Spearman's rank correlation of two sample populations X and Y. The result is a two-element vector containing the rank correlation coefficient and the two-sided significance of its deviation from zero. The significance is a value in the interval [0.0, 1.0]; a small value indicates a significant correlation.

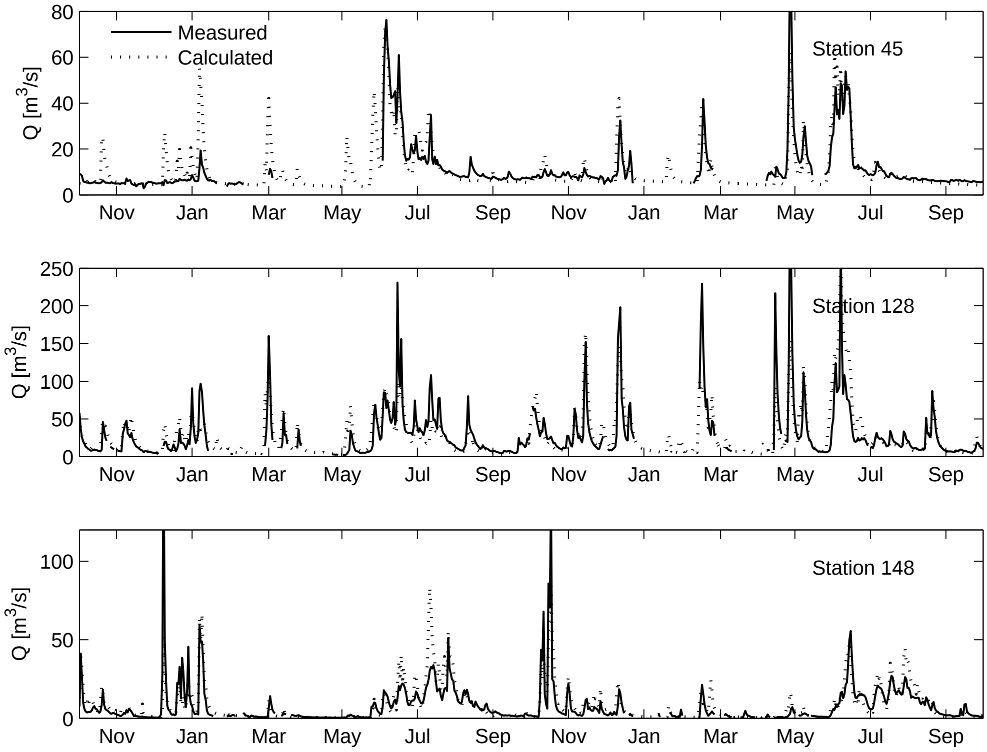

Figure 5: Comparison of measured (solid lines) and calculated (dashed lines) runoff from September 1, 1998 to August 31 2000 at stations 45, 128 and 148.

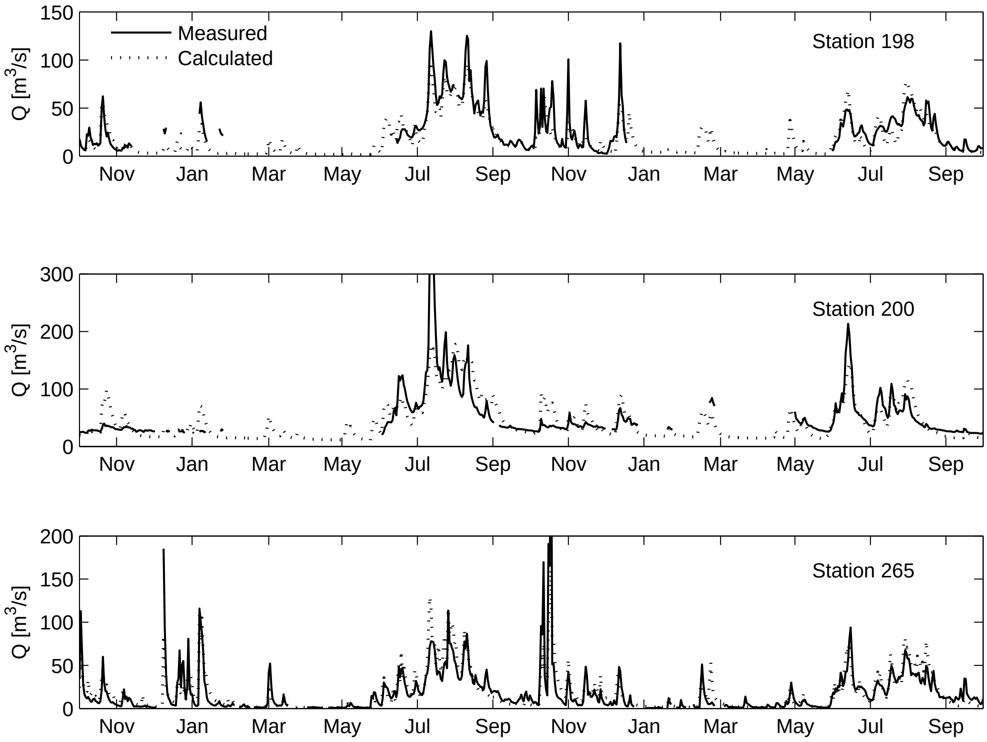

Figure 6: Comparison of measured (solid lines) and calculated (dashed lines) runoff from September 1, 1998 to August 31 2000 at stations 198, 200, 265.

value of 0.019. The simulated precipitation is within estimated observational error-margins for 5 out of 10 winters for Dyngjujökull, 9 out of 11 for Brúarjökull and 5 out of 7 for Langjökull ice cap.

4.2 Comparison with hydrological model data

Runoff from the six Icelandic watersheds used in this study is strongly influenced by snow accumulation and

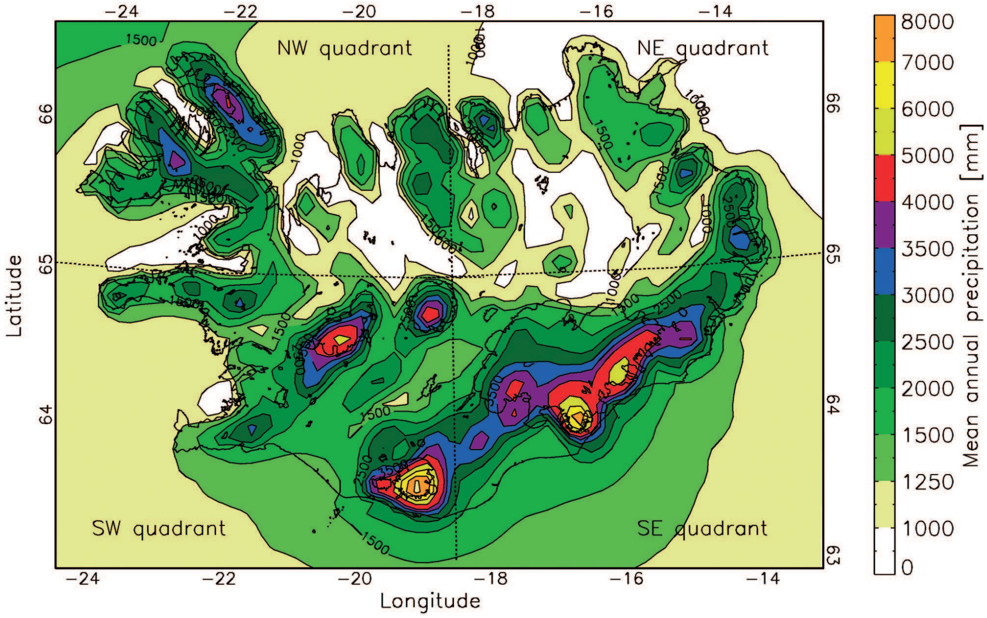

Figure 7: Mean annual precipitation from March 1988 through February 2003 as simulated by the MM5 model. Dashed lines show the definition of NW, NE, SE and SW quadrants.

snow melt. Therefore, the fit of simulated to observed runoff is highly dependent on both temperature and precipitation, while the overall water balance of water years depends primarily on precipitation data. Here, the Nash-Sutcliffe coefficient $R2$ (Nash and Sutcliffe, 1970) and $R2log$ is used to measure how well the simulated runoff fits the observed runoff. Both coefficients $R2$ and $R2log$ range from 1 to $-\infty$, where a perfect fit equals 1. The coefficient $R2$ emphasizes the fit for high flows and floods while $R2log$ puts greater weight on how well low flows are simulated.

Table 1 shows the $R2$ and $R2log$ coefficients as well as the fit of the water balance for the period September 1, 1988–August 31, 2002. The average simulated runoff is 7 % higher than the observed runoff, the $R2$ and $R2log$ values are higher than 0.6 except for one basin where they are both 0.53. Figures 5 and 6 also show observed and simulated hydrographs, for the period September 1, 1998–August 31, 2000, for the six watersheds.

4.3 Simulated time series

Figure 7 shows the mean annual precipitation as simulated with the MM5 model over the 15-year period from March 1988 to February 2003. It shows a realistic precipitation pattern with the greatest precipitation over the large ice caps in S- and SE-Iceland and over the three large ice caps in central and NW-Iceland.

Figure 8 shows simulated seasonal precipitation for lowland points, defined as model grid points below 100 metres (11 % of Iceland) and highland points (altitude above 100 metres) for the four quadrants shown in Figure 7 as well as the whole of Iceland. The greatest absolute difference between the lowland and highland points is during the winter months (December to February, DJF) and minimum difference is during the summer months (June to August, JJA). These two seasons show the greatest (DJF) and smallest (JJA) inter-annual variability. On average, the greatest difference between precipitation at low- and highland points is in the SW quadrant for all seasons, while the NE quadrant shows the smallest difference. There is considerable inter-annual variability for all quadrants, but least in the NE. The NE quadrant is the driest quadrant. Precipitation at lower altitudes sometimes exceeds precipitation in the mountains, most frequently so during SON in the NE quadrant and in JJA in the SE quadrant.

Figure 9 (left) shows the seasonal precipitation over a 15-year period from MAM 1988 through DJF 2002. The seasonal variability is clear in all quadrants and lowland precipitation is clearly considerable lower than precipitation in the mountains at most times. The exception is the NE and to a less extent, the SE quadrant from 1997 to 2002. The right panel of Figure 9 shows the seasonal precipitation for all quadrants for the same period. A negative trend can be seen in wintertime (DJF) precipitation in the western part of Iceland (cf. Figure 8, upper left panel).

Figure 10 shows the ratio of simulated low- and highland precipitation to total precipitation for each quadrant, as well as the sum of all quadrants. In the NE and to some extent in the SE, there is a positive trend in the relative proportion of lowland precipitation during winter and springtime but the greatest inter-annual variability in the precipitation of lowland to highland precipitation is during JJA in the SE quadrant. There appears to be an oscillation in the lowland precipitation during winter (DJF) and summer (JJA) in the southern quadrants with a period of about five years in this period. The greatest amplitude is found in the SE quadrant during JJA 1992–2002.

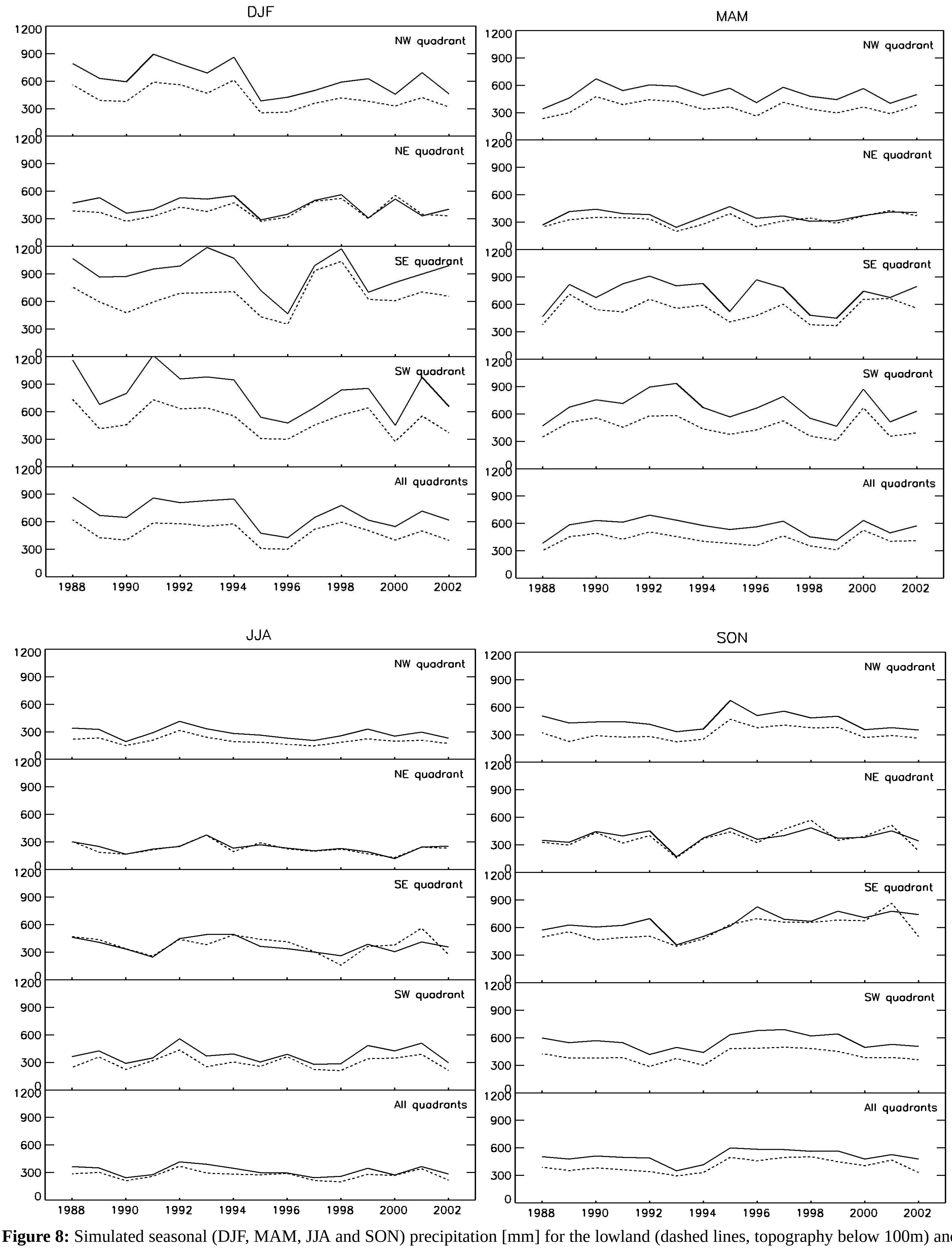

Figure 8: Simulated seasonal (DJF, MAM, JJA and SON) precipitation [mm] for the lowland (dashed lines, topography below 100m) and the highlands (solid lines, topography above 100m) from March 1988 through February 2003. The country is divided into four quadrants, NW (top panel), NE (second from top), SE (middle panel) and SW (second from bottom). The lowest panel shows the sum of all quadrants.

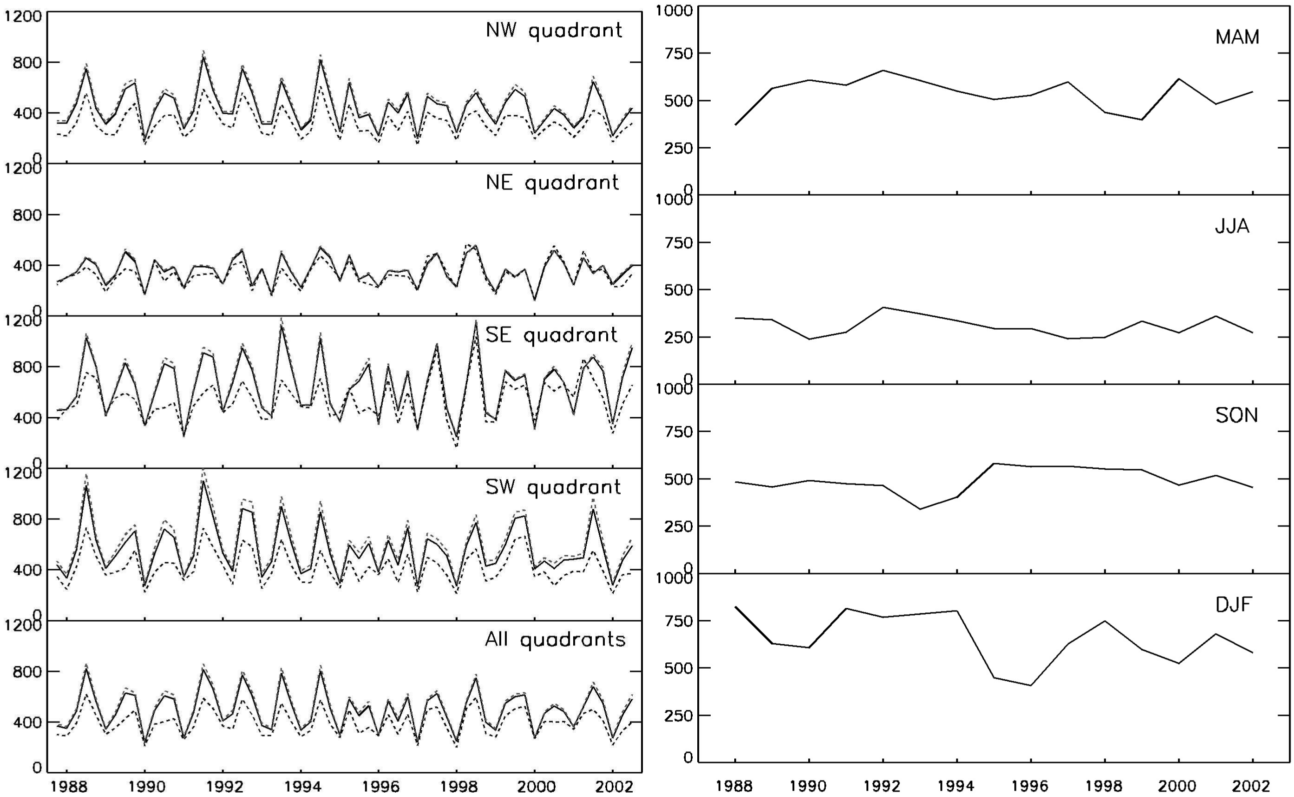

Figure 9: Simulated seasonal precipitation [mm] from MAM 1988 through DJF 2002 for the NW, NE, SE and SW quadrants and sum of all quadrants (left). Solid black line shows the total precipitation, dashed line shows the precipitation for the highlands (z>100m) and dashed black lines for the lowlands (z<100m). The right panel shows the seasonal precipitation [mm] for all quadrants for the same period.

4.4 Orographic effects

Figure 11 shows the accumulated precipitation between September 2001 and August 2002 with unmodified (CONTROL, left) and flat terrain (FLAT, right). The absolute difference between the two simulations is shown in Figure 12 (left) as well as relative difference (right). The mean monthly precipitation for both simulations is shown in Figure 13 along with the relative difference.

The mountains constitute about 40 % increase in precipitation over Iceland. The differences in monthly values range from 25 % to 55 %. The mountains cause a drying in the highlands north of the Vatnajökull ice cap and north of the two large ice caps in central Iceland. The valley areas in the central and southeast part of the NW quadrant and the two largest fjords in the northwesternmost part of Iceland are also drier when the mountains are present. The mountains cause an increase in precipitation that reaches far south of Iceland, while a decrease in precipitation is evident far to the north and northeast of Iceland.

5 Discussion

In this study, numerically simulated precipitation has been compared with unconventional observations of precipitation, i.e. runoff and snow accumulation. This type of data only provides validation on a much longer timescale than conventional rain-gauge data, and the daily error in the precipitation downscaling remains unclear. However, the comparison with the observational data shows that the climatological values of the simulated precipitation are of good quality. The correlation between observations and simulations is in fact much better than in RÖGNVALDSSON et al. (2004). The relatively poor correlation in RÖGNVALDSSON et al. (2004) is mainly because of observational errors associated with undercatchment by the rain-gauges but not because of a poor statistical model treating the rain-gauge observations or a poor quality in the numerical simulations. In this study, precipitation from the MM5 model has not been scaled in any way to fit the observed discharge. The good fit of the watershed models, particularly with regards to accumulated water balance, therefore, suggests that MM5 precipitation in these areas is close to the actual precipitation. However, no conclusions on the precision of other meteorological variables, such as temperature and wind speed, can be drawn from this study because parameters in the hydrological model involving snow melt and accumulation were adjusted to improve the fit as measured by $R2$ and $R2log$. These results do suggest that meteorological output from the MM5 models can be used with WaSiM-ETH to set up successful models of runoff in the areas of these six watersheds.

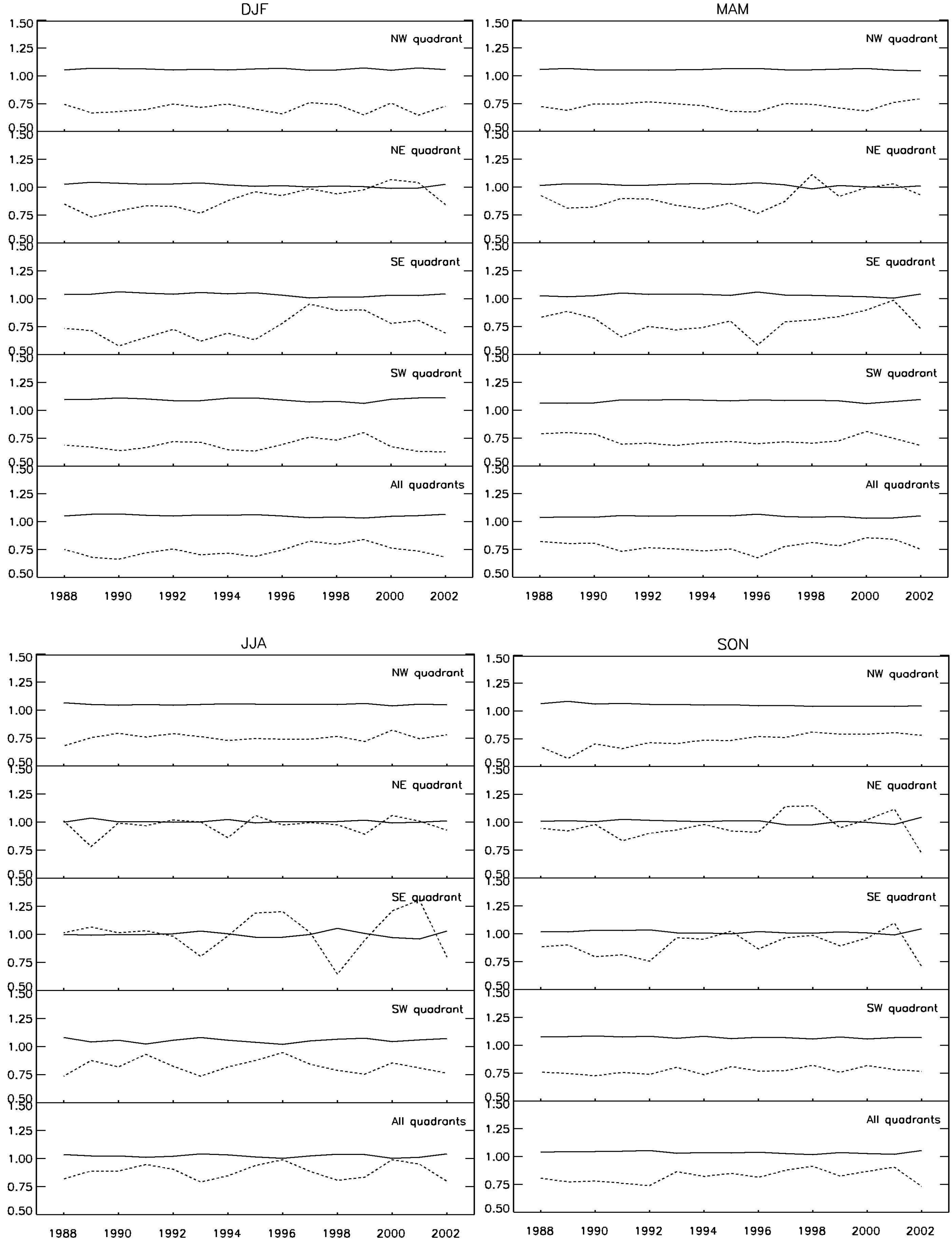

Figure 10: Ratio [%] to total simulated precipitation for lowland (dashed lines) and the highlands (solid lines) for the four seasons and individual quadrants, as well as the whole country from MAM 1988 through DJF 2002.

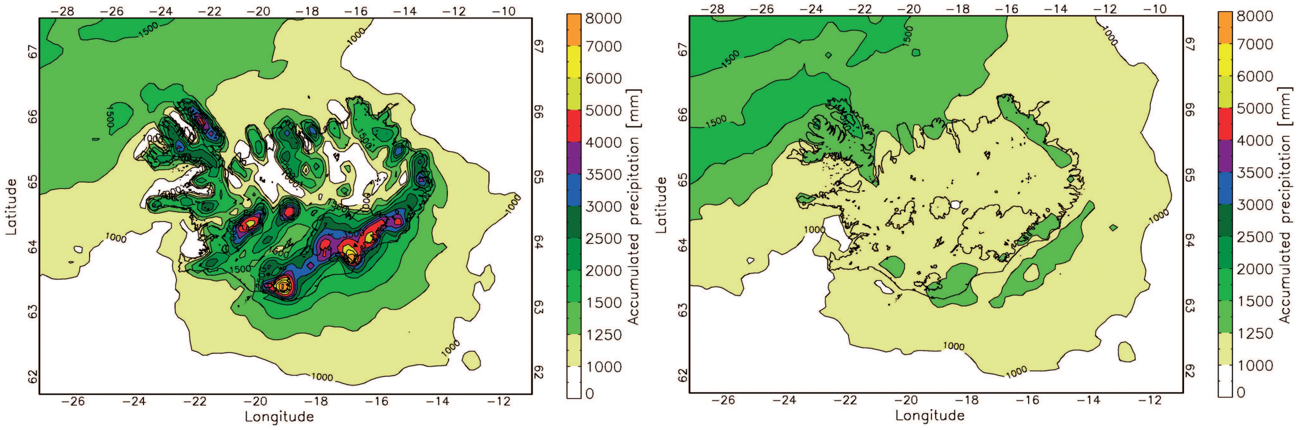

Figure 11: Simulated precipitation [mm] for 2001-02 (September through August) with unmodified terrain (CONTROL, left) and with the orography reduced to one meter (FLAT, right).

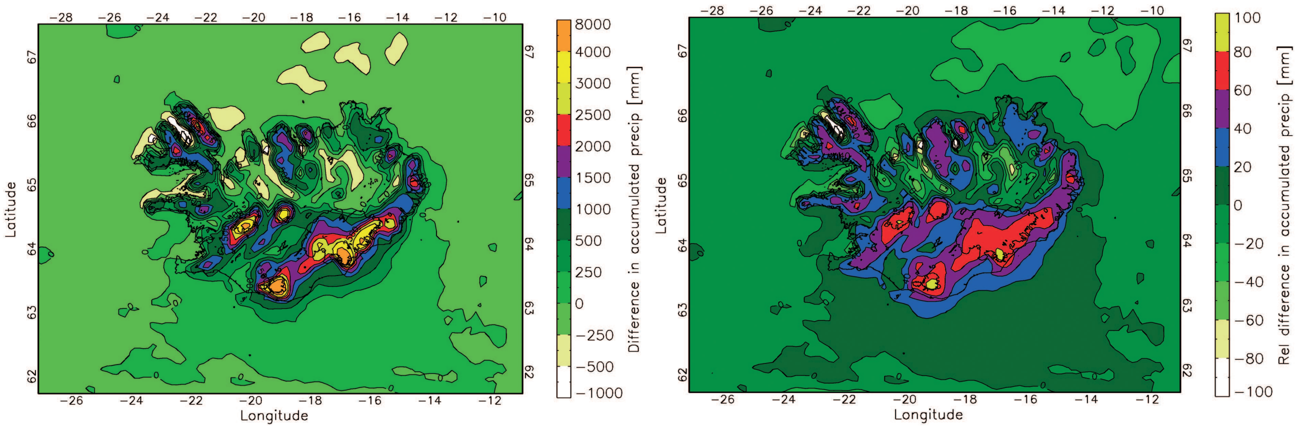

Figure 12: Absolute [mm] difference in precipitation (left) between CONTROL and FLAT and relative [%] (CONTROL-FLAT / CONTROL) difference (right).

The fit between measured and calculated discharge might be improved by adjusting the input precipitation; however this is not the purpose of the study. Also, the use of more advanced interpolation methods for the meteorological variables, with elevation dependency might improve the model. An application of more advanced evaporation schemes, according to the Penman-Monteith approach, could give a better evaluation of evapotranspiration, but as mentioned earlier the use of Penman-Monteith has been proved difficult in this study. Furthermore, the WaSiM-ETH model simulate the heat flux in the soil or subsurface, so that discharge during winter when soil is frozen might be simulated better if a different hydrological model were used. However despite these limitations, the comparison of measured and calculated discharge gives acceptable results with regard to the one-way coupling of MM5 and WaSiM-ETH.

The simulations reveal several interesting aspects of the precipitation pattern in time and space. Firstly, there is a negative trend in the precipitation, as pointed out by BROMWICH et al. (2005). However, this trend is small compared with the inter-annual variability, and by choosing different 15-year periods during the last 45 years, quite variable trends can be obtained (cf. Figure 14). The negative trend for 1988–2002 is primarily confined to the western part of Iceland (quadrants NW and SW) in winter. This happens at the same time as wintertime ratio of lowland precipitation to highland precipitation increases steadily in the eastern part of Iceland (quadrants SE and NE). Regional precipitation in Iceland is very dependent upon wind direction. Basically, most precipitation in each region falls when the winds are blowing from the ocean, while when winds are blowing from the central highlands, there is usually only little, if any precipitation (EINARSSON, 1984). On a day-to-day time scale, precipitation in the northeast is thus negatively correlated with precipitation in the southwest. On a longer time-scale, the correlation is not necessarily as simple and when the total precipitation falls to a bottom value in the west (winter of 2000), there is not a distinct peak in the precipitation in the northeast. On the other hand, the ratio of lowland precipitation to highland precipitation reaches a peak in the northeast this same winter. In general, strong winds favour precipitation in and immediately downstream of the upstream slopes (e.g. de VRIES and ÓLAFSSON, 2003), while in weak winds the flow is blocked and the orographic lifting may be very little, and may take place at some

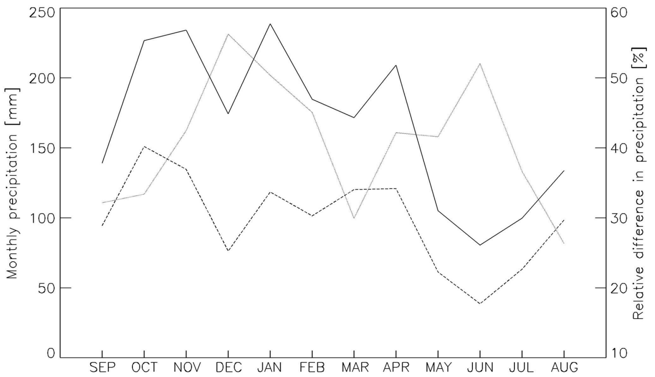

Figure 13: Accumulated monthly precipitation in Iceland [mm] as simulated in CONTROL (solid line) and FLAT (dashed line). Relative difference is shown with dotted line.

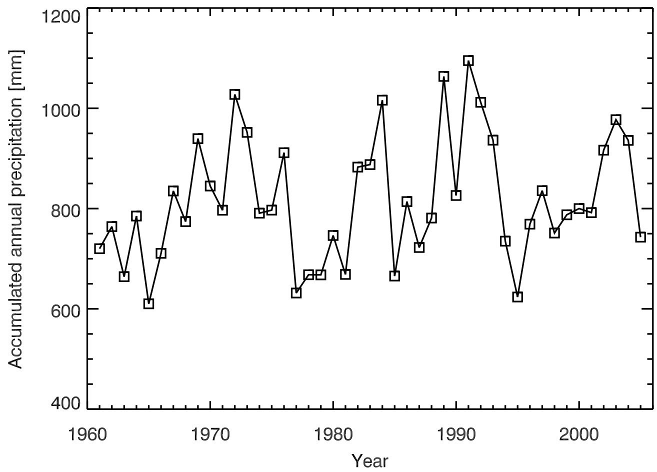

Figure 14: Observed annual precipitation [mm] at station Keflavík (WMO 4018) from 1961 to 2005.

distance upstream of the mountain. The simulated precipitation pattern indicates therefore that in the winter of 2000–2001, northeasterly, but relatively weak winds were prevailing. This was indeed the case. Investigation of observations show that in the southwest, northeasterly winds were anomalously frequent during this period, and at the northeast coast, the mean wind speed during precipitation was only 8.6 m/s, which is 1.4 m/s below the average value.

The regional variability in the proportion of precipitation falling in the lowlands can be explained by variability in the terrain. The relatively low proportion of highland precipitation in the NE is associated with the fact that there is a relatively large and dry plateau at a high elevation in the inland areas. In the NW, the lowland is sheltered and dry in northeasterly winds. Consequently, the lowland precipitation is a lower proportion of the highland precipitation than in the NE. In the SW, there is a similar sheltering of the lowlands as in the NW, but in easterly and southeasterly winds.

In general, the ratio of precipitation in the highlands to the lowlands is lowest in the summer. This is not unexpected as winds are much weaker in the summer than in the winter. This result underlines that neither summertime rain-gauge observations in the mountains nor observations of snow accumulation in the winter can be interpolated directly to the rest of the year by simple correlation with observations in the lowland, as sometimes is done.

There is substantial inter-annual variability in the proportion of precipitation in the lowlands to the highland precipitation, particularly in the summertime in the SE-part of Iceland. An investigation of weather patterns reveals that when the proportion of lowland precipitation is exceptionally low (1998), winds from the south are anomalously frequent, but winds from the east are exceptionally rare. During summers of high proportion of precipitation in the lowland (1995, 1996 and 2001), precipitation in winds from the south is less frequent than in 1998, while winds from the east are more frequent than in 1998. In winds from the east, the orographic lifting in SE-Iceland is much less than when winds are blowing from the southeast or south. In short, the large variability in the ratio of lowland precipitation to highland precipitation in SE-Iceland appears to be associated with variability in the relative frequency of wind directions.

The experiment with a flat Iceland confirms the general conception that large areas in N-Iceland are submitted to a net reduction of precipitation due to the mountains. Large parts of these areas are deserts, but that may even more a consequence of low summer temperatures, strong winds, transport of sand by wind and the volcanic nature of the soil, than due to lack of precipitation. The importance of orographic lifting for precipitation in the mountains is also confirmed by the flat Iceland experiment. This was in fact already quite clear from comparing the topography of Iceland to the simulated precipitation. In the south of Iceland, there are large areas where more than 50 % of the total precipitation is due to the impact of the mountains. In reality, this proportion may be greater, because at the current 8 km resolution, the mountains are not fully resolved (see f. inst., BROMWICH et al., 2005). The orography of Iceland contributes to some increase in precipitation as far as the domain extends to the south of Iceland, indicating that orographic lifting starts far upstream of the mountain. There is on the other hand a substantial rain shadow far offshore to the north of Iceland, indicating that it takes more than a few hundred kilometers for the precipitation systems to recover after the flow has passed a mountain range of the size of Iceland. This is in agreement with the precipitation climate of numerous regions in the world that experience rain shadow from very distant mountain ranges.

6 Summary and conclusions

A numerical weather prediction model has been shown to be very useful for mapping precipitation in complex terrain in a climate governed by extra-tropical cyclones. Snow accumulation and runoff data can be applied successfully to validate such simulations and may even be more suitable to such evaluation than traditional raingauge observations. During the period 1988–2002 there was a negative trend in wintertime precipitation in western Iceland, but a positive trend in the proportion of lowland precipitation to highland precipitation in eastern Iceland. There is substantial temporal variability in the proportion of lowland precipitation to precipitation in the mountains, and this proportion can be associated with wind speeds and prevailing wind directions. In spite of large regions in the north and in the west of Iceland being in a rain shadow, the mountains contribute to a total increase of precipitation in Iceland of the order of 40 %.

Acknowledgements

This work has been sponsored by the Icelandic Science Fund (RANNÍS), the Icelandic Energy Fund (Orkusjóður) and the National Power Company (Landsvirkjun). It is part of the Nordic and national research projects Climate and Energy (CE) and Veður og orka (VO). The authors wish to thank Tómas JÓHANNESSON and Oddur SIGURÐSSON for discussions and for providing data from the Hofsjökull ice cap. Comments from two anonymous reviewers further improved the article.

References

BARSTAD, I., R. B. SMITH, 2005: Evaluation of an Orographic Precipitation Model. – J. Hydrometeor. **6**, 85–99.

BENOIT R, P. PELLERIN, N. KOUWEN, H. RITCHIE, N. DONALDSON, P. JOE, E.D. SOULIS, 2000: Toward the use of coupled atmospheric and hydrologic models at regional scale. – Mon. Wea. Rev. **128**, 1681–1706.

BJÖRNSSON, H., F. PÁLSSON, M. T. GUÐMUNDSSON, H. H. HARALDSSON, 1998: Mass balance of western and northern Vatnajökull, Iceland, 1991–1995. – Jökull **45**, 35–58.

BJÖRNSSON, H., F. PÁLSSON, H. H. HARALDSSON, 2002: Mass balance of Vatnajökull (1991–2001) and Langjökull (1997–2001), Iceland. – Jökull **51**, 75–78.

BROMWICH, D. H., J. J. CASSANO, T. KLEIN, G. HEINEMANN, K. M. HINES, K. STEFFEN, J. E. BOX, 2001: Mesoscale modeling of katabatic winds over Greenland with the Polar MM5. – Mon. Wea. Rev. **129**, 2290–2309.

BROMWICH, D. H., L. BAI, G. G. BJARNASON, 2005: High-Resolution Regional Climate Simulations over Iceland Using Polar MM5. – Mon. Wea. Rev. **133**, 3527–3547.

BUZZI A., N. TARTAGLIONE, P. MALGUZZI, 1998: Numerical Simulations of the 1994 Piedmont Flood: Role of Orography and Moist Processes. – Mon. Wea. Rev. **126**, 2369–2383.

CASSANO, J. J., J. E. BOX, D. H. BROMWICH, L. LI, K. STEFFEN, 2001: Evaluation of Polar MM5 simulations of Greenland's atmospheric circulation. – J. Geophys. Res. **106**, 33867–33890.

CHEN, F., J. DUDHIA, 2001: Coupling an Advanced Land-Surface/Hydrology Model with the Penn State/NCAR MM5 Modeling System. Part I: Model Implementation and sensitivity. – Mon. Wea. Rev. **129**, 569–585.

CHIAO, S., Y.-L. LIN, M. L. KAPLAN, 2004: Numerical Study of the Orographic Forcing of Heavy Precipitation during MAP IOP-2B. – Mon. Wea. Rev. **132**, 2184–2203.

DICKINSON, R. E., R. M. ERRICO, F. GIORGI, G. T. BATES, 1989: A regional climate model for the western United States. – Climate Change **15**, 383–422.

EINARSSON, M. A., 1984: Climate of Iceland - In: H. van Loon (Eds.): World Survey of Climatology, Vol. 15, Climate of the Oceans, Elsevier, 673-697.

FEDERER, C.A., D. LASH, 1983: BROOK - a hydrologic simulation model for eastern forests. – Water Resources Research Center, University of New Hampshire, Durham. Research Report No. 19, 84 pp.

GIORGI, F., 1990: On the simulation of regional climate using a limited area model nested in a general circulation model, – J. Climate **3**, 941–963.

GIORGI, F., L. O. MEARNS, 1999: Introduction to special section: Regional climate modeling revisited. – J. Geophys. Res. **104**, No. D6, 6335–6352.

GIORGI, F., L. O. MEARNS, C. SHIELDS, L. MAYER, 1996: A Regional Model Study of the Importance of Local versus Remote Controls of the 1988 Drought and the 1993 Flood over the Central United States. J. Climate **9**, 1150-1162.

GRELL, G. A., J. DUDHIA, D. R. STAUFFER, 1994: A description of the fifth-generation Penn State/NCAR Mesoscale Model (MM5). – NCAR Tech. Note NCAR/TN-398+STR, 138 pp.

HAY, L. E., M. P. CLARK, R. L. WILBY, W. J. GUTOWSKY, JR., G. H. LEAVESLEY, Z. PAN, R. W. ARRITT, E. S. TAKLE, 2002: Use of Regional Climate Model Output for Hydrological Simulations. – J. Hydrometeor. **3**, 571–590.

HYDROLOGICAL MODELING SYSTEM (HEC-HMS) – Technical Reference Manual, 2000: Technical report. – Hydrological Engineering Center, U.S. Army Corp of Engineers, Davis, California, USA, 157 pp.

ICELANDIC METEOROLOGICAL OFFICE, National Land Survey of Iceland. – Science Institute, University of Iceland, and National Energy Authority, 2004: A 500x500 m DTM of Iceland. Available on the web: http://www.os.is/ce.

JASPER, K., P. KAUFMANN, 2003: Coupled runoff simulations as validation tools for atmospheric models at the regional scale. – Quart. J. Roy. Meteor. Soc. **129**, 673–692.

JASPER, K., J. GURTZ, H. LANG, 2002: Advanced flood forecasting in Alpine watersheds by coupling meteorological observations and forecasts with a distributed hydrological model. – J. Hydro. **267**, 40–52.

JÓHANNESSON, T., O. SIGURÐSSON, B. EINARSSON, TH. THORSTEINSSON, 2006: Mass balance modeling of the

Hofsjökull ice cap based on data from 1988–2004. – Reykjavík, National Energy Authority, Report OS-2006/004, 50 pp.

JÓNSDÓTTIR, J. F., J. S. ÞÓRARINSSON, 2004: Comparison of HBV models, driven with weather station data and with MM5 meteorological model data. – Reykjavík, National Energy Authority, Report OS-2004/17. ISBN 9979-68-147-0, 17 pp.

KLOK, E. J., K. JASPER, K. P. ROELOFSMA, J. GURTZ, A. BADOUX, 2001: Distributed hydrological modelling of a heavily glaciated Alpine river basin. – Hydrol. Sci. J., Journal Des Sciences Hydrologiques **46**, 553–570.

KUNSTMANN, H., C. STADLER, 2005: High resolution distributed atmospheric-hydrological modeling for Alpine catchments. – J. Hydrol. **314**, 105–124.

LIANG, X.-Z., L. LI, K. E. KUNKE, 2004: Regional Climate Model Simulation of U.S. Precipitation during 1982-2002. Part I: Annual Cycle. – J. Climate **17**, 3510-3529.

NASH, J. E., J. V. SUTCLIFFE, 1970: River flow forecasting through conceptual models part I – A discussion of principles. – J. Hydrol. **10**, 282–290.

PÁLSSON, F., E. MAGNÚSSON, H. BJÖRNSSON, 2002a: The surge of Dyngjujökull 1997–2000. Mass transport, ice flow velocities and effects on mass balance and runoff. – Reykjavík, Science Institute – University of Iceland, Report RH-01-2002.

PÁLSSON, F., H. BJÖRNSSON, H. H. HARALDSSON, 2002b: Vatnajökull: Mass balance, meltwater drainage and surface velocity of the glacial year 2000–2001. – Reykjavík, Science Institute – University of Iceland and the National Power Company, Report RH-02-2002.

PÁLSSON, F., H. BJÖRNSSON, E. MAGNÚSSON, 2004a: Afkomu- og hraðamælingar á Langjökli jökulárið 2003-2004 (Measurements of mass balance and ice flow velocities on Langjökull, glacial year 2003-2004). – Reykjavík, Raunvísindastofnun Háskólans og Landsvirkjun (Science Institute - University of Iceland and the National Power Company), Report RH-18-2004 (in Icelandic).

PÁLSSON, F., H. BJÖRNSSON, H. H. HARALDSSON, 2004b: Vatnajökull: Mass balance, meltwater drainage and surface velocity of the glacial year 2001–2002. – Reykjavík, Science Institute – University of Iceland and the National Power Company, Report RH-21-2004.

PÁLSSON, F., H. BJÖRNSSON, E. MAGNÚSSON, H. H. HARALDSSON, 2004c: Vatnajökull: Mass balance, meltwater drainage and surface velocity of the glacial year 2002–2003. – Reykjavík, Science Institute – University of Iceland and the National Power Company, Report RH-22-2004.

PHILIP, J. R., 1969: The theory of infiltration. – In: CHOW, V.T. (Ed.): Advances in Hydrosciences. – Academic Press, New York, 216–296.

QIAN, J.-H., A. SETH, S. ZEBIAK, 2003: Reinitialized versus Continuous Simulations for regional Climate Downscaling. – Mon. Wea. Rev. **131**, 2857–2874.

RICHARDS, L. A., 1931: Capillary conduction of liquids through porous medium. – Physics **1**, 318–333.

RÖGNVALDSSON, Ó., P. CROCHET, H. ÓLAFSSON, 2004: Mapping of precipitation in Iceland using numerical simulations and statistical modeling. – Meteorol. Z. **13**(3), 209–219.

SIGURÐSSON, O., 1989: Afkoma Hofsjökuls 1987–1988 (Mass balance of Hofsjökull 1987–1988). – Reykjavík, National Energy Authority, Report OS-89005/VOD-02 B (in Icelandic).

—, 1990: Afkoma Hofsjökuls 1988-1989 (Mass balance of Hofsjökull 1988-1989). – Reykjavík, National Energy Authority, Report OS-91052/VOD-08 B (in Icelandic).

—, 1993: Afkoma nokkurra jökla á Íslandi 1989-1992 (Mass balance of a number of Icelandic glaciers 1989-1992). Reykjavík, National Energy Authority, Report OS-93032/VOD-02 (in Icelandic).

SIGURÐSSON, O., Ó. J. SIGURÐSSON, 1998: Afkoma nokkurra jökla á Íslandi 1992–1997 (Mass balance of a number of Icelandic glaciers 1992–1997). – Reykjavík, National Energy Authority, Report OS-98082 (in Icelandic).

SIGURÐSSON, O., TH. THORSTEINSSON, S. M. ÁGÚSTSSON, B. EINARSSON, 2004: Afkoma Hofsjökuls 1997–2004 (Mass balance of Hofsjökull 1997-2004). – Reykjavík, National Energy Authority, Report OS-2004/029 (in Icelandic).

SMITH, R. B., I. BARSTAD, L. BONNEAU, 2005: Orographic Precipitation and Oregon's Climate Transition. – J. Atmos. Sci. **62**, 177–191.

SÆLTHUN, N. R., 1996: The "Nordic" HBV model-version developed for the project "Climate Change and Energy Production". – NVE Publication no. **7**, Norwegian Water Resources and Energy Administration, Oslo.

TÓMASSON, G. G., H. ÓLAFSSON, Ó. RÖGNVALDSSON, 2005: Meteorological and hydrological modeling of an extreme precipitation event in S-Iceland. – International Conference on Alpine Meteorology and MAP-Meeting 2005, 23–27 May 2005, Zadar, Croatia, 558–561. Available on the web: www.map.meteoswiss.ch/map-doc/icam2005/pdf/poster-sesion-d/D41.pdf

VRIES, M. DE, H. ÓLAFSSON, 2003: Precipitation across a mesoscale mountain ridge: The Reykjanes EXperiment (REX). – International Conference on Alpine Meteorology and MAP-Meeting 2003, MeteoSwiss, No. 66, Brig, Switzerland, 113–116.

WARNER, T. T., R. A. PETERSON, R. E. TREADON, 1997: A Tutorial on Lateral Boundary Conditions as a Basic and Potentially Serious Limitation to Regional Numerical Weather Prediction. – Bull. Amer. Meteor. Soc. **78**, 2599–2617.

WESTRICK, K. J., P. STORCK, C. F. MASS, 2002: Description and Evaluation of a Hydro-meteorological Forecast System for Mountainous Watersheds. – Wea. Forecasting **17**, 250–262.

Paper III: Sensitivity Simulations of Orographic Precipitation with MM5 and Comparison with Observations in Iceland during the Reykjanes EXperiment

Meteorologische Zeitschrift, Vol. **16**, No. 1, 087-098 (February 2007)
© by Gebrüder Borntraeger 2007

Article

Sensitivity simulations of orographic precipitation with MM5 and comparison with observations in Iceland during the Reykjanes Experiment

ÓLAFUR RÖGNVALDSSON*[1,2], JIAN-WEN BAO[3] and HARALDUR ÓLAFSSON[1,4,5,6]

[1]Institute for Meteorological Research, Reykjavík, Iceland
[2]University of Bergen, Bergen, Norway
[3]NOAA/Earth System Research Laboratory, Boulder, Colorado, USA
[4]University of Iceland, Reykjavík, Iceland
[5]Icelandic Meteorological Office, Reykjavík, Iceland
[6]currently at Bergen School of Meteorology, Geophysical Institute, University of Bergen, Norway

(Manuscript received October 30, 2006; in revised form November 27, 2006; accepted December 5, 2006)

Abstract

This paper presents a study of the sensitivity of numerically simulated precipitation across a mesoscale mountain range to horizontal resolution, cloud condensation nuclei (CCN) spectrum, initiation of cloud ice, numerical treatment of horizontal diffusion and initial and boundary conditions. The fifth generation Penn State/National Center for Atmospheric Research (PSU/NCAR) Mesoscale Model (MM5) is used in the study, in which the model is run at 8, 4 and 2 km horizontal resolutions and with a number of microphysical and numerical configurations. The model simulated precipitation is compared to the observed precipitation over the Reykjanes mountain ridge during the Reykjanes Experiment in Southwest Iceland in the autumn of 2002. Improvements in representation in topography at increasing horizontal resolutions yield large improvements in the accuracy of the simulated precipitation. At 8 km horizontal resolution the simulated maximum precipitation is too low, but the simulated precipitation upstream of the mountains is too high. The absolute values and the pattern of the precipitation field improve stepwise when going from horizontal resolutions of 8 km to 2 km, with the main contribution being when going from 8 km to 4 km. Calculations of diffusion and ice initiation do not seem to have a large impact on the simulated precipitation, which is on the other hand quite sensitive to the CCN spectrum. The simulations underestimate the precipitation over the downstream slopes of the mountain ridge by factors of 2–3. There are indications that this underestimation may be associated with a systematic overestimation of downslope winds, and possibly descending motion, by the model.

Zusammenfassung

In dieser Publikation wird die Empfindlichkeit des simulierten Niederschlags über mesoskaligem Gebirge bezüglich der horizontalen Auflösung, dem Spektrum der Kondensationkerne (CCN), der Aktivierung der Eisbildung, der numerischen Behandlung der horizontalen Diffusion sowie der Anfangs- und der Randbedingungen studiert. Hiezu wurde das von PSU/NCAR entwickelte mesoskalige Modell MM5 eingesetzt und Simulationen mit horizontalen Auflösungen von 8, 4 und 2 km und mit mehreren mikrophysikalischen und numerischen Konfigurationen durchgeführt. Der simulierte Niederschlag wird mit den Messungen über dem Reykjanes Gebirge während des REX Experimentes in Südwest-Island im Herbst 2002 verglichen. Die Verfeinerung der räumlichen Auflösung der Topographie bewirkt eine wesentliche Verbesserung der Genauigkeit des simulierten Niederschlags. Bei 8 Kilometer Auflösung ist der simulierte maximale Niederschlag zu niedrig, der simulierte Niederschlag im Luv der Gebirgskette jedoch zu hoch. Die Absolutwerte und das räumliche Muster des Niederschlags verbessern sich schrittweise wenn man die horizontale Auflösung von 8 km auf 2 km erhöht, wobei der Hauptanteil beim Schritt von 8 km auf 4 km liegt. Unterschiedliche Berechnungen der Diffusion sowie der Aktivierung der Eisbildung scheinen keine großen Auswirkungen auf den simulierten Niederschlag zu haben. Auf die Wahl des CCN Spektrums ist er hingegen ziemlich empfindlich. Die Simulationen unterschätzen den Niederschlag im Lee der Gebirge um Faktoren von 2 bis 3. Es gibt Hinweise, dass diese Unterschätzung mit einer Überschätzung des leeseitigen Hangabwindes und einer generellen Absinkbewegung durch das Modell einher geht.

1 Introduction

Improving quantitative precipitation forecasting (QPF) over complex topography has long been a target of research campaigns organized in the numerical weather prediction (NWP) community. Recent examples of such campaigns are the Mesoscale Alpine Program (BOUGEAULT et al., 2001) and IMPROVE[1] (STOELINGA et al., 2003). Although forecasting skills

*Corresponding author: Ólafur Rögnvaldsson, Institute for Meteorological Research, Orkugarður Grensásvegur 9, 108 Reykjavík, Iceland, e-mail: or@os.is

[1]J. Atmos. Sci. **62**(10), October 2005, is a special issue on IMPROVE.

0941-2948/2007/0181 $ 5.40

DOI: 10.1127/0941-2948/2007/0181
© Gebrüder Borntraeger, Berlin, Stuttgart 2007

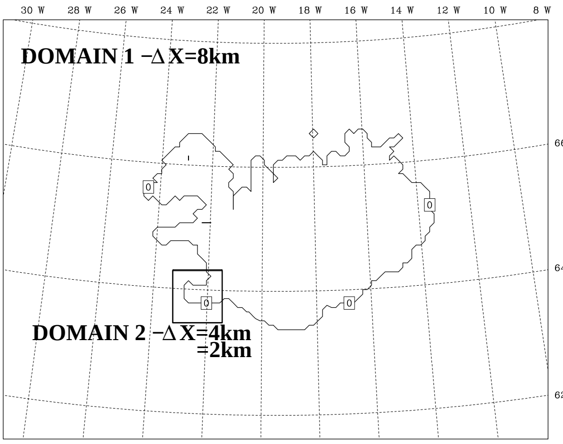

Figure 1: The domain setup as used in the simulations. Domain 1 is 123×95 points (approximately 975×750 km^2). The 4 and 2 km resolution domains are identical in size (approximately 145×130 km^2) and are 37×33 and 73×65 points in dimension, respectively.

of NWP models have improved considerably for many variables (e.g. geopotential height and temperature) over the past years and decades, precipitation has remained somewhat elusive (BOSART, 2003). One reason for this is that the physics governing the formation of precipitation are highly complicated, rendering parameterization difficult. Another reason is that the distribution of precipitation (particularly solid precipitation) over complex topography as simulated by NWP models is very sensitive to the dynamic and thermal characteristics of impinging wind (e.g. CHIAO et al., 2004).

Several investigations have been made on the sensitivity of numerically simulated precipitation to parameterizations of microphysical processes and numerical resolution. GRUBIŠIĆ et al. (2005) investigated wintertime storms in the Sierra Nevada. They found that the QPF skill score is greater on the windward side than the lee side. Interestingly, the low scores on the lee side cannot be improved by increasing model resolution.

COLLE and ZENG (2004a) also show that the precipitation over the Sierra Nevada is most sensitive to the parameters in the microphysical scheme that are associated with the distribution of snow and the fall speed of hydrometeors. There is, however, less sensitivity to the parameters associated with ice initiation and cloud water autoconversion. An investigation of the sensitivity of precipitation to barrier width (COLLE and ZENG, 2004b) indicates that for relatively wide ridges (with half-width greater or equal to 30 km) precipitation over the windward side is more sensitive to parameters related to snow, such as slope intercept for number concentrations and fall speeds, than to parameters related to rain and graupel. This is due to the fact that wide barriers allow more time for snow growth aloft. Consequently, precipitation over narrow barriers is more sensitive to rain and graupel processes such as cloud water autoconversion and graupel fall speed.

It has long been recognized that the precipitation intensity over complex topography is very sensitive to the dynamic characteristics of the flow. Modelling studies of flow over complex topography (e.g., ZÄNGL, 2002 and ZÄNGL et al., 2004) show that mountainous flow is not only dependent on model resolution and/or physical parameterizations but can also be greatly influenced by how advection and diffusion of temperature and moisture are calculated. The simulated precipitation can differ by as much as 35 % depending on how horizontal diffusion is calculated by the numerical model (ZÄNGL, 2004).

This paper presents a study in which precipitation over the Reykjanes peninsula in SW-Iceland is simulated and compared to observations made during the Reykjanes EXperiment (REX) in September and October 2002. Special focus will be on precipitation simulated numerically during intensive observation period 5 (IOP5) of REX, 3–7 October 2002. Results from the simulations of other IOPs are discussed briefly.

The paper is structured as follows: In the next section the model configurations are explained and the various sensitivity simulations are described. Section 3 gives a short description of the available observational data. The results are presented in Section 4, followed by discussion and concluding remarks.

2 Model setup

The evolution of the atmosphere over a six week period in September and October 2002 is simulated with the PSU/NCAR MM5 model (GRELL et al., 1994). In this study, the turbulent boundary layer physics is parameterized according to HONG and PAN (1996), and the physics of cloud and precipitation is parameterized according to GRELL et al. (1994) and THOMPSON et al. (2004), respectively. The simulations are carried out with horizontal resolution of 8, 4 and 2 km with initial and boundary conditions (operational analysis) from both the European Centre for Medium-Range Weather Forecasts (ECMWF) and National Centers for Environmental Prediction (NCEP). The horizontal resolution of the ECMWF data is $0.5^\circ \times 0.5^\circ$ and of the NCEP data $1^\circ \times 1^\circ$. Vertical levels are the same for both data sets, i.e. along standard pressure levels. The 4 and 2 km simulations are initialized by one way nesting of the 8 km resolution simulation. The 8 km domain has 123×95 points (approximately 975×750 km^2) with 23 vertical levels. The model top is at 100 hPa in all simulations. The output of the 8 km resolution simulation is written once every hour in order to provide the necessary tempo-

Table 1: Overivew of the simulations.

Abbre-vation	Obs. period	Horiz. resolution	Vertical resolution	IC & BC	Horiz. diffusion	CNP value	Ice init. method
REX8-CNTR	All IOPs	8 km	23 σ-levels	ECMWF	Standard	100	Cooper
REX8-THoriz	IOP5	8 km	23 σ -levels	ECMWF	Truly horiz.	100	Cooper
REX8-NCEP	All IOPs	8 km	23 σ -levels	NCEP	Standard	100	Cooper
REX4-CNTR	All IOPs	4 km	40 σ -levels	ECMWF	Standard	100	Cooper
REX4-THoriz	IOP5	4 km	40 σ -levels	ECMWF	Truly horiz.	100	Cooper
REX4-NCEP	IOP5	4 km	40 σ -levels	NCEP	Standard	100	Cooper
REX4-Fletcher	IOP5	4 km	40 σ -levels	ECMWF	Standard	100	Fletcher
REX4-Meyer	IOP5	4 km	40 σ -levels	ECMWF	Standard	100	Meyers
REX4-CNP200	IOP5	4 km	40 σ -levels	ECMWF	Standard	200	Cooper
REX4-CNP50	IOP5	4 km	40 σ -levels	ECMWF	Standard	50	Cooper
REX4-CNP30	IOP5	4 km	40 σ -levels	ECMWF	Standard	30	Cooper
REX4-CNP30-THoriz	IOP5	4 km	40 σ -levels	ECMWF	Truly horiz.	30	Cooper
REX2-CNTR	All IOPs	2 km	40 σ -levels	ECMWF	Standard	100	Cooper
REX2-THoriz	IOP5	2 km	40 σ -levels	ECMWF	Truly horiz.	100	Cooper
REX2-CNP30	IOP5	2 km	40 σ -levels	ECMWF	Standard	30	Cooper
REX2-CNP30-THoriz	IOP5	2 km	40 σ -levels	ECMWF	Truly horiz.	30	Cooper

ral resolution for the nestdown[2] procedure. The 4 and 2 km resolution domains have 37×33 and 73×65 points (approximately 145×130 km^2), respectively. There are 40 vertical levels in all the 4 km and 2 km simulations. The values of the three lowest full-sigma levels in the simulations with horizontal resolution of 4 and 2 km are 0.9885, 0.9975 and 1.0. For the 8 km resolution simulations, these values are 0.985, 0.995 and 1.0. A number of simulations are carried out in order to investigate the sensitivity of simulated precipitation to model configuration (cf. Table 1). All simulations are done using version 3-7-3 of the MM5 model. The domain setup is shown in Figure 1.

[2]We used the NESTDOWN post-processing program that comes with the MM5 modeling suite to interpolate (both vertically and horizontally) the coarse resolution data (i.e. from the 8 km simulations) to be used as initial and boundary data for the 4 and 2 km simulations. The advantages of this method are that the model has lateral boundary conditions that use consistent physics with the coarse grid model, the lateral boundary conditions are available at a high temporal frequency and the vertical structure of the atmosphere is not significantly modified through vertical interpolation.

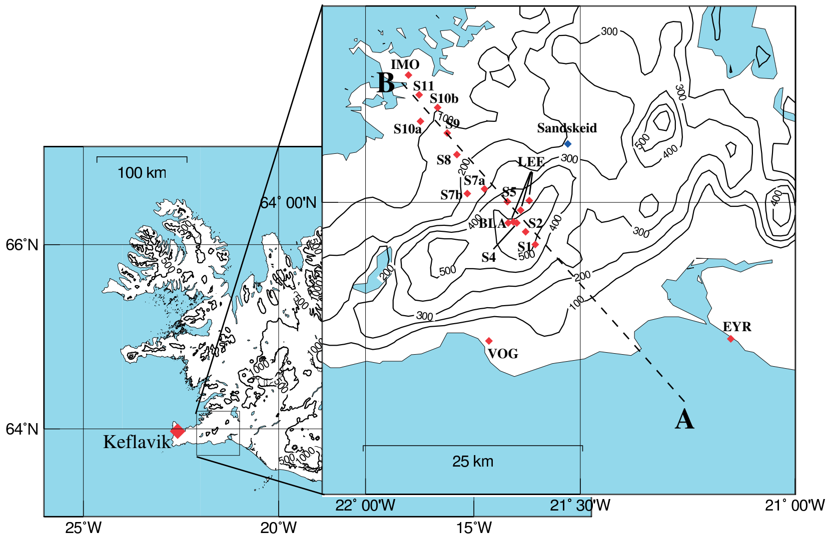

Figure 2: Overview of station location during REX. Stations EYR (Eyrarbakki), VOG (Vogsósar), BLA (Bláfjöll), IMO (Icelandic Meteorological Office, WMO 4030) and Keflavík (WMO 4018) are part of the operational network in Iceland. Other stations, S1, S2, S4, S5, LEE (taken as mean of three stations), S7a, S7b, S8, S9, S10a, S10b and S11 were installed specifically for the Reykjanes EXperiment. Station Sandskeið is shown in blue. Topography is shown with height intervals of 100 meters. Results along cross section AB are shown in Figures 4 to 8.

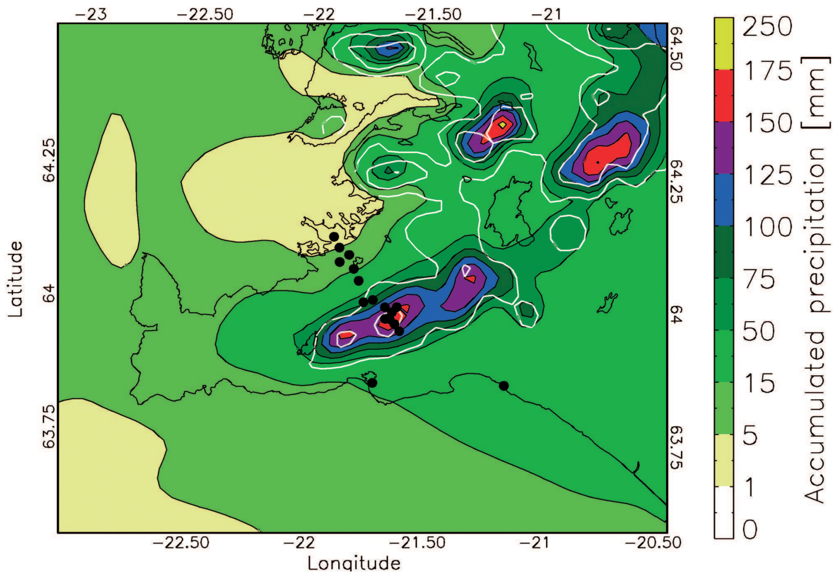

Figure 3: Terrain and accumulated precipitation during IOP5 as simulated in the REX2-CNP30 run (cf. Table 1). Contour lines (white) of the terrain are plotted every 250 meters. Location of observation sites are shown by black dots.

In order to investigate the model sensitivity to various parameterizations of the nucleation of cloud ice, three types of simulations are performed[3] by using (1) a modified Reisner2 bulk microphysics parameterization (BMP) scheme (THOMPSON et al., 2004) using the method of FLETCHER (1962), (2) the unmodified Reisner2 scheme based on the method of COOPER (1986), and (3) the slightly modified Reisner2 BMP scheme based on the method of MEYERS and COTTON (1992).

[3]This was done through modifications to files/programs paramr.F and exmoisg.F in the MM5 modeling system suite.

Another issue in the BMPs is the sensitivity to aerosol and/or cloud condensation nuclei (CCN) concentrations. CCN is not used directly in the Reisner2 scheme, but there is a parameter that sets the cloud droplet number concentrations (CNP), which determines the amount of cloud-to-rain autoconversion[4] (THOMPSON et al., 2004). To test the model sensitivity to the CCN spectra, simulations are carried out with

[4]The collision and coalescence of cloud droplets to form raindrops is parameterized by autoconverting between the mixing ratios of the two hydrometeor species q_c (i.e. cloud) and q_r (i.e. rain).

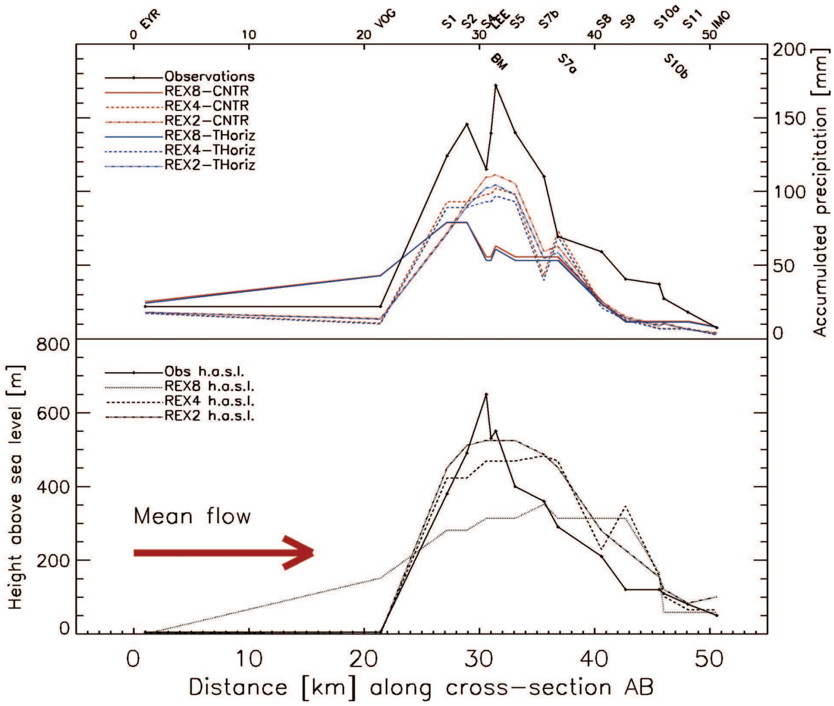

Figure 4: Observed and simulated accumulated precipitation during IOP5 along cross section AB in Figure 2. Model resolution varies; solid, dashed and dot-dashed lines represent 8, 4 and 2 km resolution, respectively, as well as treatment of horizontal diffusion (truly horizontal in blue and standard in red). Observed precipitation is shown by solid black line and station locations are indicated by crosses. Bottom panel shows the orography along cross section AB in Figure 2, observed (solid line), 8 km resolution (dotted line), 4 km (dashed line) and 2 km resolution (dot-dashed line).

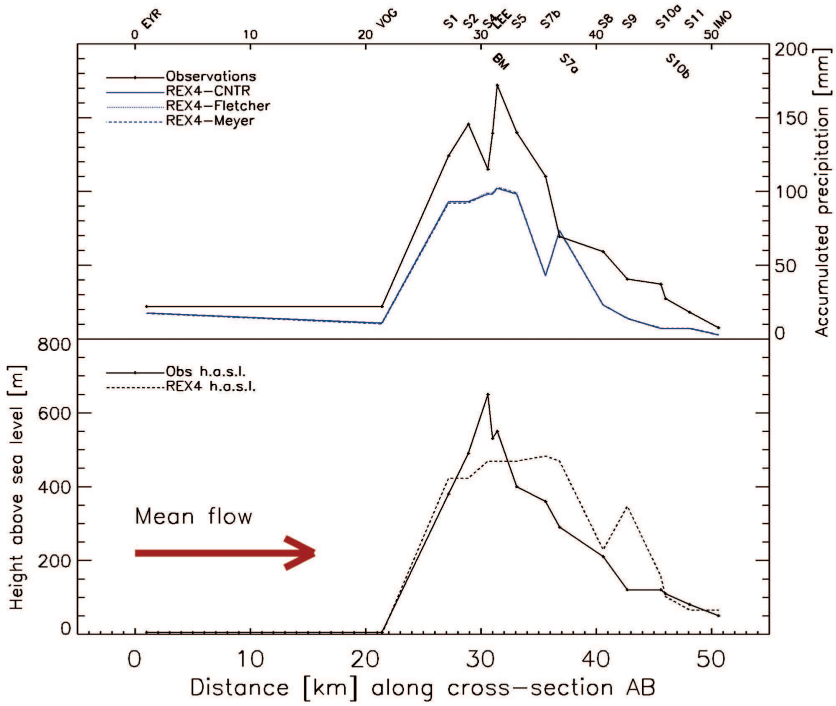

Figure 5: Sensitivity to different ice initiation methods as simulated by REX4-CNTR (solid line), REX4-Fletcher (dot-dashed line) and REX4-Meyer (dashed line), cf. Table 1. All three lines coincide with each other. Bottom panel shows the model and actual orography along cross section AB in Figure 2.

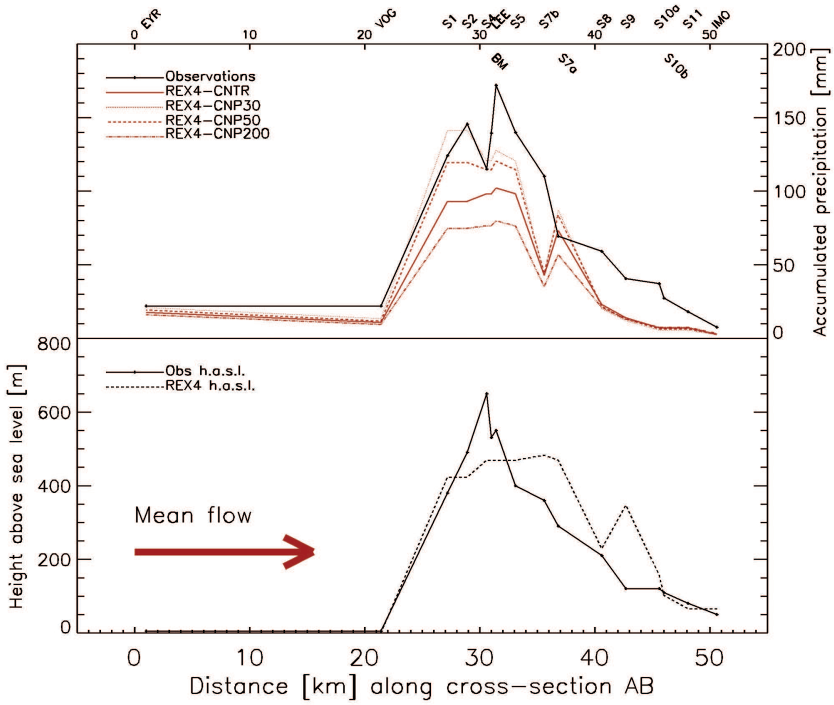

Figure 6: Sensitivity to different values of CNP at 4 km horizontal resolution, CNP = 100 (CNTR, solid line), CNP = 30 (dotted line), CNP = 50 (dashed line) and CNP = 200 (dot-dashed line). Bottom panel shows the model and actual orography along cross section AB in Figure 2.

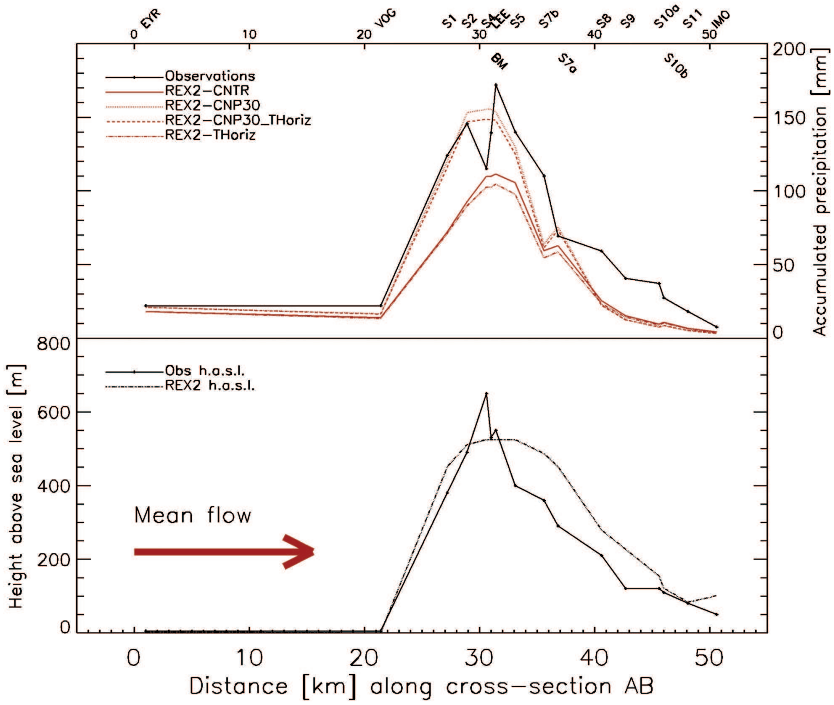

Figure 7: Sensitivity to various CNP values and treatment of horizontal diffusion at 2 km horizontal resolution. REX2-CNTR (solid line), REX2-THoriz (dot-dashed line), REX2-CNP30 (dotted line) and REX2-CNP30_THoriz (dashed line), cf. Table 1. Bottom panel shows the model and actual orography along cross section AB in Figure 2.

different values of CNP[5] (30, 50, 100 and 200 droplets per cubic centimetre). Here, CNP = 30, represents a maritime spectrum of CCN, whilst CNP = 200 represents a more continental CCN spectrum.

Sensitivity of simulated precipitation to how horizontal diffusion of temperature and moisture is calculated is tested, i.e. whether the diffusion is calculated along

[5]The value of CNP is defined in file paramr.F in the MM5 modeling system suite.

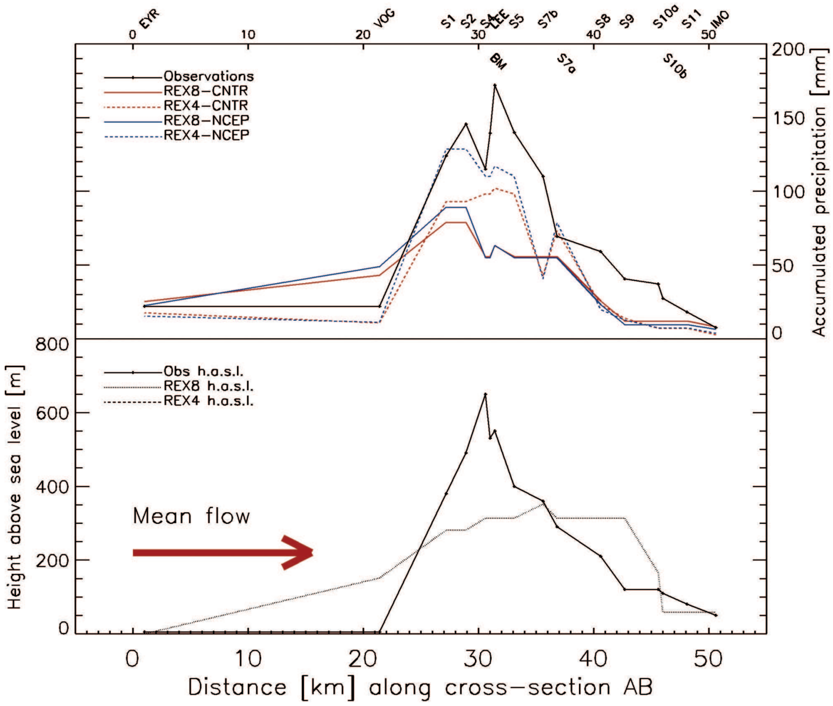

Figure 8: Sensitivity to different initial and boundary conditions. Simulations using the ECMWF operational analysis is shown in red and the NCEP operational analysis in blue, for 8 (solid lines) and 4 (dashed lines) km horizontal resolutions. Bottom panel shows model and actual the orography along cross section AB in Figure 2.

the terrain-following sigma coordinates (referred to as "standard" in Table 1) or along truly horizontal levels[6] (referred to as "Truly horiz." in Table 1).

All observation periods are simulated on 8, 4 and 2 km horizontal resolution using the ECMWF operational analysis and on 8 km resolution using the NCEP operational analysis. Table 1 gives an overview of the simulations carried out for this study.

3 Observational data

The Reykjanes mountain ridge in Southwest-Iceland is about 20 km wide with a crest at about 700 m.a.s.l. (cf. Figures 1 and 2). During autumn 2002, precipitation was observed at 18 locations around and across the mountain ridge in SW-Iceland (de Vries and Ólafsson, 2003). The precipitation was observed by conventional raingauges of which most were at ground level (Figure 2). The experiment took place from early September until the middle of October and during the whole period, only liquid precipitation was observed. The maximum mean precipitation in the mountains during the experiment was observed to be 3–4 times the mean precipitation at the south coast of the peninsula (upstream) and 5–6 times the precipitation at the north coast of the peninsula (downstream). There was a distinct connection between the wind speed and the topographic precipitation gradient; the ratio of precipitation in the mountains to the precipitation upstream of the mountains in strong winds was substantially greater than in cases of weak winds. In addition to the conventional raingauge data, automatic observations of wind, temperature and precipitation were made at high temporal resolution close to the crest of the mountain range (station BLA). The observation periods of REX were as follows: IOP1: 9–10 September, IOP2: 12–19 September, IOP3: 19–27 September, IOP4: 29 September–3 October, IOP5: 3–7 October and IOP6: 8–14 October. During the IOPs, precipitation was observed in winds from the south and/or southeast, with the exception of IOP2, which had easterly winds.

4 Results

4.1 Sensitivity tests during IOP5

Figure 3 shows the accumulated precipitation simulated using 2 km horizontal resolution and the initial and boundary conditions from the ECMWF and a CNP value equal to 30 (REX2-CNP30 in Table 1). A very close correspondence of the precipitation pattern to local orographic feature is evident, as the precipitation isolines coincide largely with the topography. The simulated precipitation is typically about 20–30 mm at the south coast, while in the mountains the simulated precipitation is 5–6 times greater than at the south coast.

[6] This is done by giving the parameter ITPDIF a value of "2" in the mmlif file of the MM5 modeling suite.

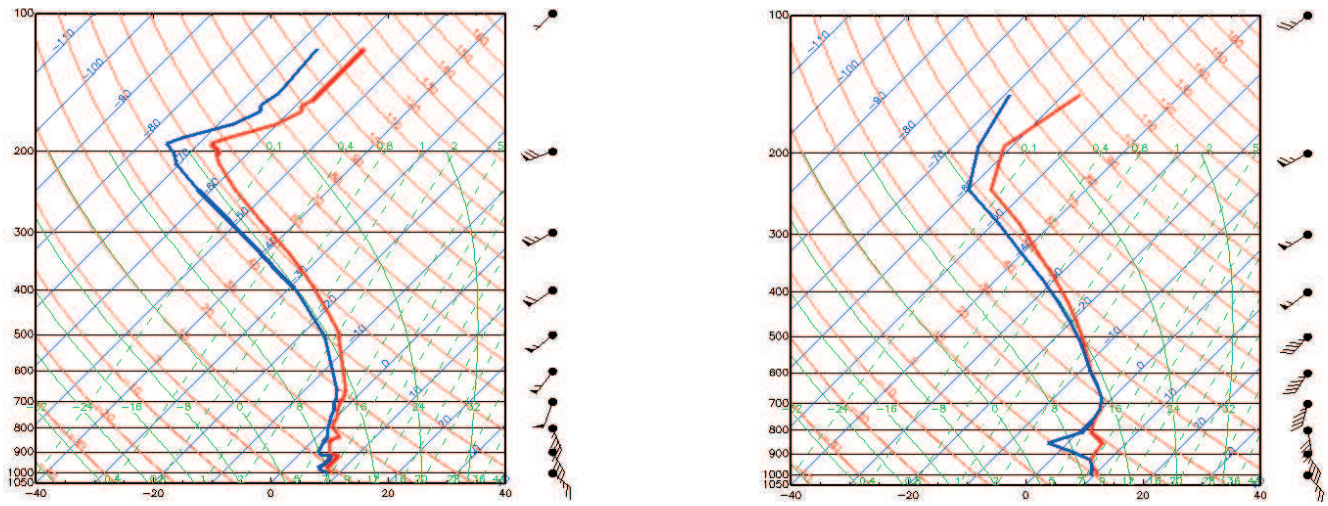

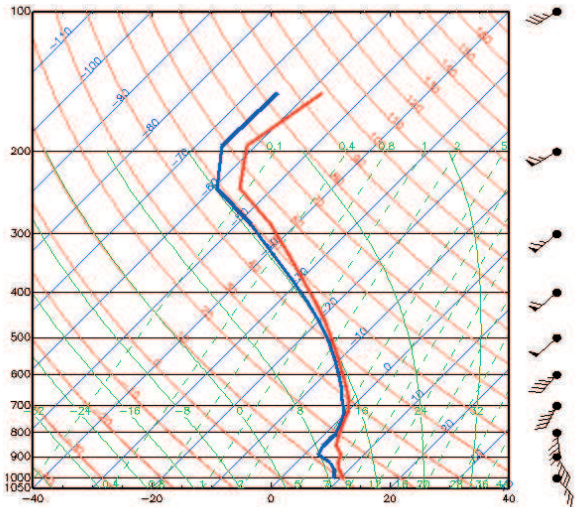

Figure 9: Observed (upper left) and simulated soundings at station Keflavík (WMO 4018) at 00 UTC October 5, based on ECMWF (upper right) and NCEP (lower left) analysis. Here, an overly dry layer is present in the ECMWF, and to a considerably less extent the NCEP, based simulation at approximately 850 hPa.

4.1.1 Sensitivity to horizontal resolution and calculations of horizontal diffusion

Figure 4 compares the observed precipitation distribution with precipitation simulated using different horizontal resolutions and different ways of calculating horizontal diffusion. Upstream of the mountain, the precipitation is slightly underestimated in the model at the higher resolutions, but it is overestimated at 8 km resolution. In the vicinity of the crest of the mountain ridge, the 4 km and particularly the 2 km resolutions give much greater, and more correct, precipitation than the simulation with 8 km horizontal resolution. Further downstream, all the simulations converge towards the same values that are only about half the observed values. Calculating diffusion along truly horizontal levels gives slightly less precipitation than the control simulations for all resolutions, but the differences are relatively small.

4.1.2 Sensitivity to microphysics

Figures 5 and 6 show the accumulated precipitation as calculated with different cloud ice initiation methods at 4 km resolution and for different values of the droplet concentration (CNP) at 4 km horizontal resolution. The simulations reveal no sensitivity to the ice initiation methods. There is however a substantial sensitivity to the droplet concentration. Increasing the CNP to 200 gives a significant reduction in precipitation, while a reduction in the CNP value increases the simulated precipitation substantially. At CNP = 30 the simulated precipitation is comparable with the observations values at the mountain crest and immediately upstream. Moving downstream from the mountain crest, the simulations with different droplet concentrations converge rapidly to giving similar amounts of precipitation. Figure 7 shows the sensitivity of the simulated precipitation to the droplet concentration and using different ways of calculating horizontal diffusion. Calculating diffusion at true horizontal levels gives slightly less precipitation than when us-

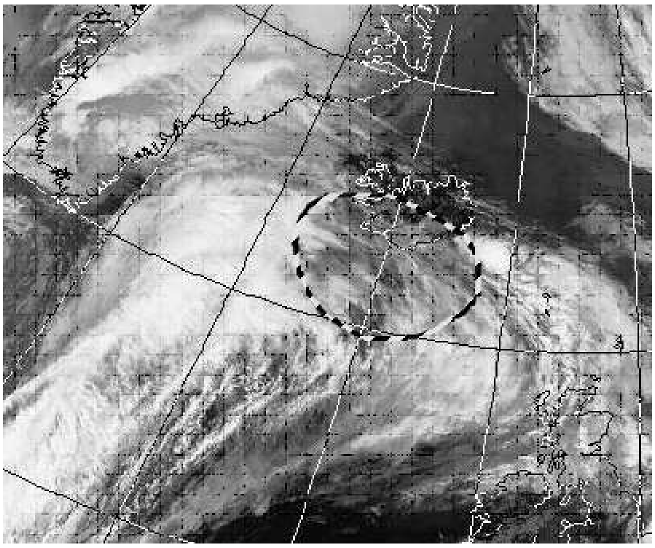

Figure 10: Satellite image taken at 14:30 UTC on 4 October, 2002, showing a relatively dry layer south of Iceland between two frontal systems (encircled area). Photo courtesy of the NERC Satellite Receiving Station, Dundee.

ing the standard method. Consequently, the calculated precipitation appears not to be sensitive to the methods of calculating the diffusion, independent of whether the droplet concentration is high or low (CNP 30 or 100).

4.1.3 Sensitivity to initial and boundary conditions

At 4 km resolution the simulation with the NCEP analysis at the lateral boundaries produces considerably greater precipitation in the mountains than the simulation forced with data from the ECMWF (cf. Figure 8). A similar pattern appears at 8 km horizontal resolution. To give an example of differences between simulations with the two different data sources, the two 4 km simulations initialized separately using the NCEP and the ECMWF analyses are compared during a sub-period of IOP5. The upper air observations at 00 UTC on 5 October from Keflavík (WMO 4018) reveal a relatively dry layer close to 850 hPa in the simulation with boundary data from the ECMWF analysis. No such layer is present in neither the observations nor in the simulation with boundary data from NCEP analysis (Figures 9a–c).

A satellite image taken at 14:30 UTC on 4 October (Figure 10) shows a relatively dry region south of Iceland between two frontal systems. This region is present at 850 hPa height in simulations initialized using both the ECMWF and NCEP analyses (Figure 11). In the simulation based on data from the ECMWF analysis, part of this layer is being advected over the Reykjanes peninsula, SW-Iceland, at 00UTC on 5 October. This layer is also present in the NCEP based simulation but is largely limited to the area south and southeast of Iceland.

4.2 Other observation periods

The downslope dryness in the simulated precipitation, as shown in the case study for IOP5, is apparent for all of the IOPs. Figure 12 shows this clearly. Here, "upstream" is defined as the mean of points EYR and VOG in Figure 1. Further, "top" and "downstream" are defined as the mean of points S2, BLA and S4 and points S10a, S10b, S11 and IMO, respectively (cf. Figure 2). For the sake of clarity, Figure 12 only shows results at 8 and 2 km horizontal resolution. On the upstream side, the simulated precipitation decreases consistently with increasing resolution. Close to the crest (mountain top), there is consistently greater and in most cases more correctly simulated precipitation at horizontal resolution of 2 km than at 8 km. Downstream, the 2 km simulations give either similar or more precipitation than the 8 km simulations. In all, except IOP2, the downstream precipitation is grossly underestimated by the simulations. In general, the simulations based on NCEP data are either similar or wetter than those that are based on ECMWF data.

5 Discussions and conclusions

The sensitivity of precipitation to horizontal resolution corresponds with the representation of the topography at the different resolutions. As the resolution is increased from 8 to 2 km, the numerical model is able to reproduce the precipitation observed in REX quite realistically close to the crest of the mountain range. However, as in GRUBIŠIĆ et al. (2005), simulated precipitation downstream of the ridge does not improve as model resolution is increased. The model underestimates the precipitation over the lee slopes regardless of horizontal resolution. This systematic underestimation of the precipitation downstream may be one of the key results of this study and it calls for further discussion. Figure 13 shows observed (at approximately 10 m.a.g.) and modelled (REX2-CNTR, approximately 50 m.a.g.) surface wind speed at Keflavík, about 30 km west of the mountains and at Sandskeið (cf. Figure 2)[7]. The southerly winds giving precipitation during REX are basically unperturbed by the mountains when they pass over Keflavík, while Sandskeið is located on the downstream side of the Reykjanes mountains (cf. Figure 2) . The figure reveals that the model overestimates the winds and that the overestimation is greater at Sandskeið than at Keflavík. There is greatest wind overestimation in IOP1, which along with IOP4, IOP5 and IOP6 give the greatest underestimation of the downstream precipitation. These results indicate that the downslope winds and possibly the descending motion downstream of the mountain

[7]Winds are retrieved from the second lowest half-sigma level, which is close to 50 m above the ground. Of all levels, including 10 m above the ground, this level gives winds that are closest to observations.

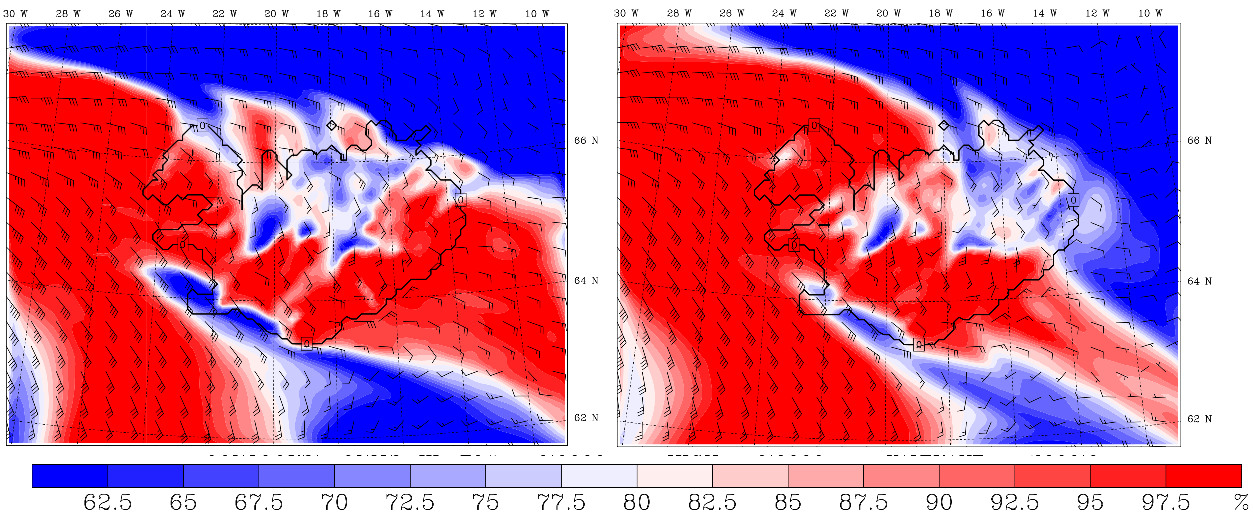

Figure 11: Simulated surface winds [m/s] and relative humidity [%] at 850 hPa for REX8-CNTR (left) and REX8-NCEP (right) at 00UTC on 5 October.

crest may be systematically overestimated by the model. Overestimation of the winds aloft can lead to an overestimation of the spill-over (see GARVERT et al., 2005) but an overestimation of the downdrafts can lead to an overestimation of the evaporation (see COLLE, 2004 for related tests). This calls for 3D verifications of the simulated flow fields by for instance airborne lidar observations. Such observations will hopefully be carried out in the upcoming field experiments (OFF-GREEN and GREENEX-THORPEX) in association with the International Polar Year.

Other processes may also be responsible for at least some of the downstream precipitation deficit, such as underestimation of snow in the model (see COLLE et al., 2005). Snow has lower fall speed than graupel or rain and is consequently advected downstream more easily. The existence of cold air pools acting as a virtual extension of the mountain should also not be ruled out. If such a pool is not reproduced by the model, the descending motion will be overestimated in the model and consequently the evaporation too (see ZÄNGL, 2005). However, most of the time, wind speeds are too high to allow for such a flow pattern and if they exist at all in our experiment, they are presumably only present for a very short time. Further, if the simulated upstream precipitation is unrealistically efficient (see LYNN et al., 2005) such that a small amount of hydrometeors is left in the flow passing over the mountain peak, one would expect similar results as presented in this paper. Lastly, it can not be ruled out that the incoming flow is unrealistically dry.

The model shows considerable sensitivity to cloud droplet concentration spectra on the windward side of the mountain and close to the mountain top, but no sensitivity to the ice initiation methods. This is in line with the sensitivity tests by COLLE and ZENG (2004a, 2004b; see also COLLE et al., 2005) and underlines the importance of the cloud droplet spectrum for precipitation simulations.

There is not much sensitivity to how the horizontal diffusion is calculated. This result deviates somewhat from ZÄNGL (2004), but may be associated with the fact that winds are relatively strong in our cases.

A relatively dry layer close to 850 hPa is erroneously represented in the ECMWF operational analysis during a brief subperiod of IOP5. The layer appears to contribute to the underestimation of precipitation on the crest of the mountain range, but the layer is only present for a very short period in time (approximately 3 hours) and has little impact on the overall results. General conclusions can hardly be drawn from the presence of such a layer, but a detection of an error of this kind may be helpful in improving the analysis procedures of the ECMWF model.

The results from this study indicate that the precipitation mapped at 8 km resolution as in BROMWICH et al. (2005) and RÖGNVALDSSON et al. (2004 and 2007) gives too small maxima over the mountain crest and far too little precipitation directly downstream of the crest. The former was in fact tested by BROMWICH et al. (2005). This can have considerable economical implications, as the spatial distribution of precipitation plays a key part in planning and use of water resources.

Quantitative precipitation forecasts in the mountains of Iceland are of economic and social value. Currently, the MM5 model is run for weather forecasting for Iceland with a 3 km horizontal resolution and the results presented here indicate that the precipitation forecasts close to the crest and immediately upstream of mountain ranges of the size of the Reykjanes mountains may be improved by decreasing the CNP value from the default value (i.e. CNP = 100).

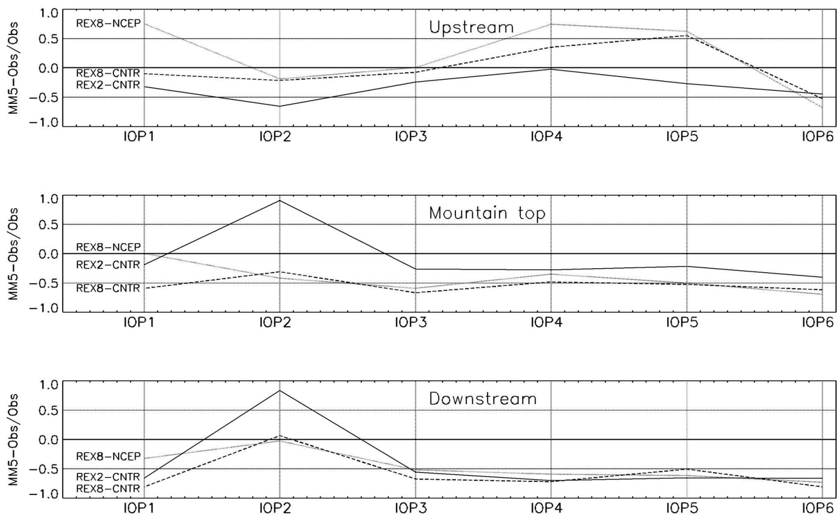

Figure 12: Ratio of simulated minus observed to observed precipitation upstream (top panel), at mountain top (middle panel) and downstream (bottom panel) for REX8-CNTR (dashed), REX8-NCEP (dots) and REX2-CNTR (solid) for all IOPs. The zero line indicates a perfect fit between observations and simulations.

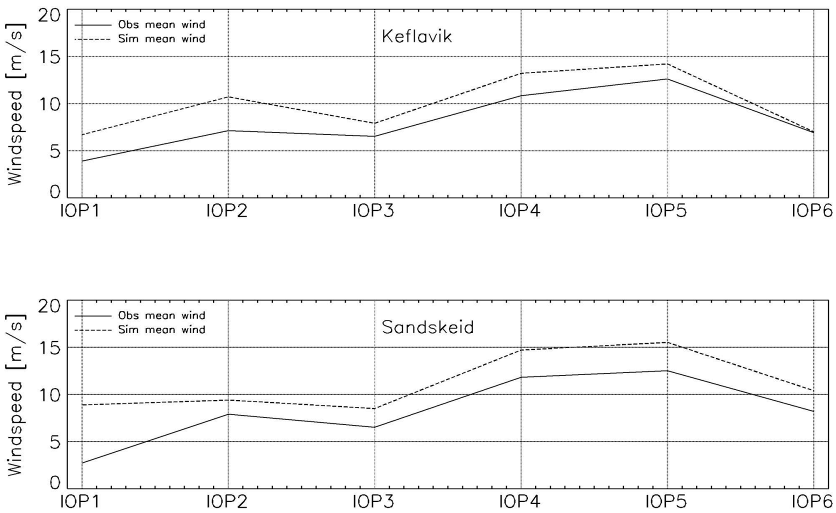

Figure 13: Simulated (REX2-CNTR, dashed line) and observed (solid line) surface mean winds, during precipitation at Bláfjöll station, at Keflavík (top) and Sandskeið (bottom). For station location see Figure 2. Simulated wind is at approximately 50 m.a.g. and observed at 10 m.a.g.

The tests presented in this paper further emphasize the well known importance of initial and boundary data for high-resolution simulations. The current operational forecasting suite in Iceland uses only initial and boundary data from the ECMWF. Implementing parallel forecasting suites using other available data sources, such as the NCEP (GFS) may provide useful information for operational forecasting.

The observations during REX and the simulations presented in this paper underline the variability in the precipitation pattern in a small mountain range. Our study strongly suggests that in order to validate numerical simulations and map the precipitation in this region and in similar regions of the world, a dense observation network is needed. The temporal resolution of precipitation observations should be at least one hour, and preferably higher. In order to improve the quality of the numerical simulations and in particular to explain and reduce the dryness of the simulations on the downstream side, four-dimensional observations of the flow and the microphysics should also be undertaken. This will hopefully be dealt with in future REX programmes.

From the numerical simulations and comparisons with observations during the REX experiment in SW-Iceland, it can be concluded that much is to be gained in quantitative precipitation mapping and forecasting by going from 8 km to at least 2 km horizontal resolution. Our current tool, the MM5 model, produces precipitation which is quite sensitive to the droplet spectrum, but not to the ice initiation method. The downslope precipitation is systematically underestimated and this calls for 3 to 4 dimensional observations to validate the flow field. Such a task will hopefully be undertaken in the upcoming field experiments of the International Polar Year.

Acknowledgements

This work has been sponsored by the Icelandic Science Fund (RANNÍS) and the Icelandic Energy Fund (Orkusjóður) and was part of the Nordic CWE (Climate, Water and Energy) project. Support was also given by the HRAS/RÁV projects for weather forecasting in Iceland. The first author is further indebted to NOAA/Earth System Research Laboratory (formerly Environmental Technology Laboratory) for hosting him as a visiting scientist in 2003. Comments from two anonymous reviewers further improved the article.

References

BOUGEAULT, P. , P. BINDER, A. BUZZI, R. DIRKS, R. HOUZE, J. KUETTNER, R. B. SMITH, R. STEINACKER, H. VOLKERT, 2001: The MAP Special Observing Period. – Bull. Am. Meteor. Soc. **82**, 433–462.

BOSART, L. F., 2003: Whither the Weather Analysis, Forecasting Process? – Wea. Forecasting **18**, 520–529.

BROMWICH, D. H. L. BAI, G. G. BJARNASON, 2005: High-Resolution Regional Climate Simulations over Iceland Using Polar MM5. – Mon. Wea. Rev. **133**, 3527–3547.

CHIAO, S. Y-L LIN, M. L. KAPLAN, 2004: Numerical Study of the Orographic Forcing of Heavy Precipitation during MAP IOP-2B. – Mon. Wea. Rev. **132**, 2184–2203.

COLLE, B. A., 2004: Sensitivity of orographic precipitation to changing ambient conditions and terrain geometries: An idealized modeling perspective. – J. Atmos. Sci. **61**, 588–606.

COLLE, B. A., Y. ZENG, 2004a: Bulk Microphysical Sensitivities within the MM5 for Orographic Precipitation. Part I: The Sierra 1986 Event. – Mon. Wea. Rev. **132**, 2780–2801.

—, —, 2004b: Bulk Microphysical Sensitivities within the MM5 for Orographic Precipitation. Part II: Impact of Barrier Width, Freezing Level. – Mon. Wea. Rev. **132**, 2802–2815.

COLLE, B. A. J. B. WOLFE, W. J. STEENBURGH, D. E. KINGSMILL, J. A. W. COX, J. S. SHAEFER, 2005: High-Resolution Simulations, Microphysical Validation of an Orographic Precipitation Event over the Wasatch Mountains during IPEX IOP3. Mon. Wea. Rev. 133, 2947-2971.

COOPER, W. A., 1986: Ice initiation in natural clouds. Precipitation Enhancement – A Scientific Challenge. – Meteor. Monogr. No. **43**, Amer. Meteor. Soc. 29–32.

FLETCHER, N. H., 1962: The Physics of Rain Clouds. – Cambridge University Press, 386 pp.

GARVERT, M. F., B. A. COLLE, C. F. MASS, 2005: The 13-14 December 2001 IMPROVE-2 Event. Part I: Synoptic and Mesoscale Evolution and Comparison with a Mesoscale Model Simulation. – J. Atmos. Sci. **62**, 3474–3492.

GRELL, G. A. J. DUDHIA, D. R. STAUFFER, 1994: A description of the fifth-generation Penn State/NCAR Mesoscale Model (MM5). – NCAR Tech. Note NCAR/TN-398+STR, 138 pp.

GRUBIŠIĆ V., R. K. VELLORE, A. W. HUGGINS, 2005: Quantitative Precipitation, Forecasting of Wintertime Storms in the Sierra Nevada: Sensitivity to the Microphysical Parameterization, Horizontal Resolution. – Mon. Wea. Rev. **133**, 2834–2859.

HONG, S. Y., H. L. PAN, 1996: Nonlocal boundary layer vertical diffusion in a medium-range forecast model. – Mon. Wea. Rev. **124**, 2322–2339.

LYNN, B. H., A. P. KHAIN, J. DUDHIA, D. ROSENFELD, A. POKROVSKY, A. SEIFERT, 2005: Spectral (Bin) Microphysics Coupled with a Mesoscale Model (MM5). Part I: Model Description and First Results. – Mon. Wea. Rev. **133**, 44–58.

MEYERS, M. P., W. R. COTTON, 1992: Evaluation of the potential for wintertime quantitative precipitation forecasting over mountainous terrain with an explicit cloud model. Part I: Two-dimensional sensitivity experiments. – J. Appl. Meteor. **31**, 26-50.

RÖGNVALDSSON, Ó., P. CROCHET, H. ÓLAFSSON, 2004: Mapping of precipitation in Iceland using numerical simulations, statistical modeling. – Meteorol. Z., **13**(3), 209–219.

RÖGNVALDSSON, Ó., J. F. JÓNSDÓTTIR, H. ÓLAFSSON, 2007: Numerical Simulations of Precipitation in the Complex Terrain of Iceland - Comparison with Glaciological and Hydrological Data. – Meteorol. Z., **16**(1), 71-85.

STOELINGA, M., P. V. HOBBS, C. F. MASS, J. D. LOCATELLI, B. A. COLLE, R. A. HOUZE, A. L. RANGO, N. A. BOND, B. F. SMULL, R. M. RASMUSSEN, G. THOMPSON, B. R. COLEMAN, 2003: Improvement of Microphysical Parameterizations through Observational Verification Experiments IMPROVE. – Bull. Amer. Meteor. Soc. **84**, 1807–1826.

THOMPSON, G, R. M. RASMUSSEN, K. MANNING, 2004: Explicit Forecasts of Winter Precipitation Using a Improved Bulk Microphysics Scheme. Part I: Description, Sensitivity Analysis. – Mon. Wea. Rev. **132**, 519–542.

VRIES, M. DE, H. ÓLAFSSON, 2003: Precipitation across a mesoscale mountain ridge: The Reykjanes EXperiment (REX). International Conference on Alpine Meteorology. – MAP-Meeting 2003, MeteoSwiss, No. 66, Brig, Switzerland, 113–116.

ZÄNGL, G., 2002: An Improved Method for Computing Horizontal Diffusion in a Sigma-Coordinate Model, Its Application to Simulations over Mountainous Topography. – Mon. Wea. Rev. **130**, 1423–1432.

—, 2004: The sensitivity of simulated orographic precipitation to model components other than cloud microphysics. – Quart. J. Roy. Meteor. Soc. **130**, 1857–1975.

—, 2005: The impact of lee-side stratification on the spatial distribution of orographic precipitation. – Quart. J. Roy. Meteor. Soc. **131**, 1075–1091.

ZÄNGL, G. L. GANTNER, G. HARTJENSTEIN, H. NOPPEL, 2004: Numerical errors above steep topography: A model intercomparison. – Meteorol. Z. **13**(2), 69–76.

Paper IV: Extracting Statistical Parameters of extreme Precipitation from a NWP Model

Hydrol. Earth Syst. Sci., 13, 2233–2240, 2009
www.hydrol-earth-syst-sci.net/13/2233/2009/
© Author(s) 2009. This work is distributed under
the Creative Commons Attribution 3.0 License.

Hydrology and Earth System Sciences

Extracting statistical parameters of extreme precipitation from a NWP model

J. Eliasson[1], O. Rögnvaldsson[2], and T. Jonsson[3]

[1]University of Iceland, Institute of Environmental and Civil Engineering, Iceland
[2]Institute for Meteorological Research, Reykjavik, Iceland
[3]Icelandic Meteorological Office, Iceland

Received: 8 June 2009 – Published in Hydrol. Earth Syst. Sci. Discuss.: 7 July 2009
Revised: 27 October 2009 – Accepted: 10 November 2009 – Published: 25 November 2009

Abstract. Precipitation simulations on an 8 8 km grid using the PSU/NCAR Mesoscale Model MM5 are used to estimate the M5 and C_i statistical parameters in order to support the M5 map used for flood estimates by Icelandic engineers. It is known a priori that especially wind anomalies occur on a considerably smaller scale than 8 km. The simulation period used is 1962–2005 and 73 meteorological stations have records long enough in this period to provide a validation data set. Of these only one station is in the central highlands, so the highland values of the existing M5 map are estimates. A comparison between the simulated values and values based on station observations set shows an M5 average difference (observed-simulated) of 5 mm/24 h with a standard deviation of 17 mm, 3 outliers excluded. This is within expected limits, computational and observational errors considered. A suggested correction procedure brings these values down to 4 mm and 11 mm, respectively.

1 Introduction

In this paper the statistical parameters M5 and C_i (Eliasson, 2000) for annual precipitation extremes in Iceland are estimated. The estimates are based on a NWP model: The fifth-generation Pennsylvania State University-NCAR Mesoscale Model-MM5 (Grell et al., 1995). It has been widely used in forecasting and usually found reliable. (Anders et al., 2007) found good agreement between gauge precipitation and cumulative MM5 precipitation simulations for all seasons in their investigation of the small-scale spatial gradients in climatological precipitation on the Olympic peninsula, a geographical region even more mountainous than Iceland. The sum of the 10 largest simulated events compared well with the precipitation gauges, although some of the individual events are significantly over- or undersimulated. In this paper we follow a similar methodology, extract statistical parameters from MM5 computed annual extreme rainfalls, without considering discrepancies in the time histories of computed and observed values, and then compare the results with available statistical parameters based on observations.

Great care has to be taken in selecting the parameterization scheme used in MM5 precipitation simulations. Convective precipitation is one of the most difficult. Here the Grell cumulus parameterization scheme (CPS) and the Reisner1 microphysics scheme (Reisner et al., 1998) is used as recommended by (Chien and Jou, 2004). Other combinations were found to lead to a general underforecast. However, some investigations have shown that all microphysical schemes produce a similar precipitation field and none of them perform significantly better than the others (Serafin and Ferretti, 2007). CPS will be discussed in more detail in the next section.

Major precipitation errors for individual storms seem to exist even in model runs with excellent overall performance. (Minder et al., 2008) found MM5 very good in simulating small-scale pattern of precipitation at seasonal time-scales while major errors exist for individual storms. Other analyses clearly show a tendency to form local precipitation maxima in the lee of individual mountain ridges (Zangl et al., 2008) while yet other research indicates exactly the opposite (Rögnvaldsson et al., 2007a).

Correspondence to: J. Eliasson
(jonase@hi.is)

Published by Copernicus Publications on behalf of the European Geosciences Union.

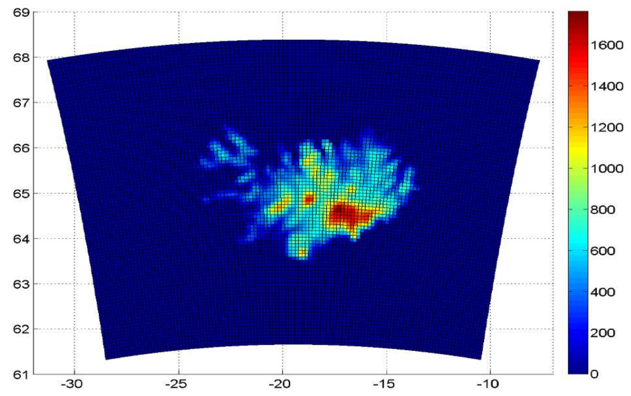

Fig. 1. Elevation data of the MM5 simulation area (color scale in meters), geographical longitude (Degrees East) on horizontal axis, latitude (Degrees North) on vertical axis.

The purpose of this analysis is to review an M5 map presently used by Icelandic engineering hydrologists to estimate peak runoff. The M5 – annual extreme 24 h rainfall with 5 years return period – (Eliasson, 2000) is used as an index variable in these estimations hence a good M5 map is needed. The basic data for the M5 is the uncorrected annual maximum 24 h precipitation. Various correction methods do exist (Crochet, 2007) but these can be applied to the values on the map by the users as the corrections apply to varying wind speeds in the range 0–6.5 m/s but annual maximum precipitation events in Iceland usually occur in storms with wind speeds larger than 6.5 m/s, but above this wind speed the correction factors depend on rain intensity only. The reliability of the correction factors is also an open question in rain intensities larger than 60–80 mm/24 h.

Another parameter is needed for quantile estimation, the C_i parameter. Together these two replace the mean value and the standard deviation in the Gumbel distribution, but this distribution is found valid for the Icelandic data (Eliasson, 1997). The map is also used for PMP (Probable Maximum Precipitation) estimation (Eliasson, 1994) so the map is used for a wide range of quantile estimates in engineering design.

The North Atlantic experienced increased cyclonic activity with increased storminess from the early 1960s until the mid nineties after a relatively quiescent period from about 1930 (Hanna et al., 2008). The climatic stability and therefore the justification for using an index parameter extracted from the last 100 years of observations is an open question. It is necessary to bear in mind the complex composition of precipitation extremes and how individual precipitation components in Iceland do differ from those of central Europe. The main difference in extreme precipitation climatology is that orographically enhanced precipitation is the dominating component in Iceland rather than convective precipitation (Hanna et al., 2004).

2 The MM5 model simulation for 1961 to 2006

An MM5 simulation for the period January 1961 to July 2006 was completed in 2006 based on ERA40 initial and boundary data from the European Centre for Medium-range Weather Forecasts (ECMWF). General results are discussed by (Rögnvaldsson et al., 2009). Prior to this, atmospheric flow over Iceland had been simulated for the period September 1987 through June 2003, using an older version of the PSU/NCAR MM5 mesoscale model driven by initial and boundary data from ECMWF (Rögnvaldsson et al., 2007b). Furthermore, an investigation of the seasonal and interannual variability of the precipitation simulations revealed a negative trend in winter precipitation in W-Iceland, a positive trend in the ratio of lowland precipitation to mountain precipitation in E-Iceland and a substantial inter-annual variability in the ratio of lowland precipitation to precipitation in the mountains. It was found that the mountains contribute to a total increase of precipitation in Iceland of the order of 40%. Because of the good experience with this preliminary run it was decided to extend the simulation period and make a statistical analysis of the precipitation extremes. The calculations were done on an 8 8 km net shown in Fig. 1.

If Fig. 1 is compared to a topographic map of Iceland it reveals that the computational net is rather coarse compared to many landscape features that may be expected to have an effect on the atmospheric flow. This can influence the results significantly. Figure 2, computed in a 1 km grid, shows the simulation results of a storm on 16 June 2008 (simulated with the AR-WRF model 2). Here, local wind speed extremes and high spatial gradients can clearly be seen on the south side of the landmass, which is the westward pointing peninsula at approximately 65 N in Fig. 1. Increasing the grid size to 3 km made the local features completely disappear. Calculation in a 9 km grid showed even less gradients than the 3 km grid but the difference was greatest between the 1 km and 3 km grid results. These grid-size dependent discrepancies cannot be mended by parameterization, but wrong parameterization can make them considerably worse. Therefore it is possible that spatial gradients in the 8 km MM5 grid are much too small to rely on the results in small-catchment hydrological simulations. Nevertheless, local results that do not depend upon a short time history (like statistical estimates based on annual extremes) can be accurate enough for many applications.

Forecast skills of numerical weather prediction (NWP) models have improved considerably for many variables (e.g. geopotential height and temperature) over the past years and decades but precipitation has remained somewhat elusive (Bozart, 2003). One reason for this is that the physics governing the formation of precipitation are highly complicated and only partly understood, so parameterization is difficult. Another reason is that the distribution of precipitation (particularly solid precipitation) over complex topography, as simulated by NWP models, is very sensitive to the

Table 1. MM5 output results.

Run time	1961–2006	AD
Grid size	8 8	km
Number of cells North West	94 122	
Output time step	6	h
Precipitation on boundary	0	mm/6 h
Output files produced	60 000	

Table 2. MM5 data transformation results.

Used data	1962–2005	AD
Number of 6 h time series	11 468	
Running average series	24 h	
Annual maxima isolated in each cell	44	
Precipitation on boundary	0	mm/6 h
Number of M5 and C_i values computed	11 464	

dynamic and thermal characteristics of the impinging winds (e.g. Chiao et al., 2004).

The output files of the simulation were now transformed as follows in Table 2.

3 Estimation of M5 and Ci

The procedure for estimating M5 and C_i is described by (Eliasson, 2000). The stability of the M5 estimate is of great concern. The M5 estimates cannot be taken as scatter free but must be assigned an uncertainty value, just as the model values must be. The common practice is not to use M5 estimates with fewer than 20 annual extremes behind them. One reason for this are the previously mentioned long term fluctuations in the climate. Another reason is statistical uncertainty due to the limited length of the time-series. The influence of the effects of this on the M5 estimate may be clearly seen in Fig. 3.

In the Fig. 3 example it is clearly seen that the number of station years behind an M5 estimate should preferably be greater than 40 in order to achieve reasonable stability. Only 32 meteorological stations have more than 40 station years and of those only 11 have more than 60 years. The station observations considered here are in all cases directly gauged values without wind corrections as previously explained. The MM5 model simulated M5 values used in this study are based on 44 calculated annual extreme values at each grid point and should therefore be reasonably stable.

Another way of assessing the stability in estimated M5 values is to study the differences between a short and a longer period in many points. Figure 4 shows the differences in meteorological M5 station values, between the observation period up to 1990 (Eliasson, 1997) and values covering the period up to 2006. There is a minimum of 20 years behind each M5 value so the data sets of each station overlap by an amount of years that depends upon the period of operation of that station. The difference in M5 is within 10 mm but depends strongly on the number of station years. Above 60 station years this difference seems to be within 5 mm. The average value of the difference is 1 mm but the standard deviation is 3.6 mm. It therefore seems appropriate to assume that the M5 values estimated at the meteorological stations are within   4 mm for each location. This indicates that the stability of the M5 estimates is good enough so observed and simulated values can be compared, even though the observation periods of the individual stations do not cover exactly the same 44 year period as the simulation does.

The 4 mm value may then be taken as an estimate of the uncertainty of the M5 estimate based on station observations caused by the difference in observation periods from the simulation period. On top of this there are instrumental errors and effects of spatial variability that will increase this

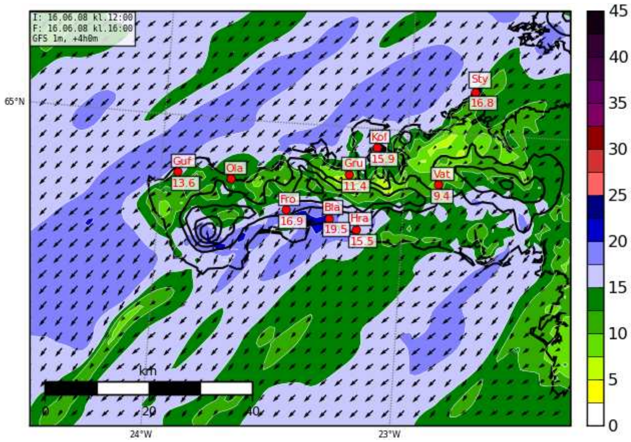

Fig. 2. Local wind anomalies (small blue spots in the lee zone) in Snæfellsnes, only found in a 1 km grid, not 9 or 3 km. Red figures in Squares: Meteorological station names and wind speed in m/s. Colour scale: Computed wind speed in m/s.

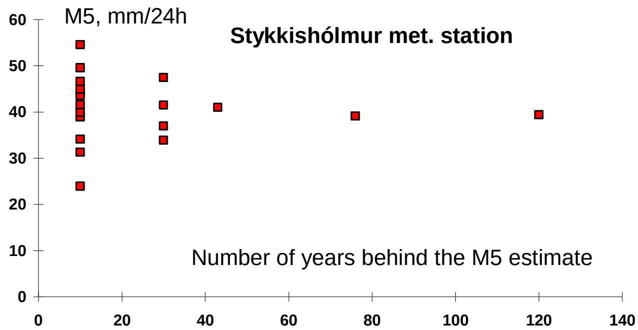

Fig. 3. Scatter of the M5 estimate and its dependence on number of station years. M5 estimates from other long-term stations show similar sensitivity to number of station years (not shown).

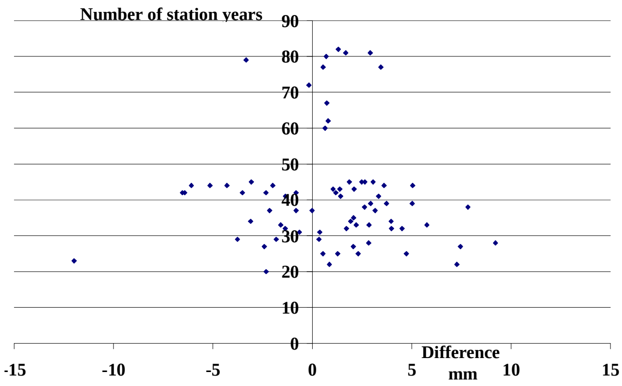

Fig. 4. The difference between M5 data in the 1990 and 2006 data sets.

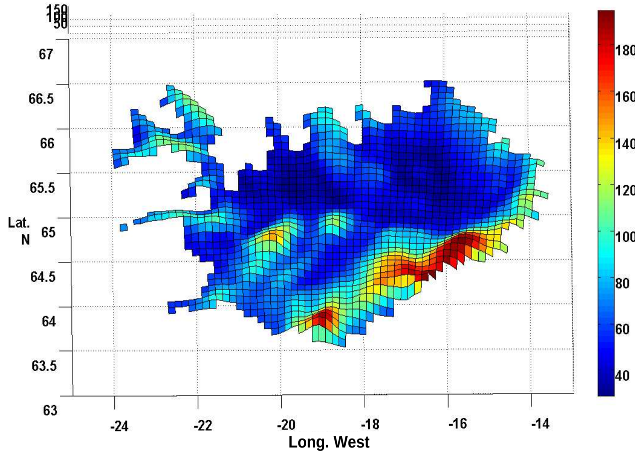

Fig. 5. Surface map of the MM5 model values for M5 showing the orographic effect. Colour bar and z scale: M5 in mm/24 h.

uncertainty. It must therefore be kept in mind, that the simulation period is the 44 years between 1962–2005 in all grid points, but the observation period for individual meteorological stations is normally different.

The statistical distribution of pooled normalized annual maximum precipitation data in Iceland follows a Gumbel probability distribution rather well (Eliasson, 1997). This distribution was therefore used to estimate the M5 and C_i values from the mean and the standard deviation of the station values used in the normalization.

The stability of the C_i estimate is also an issue, but the effect of scatter in this parameter is much more limited than the effect of scatter in M5. Most station values of C_i in Iceland are below 0.2. The effect of a variability in C_i on a quantile estimate can be seen from the following equation (Eliasson, 2000):

$$MT/M5 = 1 + C_i(y - 1.5) \tag{1}$$

MT=24 h annual precipitation maximum with return period T years
y=Gumbel's parameter= $-\ln(-\ln(1-1/T))$

The largest y value used in engineering design is around 7 (T=1000). This will produce the greatest impact of a scatter in C_i, but a deviation of 10% in the C_i will only produce a 5% deviation in the MT estimate for y=7. For lower T values this effect is smaller and it disappears altogether around the 5 year y value. This relatively little importance of the C_i value in practical quantile estimates is the main reason for replacing the mean value and the standard deviation in the Gumbel probability distribution function with M5 and C_i.

4 Comparison with earlier results

Only 1650 of the 11 468 grid-cells are on land. This is a great improvement over the M5 estimates based on station observations, as only 73 stations exist that can be compared to this simulation result. There is no doubt that a substantial improvement can be gained in the model results by using a finer grid and a shorter time step. Such simulations will undoubtedly be produced in the future.

For a qualitative examination it is instructive to study the map in Fig. 5 which clearly shows the strong orographic effect on the precipitation. Areas with M5>120 are seen to be on the glaciers, they are the highest parts of the country, 1000–2000 m a.s.l., while the highland plateau around them is around 600 m a.s.l. The figure shows that the largest precipitation amounts are not found in the lee zones as found by (Zangl et al., 2008). In fact they are located directly on the mountain tops.

The qualitative comparison with the earlier M5 map compiled from precipitation observations until 1990 is shown in Fig. 6. The reader is asked to note, that detailed examination of the maps can be made by zooming the pdf published on the journal's website until the text on the M5 map is clearly readable. Figure 6a is a reproduction of the original map on the referred website, the Icelandic text has no significance to the contents of this paper.

The two isoline maps are not identical, but much closer than might have been expected, especially in the ungauged regions (punctuated lines on the M5 map). The main differences can be qualitatively described as follows:

The valley of low values between the high M5 values in the south and the lower values in the north is 60–80 mm/24 h in the earlier map while the simulated values are 40–60 mm/24 h. The line through the high points is along the main water divide between the north and the south parts of the country.

The 120 mm line reaches in between the two glaciers of the south in the earlier map but not in the simulated results.

The low value areas in the north are larger according to the new model.

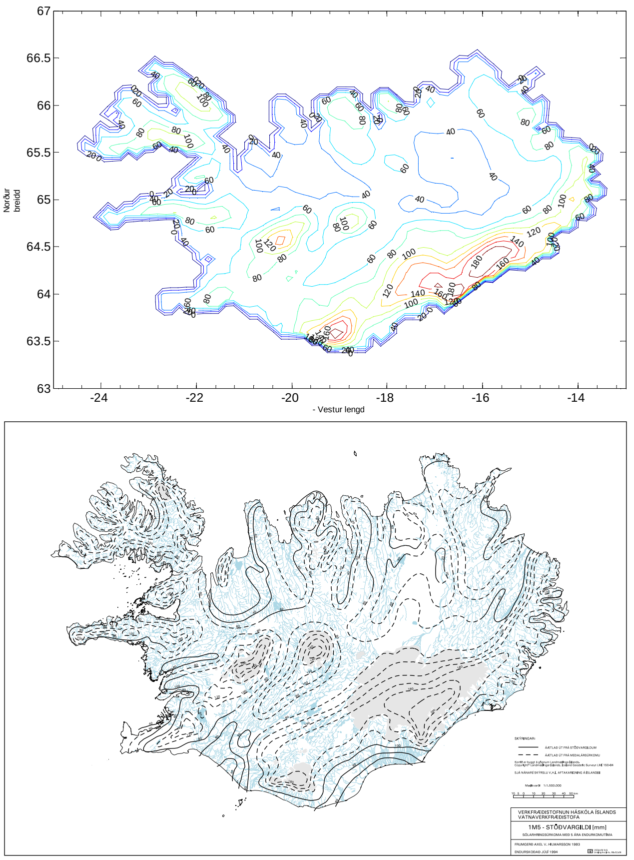

Fig. 6. Existing M5 map (http://www2.verk.hi.is/vhi/vatnaverkfrstofa/Kort/1M5_Yfirlit.pdf) punctuated lines estimated values above, compared to MM5 model M5 (below). Contour lines for each 20 mm/24 h on both maps. (For reading the figures text: Zoom in the picture.)

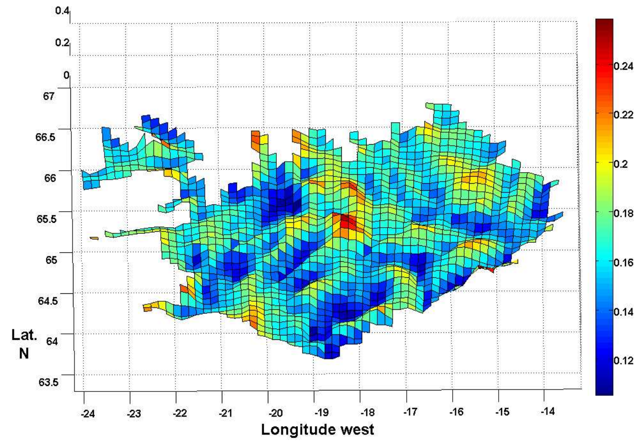

Fig. 7. Surface map of the C_i values from the MM5 run, smaller orographic effect than in Fig. 5. Colour bar and z scale: C_i, dimensionless value.

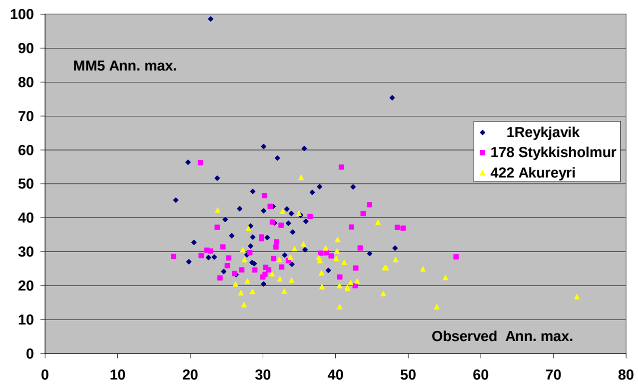

Fig. 8. Example of scatter of observed and simulated annual maxima 1962–2005, 3 stations.

The largest areas based on gauged values in the earlier map (solid lines in the map) are very similar in the simulations.

The qualitative result of this comparison is that the model produces similar M5 values as found from meteorological measurements where they are available, in the ungauged regions the estimated values in the earlier map are higher than the simulated values and this difference is of the order of magnitude 10–20 mm or 20–30%.

The results for the C_i coefficients are very much along the same lines.

The computed C_i values range from 0.12–0.23, this is the same range as found from data from the meteorological stations. It is impossible to compile an areal distribution comparable to Fig. 7 from the 73 observations because while the punctuated lines in the M5 map could be estimated from reliable M5–AAR (annual average rainfall) relations, no such relation seems to exist for the C_i. It was therefore recommended to use the value C_i=0.19 with the M5 map, or the value from the closest meteorological station.

Figure 7 shows that the MM5 simulations justify this recommendation. The average C_i value is closer to 0.17, but a recommended value to be used in practical applications should be a little higher than the average to prevent underdesign.

The simulated annual maxima for individual years show a great scatter when compared with observations as is done in Fig. 8. Besides this scatter in the numerical values, observed and simulated maxima do not usually occur on the same day. It is not anticipated that simulations in a finer grid will mend this scatter.

In the quantitative comparison between the meteorological stations and the simulation the closest gridpoint (NP0) is used together with the 8 neighbor points to NP0 (NP1–NP8). This is because simulated M5's are cell averages while the observations are point values so no gridpoints correspond exactly to the stations. The cluster NP1–NP4 is the closest 4 points (N–S and E–W), NP1–NP8 the cluster of the closest 8 points in the grid.

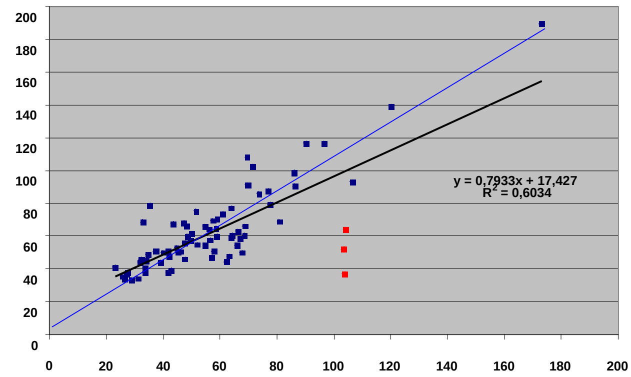

Fig. 9. Simulated NP0 point values for M5 (vertical axis) compared to observed values at the 73 meteorological stations (horizontal axis). Trend lines are for all points (black) and outliers excluded (blue).

These two clusters were studied in an attempt to find explanations to the larger differences between gauge M5 and NP0. The distance MS–NP0 can be up to 5.7 km and the differences in M5 values between the NP points will show the spatial variation in the computational grid and this variation can explain a part of the gauge–NP0 difference in the M5 values, when the spatial variation in the NP1–NP8 cluster is regular and the distance from the gauge to NP0 is a few kilometers. Various schemes to interpolate and estimate the "best computed value" at the meteorological station in order to compare that value to the observation M5 value may be used.

On top of this "regular" spatial variation there is the precipitation effect due to landscape forms on a scale <8 km that are flattened out by the grid but felt by the meteorological stations.

Figure 9 shows a direct comparison between simulated M5 values at the NP0 points and the M5 based on precipitation measurements from the meteorological stations, again with no corrections applied. The RMS difference of the station and simulated M5 values in Fig. 9 is 17 mm and the average difference is 5 mm (model values higher than the gauges), the correlation coefficient is $R=0.78$ (black line). If the three red outliers are excluded (see below), the correlation improves somewhat ($R=0.9$; blue line). Of the 73 gauges 57 are in the range 40–80 mm and 80% of these points (63% of the total) are within 10 mm which is the outer range for the scatter in Fig. 4. Differences between the station and simulated M5 values are given in Tables 3 and 4.

The magnitude of the measurement error depends on the wind-speed and the under-catch is more pronounced for solid (especially snow) than liquid precipitation (Førland et al., 1996). The values of the differences in Table 3 and the estimated underlying causes of the differences are listed in Table 4. The differences marked A and B in Table 3 have a cause marked A and B in Table 4. They speak for themselves

Table 3. Differences between meteorological stations and NP0 values.

A1.	Average difference of meteorological stations and NP0	5 mm
A2.	Closest 63% of differences	<10 mm
B1.	Full standard error of the estimate (rms of diffs)	17 mm
B2.	Max error, outliers (total 3 or 4.1%) excluded	35 mm

Table 4. Order of magnitude values of possible causes of the differences in Table 3.

A1.	Wind effect in MS[a] average (1/3 of ann. max. affected)	5 mm
A2.	The MS[a] – NP0 distance effect, rms value	5 mm
A3.	Different estimation periods	4 mm
B.	Course grid effect (0–50% in 4% of points) rms	10 mm

[a] Meteorological Station

except that the outliers indicated by the red symbols in Fig. 9 and noted in line B2 of Table 3 need closer examination.

In Fig. 10 we examine the three red outliers in Fig. 9, together with the point directly above them. In all these points the gauge value is approximately the same, (103–106) so this value is represented by a thick green line in Fig. 10. The large cluster NP1–NP2 is used.

In Fig. 10 we see that the "normal" station 615 (yellow columns) has an average deviation within the 17 mm mark, but the spatial variation around the NP0 value is greater than in the other points. The same large spatial variation is seen in the results from station 620, but here the simulated M5 value is only 60% of the gauge value. The two other points are less than 50% of the gauge value and the spatial variation is small with the exception of NP9 for station 234 (red column). This shows that a small spatial variation in the NP values may not imply an accurate result. It is believed that hills in the landscape around stations 103 and 234, that are flattened out in the grid, cause the large deviations at these stations and this effect could also affect the low simulation results at station 620. This cannot be verified except by simulations in a finer grid that have so far not been carried out. Nevertheless, this opens up the possibility that several grid points in the simulation, possibly anywhere in the grid, can be rather inaccurate. Carefully interpolated values to the stations locations in Fig. 8, statistical analysis of the differences and subsequent correction of all of the 1650 cell values does only have a minor chance of improving the simulation results.

5 Discussion

The simulation has provided M5 results for around 1500 locations in Iceland where no information was available before.

Where we have station information, the largest single group (63% of the total gauge values) NP0 and gauge values fall within 10 mm/24 h (Table 3). Of these about 4 mm may be due to different estimation periods (Table 4). Effects of wind and distance between station locations and NP0 can explain differences up to 10 mm (Table 4).

The rest of the values (37%) show greater scatter. These discrepancies are presumably due to a combination of all errors listed in point 4 and errors in the precipitation measurements. Due to the strong orographic effect in the precipitation, local landscape features on length-scales <8 km can be felt by the gauges without having any effect in the simulations. Three outliers may show a large effect of this type. There the simulated MM5 precipitation value is only 50% of the gauge value so the total difference is 40–60 mm instead of the maximum 35 mm at the other points. There may be an unknown number of such points in the simulated data set; they can only be identified by more accurate simulations.

The least squares line is M5sim=4+1.05 M5MS (outliers excluded), but using the relation M5=(M5sim–4)/1.05 to produce a new M5 map has very little effect and does not mend the real problems. The result of this discussion is therefore, that a general trend function that can be applied to the new simulated M5 values for use in ungauged regions cannot be seen. The simulated values are already so good that differences between gauge values and simulated results falls within the range to be expected when the model grid inaccuracy and the accuracy of the estimation of the gauge M5's on one hand, and the general MM5 model inaccuracy on the other hand are combined. Such differences are generally not randomly distributed, as least square lines assume.

6 Conclusions

This paper describes the M5 parameter, as computed from the annual precipitation maxima, simulated by the MM5 atmospheric model. The simulated M5 values were compared to all meteorological stations where estimates of observed M5 values were available. The results can be summarized as follows.

- The observed values show sufficient stationarity so the comparison does not have to be restricted to observations within the simulation period 1962–2005.
- The comparision reveals a few outliers (4%) where the difference between simulated and observed values is large and of uncertain origin.
- The difference between simulated and observed values is within 10 mm (for   2/3 of the values) in the range 20–160 mm/24 h
- There are no systematic deviations that can be mended by a trend function.

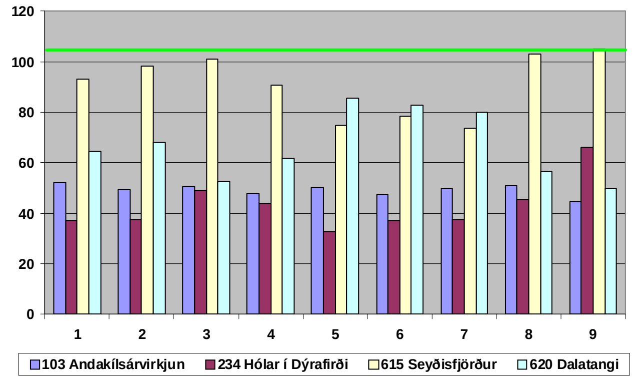

Fig. 10. Outlier points in Fig. 9 (red). Meteorological stations number 103, 234 and 620 compared to "normal" difference station 615. Numbers on the horizontal axis are the NP point numbers. Vertical axis: M5 values in mm/24 h

- In making a new M5 map 1650 simulated values are available along with the 73 observed ones.

In making a new M5 map the following policy is recommended to correct the simulation values:

Gauged regions

Areas where the difference is <10 mm: No correction.

Other areas (30 meteorological station points available): Correction by expert opinion.

For ungauged regions the following procedure is recommended

All regions where the original map and the M5sim value is <60 mm: No correction.

Other regions, original map value up to 80 mm: Correction 0–20, linearly increasing.

In regions with original map value >80: Add 20 to the simulated values.

The suggested procedure is believed to be more consistent than the flat trendline. It brings the overall differences down to the average   4 and rms 11 instead of the   5 and 17 in Table 3.

Future research on M5 and the basis of flood estimation in Iceland will be concentrated in three main areas:

1. Checking the probability distribution function of the annual precipitation maxima region for region in order to find if there are discrepancies in the a priori assumption that they follow the 2-parameter General Extreme Value distribution as previously found (Eliasson, 1997).
2. Searching for statistically significant M5-AAR (Average annual rainfall) and C_i-AAR relations.

3. Working towards a new simulation 1961–2007 in as fine a grid as possible.

Acknowledgements. The authors wish to thank the Energy Research Fund of the National Power Company of Iceland for supporting this research project. This study was also funded in part by the Nordic Climate and Energy (CE) research project and the corresponding Icelandic national project Veður og orka (VO).

Edited by: N. Verhoest
Reviewed by: T. Johannesson and G. Villarini

References

Anders, A. M., Roe, G. H., Durran, D. R., and Minder, J. R.: Small-scale spatial gradients in climatological precipitation on the Olympic peninsula, J. Hydrometeorol., 8(5), 1068–1081, 2007.

Chien, F. C. and Jou, B. J. D.: MM5 ensemble mean precipitation forecasts in the Taiwan area for three early summer convective (mei-yu) seasons, Weather and Forecasting, 19(4), 735–750, 2004.

Chrochet, P.: A study of regional precipitation trends in Iceland using a high-quality gauge network and ERA-40, J. Climate, 20(18), 4659–4677, 2007.

Eliasson, J.: Statistical Estimates of PMP Values, Nordic Hydrology, 25(4), 301–312, 1994.

Eliasson, J.: A statistical model for extreme precipitation, Water Resour. Res., 33(3), 449–455, 1997.

Eliasson, J.: Design values for precipitation and floods from M5 values, Nordic Hydrology, 31(4–5), 357–372, 2000.

Grell, G. A., Dudhia, J., and Stauffer, D. R.: A Description of the Fifth-Generation Penn State/NCAR Mesoscale Model (MM5), NCAR/TN-398+STR. National Center for Atmospheric Research, Boulder, CO, 107 pp., 1995.

Førland, E. P., Allerup, P., Dahlström, B., Eloma, E., Jónsson, T., Madsen, H., Perälä, J., Rissanen, P., Vedin, H., and Vejen, F.: Manual for operational correction of Nordic precipitation data, Klima Report 24/96, The Norwegian Meteorological Institute, Norway, 1996.

Hanna, E. Cappelen, J., Allan, R., et al.: New Insights into North European and North Atlantic Surface Pressure Variability, Storminess, and Related Climatic Change since 1830, J. Climate, 21(24), 6739–6766, 2008.

Hanna, E., Jonsson, T. and Box, J. E.: An analysis of Icelandic climate since the nineteenth century, Int. J. Climatol., 24(10), 1193–1210, 2004.

Haraldsdóttir, S. H., Ólafsson, H., Durand, Y., Mérindol, L., Giraud, G.: SAFRAN-Crocus snow simulations in an unstable and windy climate, Ann. Glaciol., 32, 339–344, 2001.

Minder, J. R., Durran, D. R., Roe, G. H., and Anders, A. M.: The climatology of small-scale orographic precipitation over the Olympic Mountains: Patterns and processes, Q. J. Roy. Meteorol. Soc., 134(633), 817–839, 2008.

Reisner, J., Rassmussen, R. J., Bruintjes, R. T.: Explicit forecasting of supercooled liquid water in winter storms using the MM5 mesoscale model, Q. J. Roy. Meteorol. Soc., 124B, 1071–1107, 1998.

Rognvaldsson, O., Bao, J.-W., and Olafsson, H.: Sensitivity simulations of orographic precipitation with MM5 and comparison with observations in Iceland during the Reykjanes Experiment, Meteorologische Zeitschrift, 16(1), 87–98, 2007a.

Rognvaldsson, O., Jonsdottir, J. F., and Olafsson, H.: Numerical simulations of precipitation in the complex terrain of Iceland – Comparison with glaciological and hydrological data, Meteorologische Zeitschrift, 16(1), 71–85, 2007b.

Rognvaldsson, O., Jonsdóttir, J. F., and Olafsson, H.: Dynamical downscaling of precipitation in Iceland 1961–2006, Hydrol. Res., in revision, 2009.

Serafin, S. and Ferretti, R.: Sensitivity of a mesoscale model to microphysical parameterizations in the MAP SOP events IOP2b and IOP8, J. Appl. Meteorol. Climatol., 46(9), 1438–1454, 2007.

Zangl, G., Aulehner, D., Wastl, C., and Pfeiffer, A.: Small-scale precipitation variability in the Alps: Climatology in comparison with semi-idealized numerical simulations, Q. J. Roy. Meteorol. Soc., 134(636), 1865–1880, 2008.

Paper V: Validation of Numerical Simulations of Precipitation in Complex Terrain at high Temporal Resolution

164 © IWA Publishing 2010 Hydrology Research | 41.3–4 | 2010

Validation of numerical simulations of precipitation in complex terrain at high temporal resolution

Teitur Arason, Ólafur Rögnvaldsson and Haraldur Ólafsson

ABSTRACT

Atmospheric flow over Iceland has been simulated for the period January 1961 to July 2006, using the mesoscale MM5 model driven by initial and boundary data from the ECMWF. A systematic comparison of results to observed precipitation has been carried out. Undercatchment of solid precipitation is dealt with by looking only at days when precipitation is presumably liquid or by considering the occurrence and non-occurrence of precipitation. Away from non-resolved orography, the long term means (months, years) of observed and simulated precipitation are often in reasonable agreement. This is partly due to a compensation of the errors on a shorter timescale (days). The probability of false alarms (the model predicts precipitation, but none is observed) is highest in N Iceland, particularly during winter. The probability of missing precipitation events (precipitation observed but none is predicted by the model) is highest in the summer and on the lee side of Iceland in southerly flows.

Key words | dynamical downscaling, Iceland, MM5, QPF, rain gauge data, validation

Teitur Arason
Faculty of Earth Sciences,
University of Iceland, 101 Reykjavík,
Iceland
Icelandic Meteorological Office,
Bústaðavegur 9, 150 Reykjavík,
Iceland

Ólafur Rögnvaldsson (corresponding author)
Institute for Meteorological Research,
Orkugarður, Grensásvegur 9,
108 Reykjavík,
Iceland
Bergen School of Meteorology,
Geophysical Institute, University of Bergen,
N-5007 Bergen,
Norway
E-mail: *or@belgingur.is*

Haraldur Ólafsson
Faculty of Earth Sciences,
University of Iceland, 101 Reykjavík,
Iceland
Bergen School of Meteorology,
Geophysical Insitute, University of Bergen,
N-5007 Bergen,
Norway

INTRODUCTION

The 6-hourly ERA40 re-analysis (Uppala *et al.* 2005) of the ECMWF (European Centre for Medium-Range Weather Forecasts) has been dynamically downscaled for the period 1961–2006 using the numerical model MM5 (Grell *et al.* 1995) run at 8 km horizontal resolution on a 123 × 95-point grid with 23 vertical levels. The model set-up included the Grell cumulus scheme (Grell *et al.* 1995), the Reisner2 microphysics scheme (Thompson *et al.* 2004) and the MRF (Hong & Pan 1996) planetary boundary layer (PBL) scheme. The modelling approach is described in greater detail in Rögnvaldsson *et al.* (2007*a*) and Rögnvaldsson & Ólafsson (2008).

Previous studies (Rögnvaldsson *et al.* 2004, 2007*a*; Bromwich *et al.* 2005) have shown the combination of the Grell cumulus scheme, the Reisner2 microphysics scheme and the MRF PBL scheme to be a reliable set-up for simulating precipitation over Iceland at 8 km resolution. Rögnvaldsson & Ólafsson (2002) also tested the sensitivity of simulated precipitation to the number of vertical levels (23 vs. 40) and to the size of the simulation domain. They found that the simulated precipitation is neither sensitive to domain size nor vertical resolution.

The 8 km grid size is a compromise between resolution and available computer resources. Simulation time is roughly proportional to the increase in horizontal resolution to the power of three. Hence, a 1 km grid would take 512 times longer to simulate than an 8 km grid. The issue of computational resources is one reason to simulate precipitation using a simpler and faster model. Crochet *et al.* (2007) used a linear model of orographic precipitation that included airflow dynamics, condensed water advection and downslope evaporation to simulate precipitation over

doi: 10.2166/nh.2010.133

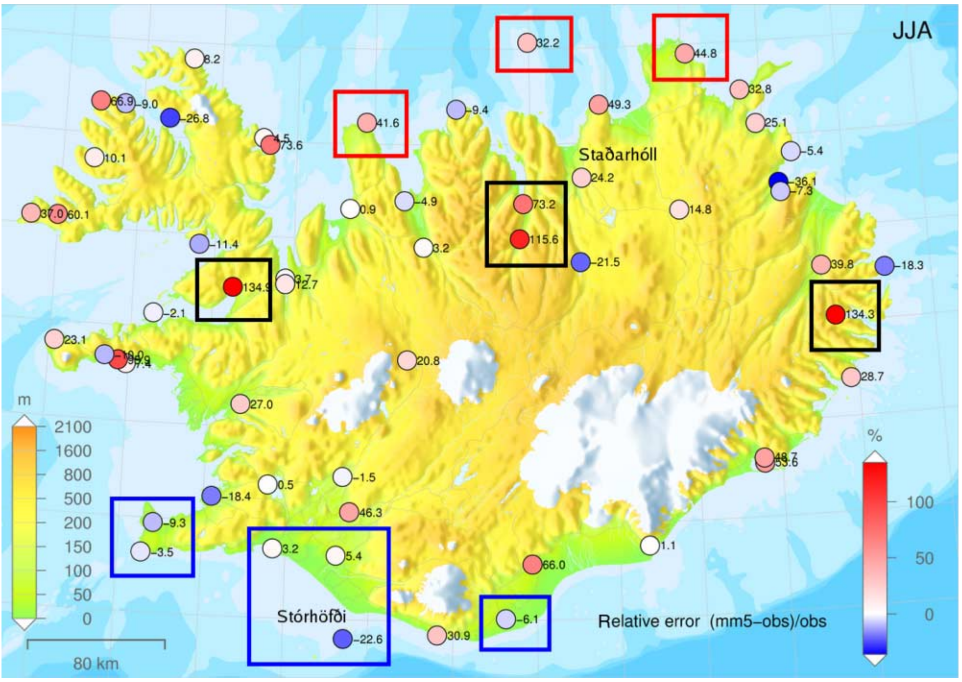

Figure 1 | A topographic map of Iceland showing relative difference between simulated and observed accumulated precipitation, (mm5-obs)/obs, in June, July and August (JJA). Each coloured circle corresponds to a synoptic weather station. Station names are included at the stations referred to in this paper. The colour of the circle denotes the relative error in the simulations (colourbar to the right). The blue boxes enclose a few stations on flat land in S Iceland where the observations and simulations are in reasonable agreement. The red boxes draw attention to stations in N Iceland where the model overestimates precipitation, despite these stations being on flat land. Stations that have huge overestimation, which is almost certainly due to non-resolved orography, are enclosed in black boxes. The full colour version of all figures in this paper can be accessed by subscribers online at http://www.iwaponline.com/nh/toc.htm

Iceland at a 1 km horizontal resolution. The model was forced using the ERA40 dataset for the period 1958–2002. Their results suggested that the linear model did capture the main physical processes governing orographic generation of precipitation in the mountains of Iceland.

Climatological downscaling of precipitation is not only of use for hydrological purposes. The MM5 model, using a similar set-up as used in this study, is in operational use in Iceland for production of short- to medium-range weather forecasts. Although a hydrologist and a weather forecaster

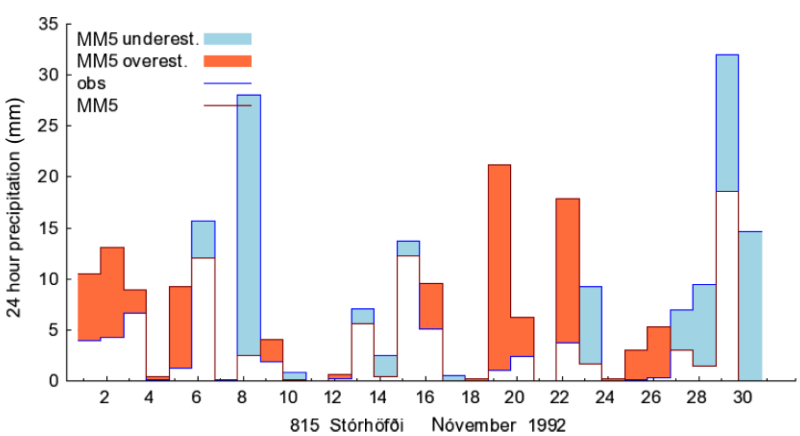

Figure 2 | Data from Stórhöfði, S Iceland, accumulated 24 h precipitation (mm) (observed and simulated) for November 1992. Blue colour denotes the amount of MM5 underestimation and red denotes the MM5 overestimation.

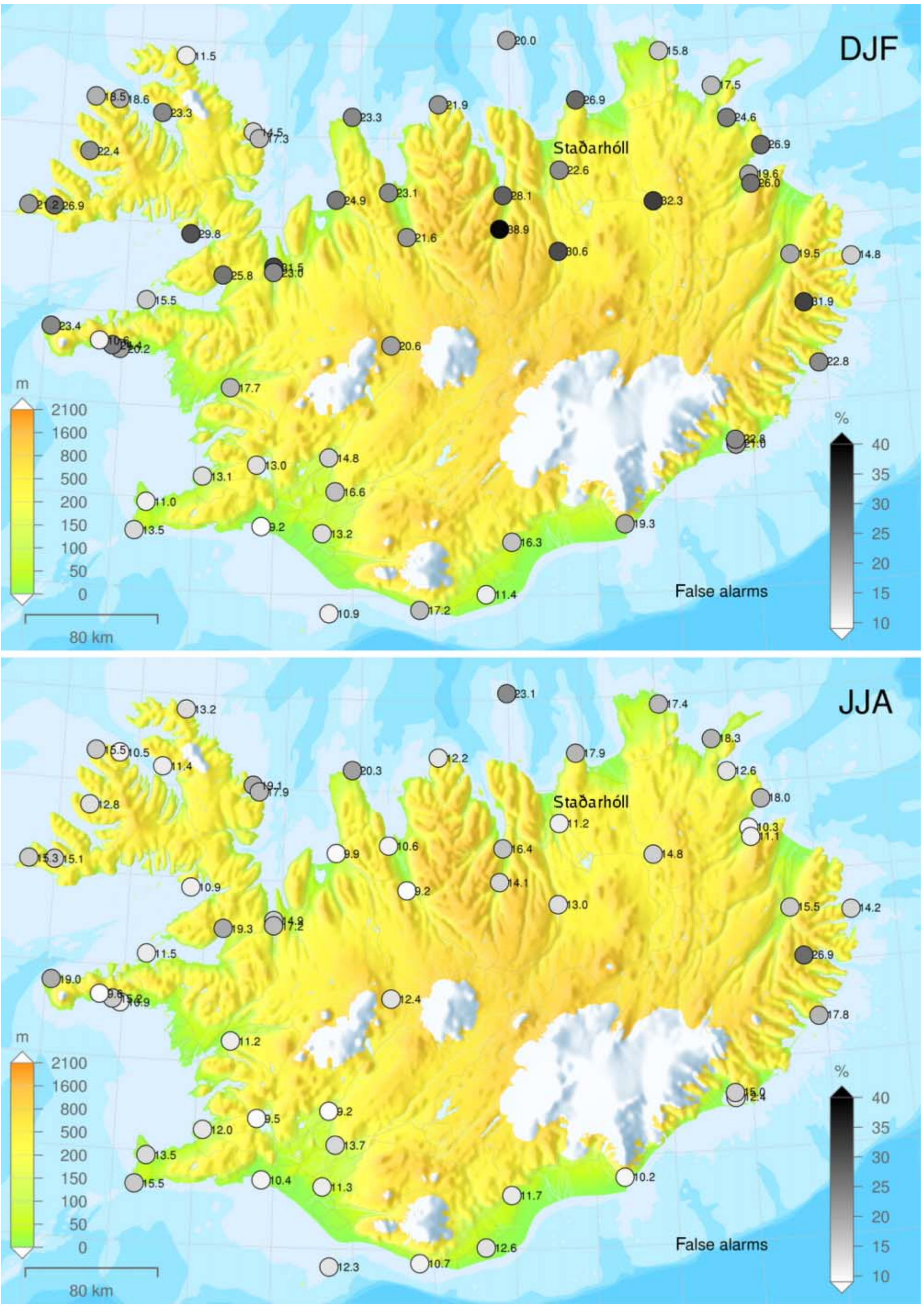

Figure 3 | Ratio (%) of “false alarms” (mm5 wet, obs dry) during winter (DJF, top) and summer (JJA, bottom).

would both like to be able to predict precipitation, their interests lie on different timescales.

In this paper we evaluate the quality of the simulations by comparing them to rain gauge measurements. This can be done by comparing long term means (months, years) of simulated and observed precipitation. Such a comparison would be of use to a hydrologist but of somewhat limited value to a forecaster. We therefore set out to make comparisons that would assess strong and weak points of the simulations to aid forecasters. We want to know how the errors in the simulated precipitation relate to other meteorological factors and if the performance depends on the temporal resolution of the data and geographical location. This work should shed a light on which aspects need improvement. Increased understanding of the limitations of the simulations on a short timescale will also be beneficial to their use in hydrological purposes at all timescales.

In this paper we describe the rain gauge data used in this study and how simulated precipitation compares to observations, followed by discussion and concluding remarks.

RAIN GAUGE DATA

The dynamic downscaling of ECMWF data, using version 3–7–3 of the MM5 model, has been compared to precipitation observations from synoptic stations for the sub-period 1987–2003. Precipitation is measured at 18 UTC. The MM5 output was saved every 6 h, at 00, 06, 12 and 18. The comparison period is therefore 24 h (from 18 to 18). That period will from now on be referred to as an "event" in this paper.

The model output from a grid point can be considered as an area-averaged precipitation over an area of 64 km^2. Therefore we do not expect the simulations to agree with measurements in areas with topography that is not resolved by the model. When comparing simulated and observed precipitation we must also bear in mind the general problems of precipitation observations. The most significant of these is the large undercatchment of solid precipitation in cold and windy climate, as in Iceland (Førland *et al.* 1996). Undercatchment of solid precipitation is dealt with by looking only at days when precipitation is presumably liquid (summer or temperature criteria) or by considering the occurrence and non-occurrence of precipitation.

COMPARISON WITH OBSERVED PRECIPITATION

Figure 1 shows the relative error of the simulations, (mm5-obs)/obs, for the summer months June, July and August (JJA). It can be seen that the model behaves differently in N and S Iceland for stations on flat land (minimal effect of non-resolved orography). For stations on flat land in the south, the simulations and observations are in overall reasonable agreement (see the stations in blue boxes in Figure 1). The model does, however, underestimate precipitation in flows from the SE (not shown). The model overestimates the precipitation for flat land stations in the north (see the red boxes in Figure 1). This is particularly true in northerly flow. For stations situated in orography that is obviously not resolved by the model (see the black boxes in Figure 1), the somewhat expected result of huge relative errors is clearly visible.

The 24 h precipitation amounts (observed and simulated) for November 1992 at Stórhöfði, S Iceland, is shown in Figure 2. The sums of observed and simulated precipitation for this month are almost identical. It is, however, clear that the agreement of the monthly sums is in large part due to compensation of the errors on a daily timescale. We define a "false alarm" event as a period of 24 h (from 18 to 18) where there is some precipitation in the simulations ($r_{\mathrm{mm5}} > 0.1$ mm) but the observations are dry ($r_{\mathrm{obs}} \leq 0.1$ mm). Figure 3, top, shows the percentage of events that fall into the false alarm category at each of the stations during the winter months December, January and February (DJF). Comparison with Figure 3, bottom, showing the false alarm percentage during June, July and August reveals that there is a relatively high probability of false alarms in winter, most notably for inland areas in N Iceland. In Figure 4 all false alarm events at Staðarhóll have been categorized according

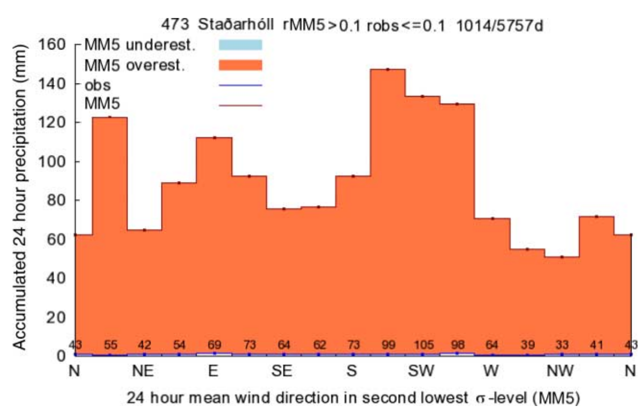

Figure 4 | All "false alarm" events from Staðarhóll, NE Iceland. The horizontal axis shows bins for 16 wind directions. The vertical axis shows the accumulated precipitation in each bin.

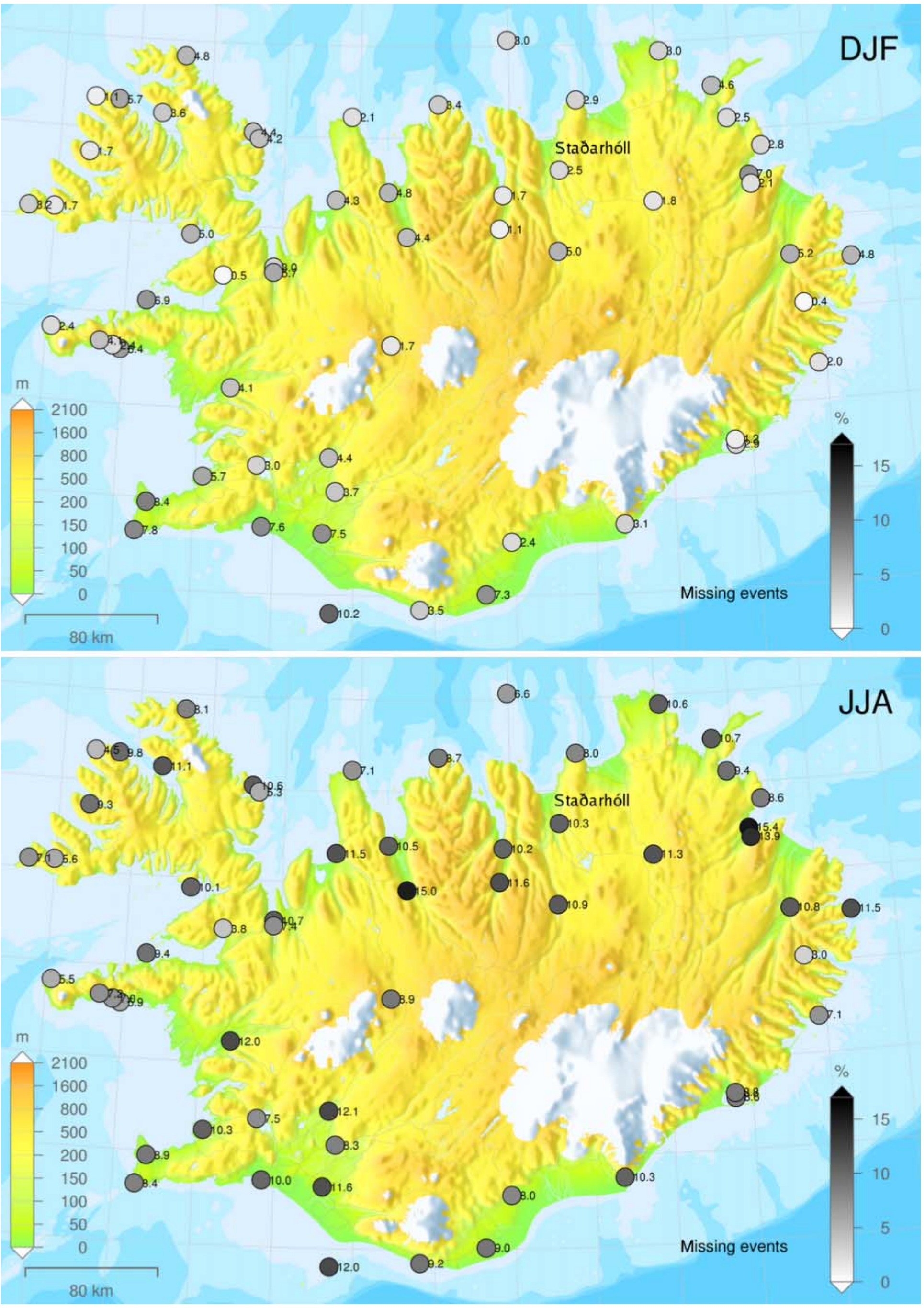

Figure 5 | Ratio (%) of "missing" events (mm5 dry, obs wet) during winter (DJF, top) and summer (JJA, bottom).

to wind direction. We see that much of the precipitation during false alarm events is associated with southerly winds, which are generally not associated with precipitation in this area. A "missing" event is defined as a 24 h period where the simulations are dry ($r_{\mathrm{mm5}} \leq 0.1$ mm) but the observations are wet ($r_{\mathrm{obs}} > 0.1$ mm). Figure 5, bottom, shows the percentage of missing precipitation events. It reveals that there is a low probability of missing events in the winter, but much higher in the summer. In Figure 6, the precipitation during missing events (precipitation observed, but not

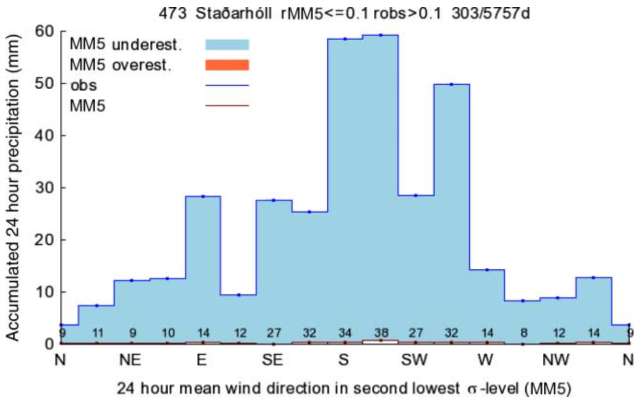

Figure 6 | Accumulated precipitation for individual wind directions during all "missing" events at Staðarhóll, N Iceland (MM5 dry, obs wet).

simulated) at Staðarhóll has been grouped according to the simulated low-level wind direction. Again, we see that southerly winds (when Staðarhóll is in the lee of Iceland) are the main culprit.

DISCUSSION

In view of the important uncertainties associated with precipitation processes and the complex nature of precipitation distribution in real flows in the vicinity of mountains, the overall results must be characterized as good. One reason for this must be the fact that most of the precipitation in Iceland is associated with large-scale systems and the precipitation distribution within such systems over complex terrain can indeed be predicted with much greater skill than the distribution of convective precipitation (Dorninger *et al.* 2008). However, it should be kept in mind that some of the results presented in this paper are valid for timescales of several months and errors on the timescale of a passing front are higher. Care should therefore be taken when interpreting the results from Figure 1 in the context of forecasting individual events.

Even though a horizontal resolution of 8 km permits the representation of most of the major mountain ranges, the steepness of the topography is underestimated at many locations. So are the strong precipitation gradients that have been observed (Brynjólfsson & Ólafsson 2009). Simulations of flow in the mountains of SW Iceland have shown that much improvement is to be gained locally when the horizontal resolution is increased from 8 to 4 km and even from 4 to 2 km (Rögnvaldsson *et al.* 2007*b*). Similar improvements of the present results through increased resolution can be expected for other parts of Iceland that also have narrow mountain ranges.

Although much of the errors in the simulations can be related to non-resolved orography, this can not easily be done for features such as the overestimation of precipitation away from the mountains in the north and underestimation of precipitation in winds from the southeast over flat land in the southwest. The reasons for these features are unclear. The overestimation of precipitation in the north emanates from cases of both southerly and northerly winds. An overestimation, reminiscent of the southerly flows, can be seen in the MM5 simulations of Schwitalla *et al.* (2008) at some distance downstream of the Black Forest mountain range (cf. Figure 7 in Schwitalla *et al.* 2008). This more distant lee-side problem should be distinguished from the excessive dryness of the model immediately above the lee slopes (Rögnvaldsson *et al.* 2007*b*; Schwitalla *et al.* 2008). A further analysis of the errors requires precipitation observations with higher temporal resolution and observations of the structure of the vertical profile of the atmosphere, including microphysical properties.

SUMMARY AND CONCLUSIONS

The numerical model MM5, run at a horizontal resolution of 8 km, has been used to downscale the 6-h analysis of the ECMWF over Iceland. A systematic comparison with observed precipitation for the period 1987–2003 has been presented. The main outcome of this comparison is:

- Away from non-resolved orography, long term (months, years) sums of simulated precipitation are quite correct in the south but too high in the north. This is partly due to compensating errors on a smaller timescale (days).
- The probability of false alarms (the model predicts precipitation, but none is observed) is highest in N Iceland, particularly during winter.
- The probability of missing precipitation events is highest in the summer and on the lee side of Iceland in southerly flows.

- Precipitation is underestimated in southeasterly flows at the SW coast of Iceland and is overestimated at the N coast of Iceland. This cannot only be explained by non-resolved orography.

ACKNOWLEDGEMENTS

This study was funded in part by the Nordic Climate and Energy Systems (CES) research project and the corresponding Icelandic national project Lofthjúpsbreytingar og áhrif þeirra á OrkuKerfi og Samgöngur (LOKS, see http://en.vedur.is/ces).

The authors would like to thank two anonymous reviewers for their helpful comments.

REFERENCES

Bromwich, D. H., Lesheng, B. & Bjarnason, G. G. 2005 High-resolution regional climate simulations over Iceland using polar MM5. *Mon. Weather Rev.* **133**, 3527–3547.

Brynjólfsson, S. & Ólafsson, H. 2009 Precipitation in the Svarfaðardalur region, North-Iceland. *Meteorol. Atmos. Phys.* **103**, 57–66.

Crochet, P., Jóhannesson, T., Jónsson, T., Sigurðsson, O., Björnsson, H., Pálsson, F. & Barstad, I. 2007 Estimating the spatial distribution of precipitation in iceland using a linear model of orographic precipitation. *J. Hydrometeorol.* **8**(6), 1285–1306.

Dorninger, M., Schneider, S. & Steinacker, R. 2008 On the interpolation of precipitation data over complex terrain. *Meteorol. Atmos. Phys.* **101**, 175–189.

Førland, E. J., Allerup, P., Dahlström, B., Elomaa, E., Jónsson, T., Madsen, H., Perälä, J., Rissanen, P., Vedin, H. & Vejen, F. 1996 *Manual for Operational Correction of Nordic Precipitation Data*. DNMI report no. 24/96 Klima, Norwegian Meteorological Institute, Oslo.

Grell, G. A., Dudhia, J. & Stauffer, D. R. 1995 *A Description of the Fifth-generation Penn State/NCAR Mesoscale Model (MM5)*. NCAR tech. note NCAR/TN-398 + STR. National Center for Atmospheric Research, Boulder, Colorado.

Hong, S. H. & Pan, H. L. 1996 Nonlocal boundary layer vertical diffusion in a medium-range forecast model. *Mon. Weather Rev.* **124**, 2322–2339.

Rögnvaldsson, Ó., Crochet, P. & Ólafsson, H. 2004 Mapping of precipitation in Iceland using numerical simulations and statistical modeling. *Meteorol. Z.* **13**(3), 209–219.

Rögnvaldsson, Ó., Jónsdóttir, J. F. & Ólafsson, H. 2007*a* Numerical simulations of precipitation in the complex terrain of Iceland - comparison with glaciological and hydrological data. *Meteorol. Z.* **16**(1), 71–85.

Rögnvaldsson, Ó., Bao, J.-W. & Ólafsson, H. 2007*b* Sensitivity simulations of orographic precipitation with MM5 and comparison with observations in Iceland during the Reykjanes Experiment. *Meteorol. Z.* **16**(1), 87–98.

Rögnvaldsson, Ó. & Ólafsson, H. 2002 *Downscaling Experiments With The MM5 Model: Determining an Optimal Configuration for Climatological Downscaling Studies of Precipitation in Iceland*. Icelandic Meteorological Office. Available at: http://www.vedur.is/\verb + ~ + haraldur/urkoma.pdf

Rögnvaldsson, Ó.& Ólafsson, H. 2008 Dynamical downscaling of precipitation—Part I: Comparison with glaciological data. *Proceedings of the XXV Nordic Hydrological Conference, Reykjavík, Iceland*, pp. 236–245. Available at: http://www.vedur.is/media/vatnafar/saga/NHC2008_volume1_web.pdf

Schwitalla, T., Bauer, H.-S., Wulfmeier, V. & Zängl, G. 2008 Systematic errors of QPF in low-mountain regions as revealed by MM5 simulations. *Meteorol. Z.* **17**(6), 903–919.

Thompson, G., Rasmussen, R. M. & Manning, K. 2004 Explicit forecasts of winter precipitation using a improved bulk microphysics scheme. Part I: Description, sensitivity analysis. *Mon. Weather Rev.* **132**, 519–542.

Uppala, S. M., KÅllberg, P. W., Simmons, A. J., Andrae, U., Bechtold, V. DaCosta, Fiorino, M., Gibson, J. K., Haseler, J., Hernandez, A., Kelly, G. A., Li, X., Onogi, K., Saarinen, S., Sokka, N., Allan, R. P., Andersson, E., Arpe, K., Balmaseda, M. A., Beljaars, A. C. M., Van De Berg, L., Bidlot, J., Bormann, N., Caires, S., Chevallier, F., Dethof, A., Dragosavac, M., Fisher, M., Fuentes, M., Hagemann, S., Hólm, E., Hoskins, B. J., Isaksen, L., Janssen, P. A. E. M., Jenne, R., Mcnally, A. P., Mahfouf, J.-F., Morcrette, J.-J., Rayner, N. A., Saunders, R. W., Simon, P., Sterl, A., Trenberth, K. E., Untch, A., Vasiljevic, D., Viterbo, P. & Woollen, J. 2005 The ERA-40 re-analysis. *Q. J. R. Meteorol. Soc.* **131**, 2961–3012.

First received 15 December 2008; accepted in revised form 25 June 2009. Available online April 2010

Paper VI: Dynamical Downscaling of Precipitation in Iceland 1961–2006

153 © IWA Publishing 2010 Hydrology Research | 41.3–4 | 2010

Dynamical downscaling of precipitation in Iceland 1961–2006

Ólafur Rögnvaldsson, Jóna Finndís Jónsdóttir and Haraldur Ólafsson

ABSTRACT

Atmospheric flow over Iceland has been simulated for the period January 1961 to July 2006, using the mesoscale MM5 model driven by initial and boundary data from the European Centre for Medium Range Weather Forecasts (ECMWF). Firstly, the simulated precipitation is compared to estimates derived from mass balance measurements on the Icelandic ice caps. It is found that the simulated precipitation compares favourably with the observed winter balance, in particular for Hofsjökull, where corrections to take liquid precipitation and/or winter ablation into account have been made, and for the outlet glaciers Dyngjujökull and Brúarjökull. Secondly, the model output is used as input to the WaSiM hydrological model to calculate and compare the runoff with observed runoff from six watersheds in Iceland. It is found that model results compare favourably with observations. Overall, the MM5 V3–7 is somewhat better than the MM5 V3–5. The V3–7 is drier than V3–5 on upstream slopes.

Key words | dynamical downscaling, glaciological data, hydrological data, MM5, precipitation, WaSiM

Ólafur Rögnvaldsson (corresponding author)
Institute for Meteorological Research,
Orkugarður, Grensásvegur 9,
108 Reykjavík,
Iceland
and
Bergen School of Meteorology,
Geophysical Institute, University of Bergen,
Bergen,
Norway
E-mail: *or@belgingur.is*

Jóna Finndís Jónsdóttir
Formerly at the Hydrological Service,
National Energy Authority,
Reykjavík,
Iceland

Haraldur Ólafsson
Faculty of Earth Sciences,
University of Iceland,
101 Reykjavík,
Iceland
and
Bergen School of Meteorology,
Geophysical Institute, University of Bergen,
Bergen,
Norway

INTRODUCTION

The geographical distribution of precipitation in Iceland is poorly known but very important for hydrological applications, both in general and particularly in the context of climate change. Therefore, an extensive task carried out in the recent VO/CE project (Jóhannesson *et al.* 2007; further information on the Veður og orka – Climate and Energy (VO/CE) project can be found on the web: http://www.os.is/ce) was concerned with modelling of precipitation and a compilation of precipitation datasets on a regular grid covering the whole country. These datasets provide the opportunity to model river runoff and glacier mass balance both in the current climate and also in a hypothetical future climate based on climate change scenarios. Thus, climatological downscaling of precipitation is of great use for hydrological purposes. Furthermore, the MM5 model, using a similar set-up as used in this study, is in operational use in Iceland for the production of short to medium range weather forecasts. Improvements in the numerical tools do therefore benefit both the hydrology community as well as weather forecasting, although the interests of these two communities lie in different timescales.

The climate of Iceland is largely governed by the interaction of orography and extra-tropical cyclones, both of which can be described quite accurately by present-day atmospheric models. As a result, dynamical downscaling of the climate, using physical models, can be expected to give reliable information about precipitation distribution, especially in the data-sparse highlands.

In this paper we compare dynamical downscaling of large-scale meteorological fields provided by the ERA40 reanalysis (Uppala *et al.* 2005) to precipitation estimates derived from mass balance measurements on the Icelandic

doi: 10.2166/nh.2010.132

ice caps. The dynamical downscaling is done by using the mesoscale MM5 model (Grell *et al.* 1995). We also use output from the MM5 model as input to the WaSiM hydrological model (Jasper *et al.* 2002) for the same six watersheds as used for validation purposes of a 15-year time series described by Rögnvaldsson *et al.* (2007, hereafter referred to as RJO07) and compare the simulated discharge with the observed discharge.

Previous studies (Rögnvaldsson *et al.* 2004, 2007; Bromwich *et al.* 2005) have shown the combination of the Grell cumulus scheme, the Reisner2 microphysics scheme and the MRF PBL scheme to be a reliable set-up for simulating precipitation over Iceland at 8 km resolution. Rögnvaldsson & Ólafsson (2002) also tested the sensitivity of simulated precipitation to the number of vertical levels (23 vs. 40) and to the size of the simulation domain. They found that the simulated precipitation is neither sensitive to domain size nor vertical resolution.

This paper begins with a description of the model approach, followed by comparison of the model results to glaciological data and a comparison of modelled discharge to observed discharge. The results are discussed in brief, followed by concluding remarks.

MODELLING WITH THE MM5 MODEL

Atmospheric flow over Iceland was simulated for the period January 1961 through June 2006 using V3–7 of the PSU/NCAR MM5 mesoscale model (Grell *et al.* 1995). The domain used is 123 × 95 points, centered at 64°N and 19.5°W, with a horizontal resolution of 8 km. There are 23 vertical levels with the model top at 100 hPa and model output is every 6 h. The domain set-up is shown in Figure 1.

The MM5 model was used with initial and lateral boundaries from the ERA40 re-analysis project to 1999. After that date, operational analyses from the ECMWF were used. The ERA40 data were interpolated from a horizontal grid of 1.125° to 0.5° prior to being applied to the MM5 modelling system. The modelling approach differs from that used by Bromwich *et al.* (2005). Instead of applying many short term (i.e. of the order of days) simulations and frequently updating the initial conditions, the model was run over a period of approximately six months with only lateral boundary conditions updated every six hours. This was made possible by taking advantage of the NOAH land surface model (Koren *et al.* 1999; Ek *et al.* 2003).

For discussions regarding the use of limited-area models for regional climate studies and the use of run-off measurements for validation of precipitation simulated by atmospheric models we refer to RJO07 and references therein.

PREVIOUS VERIFICATION OF SIMULATED PRECIPITATION

RJO07 simulated atmospheric flow over Iceland for the period September 1987 through June 2003 using V3–5 of MM5 driven by initial and boundary data from the ECMWF. The simulated precipitation was compared with two types of indirect precipitation observations. Firstly, winter balance on two large outlet glaciers in SE Iceland and on two large ice caps in central Iceland. Secondly, model output was used as input to the WaSiM hydrological model to calculate and compare the simulated run-off with observed run-off from six watersheds in Iceland for the water years 1987–2002. Model precipitation compared favourably with both types of validation data.

In this paper we extend the RJO07 study to a 45-year period using a new version of the MM5 model and more glaciological and hydrological data.

COMPARISON WITH GLACIOLOGICAL DATA

The spatial variability of the mass balance on large ice masses, such as Vatnajökull and Langjökull ice caps, can be mapped given data along several profiles extending over the elevation range of the ice caps. Mass balance has been observed on parts of Vatnajökull ice cap in SE Iceland since 1991 (Björnsson *et al.* 1998) and from 1996 on Langjökull ice cap, central Iceland (Björnsson *et al.* 2002) (see location on Figure 2). Here, we use measurements of accumulated winter mass balance, expressed in terms of liquid water equivalents. Björnsson *et al.* (1998) estimated the uncertainty of the areal integrals of the mass balance to be a minimum of 15%. Due to surging of the Dyngjujökull glacier in 1998–2000, the uncertainty is considerably greater for this period and the following winter (Pálsson *et al.* 2002*b*).

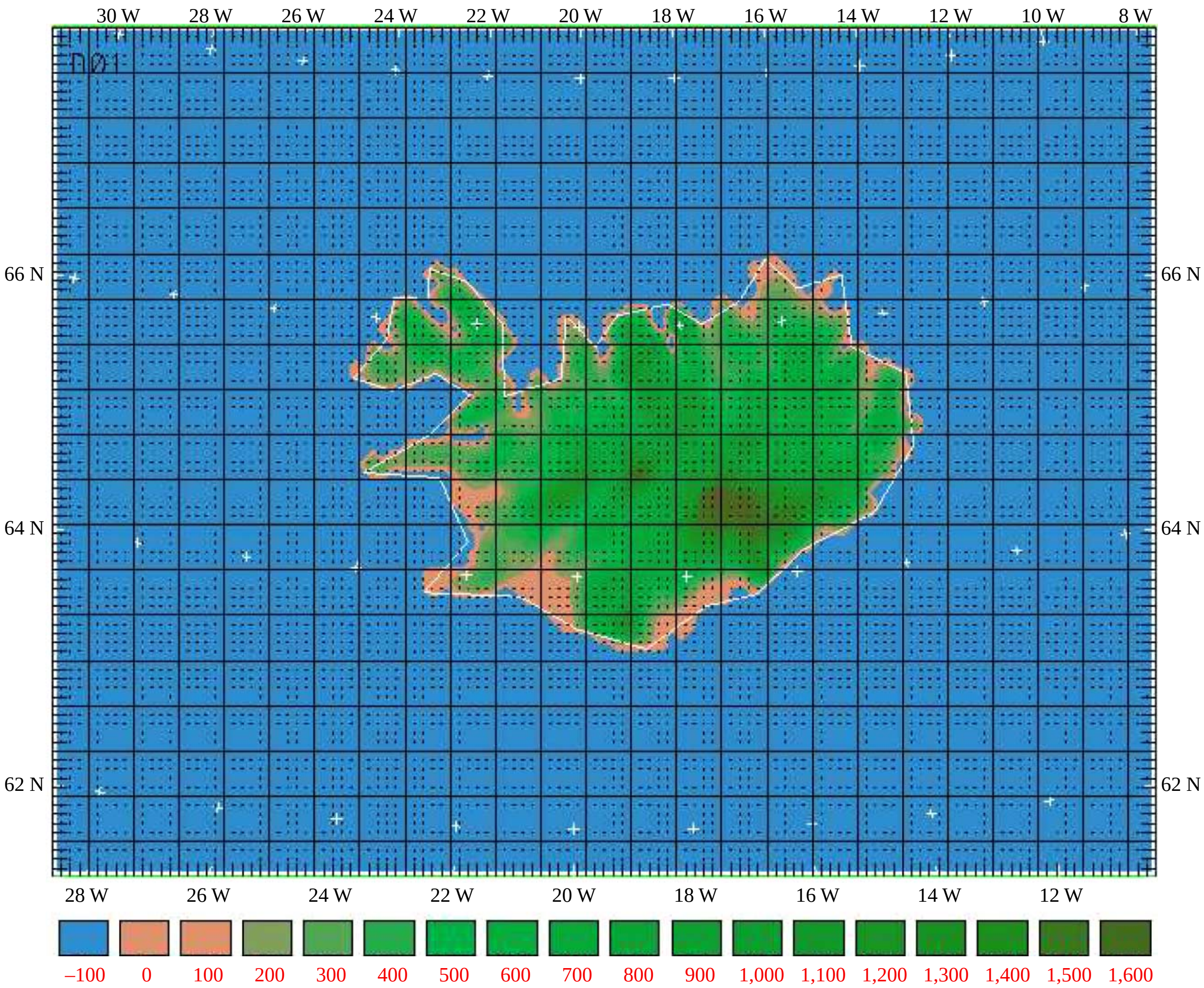

Figure 1 | Domain set-up of the MM5 model: horizontal grid size is 8 km and the number of grid points is 123 × 95 with 23 vertical levels.

As yet unpublished data for the past few winters are from Björnsson & Pálsson (Helgi Björnsson and Finnur Pálsson, Institute of Earth Sciences and Science Institute, University of Iceland, personal communication). The ice caps and typical locations of the mass balance stakes are depicted in Figure 2.

Mass balance on Hofsjökull ice cap has been observed at sites along the profile HN (cf. Figure 2) since 1987 and along profiles HSV and HSA since 1988 (Sigurðsson *et al.* 2004). Due to the relatively coarse horizontal resolution in our model configuration the maximum elevation of the Hofsjökull ice cap is approximately 1,540 m, i.e. more than 250 m lower than in reality. Hence, we use area-integrated data from an elevation range of approximately 1,450–1,650 m along the three profiles HN, HSV and HSA (Jóhannesson *et al.* 2006*b*). The number of observational data points ranges from 3 (1987–1988) to 10 (2000–2001), the most common number being 7 or 8 (16 winters out of the 19 studied here). The winter balance on Hofsjökull has been modelled to estimate the amount of precipitation that falls as rain and ablation that may take place during the winter season. These estimates have been added to the measured winter balance to produce estimates of total precipitation at the measurement sites. The methodology behind this procedure is described in detail in Jóhannesson *et al.* (1995, 2006*a*, pp 31–37). This correction has not been carried out for Vatnajökull and Langjökull ice caps as a whole.

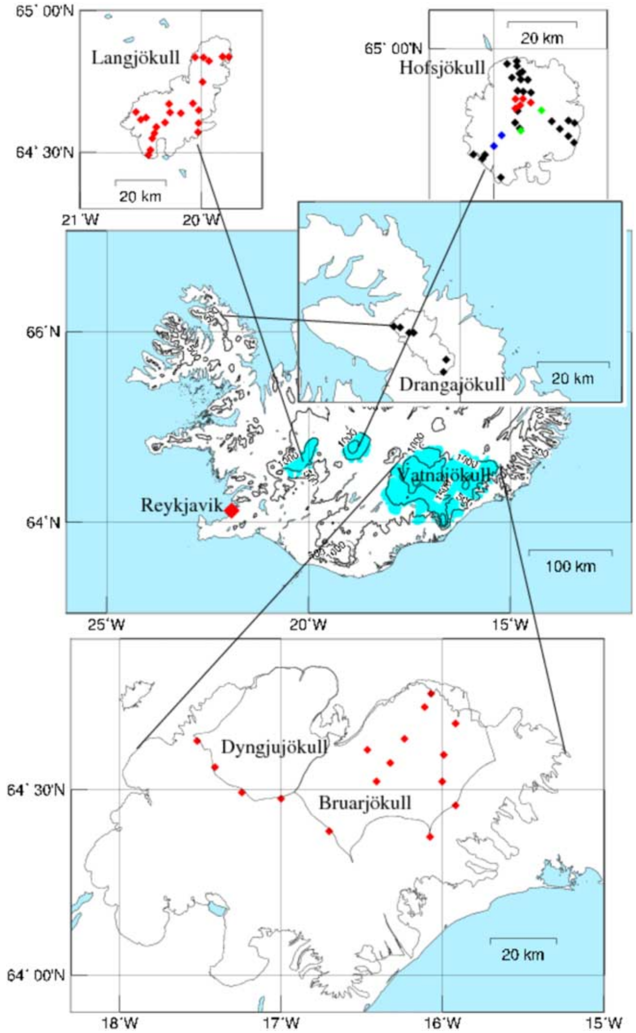

Figure 2 | Overview of the six ice caps and glaciers used for validation purposes, where dots indicate a typical location of an observation site. Red dots on Hofsjökull glacier are along profiles HN (N part), blue dots along profile HSV (SW part) and green dots along profile HSA (SE part). Observations at locations shown in black at Hofsjökull have not been used in this study. Drangajökull is split up in two regions, NW and SE parts (cf. Table 2). See Figure 1 in RJO07 for comparison.

The simulated winter precipitation at Hofsjökull ice cap is in good agreement with observations (cf. Figure 3) over the northern part of the ice cap (HN, red dots, cf. Figure 2), the SE part (HSA, green dots, cf. Figure 2) and the SW part (HSV, blue dots, cf. Figure 2). The solid line in Figure 3 shows the average of the observed winter precipitation, corrected to take liquid precipitation and/or winter ablation into account, at altitudes between 1,450 and 1,650 m at locations HN, HSA and HSV. The dashed line represents precipitation simulated by MM5 (nine-point average) at the location of the ice cap. The simulated precipitation is within one standard deviation of the average observed winter precipitation within this altitude range for 16 out of the 19 winters during the period (1987–2006). The Spearman's rank correlation, ρ, is 0.63 with a significance value of 0.004 and the RMS error is 300 mm.

Areal integrals of winter balance over the Vatnajökull ice cap as a whole (8,100 km^2), the Dyngjujökull (1,040 km^2) and Brúarjökull (1,695 km^2) outlet glaciers on the north side of the ice cap, and the Langjökull ice cap (925 km^2) are compared with simulated wintertime precipitation by the MM5 model in Figure 4. The winter balance is not corrected to take liquid precipitation and/or winter ablation into account. The model shows least skill on Langjökull ice cap ($\rho = 0.50$; 0.14) where it has an RMS error equal to 372, and the greatest skill on Brúarjökull ($\rho = 0.83$; 0.0002) where the RMS error is equal to 171. The correlation for Dyngjujökull is 0.61 with a significance value of 0.06 and the RMS error is equal to 286. The simulated precipitation is within estimated observational error margins for 10 out of 12 winters for Dyngjujökull, 13 out of 14 for Brúarjökull and 5 out of 10 for Langjökull ice cap. The correlation for Vatnajökull ice cap

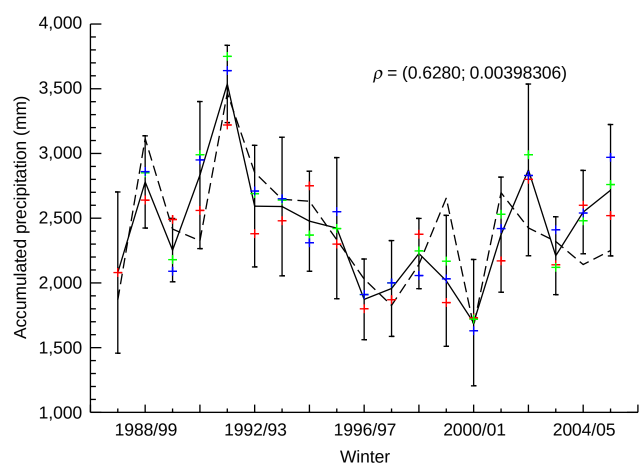

Figure 3 | Estimated mean accumulated winter precipitation (mm) along profiles HN (N part), HSA (SE part) and HSV (SW part) at altitudes between 1,450 and 1,650 m (solid line, Jóhannesson et al. 2006a). Dashed line represents simulated precipitation by MM5 (nine-point average) at Hofsjökull ice cap. Red, green and blue crosses represent mean winter balance values at stakes along profiles HN, HSA and HSV, respectively, within the altitude interval 1,450–1650 m (cf. Figure 2). Error bars indicate the standard deviation of the observations. Observed values from individual snow stakes are from Sigurðsson & Sigurðsson (1998) and Sigurðsson et al. (2004) Sigurðsson & Thorsteinsson (personal communication). See Figure 3 in RJO07 for comparison.

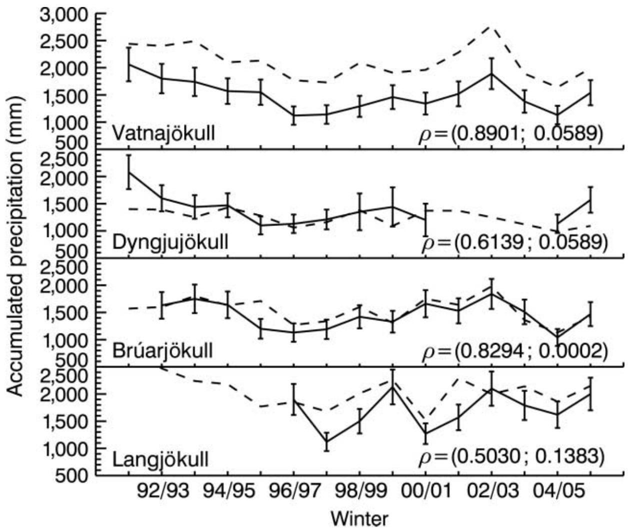

Figure 4 | Observed accumulated winter balance (solid) and precipitation simulated by MM5 (dashed) for Vatnajökull ice cap as a whole (top), Dyngjujökull (second from top) and Brúarjökull (second from bottom) outlet glaciers and Langjökull ice cap (bottom). Error bars indicate 15% uncertainty of the observations, except for 1998–2001 at Dyngjujökull where it is 25%. Glaciological data for Vatnajökull, Dyngjujökull and Brúarjökull are from Björnsson *et al.* (1998, 2002) and Pálsson *et al.* (2002*a*,*b*; 2004*b*,*c*,*d*) Data for Langjökull ice cap are from Björnsson *et al.* (2002) and Pálsson *et al.* (2004*a*). As-yet unpublished data for the past few winters are from Björnsson & Pálsson. See Figure 4 in RJO07 for comparison.

is 0.89, with a significance value of 0.06 and the RMS error is equal to 634. The relative importance of liquid precipitation and/or winter ablation is greatest for Vatnajökull as a whole because the southern margin of the ice cap reaches near sea level where rain may fall and ablation may take place at any time of the year. The north flowing outlet glaciers from Vatnajökull and Langjökull ice cap do not reach to such low altitudes so this problem is less important there. This is presumably the reason why the simulated winter precipitation is consistently about 500 mm greater than the observed winter balance for the Vatnajökull ice cap as a whole. When this constant value is added to the observations, the RMS error for Vatnajökull drops to 177 from 634.

Table 1 shows the comparison between observed accumulated precipitation and simulated precipitation using V3–5 and V3–7 of the MM5 model. The periods shown are the same as in RJO07, as well as including data from three additional winters (“starred” values in Table 1). V3–7 performs better over Dyngjujökull and Brúarjökull outlet glaciers, but worse over the Langjökull and Hofsjökull ice caps.

Mass-balance measurements at Drangajökull ice cap in NW Iceland have only been carried out since 2004. Table 2 shows a comparison between simulated and observed winter balance for the mass-balance years 2004–2005 and 2005–2006 (Oddur Sigurðsson, Hydrological Service, National Energy Authority, personal communication). The model does not appear to capture the strong observed NW–SE precipitation gradient. The single grid cell values for the SE part are very close to the observed values but they are too high for the NW part. The area-averaged values from MM5 are, however, close to the mean observed values for the NW region of the ice cap but too low for the SE part.

COMPARISON WITH HYDROLOGICAL DATA

Jónsdóttir (2008) used the latest output from V3–7 of the MM5 model as input to the WaSiM model, run at a 1 × 1 km resolution, for the period 1961–1990 to create a run-off map of Iceland. The difference between measured and modelled discharge was in general found to be less than 5%, although larger discrepancies were observed (see Figure 5). For a full list of stations we refer to Table 2

Table 1 | Comparison of observed accumulated winter balance (mm) and simulated wintertime precipitation at Langjökull and Hofsjökull ice caps and Dyngjujökull and Brúarjökull outlet glaciers (cf. Figure 2) using data from V3–5 and 3–7 of the MM5 model. “Starred” values include data for the 2003–2004, 2004–2005 and 2005–2006 winters in addition to the period shown in column 2

		RMS (mm)			Spearman’s ρ			Dev. from 0		
Glacier	Period	V3–5	V3–7	V3–7*	V3–5	V3–7	V3–7*	V3–5	V3–7	V3–7*
Langjökull	1996–2003	264	411	372	0.893	0.571	0.503	0.007	0.180	0.138
Hofsjökull	1987–2003	278	286	300	0.918	0.688	0.628	5.5×10^{-7}	0.003	0.004
Dyngjujökull	1991–2001	405	271	286	0.365	0.614	0.610	0.300	0.059	0.060
Brúarjökull	1992–2003	194	185	171	0.691	0.811	0.830	0.019	0.003	0.0002

Table 2 | Accumulated winter balance (mm) and simulated wintertime precipitation at Drangajökull, NW Iceland (cf. Figure 2). Observed winter balance is taken as the mean of stakes above 400 m altitude in the northwestern (NW) part of the ice cap and in the southeastern (SE) part. Simulated precipitation is both taken as a nine-point mean value (lower values) for the nearest grid cells as well as the nearest grid cell value (higher values)

Winter	NW_{Obs} (mm)	NW_{MM5} (mm)	SE_{Obs} (mm)	SE_{MM5} (mm)
2004/2005	1,797 (3 pts)	2,090/2,554	2,675 (2 pts)	2,072/2,603
2005/2006	1,833 (3 pts)	2,105/2,524	2,815 (2 pts)	2,127/2,604

in Jónsdóttir (2008, pp 105–106). The WaSiM model was not run with a groundwater module. Instead, precipitation simulated by MM5 was scaled in order to make the simulated water balance fit the measured water balance for individual watersheds. A detailed description of this method can be found in Section 6 in Jóhannesson *et al.* (2007, pp 50–53) and Jónsdóttir (2008, pp. 103–106). Therefore, comparison of measured and simulated water balance cannot be directly used for validation of the model-generated precipitation. According to the non-scaled MM5 output for the period 1961–1990, mean precipitation for the whole of Iceland was 1,790 mm yr^{-1}. After scaling the precipitation, this value was reduced to 1,750 mm yr^{-1}, i.e. by approximately 2%. This difference can, to some extent, be explained by the fact that precipitation falls on porous post-glacial lava in some areas and flows through groundwater aquifers to the ocean without participating in surface run-off. Earlier research (Tómasson 1982) has estimated this flow to be of the order of 33–62 mm yr^{-1}. This comparison of total accumulated scaled and non-scaled precipitation indicates that MM5 produces comparatively unbiased precipitation estimates when integrated over the whole of Iceland.

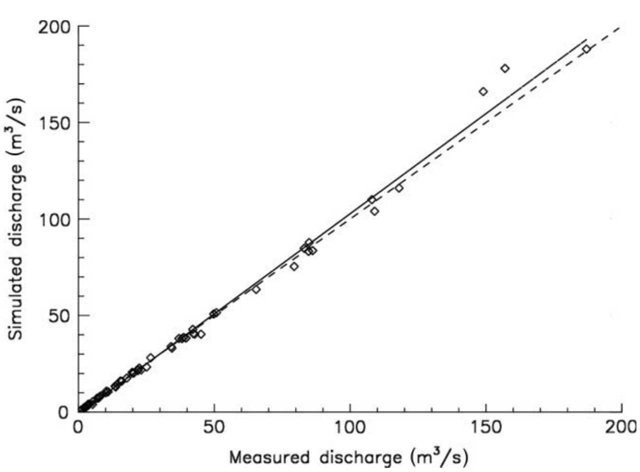

Figure 5 | Measured and simulated (WaSiM/MM5) mean discharge ($m^3 s^{-1}$) at the watershed gauges. Dashed line indicates a perfect fit, while the solid line represents the linear best fit between the measured and simulated discharge. Same as Figure 3 and 4 in Jóhannesson *et al.* (2007, p 51).

Table 3 compares observed and modelled discharge from six watersheds (cf. Figure 6) that are not much affected by groundwater flow. These discharge stations are the same as used for validation of an earlier MM5 model version (V3–5) by RJO07. The periods shown are the same (1987–2002), for comparison purposes, as well as longer periods where available ("starred" values in Table 3). Here, non-scaled precipitation is used in the hydrological modelling in order to obtain an independent validation of the precipitation generated by MM5. For the 15-year period, the difference between modelled and observed discharge (denoted by Q_{meas} in Table 3) is reduced, or remains the same, for four out of six watersheds when the newer version of the MM5 model (V3–7) is used compared with the results obtained with the earlier model version. The relative difference between the simulated and observed water balance is in the range -24.5 to 10.8%, with four of the six values in the range -5 to 9%. The relative difference between observed (denoted by Q^{*}_{meas} in Table 3) and simulated run-off for the longer simulation periods ranges between -3.0 and 5.0%.

DISCUSSIONS

In this study, numerically simulated precipitation has been compared with non-conventional observations of precipitation, i.e. snow accumulation and run-off. This type of data only provides validation on a much longer timescale than conventional rain-gauge data, and the daily error in the precipitation downscaling remains unclear. However, the comparison with the observational data shows that the climatological values of the simulated precipitation are of good quality.

Table 3 | Comparison of observed and simulated discharge ($m^3 s^{-1}$) at six discharge stations and Nash–Sutcliffe coefficients of model fit, using unscaled modelled precipitation from V3–5 and 3–7 of the MM5 model for the 15-year period 1987–2002 and for longer periods ("starred" values) for V3–7 where available (cf. Table 2 in Jónsdóttir (2008)). The longer simulation periods are, respectively, 1963–2001, 1971–2001, 1963–2001, 1976–2001, 1976–2001 and 1991–2004. The discharge stations are, respectively; Vatnsdalsá River, Norðurá River, Fossá í Berufirði River, Hvalá River, Fnjóská River and Hamarsá River. The location of the discharge areas is shown in (Figure 6)

			Q_{calc}			Difference (%)			R2			R2 log		
Station no.	Q_{meas}	Q^{*}_{meas}	V3–5	V3–7	V3–7*	V3–5	V3–7	V3–7*	V3–5	V3–7	V3–7*	V3–5	V3–7	V3–7*
45	12.3	10.3	13.4	13.4	10.8	8.9	8.9	5.0	0.69	0.62	0.54	0.60	0.57	0.46
128	26.8	22.4	29.1	29.7	22.8	8.5	10.8	2.0	0.61	0.53	0.58	0.64	0.63	0.56
148	9.1	8.2	10.4	8.64	8.4	14.3	−4.6	1.0	0.64	0.57	0.59	0.71	0.56	0.6
198	26.8	15.5	25.4	20.2	16.1	−5.2	−24.5	4.0	0.62	0.45	0.51	0.60	0.39	0.53
200	48.4	39.6	53.9	51.3	38.3	11.4	6.2	−3.0	0.53	0.50	0.51	0.53	0.53	0.55
265	19.6	19.9	20.8	18.6	20.2	6.1	−4.9	2.0	0.70	0.64	0.66	0.74	0.71	0.71

The present study is based on a horizontal resolution of 8 km. In areas where there is substantial subgrid orography, changes in the horizontal resolution will inevitably lead to locally different simulated precipitation. Such a difference may, however, not give a proportionally large signal in tests of the kind that are presented in this paper. This is because the glacier observations (apart from Drangajökull, NW Iceland) are not in the vicinity of substantial subgrid variability in orography, and because the run-off calculations are all based on averaging over a substantial area.

The discharge stations, and accompanying watersheds (cf. Figure 6) are the same as used for validation of an earlier MM5 model version (V3–5) by RJO07. As the WaSiM model was not run with a groundwater module it was necessary to compare the non-scaled simulated precipitation from the MM5 model with simulated discharge from watersheds that are not affected by groundwater flow. Looking at a geological map of Iceland (cf. Figure 7) it is clear that these watersheds are in areas where the geological formations are relatively old, i.e. from the Tertiary or late Tertiary periods. As a result the bedrock is dense with a low

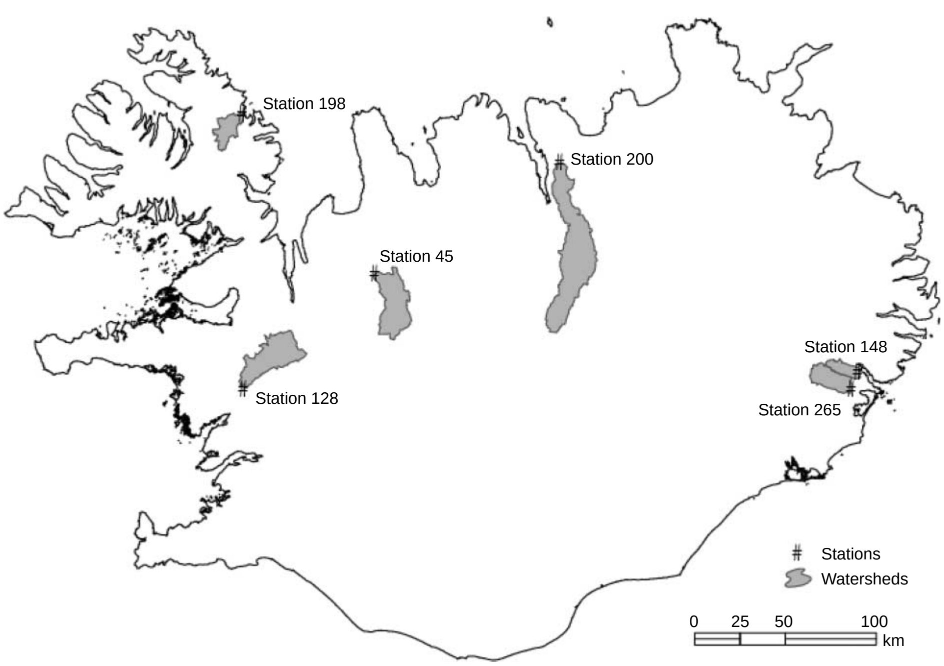

Figure 6 | The location of the six watersheds and corresponding gauging stations used for validation of the MM5 precipitation data. Same as Figure 2 in RJO07.

permeability and the groundwater flow is a negligible part of the total run-off.

There are two key differences between the MM5 model used in RJO07 and the current version. One is due to changes made in the Reisner2 microphysics scheme (Reisner *et al.* 1998). Notably, V3–5 used in RJO07 used the Kessler autoconversion scheme. Autoconversion is the process where cloud droplets collide and coalesce with each other and eventually form raindrops. As for V3–6, this scheme was swapped with that of Berry and Reinhardt as implemented by Walko *et al.* (1995). The Kessler scheme has been known to produce too much precipitation upstream of mountains. Figure 8 shows the difference in simulated precipitation between V3–5 (as in RJO07) and the current V3–7 for the period 1987–2002. As expected, the older version produces more precipitation upstream and on the upstream slopes of mountains that are well represented at the model horisontal resolution. This difference leads to V3–7 overestimating precipitation at the ice caps in central Iceland (Langjökull and Hofsjökull) relative to V3–5. However, simulated precipitation at the large outlet glaciers in N Vatnajökull (Brúarjökull and Dyngjujökull) is in considerable better agreement with observations (cf. Table 1). The second difference is that, as of V3–6, a new land surface model, called the NOAH land surface model (NOAH LSM) (Koren *et al.* 1999; Ek *et al.* 2003), is used in the MM5 model instead of the older OSU land surface model. The NOAH LSM has been shown (Mitchell 2006) to better simulate soil heat flux and to reduce cold temperature bias, especially over sparse ground vegetation. This difference is sure to affect the formation of convective precipitation

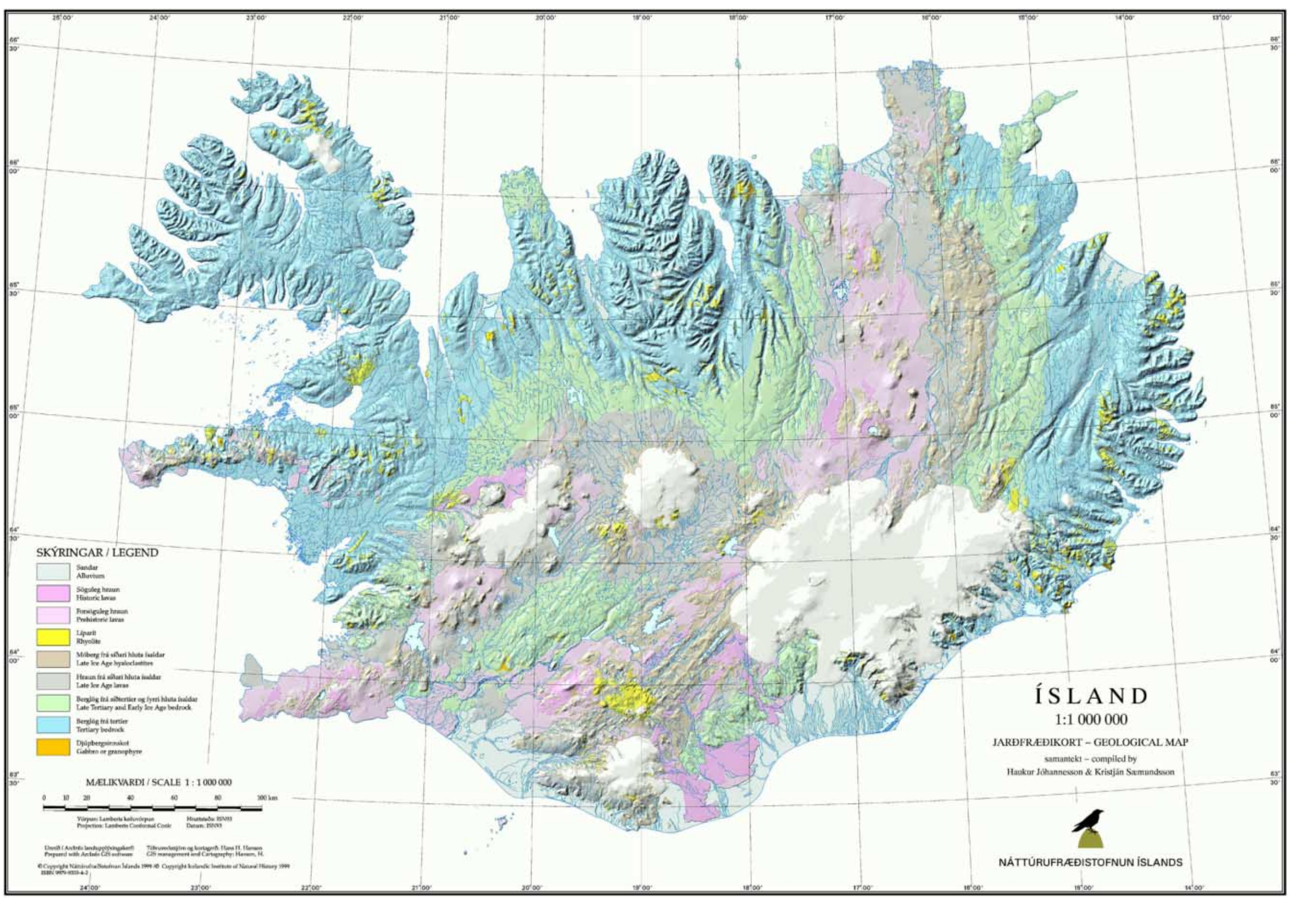

Figure 7 | Gelological map of Iceland (Jóhannesson & Sæmundsson 1999). The watersheds used for validation purposes are all located in regions where the bedrock is relatively old (denoted by blue and green legends) and dense. Consequently, the permeability is low and the effects of groundwater flow on the total run-off are at a minimum. The full colour version of this figure can be accessed by subscribers online at http://www.iwaponline.com/nh/toc.htm

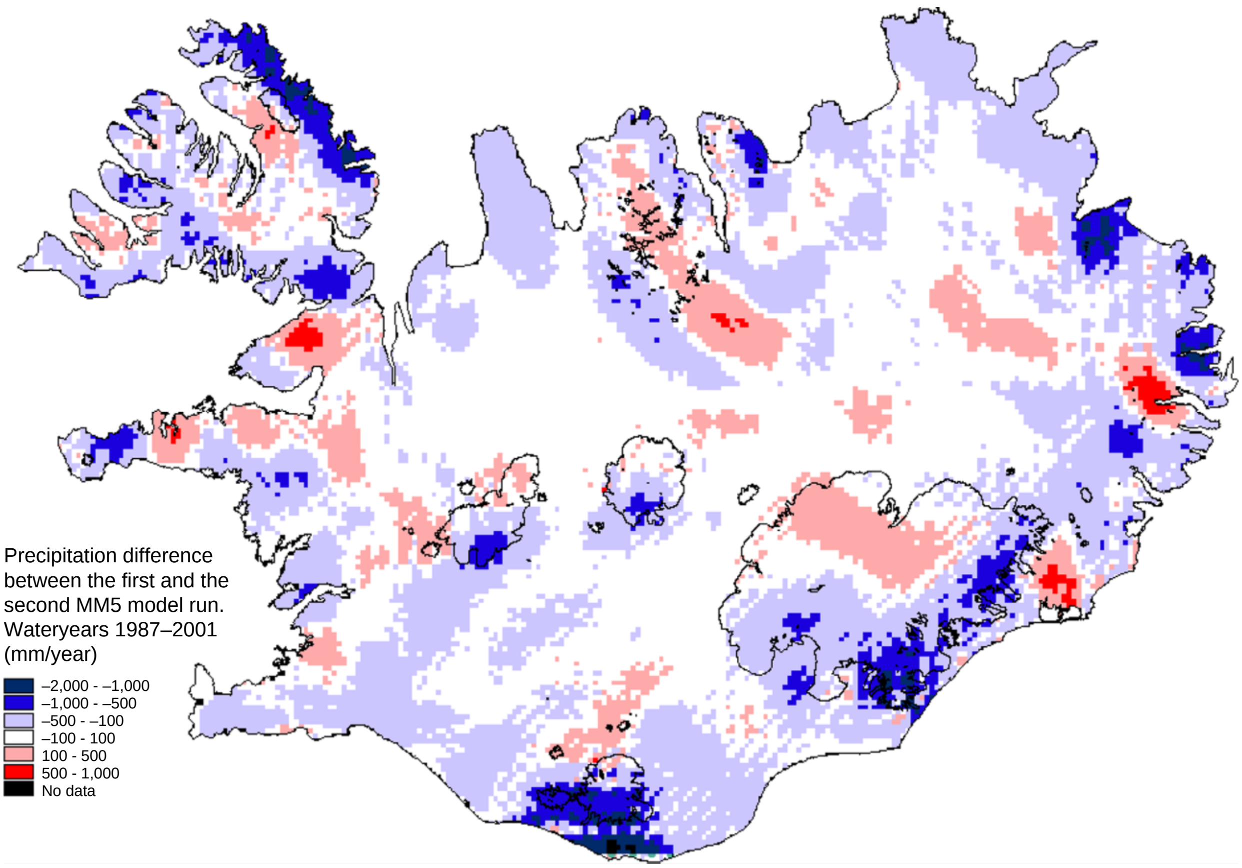

Figure 8 | Difference (MM5 V3–7 minus MM5 V3–5) in simulated mean annual precipitation for the water years 1987–2002.

in the model. However, as the ratio of simulated convective precipitation to explicitly simulated precipitation by the microphysical scheme is low (less than 5% of the total precipitation), this difference is not believed to play an important role in the difference is simulated precipitation between V3–5 and V3–7 of MM5. Other model components used in this study and the RJO07 study, such as the planetary boundary layer scheme, radiation schemes (both short and long wave) and the cumulus scheme, only experienced minor modification or bug fixes between V3–5 and 3–7.

Simulated run-off based on model data from V3–5 and V3–7 is, in general, in good agreement with observed run-off (cf. Table 3). For the 15-year period 1987–2002, the relative difference between observed and simulated run-off is reduced for three out of six watersheds when using data from V3–7 of the MM5 model. The difference remains the same for one watershed (station no. 45) and increases for two out of six watersheds. Notably, V3–7 seems to underestimate precipitation at gauging station no. 198, located in NW Iceland. However, this underestimation in run-off is not present when run-off is simulated over a longer time period (1976–2002 vs. 1987–2002). The relative difference drops from −24.5% to 4.0%. The reason for this sensitivity is unclear. The Nash–Sutcliffe coefficients of model fit remain similar for both V3–5 and V3–7, with V3–5 showing slightly greater skill. The exception being station no. 198, where the older model shows considerably greater skill, regardless of the time period in question.

When looking at long term means (weeks and/or months) of observed and simulated precipitation, as is done here, there is always the risk of compensation of errors on a shorter timescale (hours and/or days). Arason *et al.* (2010) use the same simulated data series as is done in this paper and compared the results in a systematic way to observed liquid precipitation. This was done in order to minimize the effects of undercatchment of solid precipitation in observations. They conclude that there are indeed systematic errors in the simulated precipitation, even in areas of resolved orography. Most noticable, the risk of false alarms (i.e. the model simulates precipitation, but none is observed) is highest in N Iceland, particularly during winter. The probability of missing precipitation events (i.e. precipitation is observed, but none is simulated by the model) is greatest in the summer and on the lee side of Iceland in southerly flows. This sensitivity to flow regimes could, to some extent, explain the large differences between simulated discharge (cf. Table 3, −24.5% for the period 1987–2002 vs. 4.0% difference for the period 1976–2001) at station no. 198 in NW Iceland. Subgrid orographic effects could also play an important role. Figure 1 in Arason *et al.* (2010) shows, for example, great variability in the relative error (MM5-Obs/Obs) for the two stations located in the vicinity of discharge station no. 198 in NW Iceland. The relative error of the simulated summer (i.e. June, July and August) precipitation is 4.5% and 73.6% for two stations, which are located within 15 km of each other (stations Litla Ávík and Gjögur, respectively).

Although there are some biases in the simulated precipitation, important statistical properties can still be gained from the dataset. Elíasson *et al.* (2009) have extracted statistical parameters of extreme precipitation from the simulated time series. They find the average difference between observed and simulated precipitation (Obs-MM5) at 70 out of 73 observation stations to be around $-5\,\mathrm{mm\,d^{-1}}$, with a standard error of 17 mm. As observations at the interior of Iceland are very sparse, the simulated time series gives important information about plausible return periods of extreme precipitation in these regions.

CONCLUSIONS

In general, the MM5 V3–7 model results compare favourably with the observed winter balance, in particular for Hofsjökull, where corrections to take liquid precipitation and/or winter ablation into account have been made, and for the outlet glaciers Dyngjujökull and Brúarjökull. More extensive comparison of simulated precipitation with glaciological observations needs to be made with corrected mass balance data from all the ice caps. Simulated discharge compares favourably with observed discharge for the majority of observation sites, indicating a satisfactory performance of the model.

There is an overall improvement of the simulated precipitation when going from MM5 V3–5 to MM5 V3–7. However, this improvement is both period- and site-dependent and, at some locations, the study shows a degradation in model performance. In general, V3–7 gives less precipitation on the upstream slopes.

ACKNOWLEDGEMENTS

This study was funded in part by the Nordic Climate and Energy Systems (CES) research project and the corresponding Icelandic national project Lofthjúpsbreytingar og áhrif þeirra á OrkuKerfi og Samgöngur (LOKS, see http://en.vedur.is/ces). The authors wish to thank Oddur Sigurðsson, Finnur Pálsson and Helgi Björnsson for making unpublished data available. The authors are indepted to Bergur Einarsson for running additional WaSiM simulations for evaluation purposes. Finally, the authors would like to thank two anonymous reviewers for their helpful comments.

REFERENCES

Arason, T., Rögnvaldsson, Ó. & Ólafsson, H. 2010 Validation of numerical simulations of precipitation in complex terrain at high temporal resolution. *Hydro. Res.* **41**(3–4), 164–170.

Björnsson, H., Pálsson, F., Guðmundsson, M. T. & Haraldsson, H. 1998 Mass balance of western and northern Vatnajökull, Iceland, 1991–1995. *Jökull* **45**, 35–58.

Björnsson, H., Pálsson, F. & Haraldsson, H. 2002 Mass balance of Vatnajökull (1991–2001) and Langjökull (1996–2001), Iceland. *Jökull* **51**, 75–78.

Bromwich, D. H., Bai, L. & Bjarnason, G. G. 2005 High-resolution regional climate simulations over Iceland using polar MM5. *Mon. Weather Rev.* **133**, 3527–3547.

Ek, M. B., Mitchell, K. E., Lin, Y., Rogers, E., Grunmann, P., Koren, V., Gayno, G. & Tarpley, J. D. 2003 Implementation of Noah land surface model advances in the National Centers for Environmental Prediction operational mesoscale Eta model. *J. Geophys. Res.* **108**(D22), 8851.

Elíasson, J., Rögnvaldsson, Ó. & Jónsson, T. 2009 Extracting statistical parameters of extreme precipitation from a NWP model. *Hydrol. Earth Syst. Sci.* **13**, 2233–2240.

Grell, G. A., Dudhia, J. & Stauffer, D. R. 1995 *A Description of the Fifth-generation Penn State/NCAR Mesoscale Model (MM5)*. NCAR Tech. Note NCAR/TN-398 + STR, National Center for Atmospheric Research, Boulder, Colorado.

Jasper, K., Gurtz, J. & Lang, H. 2002 Advanced flood forecasting in Alpine watersheds by coupling meteorological observations and forecasts with a distributed hydrological model. *J. Hydrol.* **267**, 40–52.

Jóhannesson, T., Aðalgeirsdóttir, G., Ahlstrøm, A., Andreassen, L. M., Björnsson, H., de Woul, M., Elvehøy, H., Flowers, G. E., Guðmundsson, S., Hock, R., Holmlund, P., Pálsson, F., Radic, V., Sigurðsson, O. & Thorsteinsson, Th. 2006*a* The impact of climate change on glaciers and glacial runoff in the Nordic countries. In: *Proc. European Conference of Impacts of Climate Change on Renewable Energy Sources, Reykjavík, Iceland, 5–6 June*. Hydrological Service–National Energy Authority, Reykjavík, Iceland, pp. 31–38.

Jóhannesson, T., Einarsson, B. & Thorsteinsson, Th. 2006*b* *Mass Balance Modeling of the Hofsjökull Ice Cap Based on Data from 1988–2004*. National Energy Authority, OS-2006/004, Reykjavík, Iceland.

Jóhannesson, T., Aðalgeirsdóttir, G., Björnsson, H., Crochette, P., Elíasson, E. B., Guðmundsson, S., Jónsdóttir, J. F., Ólafsson, H., Pálsson, F., Rögnvaldsson, Ó., Sigurðsson, O., Snorrason, Á., Sveinsson, Ó. G. B. & Thorsteinsson, Th. 2007 *Effect of Climate Change on Hydrology and Hydro-resources in Iceland*. Rep. OS-2007/011, National Energy Authority, Reykjavík.

Jóhannesson, H. & Sæmundsson, K. 1999 *Geological Map of Iceland, 1:1.000.000*. Icelandic Institute of Natural History, Reykjavík, Iceland.

Jóhannesson, T., Sigurðsson, O., Laumann, T. & Kennett, M. 1995 Degree-day glacier mass balance modelling with applications to glaciers in Iceland, Norway and Greenland. *J. Glaciol.* **41**, 345–358.

Jónsdóttir, J. F. 2008 A runoff map based on numerically simulated precipitation and a projection of future runoff in Iceland. *Hydrol. Sci. J.* **53**(1), 100–111.

Koren, V., Schaake, J., Mitchell, K., Duan, Q.-Y., Chen, F. & Baker, J. M. 1999 A parameterization of snowpack and frozen ground intended for NCEP weather and climate models. *J. Geophys. Res.* **104**(D16), 19569–19585.

Mitchell, K. 2006 The new Noah LSM in the NCEP GFS (implemented 31 May 2005). *THORPEX Workshop, 17–19 January*. Available at: http://www.emc.ncep.noaa.gov/gmb/ens/THORPEX/PI-workshop/Mitchell_THORPEX-Workshop_GFS-Noah_18Jan06.ppt

Pálsson, F., Björnsson, H., Haraldsson, H. H. & Magnússon, E. 2002*a* *Afkomu- og hraðamælingar á Langjökli jökulárið 2001–2002*. RH-26-2002, Science Institute, Reykjavík.

Pálsson, F., Magnússon, E. & Björnsson, H. 2002*b* *The Surge of Dyngjujökull 1997-2000. Mass Transport, Ice Flow Velocities, and Effects on Mass Balance and Runoff*. RH-01-2002, Science Institute, Reykjavík.

Pálsson, F., Björnsson, H. & Magnússon, E. 2004*a* *Afkomu- og hraðamælingar á Langjökli jökulárið 2003–2004*. RH-18-2004, Science Institute, Reykjavík.

Pálsson, F., Björnsson, H. & Haraldsson, H. H. 2004*b* *VATNAJÖKULL: Mass Balance, Meltwater Drainage and Surface Velocity of Glacial Year 2001–2002*. RH-21-2004, Science Institute, Reykjavík.

Pálsson, F., Björnsson, H., Magnússon, E. & Haraldsson, H. H. 2004*c* *VATNAJÖKULL: Mass Balance, Meltwater Drainage and Surface Velocity of Glacial Year 2002–2003*. RH-22-2004, Science Institute, Reykjavík.

Pálsson, F., Björnsson, H., Magnússon, E. & Haraldsson, H. H. 2004*d* *VATNAJÖKULL: Mass Balance, Meltwater Drainage and Surface Velocity of Glacial Year 2003–2004*. RH-23-2004, Science Institute, Reykjavík.

Reisner, J., Rassmussen, R. J. & Bruintjes, R. T. 1998 Explicit forecasting of supercooled liquid water in winter storms using the MM5 mesoscale model. *Q.J.R. Meteorol. Soc.* **124B**, 1071–1107.

Rögnvaldsson, Ó., Crochet, P. & Ólafsson, H. 2004 Mapping of precipitation in Iceland using numerical simulations and statistical modeling. *Meteorol. Z.* **13**(3), 209–219.

Rögnvaldsson, Ó., Jónsdóttir, J. F. & Ólafsson, H. 2007 Numerical simulations of precipitation in the complex terrain of Iceland-comparison with glaciological and hydrological data. *Meteorol. Z.* **16**(1), 71–85.

Rögnvaldsson, Ó. & Ólafsson, H. 2002 *Downscaling Experiments with the MM5 Model: Determining An Optimal Configuration for Climatological Downscaling Studies of Precipitation in Iceland*. Icelandic Meteorological Office. Available at: http://www.vedur.is/~haraldur/urkoma.pdf

Sigurðsson, O. & Sigurðsson, Ó.J. 1998 *Afkoma nokkurra jökla á Íslandi 1992–1997 (Mass balance of a number of Icelandic glaciers 1992–1997)*. Rep. OS-98082 (in Icelandic). National Energy Authority, Reykjavík.

Sigurðsson, O., Thorsteinsson, Th., Ágústsson, S. M., Einarsson, B. 2004 *Afkoma Hofsjökuls 1997–2004 (Mass balance of Hofsjökull 1997–2004)*. Rep. OS-2004/029. National Energy Authority, Reykjavík.

Tómasson, H. 1982 Vattenkraft i Island och dess hydrologiska förutsätningar (Hydropower in Iceland and its hydrological prerequisites). In: *Den nordiske hydrologiske konferense, NHK-82, Förde 28–30 June*. Rep. OS-82059/VOD-10. National Energy Authority, Reykjavík.

Uppala, S. M. *et al.* 2005 The ERA-40 re-analysis. *Q. J. R. Meteorol. Soc.* **131**, 2961–3012.

Walko, R. L., Cotton, W. R., Meyers, M. P. & Harrington, J. Y. 1995 New RAMS cloud microphysics parameterization. Part I: The single-moment scheme. *Atmos. Res.* **38**, 29–62.

First received 15 December 2008; accepted in revised form 4 January 2010. Available online April 2010

Paper VII: Downslope windstorm in Iceland – WRF/MM5 Model Comparison

Atmos. Chem. Phys., 11, 103–120, 2011
www.atmos-chem-phys.net/11/103/2011/
doi:10.5194/acp-11-103-2011
© Author(s) 2011. CC Attribution 3.0 License.

Atmospheric Chemistry and Physics

Downslope windstorm in Iceland – WRF/MM5 model comparison

Ó. Rögnvaldsson[1,2], J.-W. Bao[3], H. Ágústsson[1,4], and H. Ólafsson[4,5,*]

[1]Institute for Meteorological Research, Reykjavík, Iceland
[2]University of Bergen – UiB, Bergen, Norway
[3]NOAA/ESRL, Boulder, USA
[4]University of Iceland, Reykjavík, Iceland
[5]Icelandic Meteorological Office, Reykjavík, Iceland
[*]now at: Bergen school of meteorology, Geophysical Institute UiB, Norway

Received: 1 February 2008 – Published in Atmos. Chem. Phys. Discuss.: 1 April 2008
Revised: 8 December 2010 – Accepted: 20 December 2010 – Published: 5 January 2011

Abstract. A severe windstorm downstream of Mt. Öræfajökull in Southeast Iceland is simulated on a grid of 1 km horizontal resolution by using the PSU/NCAR MM5 model and the Advanced Research WRF model. Both models are run with a new, two equation planetary boundary layer (PBL) scheme as well as the ETA/MYJ PBL schemes. The storm is also simulated using six different micro-physics schemes in combination with the MYJ PBL scheme in WRF, as well as one "dry" run. Output from a 3 km MM5 domain simulation is used to initialise and drive both the 1 km MM5 and WRF simulations. Both models capture gravity-wave breaking over Mt. Öræfajökull, while the vertical structure of the lee wave differs between the two models and the PBL schemes. The WRF simulated downslope winds, using both the MYJ and 2EQ PBL schemes, are in good agreement with the strength of the observed downslope windstorm. The MM5 simulated surface winds, with the new two equation model, are in better agreement to observations than when using the ETA scheme. Micro-physics processes are shown to play an important role in the formation of downslope windstorms and a correctly simulated moisture distribution is decisive for a successful windstorm prediction. Of the microphysics schemes tested, only the Thompson scheme captures the downslope windstorm.

CC BY

Correspondence to: Ó. Rögnvaldsson
(or@belgingur.is)

1 Introduction

Iceland is a mountainous island located in the middle of the North Atlantic Ocean in the northern part of the storm track. Due to this, the climate and weather of Iceland are largely governed by the interaction of orography and extra-tropical cyclones. This interaction can be in the form of cold air damming by mountains or warm downslope descent. The atmosphere-mountain interaction can also cause local acceleration of the airflow or a forced ascending motion, causing extreme precipitation. As a result of this interaction, downslope windstorms are quite common in Iceland.

Mountain waves and downslope windstorms have long been a target of research campaigns as well as theoretical and numerical researches. Such windstorms are generally associated with vertically propagating gravity waves in the troposphere. Favourable large-scale flow conditions for the generation of downslope windstorms include elements such as strong low-level winds and strong static stability at low levels. A reverse vertical windshear, as described in Smith (1985), may contribute to downslope windstorm through trapping of wave energy, while a positive vertical windshear may also act positively through amplification of gravity waves (see review by Durran, 1990). The prime objective of the T-REX (Terrain-induced Rotor EXperiment) campaign (Grubišić et al., 2008) in Sierra Nevada was on observations of mountain waves, rotor flow and low- and upper-level turbulence. This was done by means of ground-based observations and state of the art remote sensors and airborne observing systems. Recently, a number of papers based on the observations of T-REX have emerged, e.g. Jiang and Doyle

Published by Copernicus Publications on behalf of the European Geosciences Union.

(2009) which investigates the impact of moisture on gravity wave activity. One of the main conclusion of the study is that waves are generally weakened by high moisture near mountain top level. Idealised cases of downslope windstorms, and the associated gravity wave activity, as well as real cases of downslope winds in many part of the world have been studied by many authors. The real flow cases include the celebrated 11 January 1972 Boulder windstorm (e.g. Doyle et al., 2000 and ref. therein), downslope windstorms in the Dinaric Alps (e.g. Smith, 1987; Belǔsić and Klaić, 2004; Belǔsić et al., 2004 and ref. therein), windstorms in Norway in westerly flow (e.g. Grønås and Sandvik, 1999; Doyle and Shapiro, 2000; Sandvik and Hartsveit, 2005) and Greenland windstorms in westerly flow (Rögnvaldsson and Ólafsson, 2003; Doyle et al., 2005) as well as easterly flow (Ólafsson and Ágústsson, 2006; Ólafsson and Ágústsson, 2009).

Research on Icelandic downslope windstorms was quite limited until recent studies by Ágústsson and Ólafsson (2007), Ólafsson and Ágústsson (2007) (hereafter ÓÁ-07), and Ágústsson and Ólafsson (2010). Yet the most violent winds in Iceland are in many if not most cases immediately downstream of mountains. One such windstorm hit Freysnes, SE-Iceland, on the morning of 16 September 2004. The windstorm was quite well forecasted in the region by the operational HRAS-system (Ólafsson et al., 2006), which at that time ran the MM5 model (Grell et al., 1995) at a 9 km horizontal resolution. Locally, the winds became however stronger than the direct model output indicated. Immediately downstream of the ice-covered Öræfajökull mountain (2110 m.a.s.l.) structural damage occurred, including a hotel that lost its roof. This windstorm was investigated in the ÓÁ-07 paper by utilising the MM5 numerical weather prediction model at high resolution and by analysing available observations. The ÓÁ-07 study revealed a flow structure characterized by a stable airmass at mountain level and a reverse vertical windshear in the lower to middle troposphere, leading to the generation and breaking of gravity waves over the mountain. The surface flow was however anomalously warm. These characteristics led to the suggestion that the Freysnes windstorm might be used as a generic name for a warm version of the bora windstorms. The Freysnes case featured at the same time strong downslope and corner winds (i.e. flow speed-up at the southern edge of Mt. Öræfajökull), underlining the fact that simple linear and even non-linear theories of uniform flows might indeed be very different from conditions in the real atmosphere. The downslope windspeed simulated by ÓÁ-07 was considerably underestimated compared to observations. The authors suggested that this might be due to too rapid deceleration of the simulated flow once it had reached the lowland, pointing out the fact that horizontal extension of downslope storms is quite sensitive to both numerical dissipation and advection as well as numerical representation of subgrid processes such as turbulence or eddy viscousity.

The objective of this study is to investigate the differences in the simulated dynamics of the downslope windstorm that are caused by the differences in the dynamical cores (including numerics) of two mesoscale models (MM5 and WRF). A further objective is to investigate the sensitivity of the simulated downslope windstorm to different micro-physics schemes available in the WRF model. This is of importance for operational numerical weather forecasts in complex orography. Especially, in light of ever increasing availability of cheap computational power, high resolution simulations are becoming more common. To study this sensitivity, ten simulations are carried out and compared for the same event as studied in ÓÁ-07. This is done by using two mesoscale models: version 3-7-3 of MM5 and version 2.2 of the Advanced Research WRF model (Skamarock et al., 2005), hereafter called WRF, and two different PBL schemes, the current ETA/MYJ planetary boundary layer model (Mellor and Yamada, 1982; Janjić, 1994, 2001) and a new two equation model (Bao et al., 2008). To investigate the impact of cloud micro-physics on the simulated windstorm, five additional simulations are done with the WRF model using different micro-physics schemes in combination with the MYJ planetary boundary layer scheme, as well as a "dry" run without any micro-physics scheme. The output from the 3 km domain of the simulation presented in ÓÁ-07 is used to initialise and drive all model simulations on a grid of 1 km horizontal resolution and 40 vertical layers with the model top at 100 hPa. Both the MM5 and WRF models are configured in as similar way as possible. Comparisons of the simulations are made using observed surface winds, temperature and precipitation.

This paper is structured as follows: in the next section we describe the synoptic overview and list the available observational data in the area. The experimental setup is described in Sect. 3. The results are presented in Sect. 4. Discussions are presented in Sect. 5, followed by concluding remarks.

2 Synoptic overview and available observational data

Figure 1 shows the mean sea level pressure, the geopotential height at 500 hPa and the temperature at 850 hPa at the time when wind gusts greater than 50 $\mathrm{ms^{-1}}$ were observed at the Skaftafell and Öræfi weather stations (see Fig. 2 for location of the stations). At the surface, the geostrophic winds are from the ESE, while over land the surface winds are from the ENE or NE. At 500 hPa, the flow is relatively weak (20–25 $\mathrm{ms^{-1}}$) and the wind direction is from the SSE. There is a sector of warm air at 850 hPa stretching from Ireland towards S-Iceland. In the early morning of 16 September, the observed 2-m temperature at Skaftafell exceeds 15 $^{\circ}$ which is about 7 $^{\circ}$ above the seasonal average. The geostrophic wind at the surface is greater than 30 $\mathrm{ms^{-1}}$ and there is a directional and a reverse (negative) vertical wind shear in the lower part of the troposphere (ÓÁ-07). Figure 2 shows the domain setup of the MM5 and WRF simulations as well as local orography and the location of automatic meteorological stations. These are Skaftafell (SKAFT), Öræfi (ORAFI), Ingólfshöfði (INGOL), Fagurhólsmýri (FAGHO) and Kvísker (KVISK). Surface wind speed and direction, gusts and temperature are all measured at these stations. At stations SKAFT, FAGHO and KVISK, accumulated precipitation is measured once to twice daily. The straight line crossing Mt. Öræfajökull shows the location of the cross sections shown in Fig. 6. Hvannadalshnjúkur, the highest peak of Mt. Öræfajökull, exceeds 2100 m above sea level while the altitude of the Öræfajökull plateau is between 1900 and 2000 m a.s.l.

3 Experimental setup

Initial and boundary data are derived from model simulations described in ÓÁ-07. In the ÓÁ-07 study, atmospheric flow was investigated using version 3-6-1 of the MM5 model (Grell et al., 1995). The subgrid turbulence was parameterized using the ETA PBL scheme (Janjić, 1994). The ÓÁ-07 simulation was run with the Grell cumulus scheme (Grell et al., 1995) and the Reisner2 explicit moisture scheme (Thompson et al., 2004). Radiation was calculated using the CCM2 scheme (Hack et al., 1993). The ÓÁ-07 three domain setup is shown in Fig. 3, the horizontal resolution being 9, 3 and 1 km. The 9 and 3 km domains are centered over Iceland and they consists of 95 × 90 and 196 × 148 gridpoints in the horizontal. The 1 km domain has 175 × 157 points and is centered over the southern part of the Vatnajökull ice cap. The calculations employ 40 vertical (full-σ) levels with the model top at 100 hPa.

In our experiment we use the ÓÁ-07 model output from the 3 km domain as initital and boundary data to all our simulations, both with MM5 (version 3-7-3) and WRF (version 2.2). The simulation domain is the same as the 1 km domain in ÓÁ-07 (cf. Fig. 2 and Fig. 3). At this resolution the Mt. Öræfajökull peak reaches 1920 m a.s.l. The MM5 model control setup (MM5/ETA) is very similar to that in ÓÁ-07 with the exception of a more recent version of the model and the use of the RRTM radiation scheme (Mlawer et al., 1997) instead of the CCM2 scheme. The MM5 model is also run with a new two equation PBL scheme (MM5/2EQ), described in Bao et al. (2008). The two equation model is based on the Mellor-Yamada level 2.5 second-moment closure (MY closure), and consists of two prognositc equations. One for the TKE and the other for the length scale multiplied by twice the TKE. As with the ÓÁ-07 simulation, both MM5 simulations use an upper radiative boundary condition.

For the WRF model (Skamarock et al., 2005) control simulation (WRF/MYJ) we use the Mellor-Yamada-Janjić (Janjić, 1994, 2001) subgrid turbulence scheme. No cumulus scheme is used as opposed to the Grell scheme in the MM5/ETA and MM5/2EQ simulations. An upgraded version of the Reisner2 scheme, the Thompson scheme (Thompson et al., 2004), is used. Long wave radiation is calculated using the RRTM long wave scheme and short wave radiation is simulated using the Dudhia (1989) scheme[1] from the MM5 model. As with the MM5 simulations the calculations

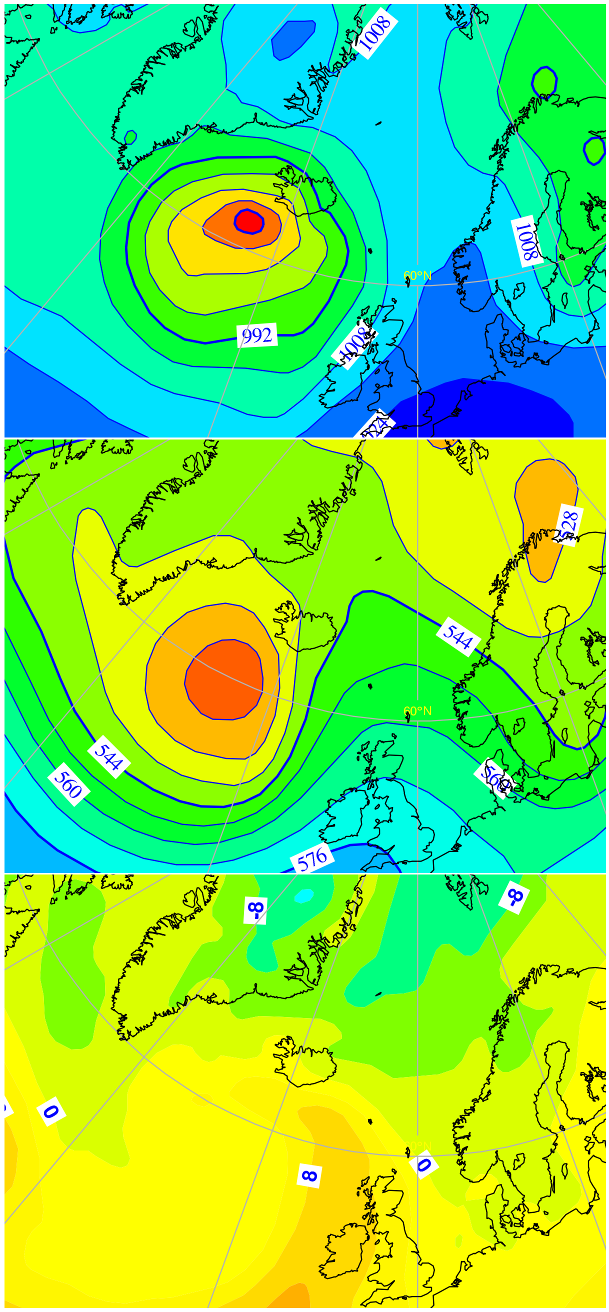

Fig. 1. Mean sea level pressure [hPa] (top), geopotential height at 500 hPa [m] (middle) and temperature at 850 hPa [°] (bottom) on 16 September 2004 at 06:00 UTC. Based on the operational analysis provided by the ECMWF.

[1]When the RRTM radiation obtion is chosen in MM5, this is the scheme used to calculate short wave radiation.

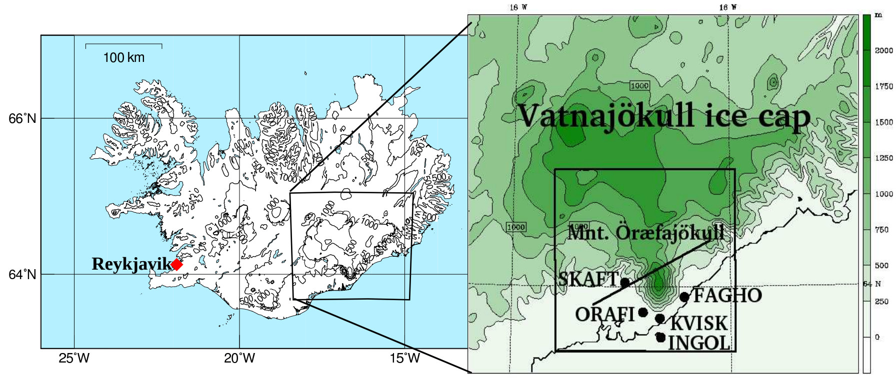

Fig. 2. The 1 km domain setup of the Vatnajökull ice cap and location of observational sites. The box on the right hand side shows the region of interest around Mt. Öræfajökull (cf. Fig. 4). The location of the Freysnes hotel coincides with location SKAFT. The colour scale to the right represents the terrain height.

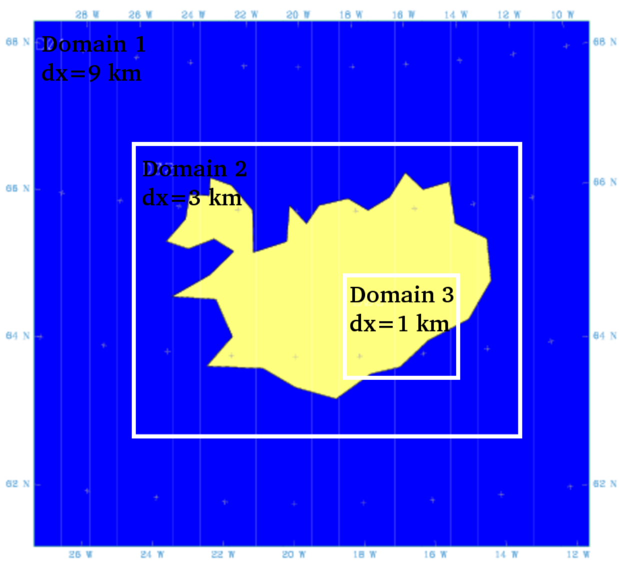

Fig. 3. MM5 domain setup of the ÓÁ-07 experiment, the number of horizontal gridpoints for domains 1, 2 and 3 are 95×90, 196×148 and 175×157, respectively. Domain 3 is the same domain as is used in this experiment. All simulations employ 40 vertical levels.

employ 40 vertical (full-η) levels with the model top at 100 hPa. No damping is imposed on the upper boundary, rather, vertical motion is damped to prevent the model from becoming unstable with locally large vertical velocities. This only affects strong updraft cores, so has very little impact on results otherwise. The WRF model was also run with the two equation PBL scheme (called WRF/2EQ).

In order to investigate the impact of various micro-physics schemes on the downslope flow we ran WRF with five different micro-physics schemes in addition to the Thompson scheme. The micro-physics schemes range from the relatively simple two class Kessler (1969) and WSM3 to the more complex WSM5 (a four class scheme without graupel) and the five class WSM6 (Hong and Lim, 2006), Lin et al. (1983) and Thompson et al. (2004) schemes. A detailed description of the WSM3 and WSM5 schemes can be found in Hong et al. (2004). Beside the differences in the micro-physics, the model setup was that of the WRF control simulation (called WRF/MYJ).

Finally, to find whether evaporation, and consequently condensation, might be a relevant factor for the flow dynamics, a "dry" simulation was carried out. This experiment was identical to the control simulation, with the exception that the microphysics and surface fluxes were turned off.

None of the simulations showed any signs of vertically reflected waves from the top of the model.

4 Results

4.1 Model sensitivity to PBL schemes

4.1.1 Surface winds, temperature and precipitation

All MM5 and WRF simulations capture strong winds over the Vatnajökull ice cap (Fig. 4) as well as over the lowlands. In all simulations the flow is decelerated upstream of Mt. Öræfajökull. The simulated near surface wind speed, taken at the lowest half-sigma level (approximately 40 m a.g.l.), has a maximum immediately downstream of the highest mountain (Mt. Öræfajökull). This maximum does not extend far downstream. There is also a secondary maximum of wind speed emanating from the edge of the same mountain (labeled corner-wind in ÓÁ-07). This secondary maximum extends far downstream. Accumulated precipitation measured at SKAFT, FAGHO and KVISK is compared with simulated precipitation in Table 1. Both models correctly simulate the dry area downstream of Mt. Öræfajökull (station SKAFT). On the windward side (station FAGHO)

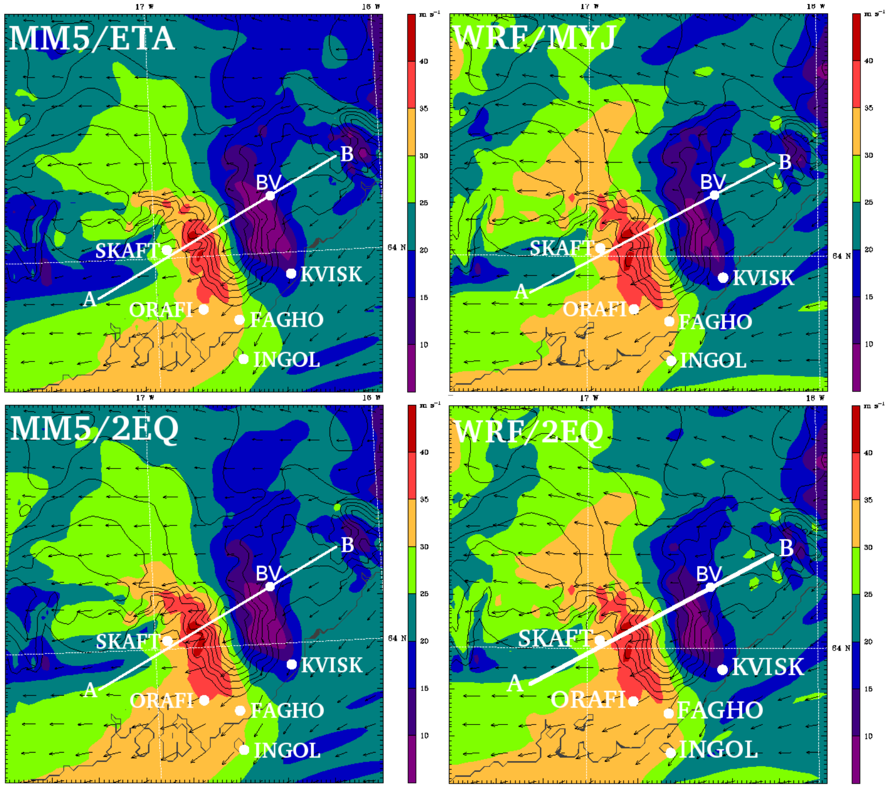

Fig. 4. Zoomed in view of simulated surface wind speed [ms^{-1}] at lowest half-sigma level (approximately 40 m a.g.l.) by MM5 (left panels) and WRF (right panels) at 16 September 2004, 06:00 UTC. Top panels show results from the ETA and MYJ boundary layer schemes and the bottom panel shows results using the new two equation PBL model. The letters "BV" show the location of the vertical profile, along which the Brunt-Väisälä frequency in Table 4 is calculated. The upstream distance from point B to the lateral boundaries of the 1 km domain is approximately 60 km.

Table 1. Observed and simulated accumulated precipitation [mm], between 15 September, 18:00 UTC and 16 September, 09:00 UTC, at stations SKAFT, FAGHO and KVISK.

Location	Observed	MM5		WRF	
		ETA	2EQ	MYJ	2EQ
SKAFT	0.0	0.0	0.0	0.8	0.8
FAGHO	42.4	49.8	47.6	74.8	74.3
KVISK	59	55.5	45.9	95.0	93.0

all four simulations tend to overestimate the precipitation. The overestimation with MM5/ETA and MM5/2EQ is 17% and 12%, respectively, while the WRF/MYJ and WRF/2EQ simulations overestimate the observed precipitation by approximately 75%. This overestimation can, to some extent, be explained by under catchment of the rain gauges due to strong winds. At location KVISK, the MM5 simulations underestimate the precipitation by 6% (MM5/ETA) and 22% (MM5/2EQ) while the WRF model overestimates the precipitation by 61% (WRF/MYJ) and 58% (WRF/2EQ). The precipitation gradient reproduced in the WRF simulations (i.e., more precipitation at KVISK than at FAGHO) is in better agreement with observed gradient than that reproduced in the MM5 simulations. However, the precipitation values in the MM5 simulations are closer to the observed values. With regard to wind speed, there exists a noticeable quantitative difference between the four simulations. Figure 5 shows observed and simulated 10-m wind speed and 2-m temperature at station SKAFT (top) and FAGHO (bottom). At location SKAFT, the WRF simulated downslope winds, using the MYJ and 2EQ PBL schemes, are in good agreement with the strength of the observed downslope windstorm, with the maximum wind speed as great as 29 and 30 ms^{-1}, respectively. The MM5 simulated surface winds, with the new two equation model, are in better agreement to observations than when using the ETA scheme. Surface winds reach 22 ms^{-1} when using the two equation model whilst the winds in the MM5/ETA simulation only reach about 17 ms^{-1}. Further, the 2-m temperature is captured considerably better by the WRF model than

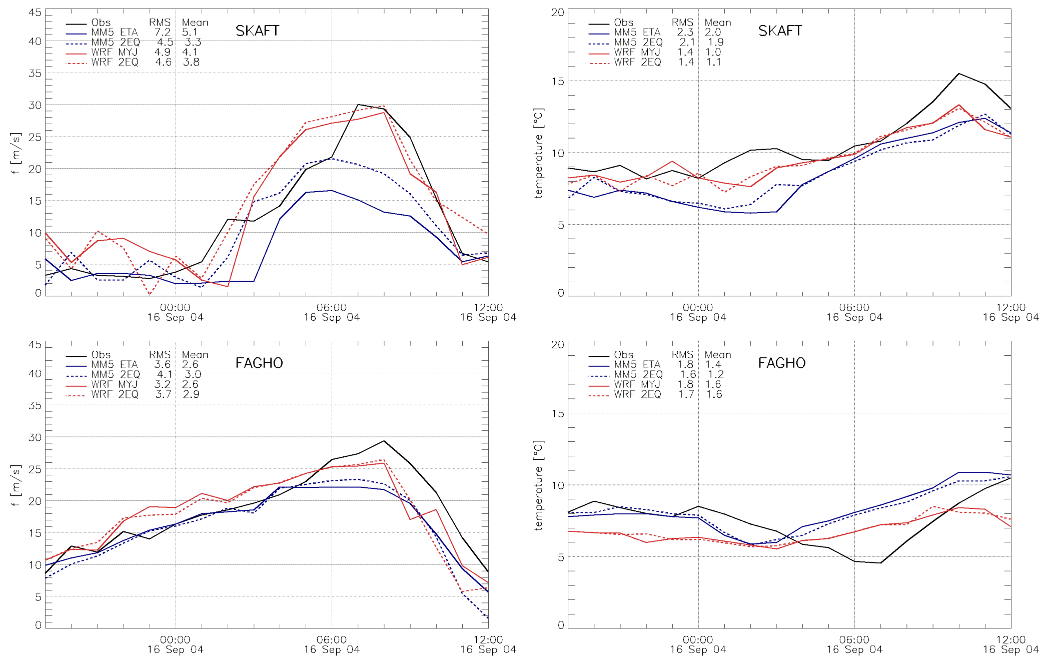

Fig. 5. Observed (solid black) and simulated (solid blue – MM5/ETA, blue dash – MM5/2EQ, solid red – WRF/MYJ, red dash – WRF/2EQ) 10 m wind speed [ms^{-1}] (left) and 2-m temperature [°] (right) at station SKAFT (WMO# 4172, top row) in the lee of Mt. Öræfajökull and at station FAGHO (bottom row).

by MM5. On average, the MM5 simulated 2-m temperature is 2–3° colder than measured while the 2-m temperature in WRF is very close to the observed surface temperature. At station FAGHO the MM5 results are very similar, both simulations correctly capture the storm at early stages but start to tail off at 23:00 UTC on 15 September. Consequently, both MM5/ETA and MM5/2EQ underestimate wind from the mountain edge during the peak of the storm and fail to capture the maximum wind strength by 7.5 and 6.5 ms^{-1}, respectively. The WRF/MYJ and WRF/2EQ simulations overestimate the winds during the early stages (i.e. between 22:00 UTC and 05:00 UTC) of the storm by 2–5 ms^{-1} but underestimate the observed maximum winds (30 ms^{-1}) by 3.5 and 3 ms^{-1}, respectively. All four runs show similar skills simulating surface temperature at FAGHO with RMS errors ranging from 1.6° (MM5/2EQ) to 1.8° (MM5/ETA and WRF/MYJ). However, at the other three stations (ORAFI, KVISK, and INGOL), the differences in temperature between the four simulations are small (not shown). At station ORAFI both WRF simulations overestimate the mean wind by approximately 5 ms^{-1} while MM5/ETA captures the wind field correctly. The MM5/2EQ simulation gives wind speed values that lie between the WRF and MM5/ETA simulated values, the wind speed being 2–3 ms^{-1} higher than observed. At KVISK both models perform similarly, the MM5 underestimates the winds slightly while WRF slightly overestimates them. With the current model configuration, station INGOL is off-shore in both models. Hence, observed and simulated fields can not be compared in a logical manner. Table 2 lists the root mean square and mean errors in simulated wind speed at all five stations during the simulation period.

4.1.2 Wave structure

Figure 6 shows a cross section along line AB (cf. Fig. 4) from the four simulations at 06:00 UTC 16 September. In both MM5 simulations, the distribution of turbulent kinetic energy (TKE) shows that there is very strong mountain wave breaking between approximately 800 and 650 hPa and very little wave activity above 500 hPa. There is intense turbulence below 700 hPa associated with the wave breaking. At the surface, there is also a layer of high TKE. In spite of common features the MM5/ETA and MM5/2EQ simulations reveal important differences in the wave and TKE structure. Between 18:00 UTC and 00:00 UTC on 15 September, there is stronger TKE between 900 and 700 hPa in the MM5/ETA simulation downslope of the mountain than in the MM5/2EQ simulation. The wave structure however remains similar. Few hours later, between 01:00 UTC and 03:00 UTC on 16 September, the wave penetrates considerably deeper in the MM5/2EQ simulation. During this time interval simulated surface wind speed at location SKAFT increases sharply from 3 to 15 ms^{-1} in MM5/2EQ whilst staying calm in the MM5/ETA simulation. This compares favourably with

Table 2. Root mean square (RMS) and mean errors [ms^{-1}] of simulated wind speed at stations SKAFT, ORAFI, INGOL, FAGHO and KVISK.

Location	MM5/ETA		MM5/2EQ		WRF/MYJ		WRF/2EQ	
	RMS	Mean	RMS	Mean	RMS	Mean	RMS	Mean
SKAFT	7.2	5.1	4.5	3.3	4.9	4.1	4.6	3.8
ORAFI	2.2	1.9	4.8	3.8	6.8	6.0	6.6	5.8
INGOL	9.3	7.4	9.0	6.9	8.0	6.6	7.8	6.5
FAGHO	3.6	2.6	4.1	3.0	3.2	2.6	3.7	2.9
KVISK	2.1	1.6	3.2	2.6	3.0	2.4	3.0	2.4

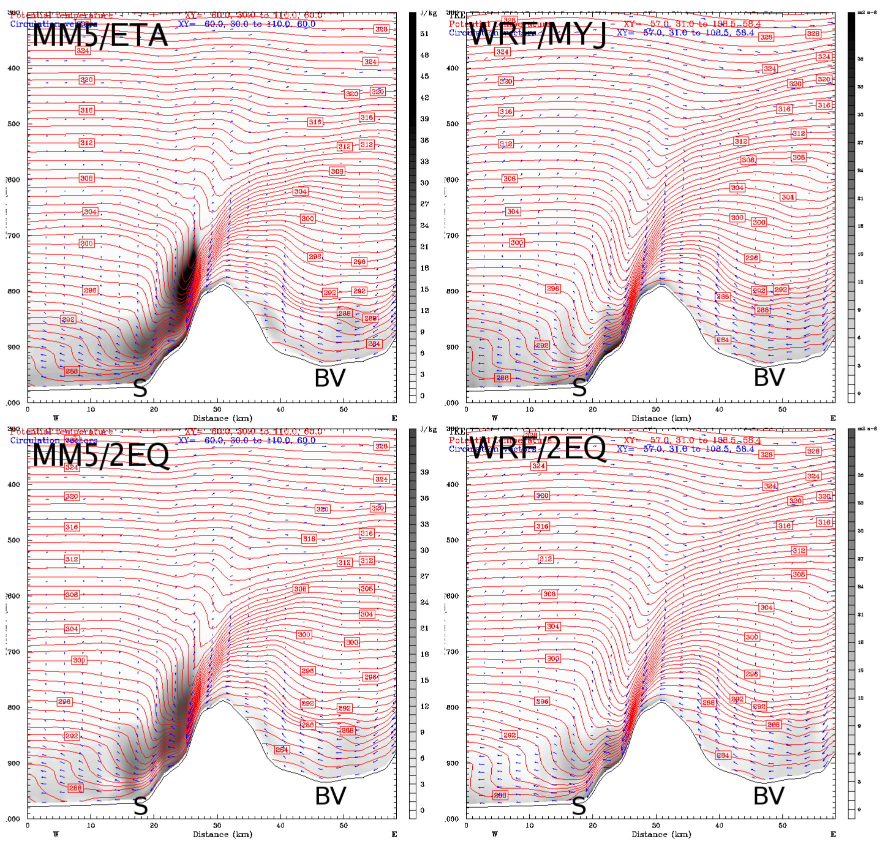

Fig. 6. Cross section along line AB (cf. Fig. 4) showing potential temperature (red lines) [K], wind along the cross section (blue arrows) [ms^{-1}] and turbulent kinetic energy (TKE) [J/kg] for MM5 (left panels) and WRF (right panels) at 16 September 2004, 06:00 UTC. Top panels show results from the ETA and MYJ boundary layer schemes and the bottom panel shows results using the new two equation PBL model. The letter "S" indicates the location of SKAFT and "BV" shows the location of the vertical profile, along which the Brunt-Väisälä frequency in Table 4 is calculated.

observations as wind speed at SKAFT increased from 5 to 12 ms^{-1} during this period. At 03:00 UTC the TKE in the lee of the mountain is confined below the $T_\theta = 286$ K isoline in the MM5/2EQ simulation but below the $T_\theta = 289$ K isoline in the MM5/ETA simulation. During the peak of the windstorm, between 06:00 UTC and 09:00 UTC on 16 September, there is stronger TKE aloft in the lee of the mountain in the MM5/2EQ simulation but the wave structure is now again very similar. After 09:00 UTC there is very little difference between the two MM5 simulations.

The wave structure simulated with the two WRF variations remains similar for the whole period. The same can not be said about the TKE distribution and intensity. The onset of strong TKE production is evident at 22:00 UTC on

15 September in WRF/MYJ and an hour later in WRF/2EQ. The maximum TKE in WRF/2EQ, between 23:00 UTC 15 September and 02:00 UTC 16 September, is confined to a narrow band (approximately 5 km wide) directly in the lee of the mountain between 750 and 900 hPa height. The TKE intensity in this region is about twice that simulated by the WRF/MYJ during the same time interval. The width of the TKE distribution in WRF/MYJ is approximately twice that of WRF/2EQ and the wave penetrates sligthly deeper (typically 10–20 hPa). For the remainder of the simulation period both schemes produce TKE of the same order of magnitude and with very similar distribution. Only during the peak of the simulated surface winds, 08:00 UTC 16 September, WRF/2EQ simulates greater values (approximately 20%) of TKE in the lee of the mountain but the upward reach is not as great as in the WRF/MYJ simulation (700 hPa vs. 650 hPa).

The wave breaking, simulated by the WRF model, differs from the wave breaking simulated by MM5. Particularly, the WRF simulated wave breaking is much weaker than that in the MM5 simulations. Interestingly, there is high TKE production at the surface in the WRF simulations as in the MM5 simulations. During hours 01:00 UTC and 03:00 UTC, downward penetration of the simulated wavestructure in the lee of the mountain is similar between the MM5/2EQ and the two WRF simulations. As with the MM5/2EQ simulation, the simulated surface wind speed at SKAFT increases significantly during this time. For WRF/MYJ the winds change from 2.5 to 15.5 ms^{-1} and the WRF/2EQ wind speed increases from 3 to 17.5 ms^{-1}. Observed wind speed changes from 5 to 12 ms^{-1} over this period.

4.2 Impact of micro-physics on the WRF/MYJ simulations

4.2.1 Precipitation

Accumulated precipitation as simulated using the various micro-physics schemes is shown in Fig. 7. The effects of increased complexity within the three WSM schemes are evident. In the simulation using the simplest three class scheme (top right) the precipitation maximum is on the lee side of the mountain. As the effects of ice and snow hydro-meteors is taken into account in WSM5 (middle left), the upslope and lee side precipitation are of the same order of magnitude. In WSM6 (bottom left), where the effects of graupel are included, the maximum of simulated precipitation has shifted to the upwind slopes of the mountain. The downslope precipitation maximum is not seen in the relatively simple Kessler scheme. Interestingly, the precipitation pattern, using the Kessler scheme, is similar to that of the more complex Lin et al., WSM6 and Thompson schemes, although the simulated maximum is greater. Table 3 compares observed precipitation to simulated precipitation using the six micro-physics schemes. In general, all schemes overestimate the downslope precipitation at location SKAFT, with the exception of the Thompson scheme. At FAGHO, the schemes overestimate the precipitation by a factor of 1.6 (WSM5) to 2.7 (Lin et al.). During the accumulation period observed wind speed at FAGHO ranged from 10 ms^{-1} at 18:00 UTC 15 September to 30 ms^{-1} at 09:00 UTC 16 September. During such high wind speeds it can be assumed that a considerable proportion of the precipitation will not be measured by a conventional rain gauge as that at FAGHO. The observed wind speed at KVISK is considerably lower during the accumulation period, ranging from 4 ms^{-1} to 15 ms^{-1}. As observed wind speed is less at KVISK than at FAGHO observations give a greater underestimation of true ground precipitation at FAGHO than at KVISK. Consequently, it can be expected that simulated precipitation at KVISK will be in better agreement with observed precipitation than at FAGHO.

Table 3. Observed and simulated accumulated precipitation [mm], between 15 September, 18:00 UTC and 16 September, 09:00 UTC, at stations SKAFT, FAGHO and KVISK using various microphysics schemes in combination with the MYJ PBL scheme in WRF.

	SKAFT	FAGHO	KVISK
Observed	0.0	42.4	59
Kessler	30.4	126.5	149.4
WSM3	9.6	70.0	57.8
WSM5	19.9	63.5	52.9
Lin et al.	13.8	148.0	128.3
WSM6	8.7	110.7	93.2
Thompson	0.8	74.8	95.0

4.2.2 Surface winds and temperature

The intensity of the simulated downslope windstorm is not only sensitive to the PBL schemes but also to the cloud micro-physics schemes.

Figure 8 shows the variation of the WRF/MYJ simulated surface wind speed (left) and temperature (right) at SKAFT that is caused by using various options of the cloud microphysics schemes. It is seen that there is a significant variation in the simulated maximum surface wind speed corresponding the different cloud micro-physics schemes, and the Thompson scheme appears to produce the result in the best agreement with the observation. The surface temperature is also best simulated with the Thompson scheme, being very close to observed temperature during the peak of the storm (04:00 UTC to 08:00 UTC on 16 September). During this period the WRF/MYJ model, using other micro-physic parameterisations, overestimates the surface temperature at Skaftafell by 1–3°. However, the model does not capture the observed temperature maximum (15.5°) at 10:00 UTC, but the Thompson scheme produces results that are closest to the observed values.

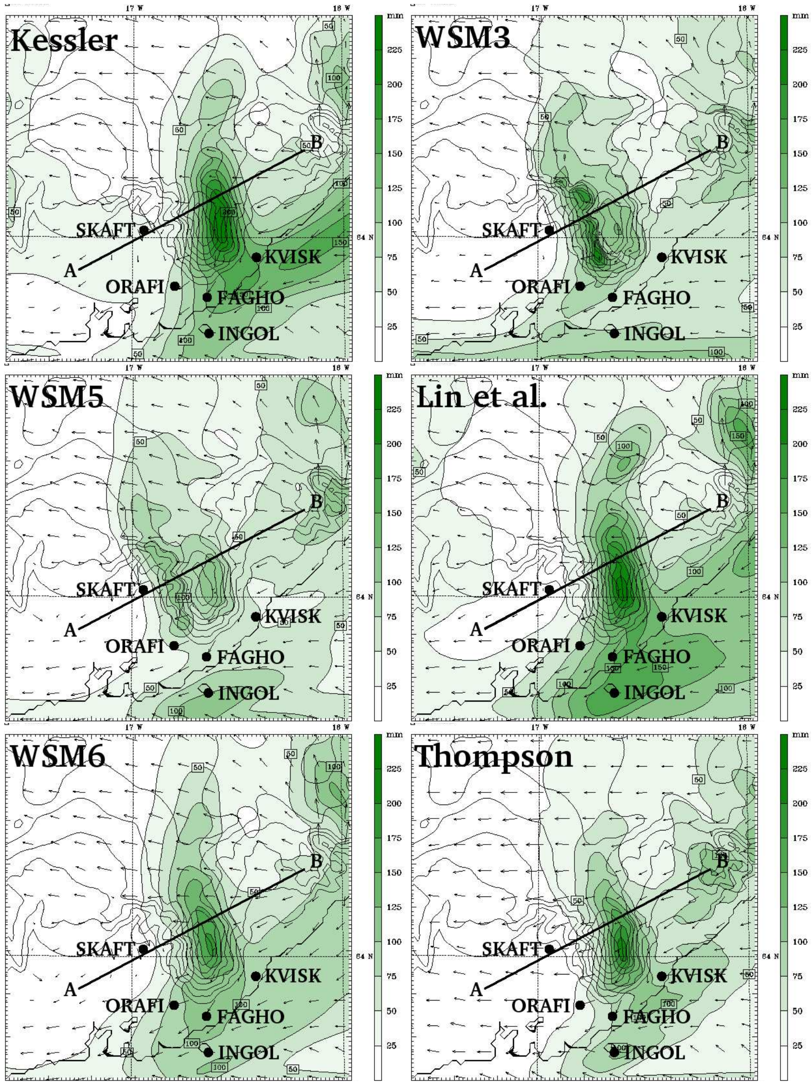

Fig. 7. Accumulated precipitation between 18:00 UTC 15 September and 09:00 UTC 16 September 2004. micro-physics schemes are, from top left to bottom right: Kessler, WSM3, WSM5, Lin et al., WSM6 and Thompson.

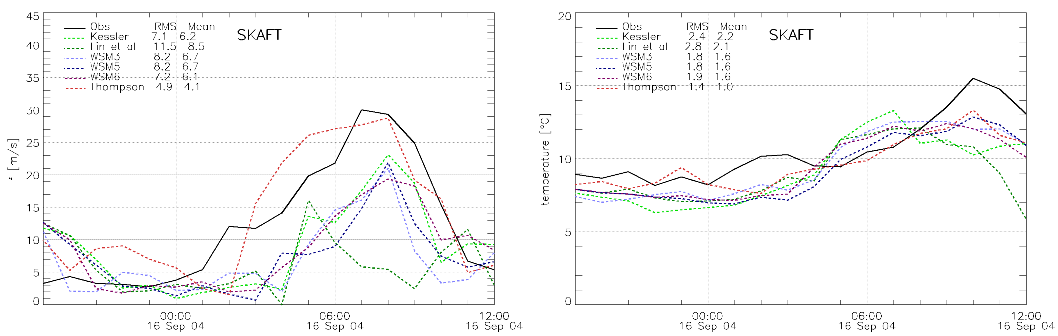

Fig. 8. Observed (solid black) and simulated (dashed) 10 m wind speed [ms^{-1}](left) and 2-m temperature [°] (right) at station Skaftafell (WMO# 4172 – SKAFT) in the lee of Mt. Öræfajökull. Various colours represent various micro-physic parameterisations within the WRF model: Light green – Kessler, dark green – Lin et al., light blue – WSM3, dark blue – WSM5, purple – WSM6 and red – Thompson scheme.

4.2.3 Hydro-meteors

There is a distinct difference between the Thompson scheme and the other five schemes when it comes to simulated surface wind speeds in the wake of Mt. Öræfajökull. The simulated wind speed is considerably less than observed wind speed at location SKAFT in all micro-physics schemes but the Thompson scheme. The six micro-physics schemes do not differ much in either distribution nor quantity of the water vapour mixing ratio. All models reveal wet cores below 700 hPa height on both sides of Mt. Öræfajökull. Over the mountain, where the air is descending, the water vapour mixing ratio is less than in the humid low level cores (not shown). Figure 9 shows a cross section along line AB (cf. Fig. 4) for the various micro-physics scheme. The simple three class schemes (i.e. Kessler and WSM3) simulate distinctly less cloud water than the other four micro-physics schemes (i.e. WSM5, Lin et al., WSM6, and Thompson). The cloud water is confined to a shallow (below 700 hPa) layer on the upslope side of the mountain. In contrast, the WSM5 and WSM6 schemes further simulate cloud water at mountain height (approximately 800 hPa) in the lee of Mt. Öræfajökull. The simulation done with the Thompson scheme produces a humid high level (between 350 and 700 hPa) plume on the lee side of the mountain. There are considerable variations in the rain water mixing ratio, both in time and space, in all microphysics schemes. Most noticeably, the Thompson scheme shows the least rain water in the lee of the mountain during the peak of the downslope wind storm. In the simulation of this storm the WSM6 and Lin et al. schemes favoured the formation of graupel to that of snow. This is in contrast to the Thompson scheme which only simulated moderate amounts of graupel between 700 and 850 hPa height, upslope of the mountain. This can clearly be seen in Fig. 10, valid at 09:00 UTC 16 September.

Yet another striking difference between the Thompson scheme and the other micro-physics schemes is the relatively low level (i.e. below 600 hPa) dryness in the lee of Mt. Öræfajökull (cf. Fig. 11) during the hours of maximum downslope wind speed. The wave activity is further much stronger when simulated with the Thompson scheme than all the other micro-physics schemes. Figure 12 shows a skew-T diagram at location B (cf. Fig. 4) for the Thompson and the WSM6 simulations. It can be seen that the temperature between 750 and 800 hPa in the Thompson scheme is less than in the WSM6 scheme by about 2.5°. The upstream moist static stability at, and above, mountain height (i.e. between 750 and 800 hPa) is greater in the Thompson simulation than the WSM6 simulation. The same holds true for all the other five micro-physics simulations. Table 4 shows the square of the dry (upper row) and moist (lower row) Brunt-Väisälä frequency (N^2) at, and above, mountain height at point BV along cross-section AB. The upslope wind speed along cross-section AB is similar in all simulations, regardless of what micro-physics scheme is used (not shown). The near surface wind speed is high (typically 25–30 ms^{-1}) but decreases with height. At mountain height (i.e. 800 hPa) the wind speed is between 8 and 10 ms^{-1} and is reduced to zero between 650 and 700 hPa.

4.3 Impact of moisture on the WRF/MYJ simulations

In order to investigate whether evaporation, and consequently condensation, might be a relevant factor for the flow dynamics a "dry" simulation was carried out. This experiment was identical to the control simulation, (called WRF/MYJ), with the exception that the micro-physics and surface fluxes were turned off.

The simulated "dry" surface flow, on the lee side of Mt. Öræfajökull (location SKAFT), is considerably stronger then in the control simulation (WRF/MYJ) with full microphysics and surface fluxes (cf. Fig. 13, left). The lee side surface temperature is however on average two to five degrees lower than the control run temperature (cf. Fig. 13, right) during the storm, while it becomes similar at the end of it.

The cross section shown in Fig. 14 reveals greater wave activity and more intence turbulence above the lee side slopes of the mountain than in the control simulation. The stability immediately upslope of Mt. Öræfajökull is considerably less than in the control simulation, although the stability is similar at point BV, as shown in Table 4. This leads to a weaker blocking in the "dry" simulation than in the control run.

5 Discussions

5.1 Sensitivity to boundary layer parameterization

The major difference between the MM5 and WRF simulations is in the wave breaking. In the MM5 simulations, there is greater dissipation in the mountain wave associated with greater TKE production below 600 hPa at all times than there is in the WRF simulations. In the WRF simulations, the dissipation takes mainly place between 950 and 700 hPa. After 03:00 UTC, 16 September, it is confined between the surface and 800 hPa. The difference in the intensity of the simulated downslope winds can be explained by less dissipation associated with turbulence in the WRF simulations than in the MM5 simulations. Since upper air observations are not available to verify the simulated wave breaking, the accuracy of the simulated surface winds and temperature is the only measurable performance of both the MM5 and WRF models for this windstorm event.

The two different boundary layer scheme perform similarily within the WRF model, and the greatest difference is found aloft. The 2EQ model gives stronger wave activity but slightly weaker sub-grid turbulence. Without observations aloft, it can not be determined which PBL scheme performs better.

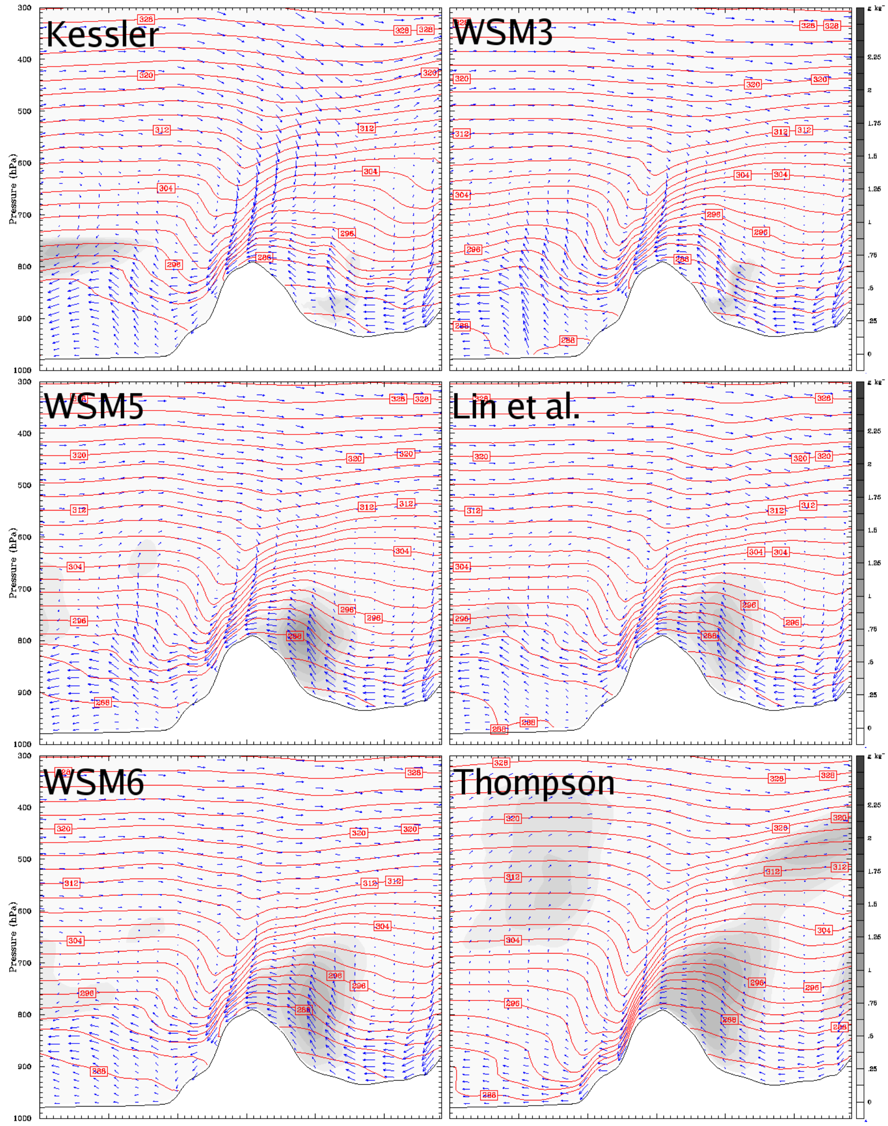

Fig. 9. Cross section along line AB (cf. Fig. 4) showing potential temperature (red lines) [K], wind along cross section (blue arrows) [ms^{-1}] and cloud water mixing ratio [g/kg] at 06:00 UTC 16 September 2004. micro-physics schemes are, from top left to bottom right: Kessler, WSM3, WSM5, Lin et al., WSM6 and Thompson.

5.2 Sensitivity to micro-physics parameterization

5.2.1 Precipitation

Different micro-physics schemes affect the simulated surface wind and temperature as well as the precipitation. The simulated precipitation in the simple Kessler scheme is similar to the simulated precipitation in the more complex WSM6, Lin et al. and Thompson schemes (cf. Fig. 7). For mountains of similar height as Mt. Öræfajökull this is in agreement with results in Miglietta and Rotunno (2006). Miglietta and Rotunno investigated moist, nearly neutral flow over a ridge in an idealistic framework. For a 700 meter high narrow ridge (i.e. with halfwidth of 10 km) the Kessler and Lin et al. schemes produced very different rain rates. The Kessler scheme had a lower rain rate and produced precipitation only on the upslope side of the ridge whilst the Lin et al. produced precipitation further upstream and had a distinct downslope maxima as well. The reason for this difference lies in a lower threshold used for autoconverting cloud water to rain in the Lin et al. scheme (7×10^{-4} gkg^{-1}) to that of the Kessler shceme (1×10^{-3} gkg^{-1}). The lower threshold values results in greater rainfall rate in the Lin et al. scheme and also in the upstream shift of the precipitation as the conversion of cloud water to rain occurs earlier. The downslope maxima in the Lin et al. scheme is generated by a downstream ice cloud

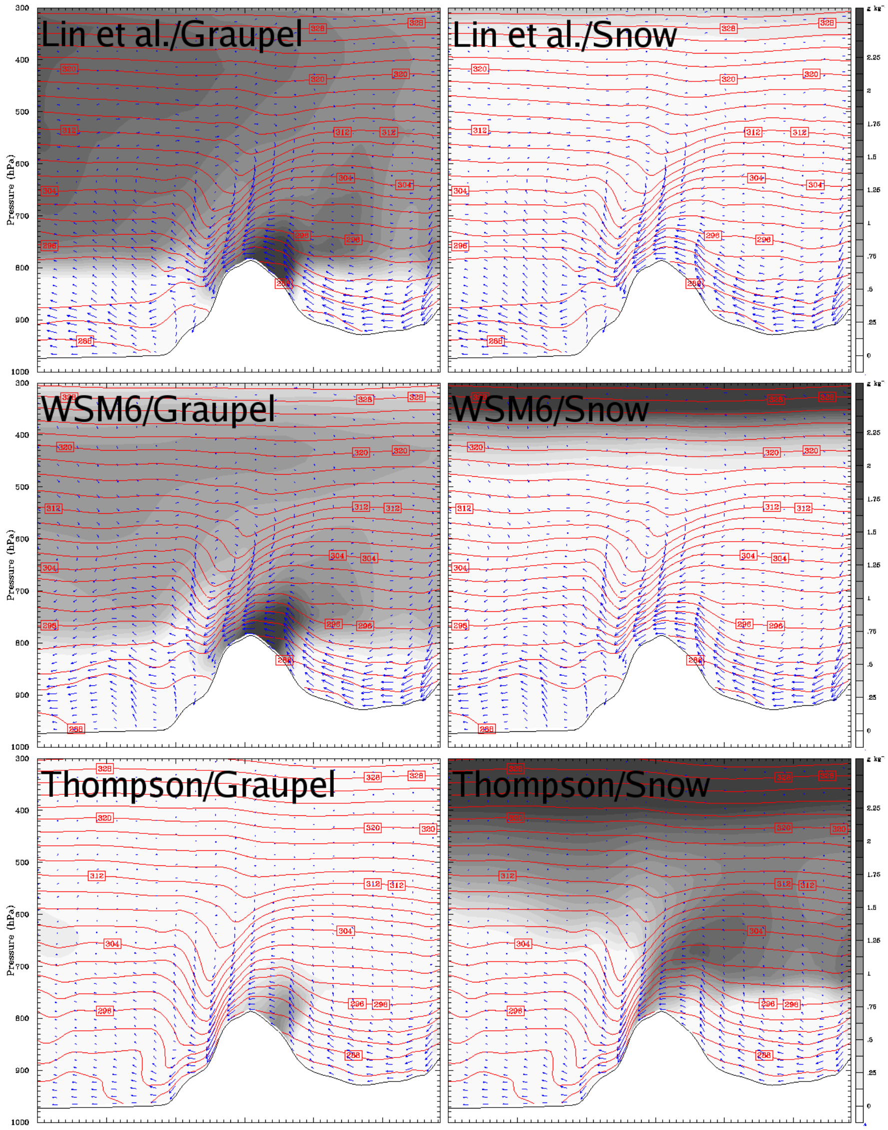

Fig. 10. Cross section along line AB (cf. Fig. 4) showing potential temperature (red lines) [K], wind along cross section (blue arrows) [ms^{-1}], graupel mixing ratio [g/kg] (left columns) and snow mixing ratio [g/kg] (right column) at 09:00 UTC 16 September 2004. micro-physics schemes are Lin et al. (top), WSM6 (middle) and Thompson (bottom).

and is the result of the ice microphysical processes that convert ice cloud to snow and then convert the snow to graupel. However, for the case of a higher (2000 m) ridge, i.e. similar to the hight of Mt. Öræfajökull, both schemes behave in a similar manner, the maximum precipitation is confined to the upstream side of the ridge with the Kessler scheme producing greater rainfall rate. The reason is that the more intense vertical motions due to a higher mountain results in much larger amounts of condensate than with a lower mountain. Consequently, the intensity and the location of the upwind precipitation maximum is not so dependent on the differing thresholds for autoconversion between the Lin et al. and Kessler shcemes. The accumulated 15 h precipitation simulated on the upslope hill of Mt. Öræfajökull is in general of the same order as the maximum 24 h precipitation values that have been observed on lowland in this area. The maximum observed 24 h precipitation was at location KVISK on 9–10 January 2002 (293.3 mm). This is a clear indication that precipitation in the mountains can be much greater than at the foothills.

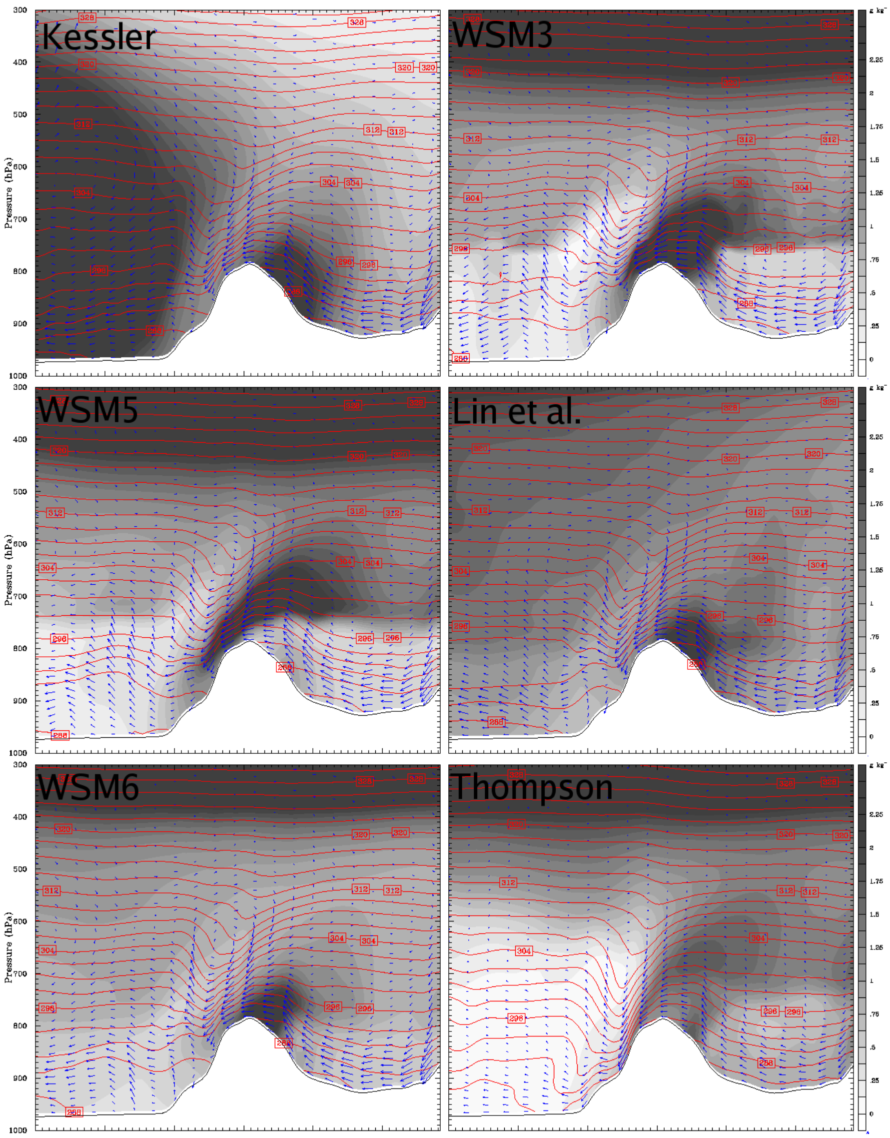

Fig. 11. Cross section along line AB (cf. Fig. 4) showing potential temperature (red lines) [K], wind along cross section (blue arrows) [ms^{-1}], and total precipitation mixing ratio [g/kg] at 09:00 UTC 16 September 2004. micro-physics schemes are, from top left to bottom right: Kessler, WSM3, WSM5, Lin et al., WSM6 and Thompson.

5.2.2 Upstream stability

Simulations done with WRF/MYJ in combination with various cloud micro-physics schemes showed little variations in upslope wind-speed along cross-section AB (cf. Fig. 4). As the Froude[2] number is a function of the characteristic mountain height, the upslope wind-speed and upslope stability, this emphasises the importance of capturing the upslope stability correctly in order to determine whether the flow will be able to cross the obstacle and cause a downslope wind storm. The upstream low-level flow at, and above, mountain top level (approx. between 700 and 800 hPa) in the Thompson scheme simulation (cf. Table 4) is noticably more stable than in the other runs. Conversely, the simulated upstream atmospheric stability below the mountain top level is slightly weaker with the Thompson scheme than with the other schemes. According to Smith (1985) greater upstream stability at mountain top level tends to produce stronger downslope winds. Furthermore, Smith et al. (2002) suggest that shallower upstream blocking contributes to stronger gravity wave activity than deeper blocking through a greater effective mountain height,

[2] Traditionally, the Froude number is a measure of the ratio of inertial and buoyant forces, i.e. whether there is a flow-over or a flow-around an obstacle.

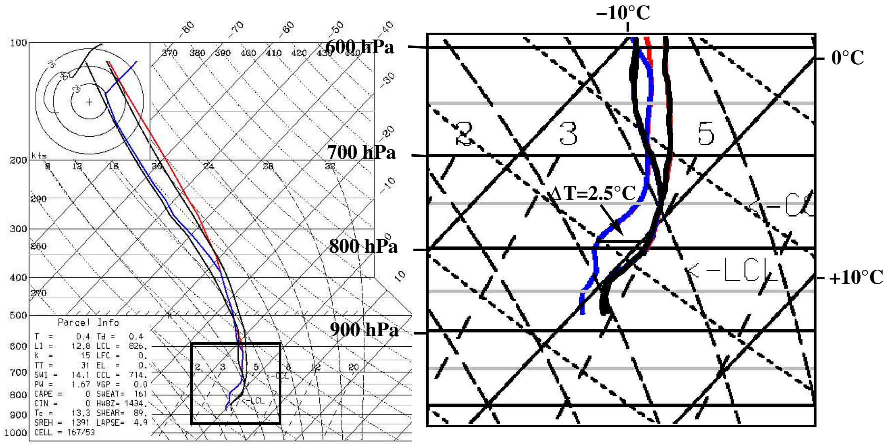

Fig. 12. Skew-T diagram at location B (cf. Fig. 4) at 06:00 UTC 16 September 2004, Thompson micro-physics scheme (blue and red lines) and the WSM6 scheme (black lines). The zoomed-in figure to the right shows that the maximum temperature difference (2.5 °) between the two schemes is at approximately 800 hPa height.

Table 4. The square of the simulated Brunt-Väisälä frequency (N^2) [s^{-2}] at point BV on 16 September, 06:00 UTC at various pressure levels for all ten simulations. Here, N is defined as $\sqrt{\frac{g}{\theta}\frac{d\theta}{dz}}$, where θ is the dry (upper row) and moist (lower row) equivelant potential temperature, g is the local acceleration of gravity, and z is geometric height.

	650–700 hPa	700–750 hPa	750–800 hPa	800–850 hPa	850–900 hPa
WRF/MYJ	13.1×10^{-5}	17.8×10^{-5}	27.3×10^{-5}	38.8×10^{-5}	12.3×10^{-5}
Kessler	0.0	15.0×10^{-5}	18.0×10^{-5}	64.0×10^{-5}	0.0
WRF/MYJ	16.3×10^{-5}	17.7×10^{-5}	22.2×10^{-5}	29.2×10^{-5}	23.2×10^{-5}
WSM3	0.0	0.0	10.0×10^{-5}	18.2×10^{-5}	13.0×10^{-5}
WRF/MYJ	15.6×10^{-5}	16.1×10^{-5}	25.2×10^{-5}	31.9×10^{-5}	21.2×10^{-5}
WSM5	3.6×10^{-5}	3.0×10^{-5}	13.0×10^{-5}	20.5×10^{-5}	9.6×10^{-5}
WRF/MYJ	17.0×10^{-5}	15.9×10^{-5}	25.8×10^{-5}	34.3×10^{-5}	18.0×10^{-5}
Line et al.	0.0	5.0×10^{-5}	24.0×10^{-5}	23.3×10^{-5}	13.5×10^{-5}
WRF/MYJ	17.1×10^{-5}	16.2×10^{-5}	23.8×10^{-5}	36.0×10^{-5}	20.4×10^{-5}
WSM6	0.0	1.0×10^{-5}	12.0×10^{-5}	25.2×10^{-5}	8.5×10^{-5}
WRF/MYJ	19.0×10^{-5}	19.4×10^{-5}	29.1×10^{-5}	30.8×10^{-5}	19.8×10^{-5}
Thompson	10.0×10^{-5}	10.0×10^{-5}	120.0×10^{-5}	0.0	0.0
WRF/MYJ	22.0×10^{-5}	17.6×10^{-5}	21.8×10^{-5}	26.6×10^{-5}	19.2×10^{-5}
Thompson dry	11.8×10^{-5}	6.3×10^{-5}	10.2×10^{-5}	15.6×10^{-5}	7.2×10^{-5}
WRF/2EQ	19.0×10^{-5}	19.4×10^{-5}	29.2×10^{-5}	31.2×10^{-5}	19.2×10^{-5}
Thompson	6.0×10^{-5}	10.0×10^{-5}	80.0×10^{-5}	0.0	0.0
MM5/ETA	18.5×10^{-5}	19.5×10^{-5}	23.1×10^{-5}	34.8×10^{-5}	18.0×10^{-5}
Reisner2	0.0	0.0	0.0	20.0×10^{-5}	0.0
MM5/2EQ	18.6×10^{-5}	19.6×10^{-5}	23.2×10^{-5}	34.8×10^{-5}	18.2×10^{-5}
Reisner2	0.0	0.0	0.0	30.0×10^{-5}	0.0

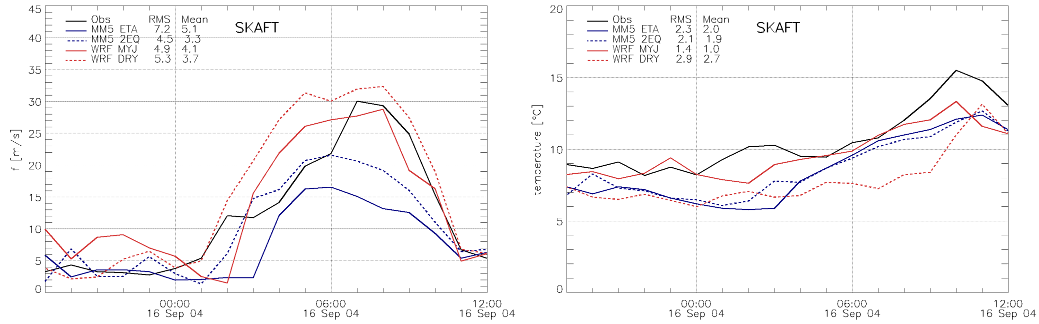

Fig. 13. Observed (solid black) and simulated (solid blue – MM5/ETA, blue dash – MM5/2EQ, solid red – WRF/MYJ, red dash – WRF/MYJ DRY) 10 m wind speed [ms^{-1}] (left) and 2-m temperature [°] (right) at station SKAFT (WMO# 4172) in the lee of Mt. Öræfajökull.

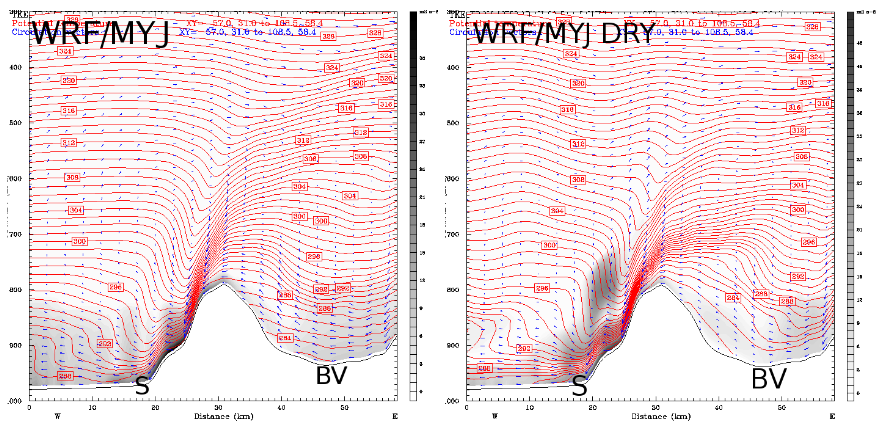

Fig. 14. Cross section along line AB (cf. Fig. 4) showing potential temperature (red lines) [K], wind along the cross section (blue arrows) [ms^{-1}] and turbulent kinetic energy (TKE) [J/kg] for WRF/MYJ (left) and WRF/MYJ DRY (right) at 16 September 2004, 06:00 UTC.

i.e. a larger part of the mountain is above the blocked flow. Jiang and Doyle (2009) use observations and simulations to reach a similar conclusion in their recent paper: firstly, that near surface moisture may enhance flow-topography interaction and lead to stronger waves through reducing the upslope blocking. Secondly, that moisture further aloft tends to dampen the wave activity through a destratification of the flow and lower buoyancy frequency. The simulated moisture distribution aloft is different for all the moisture-schemes discussed here so that these competing mechanisms have a different impact on the different simulations. In summary, a weakening of the wave activity leads to shorter downslope extent of the windstorms. Consequently a boundary layer separation occurs high on the lee slopes of the mountain in the flow simulated with all the schemes, except the Thompson scheme. Furthermore, the relatively dry downstream flow in the Thompson scheme is a result of less spillover and a greater dry-out of hydro-meteors.

5.2.3 Role of hydro-meteors

The observed sensitivity to cloud micro-physics schemes can be explained by the fact that various schemes produce different upslope distributions of precipitation and hydro-meteors, resulting in variation in the upslope static stability. Since the intensity of downslope wind is directly related to the intensity of the gravity-wave, which in turn is strongly dependent on the upslope static stability, this sensitivity is the manifestation of the great impact of the upslope precipitation on the downslope wind speed. The Thompson scheme proofed superior to the other five schemes tested in simulating the downslope windstorm. It is highly likely that this is related to the upward shift of the stable layer in the Thompson scheme (cf. Fig. 12). A possible explanation for this difference may be the different distribution function for graupel used in the Thompson scheme as well as differences in riming growth from the other micro-physics schemes. The greater formation of graupel in the Lin et al. and WSM6 schemes to that in the Thompson scheme (cf. Fig. 10) leads to more accretion (i.e. riming and/or depositional growth) which in turn leads to release of latent heat as liquid hydro-meteors are being turned into solid hydro-meteors. The Thompson scheme in contrast favours the formation of snow to that of graupel. Hence, there is less accretion and greater aggregation that takes place. As a result there is less release of latent heat than in the other two simulations and the region between 750 and 850 hPa becomes colder (cf. Fig. 11) and more stable. Previous sensitivity tests, e.g. by Colle et al. (2005) have shown that orographically influenced precipitation is in fact greatly dependent on snowfall velocity and snow size distribution. Woods et al. (2007) investigated the sensitivity of the Thompson micro-physics scheme to the representation of snow particle types. They demonstrated the defectiveness of the conventional assumption of snow particles as spheres of constant density. A more realistic empirical mass-diameter relationship resulted in an increased number of particles and a shift of the snow size distribution towards larger particles. This in turn led to increased depositional growth of snow and decreased cloud water production.

5.3 Sensitivity to atmospheric moisture

Compared to the control simulation with the Thompson micro-physics scheme, the dry simulation produces a too fast surface flow in the lee of the mountain. This is due to stronger gravity wave activity aloft, which is explained by the weaker atmospheric stability immediately above the upstream slopes of the mountain. The weaker and shallower blocking increases the effective mountain height and the flow/mountain interaction is stronger (Smith et al., 2002).

Similarly, the leeside temperature deficit in the dry simulation is a result of the weaker blocking allowing potentially colder air to ascend over the mountain and descend down the leeside than in the control simulation.

When the leeside flow in the dry simulation is compared to the flow with the other moisture schemes than Thompson, it seems plausible that in addition to less favourable upslope condition for wave formation, some of the poor model performance in the lee may be accounted for by evaporative cooling of the excessive simulated precipitation. This should lead to cooling on the leeside, and increased stability at low-levels, and hence weakens the downward penetration of the wave. This corresponds to the Kessler scheme, which gives both excessive precipitation and weak waves.

6 Conclusions

A severe windstorm downstream of Mt. Öræfajökull in Southeast Iceland is simulated on a grid of 1 km horizontal resolution by using the PSU/NCAR MM5 model and the Advanced Research WRF model. Both models are run with a new, two equation planetary boundary layer (PBL) scheme as well as the ETA/MYJ PBL schemes. The storm is also simulated using five other micro-physics schemes in combination with the MYJ PBL scheme in WRF, as well as a "dry" run. It is found that the predictability of the windstorm is strongly dependent on the parameterization schemes, with complicated interactions between the flow dynamics and different physics.

Both models capture gravity-wave formation over Mt. Öræfajökull, while the vertical structure of the lee wave differs between the two models and the PBL schemes. The simulated wave in the WRF model (using both the MYJ and the 2EQ schemes) is not as steep as in the MM5 simulations. The WRF simulated downslope winds, using the MYJ PBL scheme, are in good agreement with the strength of the observed downslope windstorm. When simulated using the new two equation scheme, surface winds are not as strong. On the contrary, the MM5 simulated surface winds, with the new two equation model, are in better agreement to observations than when using the ETA scheme. The simulated surface temperature in the WRF simulations is closer to the observations than simulated temperature in the MM5 simulations.

One of the first papers employing observational data from aloft to study the impact of moisture on gravity waves is by Jiang and Doyle (2009). They found that moisture aloft will generally weaken the wave activity while it is however dependent on both the thickness and location of the moist layer as well as wind speed near mountain top level. The current study reveals a sensitivity to cloud micro-physics that can be explained by the difference in the simulated moisture and hydro-meteors distribution. The micro-physics schemes tested here give different downslope winds and all schemes, excluding the Thompson scheme, underestimate the downslope windstorm. This is caused by different simulated stability upstream of the mountain. How general these results may be remains however unclear. This emphasises the importance of observing micro-physical properties in cases like this in order to improve our understanding of downslope windstorms, precipitation distribution and the flow pattern in general and our ability to predict them.

Furthermore, this study highlights some of the difficulties related to predicting severe downslope windstorms. The ensemble based study of Reinecke and Durran (2009) showed a strong dependence of the predictability to small-scale features in the synoptic flow. Here, merely changing a parameterization in the atmospheric model is decisive for a successful forecast. However, this study is not definite in giving the correct parameterization for downslope windstorm prediction, i.e. the 2EQ PBL and Thompson-schemes, which perform best here. Windstorms in other locations of the world and in other synoptic settings may be better represented by other parameterizations. In this light, simple ensemble prediction systems based on one or more atmospheric models employing different boundary layer and microphysics schemes may prove a valuable tool in short range severe downslope windstorm prediction.

Given the lack of upper air observations for this downslope windstorm event and the limitation of a single-case study, the results from this study are not conclusive but provide valuable information for the setup of realtime numerical forecasting systems in complex topography.

Acknowledgements. This work is part of the RÁV-project which is funded in part by the Icelandic Research Fund (Rannsóknarsjóður Íslands), grant number 70271013, and the NORA funded project "Vejrtjeneste for søberedskab", grant number 550-025. The weather stations, from which data has been used in this study, belong to the Icelandic Meteorological Office, the Icelandic Road Administration and the Icelandic Maritime Administration. The authors thank Sara Michelson for reading over the manuscript.

Comments from two anonymous reviewers are acknowledged.

Edited by: H. Wernli

References

Ágústsson, H. and Ólafsson, H.: Simulating a severe windstorm in complex terrain, Meteorol. Z., 16, 99–110, 2007.

Ágústsson, H. and Ólafsson, H.: The bimodal downslope windstorms at Kvísker, Meteor. Atmos. Phys., doi: 10.1007/s00703-010-0075-y, http://dx.doi.org/10.1007/s00703-010-0075-y, 2010.

Bao, J. W., Michelson, S. A., Kantha, L. H., and Brown, J. W.: Implementation of a Two-Equation Vertical Turbulent Mixing Scheme in a Mesoscale Atmospheric Model. NOAA Technical Memorandum OAR PSD–311, National Oceanic and Atmospheric Administration, Boulder, CO, 33 pp., 2008.

Belǔsić, D. and Klaić, Z. B.: Estimation of bora wind gusts using a limited area model, Tellus, 56A, 296–307, 2004.

Belǔsić, D., Pasarić, M., and Orlić, M.: Quasi-periodic bora gusts related to the structure of the troposphere, Q. J. Roy. Meteorol. Soc., 130, 1103–1121, 2004.

Colle, B. A., Garwert, M. F., Wolfe, J. B., Mass, C. F., and Woods, C. P.: The 13–14 December 2001 IMPROVE–2 Event. Part III: Simulated Microphysical Budgets and Sensitivity Studies, J. Atmos. Sci., 62, 3535–3558, 2005.

Doyle, J. D. and Shapiro, M. A.: A multi-scale simulation of an extreme downslope windstorm over complex topography, Meteor. Atmos. Phys., 74, 83–101, 2000.

Doyle, J. D., Durran, D. R., Chen, C., Colle, B. A., Georgelin, M., Grubišić, V., Hsu, W. R., Huang, C. Y., Landau, D., Lin, Y. L., Poulus, G. S., Sun, W. Y., Weber, D. B., Wurtele, M. G., and Xue, M.: An intercomparison of model-predicted wave breaking for the 11 January 1972 Boulder windstorm, Mon. Weather Rev., 128, 901–914, 2000.

Doyle, J. D., Shapiro, M. A., Jiang, Q. F., and Bartels, D. L.: Large-amplitude mountain wave breaking over Greenland, J. Atmos. Sci., 62, 3106–3126, 2005.

Dudhia, J.: Numerical study of convection observed during the winter monsoon experiment using a mesoscale two–dimensional model, J. Atmos. Sci., 46, 3077–3107, 1989.

Durran, D. R.: Mountain Waves and Downslope Winds, in: Atmospheric Processes Over Complex Terrain, edited by: Blumen, W., American Meteorological Society, Boston, 59–81, 1990.

Grell, G. A., Dudhia, J., and Stauffer, D. R.: A Description of the Fifth–Generation Penn State/NCAR Mesoscale Model (MM5). NCAR/TN–398+STR, National Center for Atmospheric Research, Boulder, CO, 107 pp., 1995.

Grønås, S. and Sandvik, A. D.: Numerical simulations of local winds over steep orography in the storm over North-Norway on 12 October 1996, J. Geophys. Res., 104, 9107–9120, 1999.

Grubišić, V., Doyle, J. D., Kuttner, J., Dirks, R., Cohn, S. A., Pan, L., Mobbs, S., Smith, R. B., Whiteman, C. D., Czyzyk, S., Vosper, S., Weissman, M., Haimov, S., De Wekker, S., and Chow, F. K.: The Terrain–induced Rotor Experiment: A field campaign overview including observational highlights, B. Am. Meteor. Soc., 89, 1513–1533, doi:10.1175/2008BAMS2487.1, http://journals.ametsoc.org/doi/abs/10.1175/2008BAMS2487.1, 2008.

Hack, J. J., Boville, B. P., Kiehl, J. T., Rasch, P. J., and Williamson, D. L.: Description of the NCAR Community Climate Model (CCM2) NCAR/TN–382+STR, National Center for Atmospheric Research, Boulder, CO, 120 pp., 1993.

Hong, S. Y. and Lim, J. O. J.: The WRF single–moment 6–class microphysics scheme (WSM6), J. Korean Meteor. Soc., 42, 129–151, 2006.

Hong, S. Y., Dudhia, J., and Chen, S. H.: A revised approach to ice microphysical processes for the bulk parameterization of clouds and precipitation, Mon. Weather Rev., 132, 103–120, 2004.

Janjić, Z. I.: The step-mountain eta coordinate model: Further developements of the convection, viscous sublayer and turbulence closure schemes, Mon. Weather Rev., 122, 927–945, 1994.

Janjić, Z. I.: Nonsingular Implementation of the Mellor-Yamada Level 2.5 Scheme in the NCEP Meso model. Office Note #437, National Center for Environmental Prediction, 2001.

Jiang, Q. and Doyle, J. D.: The impact of moisture on mountain waves during T-REX, Mon. Weather Rev., 137, 3888–3905, 2009.

Kessler, E.: On the distribution and continuity of water substance in atmospheric circulations, Meteor. Monogr., 32, Amer. Meteor. Soc., 84 pp., 1969.

Lin, Y. L., Farley, R. D., and Orville, H. D.: Bulk parameterization of the snow field in a cloud model, J. Appl. Meteor., 22, 1065–1092, 1983.

Mellor, G. L. and Yamada, T.: Development of a turbulence closure model for geophysical fluid problems, Rev. Geophys. Space Phys., 20, 851–875, 1982.

Miglietta, M. M. and Rotunno, R.: Further Results on Moist Neutral Flow over a Ridge, J. Atmos. Sci., 56, 2796–2810, 2006.

Mlawer, E. J., Taubman, S. J., Brown, P. D., Iacono, M. J., and Clough, S. A.: Radiative Transfer for Inhomogenious Atmosphere: RRTM, a validated correlated-K Model for the Longwave., J. Geophys. Res., 102(D14), 16663–16682, 1997.

Ólafsson, H. and Ágústsson, H.: Observational and numerical evidence of strong gravity wave breaking over Greenland, Institute for Meteorological Research ISBN 9979-9709-3-6, Ütgáfufélag-iðSlemba, Reykjavík, 2006.

Ólafsson, H. and Ágústsson, H.: The Freysnes downslope windstorm, Meteorol. Z., 16, 123–130, 2007.

Ólafsson, H. and Ágústsson, H.: Gravity wave breaking in easterly flow over Greenland and associated low level barrier- and reverse tip-jets, Meteor. Atmos. Phys., 104, 191–197, 2009.

Ólafsson, H., Jónasson, N., and Karlsdóttir, S.: Háupplausnar reikningar til almennrar spágerðar (HRAS), lokaskýrsla, Technical Report 06011, Veðurstofa Íslands, Reykjavík, available at: http://www.vedur.is/utgafa/\discretionary{-}{}{}greinargerdir/March2006, 2006 (in Icelandic).

Reinecke, P. A. and Durran, D. R.: Initial condition sensitivities and the predictability of downslope winds, J. Atmos. Sci., 66, 3401–3418, doi:{10.1175/2009JAS3023.1}, 2009.

Rögnvaldsson, Ó. and Ólafsson, H.: A case study of the Icelandic through, Proc. Int. Conf. Alp. Meteorol. (ICAM), p. 4, 2003.

Sandvik, A. D. and Hartsveit, K.: Study of a downslope windstorm over Southern-Norway, Rjukan, 16 January 2000, Tech.Rep. 18, The Norwegian Meteorological Institute (met.no), 2005.

Skamarock, W. C., Klemp, J. B., Dudhia, J., Gill, D. O., Barker, D. M., Wang, W., and Powers, J. G.: A Description of the Advanced Research WRF Version 2. NCAR Technical Note, NCAR/TN–468+(STR), National Center for Atmospheric Research, Boulder, CO, 88 pp., 2005.

Smith, R. B.: On Severe Downslope Winds, J. Atmos. Sci., 42, 2597–2603, 1985.

Smith, R. B.: Aerial observations of the Yougoslavian bora, Atmos. Sci., 44, 269–297, 1987.

Smith, R., Skubis, S., Doyle, J., Broad, A., Kiemle, C., and Volkert, H.: Mountain waves over Mt. Blanc: Influence of stagnant boundary layer, J. Atmos. Sci., 59, 2073–2092, 2002.

Thompson, G., Rasmussen, R. M., and Manning, K.: Explicit Forecasts of Winter Precipitation Using an Improved Bulk Microphysics Scheme. Part I: Description and Sensitivity Analysis, Mon. Weather Rev., 132, 519–542, 2004.

Woods, C. P., Stoelinga, M. T., and Locatelli, J. D.: The IMPROVE–1 Storm of 1–2 February 2001. Part III: Sensitivity of a Mesoscale Model Simulation of the Representation of Snow Particle Types and Testing of a Bulk Microphysical Scheme with Snow Habit Prediction, J. Atmos. Sci., 64, 3927–3948, 2007.

www.uib.no

ISBN: 978-82-308-2225-8

Graphic design: Division of Communication, UiB
Print: AIT Oslo AS